FABRICATION OF SENSORS FOR THE SENSITIVE ELECTROCHEMICAL DETECTION OF ANTI-TUBERCULOSIS DRUGS

By

Rajasekhar Chokkareddy

(Reg No: 21557680)

A thesis submitted in conformity with the requirements for the degree of Doctor of Philosophy in Chemistry in the Faculty of Applied Sciences at the Durban University of Technology

March 2018

DECLARATION

I **Rajasekhar Chokkareddy** hereby declare that the work presented in this thesis entitled **"Fabrication of sensors for the sensitive electrochemical detection of anti-tuberculosis drugs"** is my own work and has not been submitted before for any degree or examination in any university and no portion of this or any closely related work is under consideration for publication elsewhere in any medium.

Signed: 

Rajasekhar Chokkareddy Date: 08/03/2018

Signed: 

Prof. G. G. Redhi (Supervisor) Date: 08/03/2018

Signed: 

Dr N.K. Bhajanthri (Co-supervisor) Date: 08/03/2018

DEDICATION

This dissertation is dedicated to my late grandmother **Chokkareddy Dhanamma** and my late grandfather **Chokkareddy Balireddy** may your soul rest in peace.

I also wish to dedicate this work to my mother **Chokkareddy Varalakshmi**; my father **Chokkareddy Venkatarami reddy**.

ACKNOWLEDGEMENTS

First and foremost, I would like to thank Prof. **Gan. G. Redhi**, not only for gifting me this opportunity but also for the unique knowledge, sustained support and enthusiastic encouragement, he has afforded me over the past few years. Furthermore, I would like to offer a special thank you to **Dr B. Natesh Kumar** who have joined me on this long and perilous journey from the very beginning. I would also like to extend my appreciation to all members of my research group without whom this knowledge would not have been as enjoyable and I would not have developed such strong and lasting relationships.

I want to thank my family specially my mother **Chokkareddy Varalakshmi**; my father **Chokkareddy Venkatarami reddy**; my brother **Chokkareddy Niranjan reddy**; my sister **Chokkareddy Gowthami**; my aunties **Kalluru Mahalakshmi (Rosamma)** and **K Bharathi**; my grandmother **K. Shanthamma;** my friend **Golla Radhika**.

I would like to thank my uncles **Chokkareddy Vijaya Bhaskar reddy**; **Chokkareddy Manohar reddy**; **Chokkareddy Balasubramanyam reddy**; **Chokkareddy Chenga reddy**; **Patnam Narendrababu**, and my brother **Chokkareddy Jagadeesh reddy**; and my uncle **K. Jayasimha reddy**; and my late uncles **Chokkareddy Chandra reddy**; **Chokkareddy Nagi reddy**, and my friends K. Chandra Sekhar, K. Manikanta, R. Kiran Kumar, V. Satheesh Kumar, K. Ravi Teja, Mallikarjun, Bindu, Harisha, family relatives and friends for their support, encouragement and understanding.

I am also indebted to **Dr K. Suvardhan** who welcomed me to the Durban University of Technology, and made me feel at home immediately.

Last but certainly not least, I would also like to extend my acknowledgements to Dr N. Thondavada, Mr. Kabane, and Mr. Vasantha Kumar, Mrs. Pelumi, Mr. Kevel and Mr. Sabella for their much appreciated contribution to this research. I am especially grateful to lab technician Mrs. M. Xhakaza for her support and healthy research environment.

To my mother, the strongest person I have ever known. Your ability to give thanks, love, persevere, laugh, show patience, teach, learn and encourage every day is remarkable and inspiring. To my father, the smartest person I have ever known. I wish I could have shared this journey with you. I miss you every day.

I would also like to extend my acknowledgement to the Durban University of Technology for awarding me a DUT-RDG scholarship.

ABSTRACT

In this work, electrochemical biosensors have been developed and quantified the pyrazinamide, isoniazid, rifampicin, ethambutol and streptomycin drugs in various pharmaceutical samples. Electrochemical methods are versatile and powerfull analytical technique of immense value in the area of pharmaceutical analyses. In addition, due to the similarity in the biological and electrochemical reactions, it can be expected that the reduction-oxidation mechanisms occur at the electrode surface. The biologically stimulated molecules can be examined by electroanalysis and they are also outstanding tools for the detection of pharmaceutical complexes in various matrices. Although in the case of a biosensors, the analyte interacts with bioreceptor and the resultant output is measured by a specifically designed transducer.

Additionally, a reliable highly sensitive and novel biosensor was developed by using a glassy carbon electrode modified with various nanomaterials. Hence horseradish peroxidase (HRP) - Multiwalled carbon nanotubes (MWCNTs)-Titanium oxide nanoparticles (TiO_2NPs) fabricated glassy carbon electrode (GCE) were used for the determination of isoniazid. Similarly, copper oxide nanoparticles (CuONPs)-MWCNTs immobilized with Cytochrome c (Cyt c) on glassy carbon electrode were established for the detection of pyrazinamide. Furthermore, iron oxide nanoparticles (Fe_3O_4NPs) and MWCNTs composite were immobilized with Coenzyme q (Coen-q) on glassy carbon electrode for the detection of rifampicin. In addition, Cyt c immobilized with ZnONPs and MWCNTs on glassy carbon electrode for the determination of streptomycin. Finally, the glassy carbon electrode fabricated with zinc oxide nanoparticles (ZnONPs) and reduced graphene oxide (RGO) nano composite, was further immobilized with HRP to enhance the electrochemical performance of the modified electrode for the determination of ethambutol.

Abstract

Electrochemical behaviour of these first line anti TB drugs to the developed biosensors were examined by using cyclic voltammetry and differential pulse voltammetry under the optimum experimental conditions such as scan rates, pH, accumulation potential, pulse amplitude, accumulation time, voltage step time, voltage step and deposition time respectively. The prepared biosensors and nanocomposites were characterized by Fourier transform infrared spectroscopy (FT-IR), transmission electron microscopy (TEM), thermo gravimetry (TGA) and x-ray diffraction (XRD). It was observed that electrochemical methods provided good and effective techniques for the determination of isoniazid, pyrazinamide, rifampicin, ethambutol and streptomycin. Compared to the other analytical methods, the limit of detection and limit of quantifications were found to be 0.0335 μM and 0.1118 μM for isoniazid, 0.0038 μM and 0.0129 μM for pyrazinamide, 0.032 μM, and 0.413 μM for rifampicin, 0.0214 μM and 0.6713 μM for ethambutol, and 0.0028 μM and 0.5628 μM for streptomycin respectively.

TABLE OF CONTENTS

Table of Contents

LIST OF TABLES

LIST OF SCHEMES

LIST OF FIGURES

ACRONYMS AND SYMBOLS

3-FR	3-formylrifamycin SV
AA	Ascorbic acid
AC	Acetaminophen
AC	Alveolar Cells
AcINZ	Acetylisoniazid
AgNPs	Silver nanoparticles
AL	Allopurinol
ASV	Anodic Stripping Voltammetry
ATP	Adinotri phosphate
BAL	Broncho alveolar lavage
BLF	Broncho alveolar Lavage Fluid
BPH	Buspirone HCL
CE	Capillary electrophoresis
CG	Carboxylated graphene
CMEs	Chemically modified electrodes
CNTs	Carbon nano tubes

CO-en q	Coenzyme q
CPE	Carbon paste electrode
CSV	Cathodic Stripping Voltammetry
CuONPs	Copper nanoparticles
CV	Cyclic voltammetry
CVD	Chemical vapor deposition
CYP2E1	Cytochrome P450-2E1
CYP3A4	Cytochrome P450 3A4
Cyt c	Cytochrome c
DMF	N, N-dimethyl formamide
DPV	Differential pulse voltammetry
DRIF	Drifampicin
DSC	Differential Scanning Calorimetry
DSTN	Dihydrostreptomycin
EBT	Poly eriochrome black T
EC	Electro chemical detection
EC	Eastern Cape
ECL	Electro generated chemiluminescence

ECL	Electrochemiluminescense
ECS	Electrochemical sensors
EFA	Efavirenz
ERGO	Electrochemically reduced graphene oxide
ETB	Ethambutol
FASI	Fatty acid synthetase I
Fe_3O_4NPs	Iron oxide nanoparticles
f-MWCNTs	Functionalized multiwalled carbon nanotubes
FSCV	Fast Scan Cyclic Voltammetry
FT-IR	Fourier transforms infrared spectroscopy
GCE	Glassy carbon electrode
GC-MS	Gas Chromatography-Mass spectrometry
GO	Graphene oxide
GP	Gauteng Province
HDH	Hydralazine hydrochloride
HIV/AIDS	Human immunodeficiency virus/acquired immunodeficiency syndrome

HPTLC	High performance thin layer chromatography
HRP	Horseradish peroxidase
icELISA	Enzyme-linked immunosorbent assay
IM	Indomethacin
INZ	Isoniazid
ISP	Ion-selective piezoelectric
KZN	KwaZulu-Natal
LC–ESI–MS	Liquid chromatography-electro spray Ionization-Mass spectrometry
LC-ESI-MS	Liquid chromatography-electrospray mass spectrometry
LC–MS	Liquid Chromatography-Mass spectrometry
LC-MS/MS	Liquid chromatography-mass spectrometry light scattering detection
LNZ	Linezolid
LOD	Limit of detection
LOQ	Limit of quantification
LSV	Linear sweep voltammetry
LTB	Latent tuberculosis

LTBI	Latent tuberculosis infection
MAC	*Mycobacterium avium complex*
MB	*Mycobacterium bovis*
MDR	Multidrug-resistant
MDR-TB	Multidrug-resistant tuberculosis
MM	*Mycobacterium marinum*
MNPs	Metallic nanoparticles
MP	Mpumalanga
MPN	Most probable numbers
MWCNTs	Multiwall carbon nanotubes
NIRS	Near infrared spectroscopy
NPAg-HCF	Silver hexacynaoferrates
NPV	Normal Pulse Voltammetry
OPPy	Overoxidizied polypyrrole
PAG	Poly-L-arginine
PANSA	Poly (8-anilino-1-napthalene Sulphonic acid)
PAS	Paraaminosalicylic acid

PBS	Phosphate buffer solution
PEDOT	Poly (3, 4-ethylenedioxy thiophene)
PIP	Piperine
PMET	Poly-L-methionine
PSA	poly (sulfosalicylic acid)
Pt/Au electrode	Platinum/gold electrodes
PVC	Poly (vinyl chloride)
PZM	Pyrazinamide
RDE	Rotating disc electrode
RIF	Rifampicin
RNO	Rifampicin N-oxide
RP-HPLC	Reverse phase high performance liquid chromatography
RpsA	Ribosomal protein S1
RQ	Rifampicin quinone
RSD	Relative standard deviation
RVC	Reticulated vitreous carbon
SCE	Screen printed electrode
SPCE	Screen-printed carbon electrode

STN	Streptomycin
STN-SLNs	Streptomycin sulphate loaded with solid lipid nanoparticles
SV	Rifamycin SV
SV	Staircase Voltammetry
SWADCS	Square-wave adsorptive anodic stripping voltammetry
SWCNTs	Single wall carbon nanotubes
SWV	Square wave voltammetry
TB	Tuberculosis
TEM	Transmission electron microscope
TGA	Thermogravimetric analysis
TiO_2NPs	Titanium dioxide nanoparticle
UA	Uric acid
UFLC-MS	Ultra-fast liquid chromatography – mass spectrometry
WC	Western Cape
WHO	World Health Organization
XRD	X-ray diffraction
ZnONPs	Zinc oxide nanoparticles

PUBLICATIONS ARISING FROM THIS STUDY

1. **Rajasekhar Chokkareddy**, Natesh Kumar Bhajanthri, Gan G. Redhi, 2017. An enzyme induced novel biosensor for the sensitive electrochemical determination of isoniazid. Biosensors, 7, 21, 1-12.
2. **Rajasekhar Chokkareddy**, Natesh Kumar B, Gan, G. Redhi, Dhirendra G. Redhi 2017, Ultra-Sensitive Electrochemical Sensor for the Determination of Pyrazinamide. Current Analytical Chemistry, 13, 1-8.
3. **Rajasekhar Chokkareddy**, Natesh Kumar Bhajanthri, Gan G Redhi, 2017. A Novel Electrode Architecture for Monitoring Rifampicin in Various Pharmaceuticals. International journal of Electrochemical science, 12, 9190-9203.
4. **Rajasekhar Chokkareddy**, Natesh Kumar Bhajanthri, Gan G Redhi, A novel electrochemical biosensor for the detection of ethambutol in pharmaceuticals. Submitted to Indian Journal of Chemistry on 2nd February 2018.
5. N.K. Bhajanthri, V.K. Arumugam, **R. Chokkareddy**, G.G. Redhi, 2016. Ionic liquid based high performance electrochemical sensor for ascorbic acid in various foods and pharmaceuticals, Journal of Molecular Liquids, 222, 370-376.

OTHER RESEARCH PUBLICATIONS

1. N.K. Bhajanthri, **R. Chokkareddy**, G.G. Redhi 2017. Aspects of Recent Advances in Smart Ionic Liquid Based Sensors. In *Ionic Liquid Devices* RSC (321-336).
2. **Rajasekhar Chokkareddy**, Natesh Kumar Bhajanthri, Bakusele Kabane, Gan G. Redhi, 2017. Bio-sensing performance of magnetite nanocomposite for biomedical applications. Wiley-scrivener. **(Accepted)**.

3. **Rajasekhar Chokkareddy,** Niranjan Thondavada, Bakusele Kabane, Gan G. Redhi. "Current advances in biosynthesis of silver nano particles and its applications". **(Wiley) Scrivener Publishers**. (Communicated).
4. **Rajasekhar Chokkareddy,** Gan G. Redhi. "Green synthesis of metal nanoparticles and its reaction mechanisms". **(Wiley) Scrivener Publishers**. (Communicated).
5. Niranjan Thondavada, **Rajasekhar Chokkareddy,** Gan G. Redhi. "Green synthesis of platinum nanoparticles and their biomedical applications". **(Wiley) Scrivener Publishers**. (Communicated).

PRESENTATIONS

1. **Rajasekhar Chokkareddy**, Gan G Redhi, "An enzyme induced novel biosensor for the sensitive electrochemical determination of isoniazid". International conference of molecular spectroscopy (ICMS 2017), held by Mahatma Gandhi University, Kerala, India. 8-10 December 2017.
2. **Rajasekhar Chokkareddy**, Gan G Redhi, "Development of robust ionic liquid based electrochemical sensor for the determination of lamivudine: An effective anti-HIV drug". 2nd global congress & expo on Material Science and Nanoscience, 25-27 September 2107, Valencia Spain.
3. N.K. Bhajanthri, **R. Chokkareddy**, N.M. Xhakaza and G.G. Redhi 2015. Abstract proceedings of the second International conference on composite and biocomposites of nano composites (ICCBN 2015), Durban University of Technology, Durban, South Africa, 28-30 October 2015.

CHAPTER 1

INTRODUCTION

Tuberculosis (TB) is produced by the bacterium "*Mycobacterium tuberculosis"* (Mtb). Extreme cases of TB are pulmonary, which is the maximum common infecting several organisms i.e. the main infection site is in the lung. It is estimated that one third of the world's population are infected with the bacterium Mtb and approximately 9.4 million new cases of TB were diagnosed globally in 2008 and two million deaths every year. South Africa has a substantial burden of TB which is exacerbated by the simultaneous epidemic of human immunodeficiency virus (HIV). Molecular methods have been used in developed countries to study the dynamics of the TB prevalent. The development of extensively drug resistant (EDR), total drug resistant (TDR) and multidrug (MDR) resistant organisms creates a crucial demand to develop a new drug with novel mechanisms to be effective against drug resistant strains of Mtb.

Moreover, the directly observed treatment short course (DOTS) regime which is an amalgamation of the drugs i.e. Pyrazinamide (PZM), Isoniazid (INZ), Rifampicin (RIF), Ethambutol (ETB) and Streptomycin (STN) has contributed significantly to the decrease in the sum of incidences of TB, but the partial implementation of the DOTS movement has been a main cause of the high occurrences of the drug resistant strains of Mtb untied with the spread of HIV/Aids in TB endemic regions.

1.1 Drug

A drug is a chemical that interacts with proteins in the body to affect a physiological function. This is the general idea behind all **medicine**. Once these chemicals are absorbed into the systemic circulation they bind with certain proteins and this changes the functioning of the cell slightly. For example, anticancer drugs bind to proteins on the surface of cancer cells and this stimulates the cells to die. In this case cell death is the physiological action of the drug. Moreover, no drugs are exactly interacting with just one category of cell or one type of protein and this is what causes side effects.

1.2 Tuberculosis (TB)

Infectious diseases are fatal enemies of the global population and Tuberculosis (TB) is among the top ten causes global death. TB is an infection disease caused by *Mycobacterium tuberculosis* (Organization, 2000). In 1882, the microbiologist Robert Koch described the tubercle bacillus, shown in **Figure 1.1**, at a time when one of every seven deaths in Europe was affected by TB. In 2014, there were an estimated 9.6 million new TB cases: 5.4 million among men, 3.2 million among women and 1.0 million among children. There were also 1.5 million TB deaths (1.1 million among HIV-negative people and 0.4 million among HIV-positive people), of which approximately 890 000 were men, 480 000 were women and 140 000 were children. The number of TB deaths is unacceptably high: with a timely diagnosis and correct treatment, almost all people with TB can be cured.

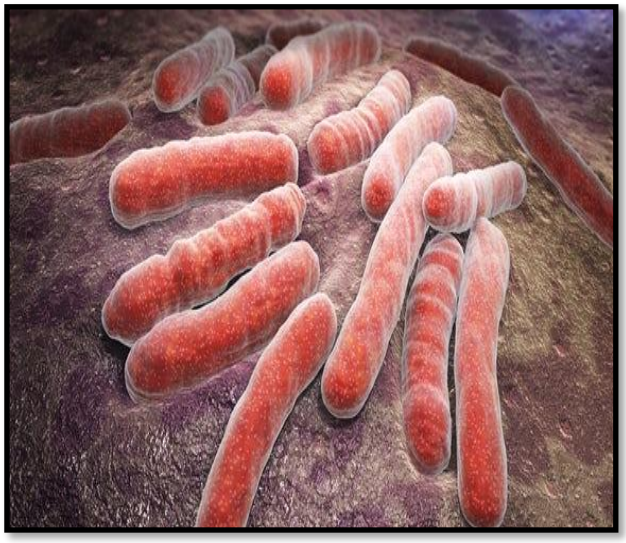

Figure 1.1: Scanning electron micrograph image of *Mycobacterium tuberculosis* (Mycobacterium Tuberculosis stock photos and images)

It is predicted that around one-third of the world's population is infected with *tuberculosis bacillus*, and every year eight million people suffer with tuberculosis disease, which yearly kills 1.8 million worldwide (Vitoria et al., 2009). Moreover, around 80% of TB cases are initiate in 23 countries; the major occurrence rates are found in Africa and South-East Asia (Raviglione and Pio, 2002). India and China only account for an expected 54% of TB cases worldwide (WHO 2015). Estimated incidence rates are shown in **Figure 1.2**. TB and human immunodeficiency virus/acquired immunodeficiency syndrome (HIV/AIDS) accelerate each other's evolution and prolong synergistic proportions of sickness and mortality. Worldwide, HIV is the robust risk issue for the expansion of TB disease, and TB is the foremost opportunistic infection and AIDS-defining disorder among people living with HIV (Stirling et al., 2008). The TB disorder has get worse over the previous two years in Africa owing to the widespread HIV/AIDS, and in Eastern Europe in association with multidrug resistance, following deterioration of the health infrastructure. TB in humans is caused mainly by *Mycobacterium tuberculosis*, but also by *M.*

africanum and *M. bovis*. In addition, these species together with *M. canettii*, *M. microti*, and additional animal-adapted *M. bovis* ecotypes make up the *M. tuberculosis* complex. Furthermore, the percentage of TB cases coinfected with HIV was highly prevalent in countries in the WHO African Region, and overdid 50% in parts of southern Africa, as shown in **Figure 1.3**.

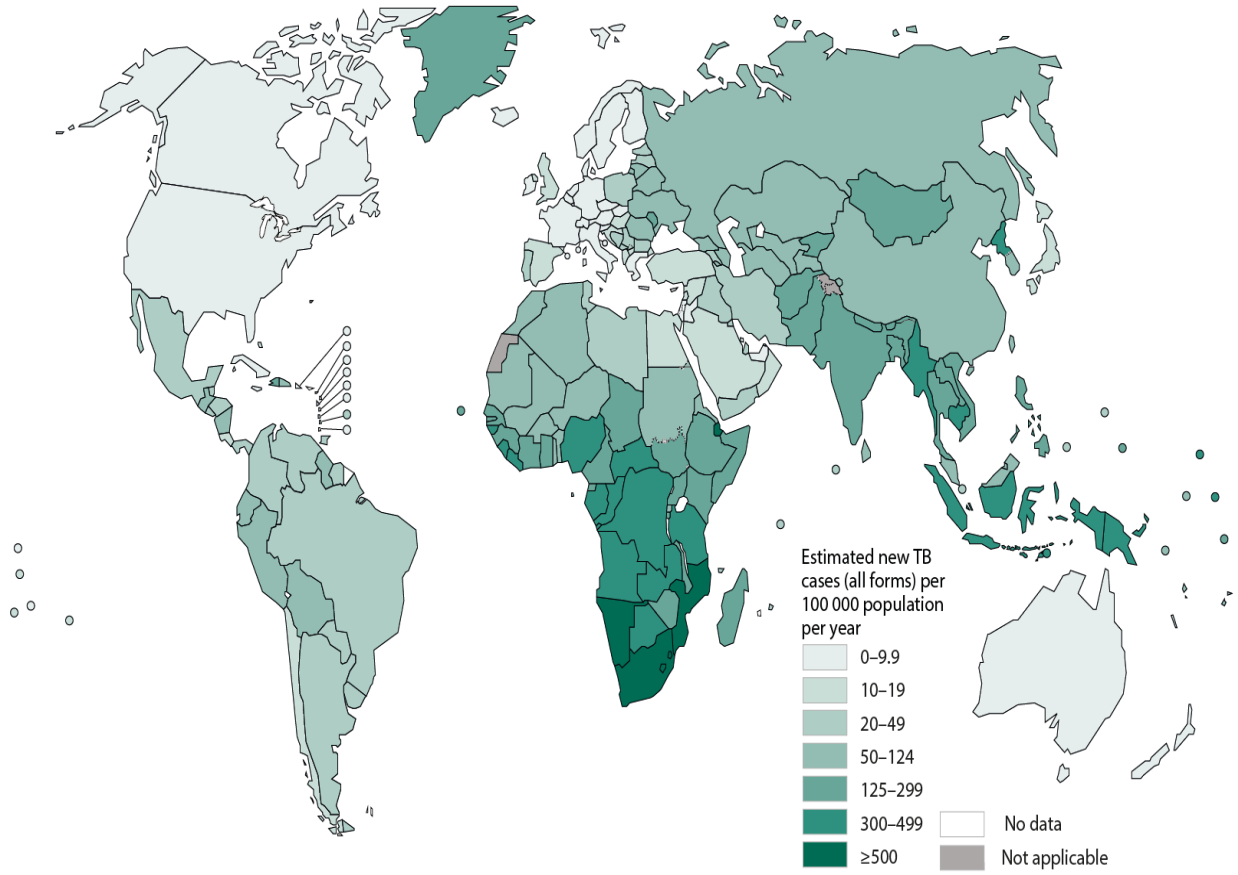

Figure 1.2: Estimated TB incidence rates, 2014 (WHO 2015)

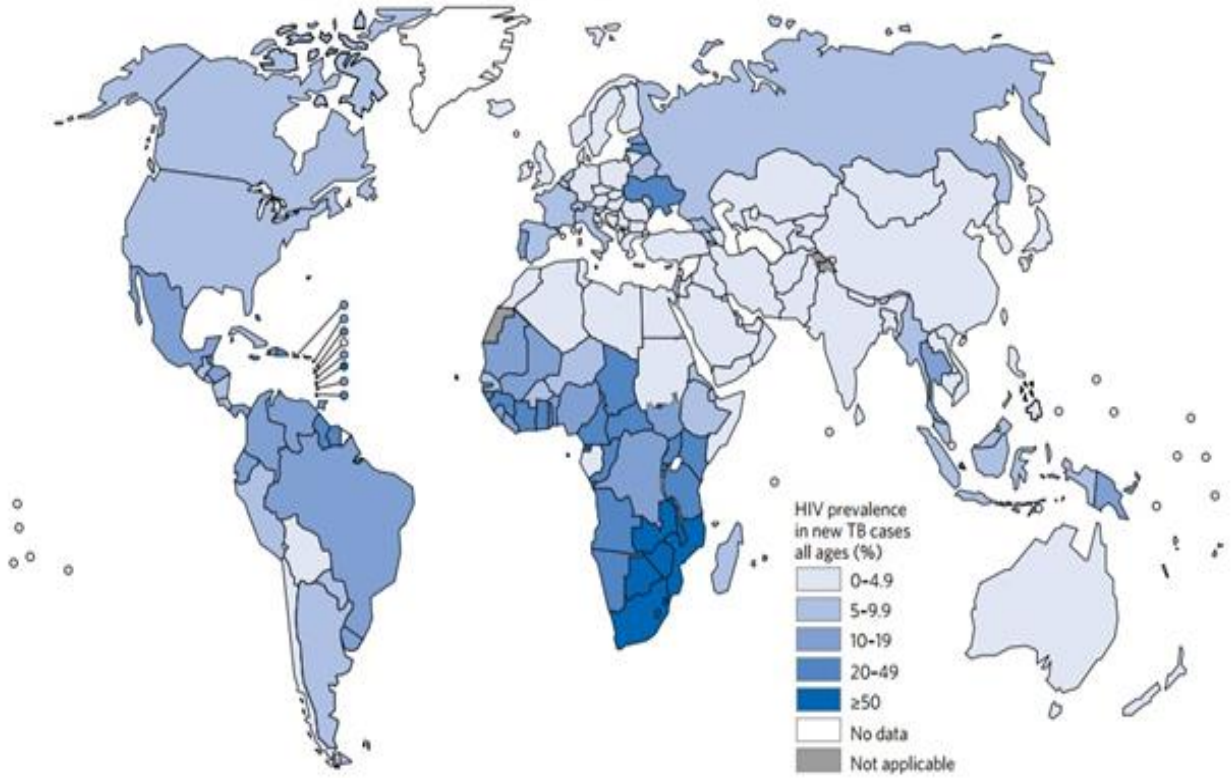

Figure 1.3: Estimated HIV incidence in new and relapse TB cases, 2015

TB usually affects the lungs, but can also affect other parts of the body. TB is generally classified into two types: (i) latent TB (ii) active TB. An analysis of latent tuberculosis (LTB), also named as latent tuberculosis infection (LTBI) means a patient is infected with *mycobacterium tuberculosis*, but the patient does not have active tuberculosis. In addition, active tuberculosis can be contagious while latent tuberculosis is not, and it is not promising to get TB from somebody with latent tuberculosis. The highest risk is that nearly 10 % of these patients (5% in the first two years after infection and 0.1% per year thereafter) will go on to advanced active tuberculosis (Resnikoff et al., 2004). This is mainly precise, and there is extra

risk, in specific circumstances such as medication that destroys the immune system. Furthermore, the identification and action of people with latent TB is a significant fragment of monitoring this disease. Many action procedures are in use to treat latent tuberculosis, which normally need to be taken for several months. If the people have active TB, the microorganisms are making ill and might be passing TB on to other people. Hence, active TB can be very dangerous to our health, but it can also be cured with a course of medication. In active TB, TB bacteria overcome the defenses of the immune system and activate to multiply, causing the progress from latent TB infection to TB disease (Floyd et al., 2002). Some people develop TB disease soon after infection, while others develop TB disease later when their immune system becomes weak. The major difference between latent TB and active TB are shown in **Table 1.1**. Utmost contagions are asymptomatic or non-progressive. The maximum collective site of infection is the lung (pulmonary TB), where TB infection naturally causes an irregular pulmonary penetrate, which undergoes caseation, cavity formation and fibrosis if it evolves.

Table 1.1: Comparison between latent TB and active TB

Latent TB	Active TB
TB germs are inactive (asleep) in our body. This stage can last for a very long time - even years.	TB germs are reproducing and distributed in our body, initiating tissue damage
We don't look or feel sick. Your chest x-ray generally is normal and it can only be identified through a blood test or TB skin test.	We frequently feel sick. Typical symptoms include: cough lasting >3 weeks, weight loss, night sweats, and fever. A chest x-ray and other tests are required to diagnose TB disease.
We can't spread TB to other people.	If the TB germs are in your lungs or voice box, We may spread TB to other people by coughing, sneezing, talking, or singing.
Commonly treated by taking one medicine for 9 months.	Treated by taking three or four medicines for at least 6 months.

Moreover, the aetiology of TB thus makes it very difficult to determine in a specific case what precisely produced 'tuberculosis'. Without the bacillus, there can be no disease, but at a time when exactly everyone had been infected, the situations which caused the immune system to fail can also be said to have brought on 'tuberculosis'. The problem is compounded by the fact that adverse environmental conditions during childhood may not manifest themselves in clinical diseases until young adulthood. The process of infection, activation and reinfection is still imperfectly understood. This complex aetiology renders epidemiological studies of the disease highly problematic.

1.3 TB in South Africa

South Africa takes the third uppermost burden of TB disease in the world, after India and China, with an expected rate of 450 000 cases of active TB in 2013, an increase of 400 % over the last 15 years (Zumla et al., 2015). Moreover, an estimated 60-73 % of the 450 000 cases have both HIV and TB infection. The occurrence of multidrug-resistant (MDR) and extensively drug-resistant TB are increasing, and South Africa has the second highest number of reported multi-drug-resistant TB (MDR-TB) cases globally (Baier et al., 2014). TB remains the leading cause of death in South Africa, contributing to 12% of deaths in 2009 (Stats, 2014). Epidemiological burden details of TB in South Africa is shown in **Table 1.2**.

Table 1.2: Epidemiological burden of TB in South Africa

Items	Statistical data
Population	52 776
TB Mortality	25
HIV+ TB mortality	64
TB Prevalence	380
TB incidence	450
HIV+ incident TB cases	270
MDR-TB cases	69

Figure 1.4 shows the rate of TB bacterial infections (2013) in SA by region. KwaZulu-Natal (KZN), Eastern Cape (EC) and Western Cape (WC) are the three provinces with the highest incidence of TB with 922; 782 and 730 cases per 100,000 populations respectively, whereas Mpumalanga (MP) at 467 cases per 100,000; Gauteng (GP) at 388/100,000 and Limpopo (LP) 354/100,000 are the three lowest ranking provinces in terms of TB incidences.

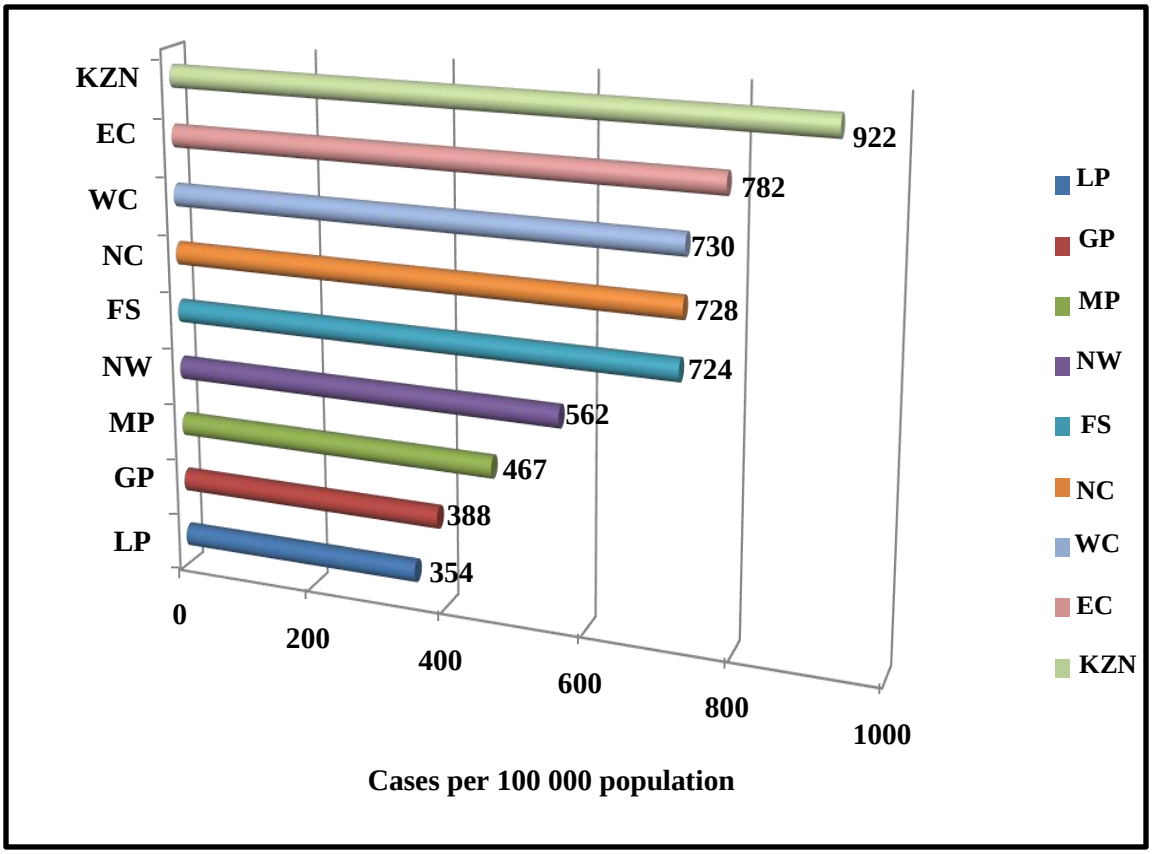

Source: District Health Barometer 2013/14

Figure 1.4: Incidence of TB in South Africa by province (2013)

Smear-positive TB patients are responsible for the transmission of TB and are then the focus of the National TB Control Programme. In addition, the South African rate of new pulmonary smear-positive TB was 234.2 per 100 000 in 2012, and different from a high of 364.9 per 100 000 in the Northern Cape to a low of 120.5 per 100 000 in Limpopo Province (Zumla et al., 2015). With the exception of 10 districts (Amathole, Chris Hani, Cacadu and Joe Gqabi (EC), Harry Gwala, uMgungundlovu and uMkhanyakude (KZN), Frances Baard, Namakwa and Pixley ka Seme (NC), Central Karoo and Eden (WC), and Ekurhuleni (GP)), the incidence of new pulmonary smear-positive TB decreased in the last five years (2009-2013) (Tzeng et al., 2014). **Figure1.5** below demonstrates the incidence of new smear positive TB patients by province.

In addition, the increasing cure rate for new pulmonary smear-positive TB, which was 75.8% in 2012, is inspiring. But, the poor performance of three boonies is responsible for South Africa falling short of the South African National TB Control Programme target of 80 % and the WHO target of 85 %. The Eastern Cape, Northern Cape, and North West provinces reported cure rates of less than 70 %, and of particularly concern are the 3 worst performing districts (Buffalo City (EC), John Taolo Gaetsewe (NC), and Dr Kenneth Kaunda (NW). Dr Kenneth Kaunda is an NHI pilot district yet the cure rate plummeted from 69.9% in 2011 to 59.4% in 2012 (HST, 2014a). **Figure 1.6** shows the new smear positive TB cure rates by province.

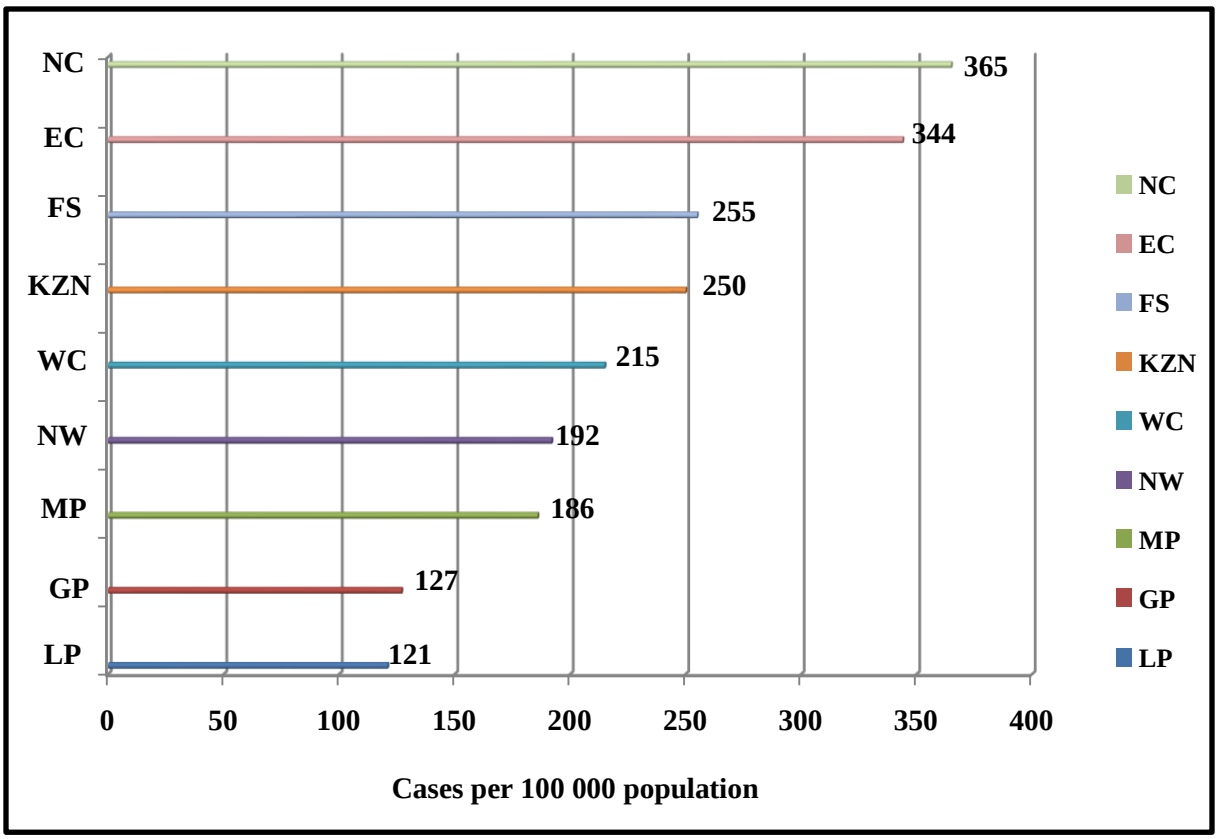

Source: District Health Barometer 2013/14

Figure 1.5: Incidence of new pulmonary smear positive TB in South Africa by province (2013)

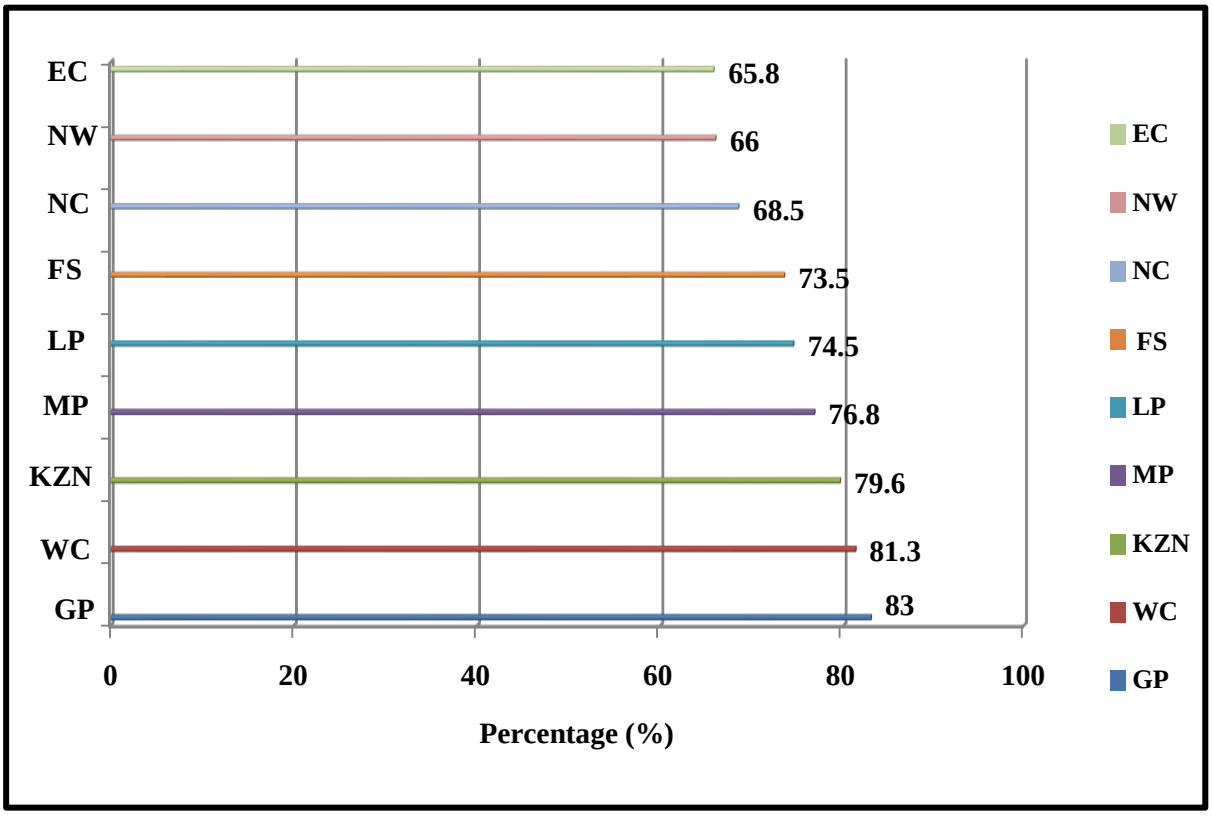

Source: District Health Barometer 2013/14

Figure 1 6: New pulmonary smear positive TB cure rate by province (2012)

1.4 Treatment for TB

Many anti-TB drugs act against various populations of bacilli. Bacilli may occur extra-cellularly or intra-cellularly. The pH in the intercellular places is usually neutral or alkaline, although it is acid intra-cellularly. In addition, most of the TB drugs act utmost in an acid environment; others enhanced in a more alkaline pH. Additionally, there are more than twenty drugs existing for TB treatment. They are used in different mixtures in various conditions.

Hence, most of the TB drugs are simply used for the action of new patients when there is no submission of any drug resistance. In many manners, some of the others are only used for the treatment of drug resistant TB. Currently, new TB drugs such as bedaquiline and delamanid are accessible for the treatment of MDR-TB while the drugs are not available. Generally, the TB drugs are classified into two types: first line anti-TB drugs and second line anti-TB drugs. First line anti-TB drugs have utmost bacterial action when used for the TB treatment. In addition, the amount of drug necessary for a TB patient to take depends on the patient's body weight. The chemical structures and dosages are shown in **Table 1.3**. Additionally, almost 90 % of people with drug susceptible TB (that is TB which is not drug resistant) can be cured in six months using a combination of "first line" TB drugs.

Drugs	Structures	Children/Adult	Dosages		
			Daily	**1×/Week**	**2×/Week**
Isoniazid	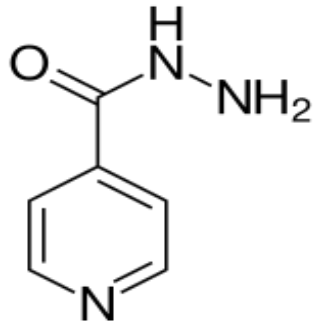	Adult (maximum)	5 mg/kg (300 mg)	15 mg/kg (900 mg)	15 mg/kg (900 mg)
		Children (maximum)	10-15 mg/kg (300 mg)	—	20-30 mg/kg (900 mg)
Pyrazinamide	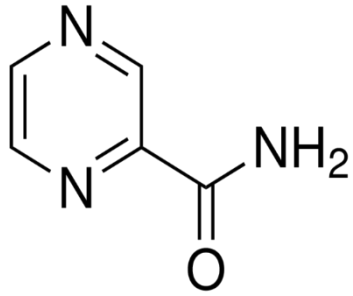	Adult	15-30 mg/kg (2.0 g)	—	50 mg/kg (4 g)
		Children (maximum)	15-30 mg/kg (2.0 g)	—	50 mg/kg (4 g)
Rifampicin	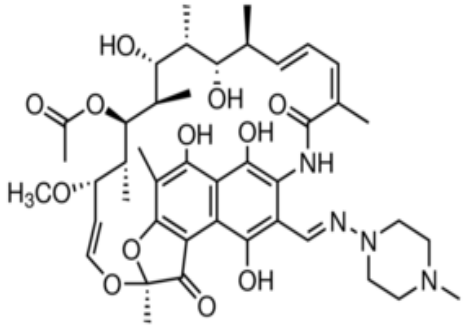	Adult	10 mg/kg (60 mg)	—	10 mg/kg (600 mg)
		Children (maximum)	10–20 mg/kg (600 mg)	—	10–20 mg/kg (600 mg)

Ethambutol	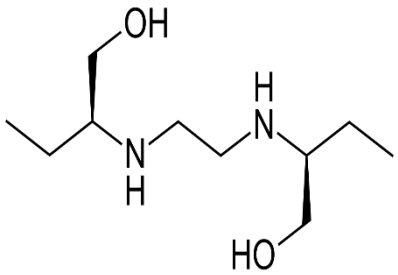	Adult (maximum)	Suggested ethambutol dosages are shown in Table 5		
		Children (maximum)	15–20mg/kg daily (1.0 g)	—	50 mg/kg (4 g)
Streptomycin	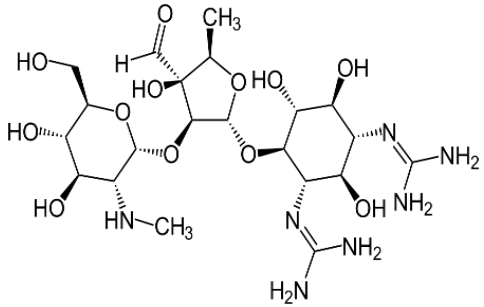	Adult (maximum)	D	D	D
		Children (maximum)	20–40 mg/kg/daily (1 g)	—	20 mg/kg
Amikacin	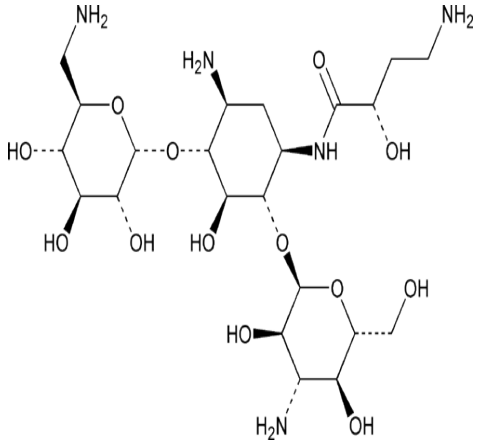	Adult (maximum)	D	D	D
		Children (maximum)	15–30 mg/kg/daily (1 g) intravenous or intramuscular as a single daily dose	—	15–30 mg/kg

kanamycin	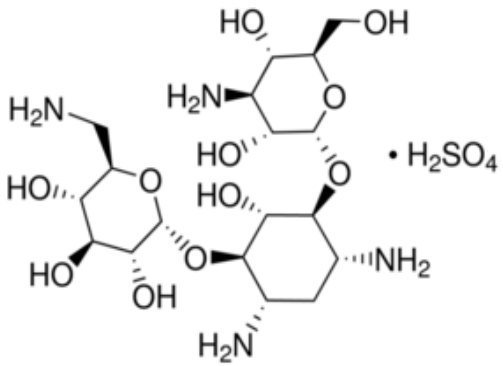	Adult (maximum)	D	D	D
		Children (maximum)	15–30 mg/kg/daily (1 g) intravenous or intramuscular as a single daily dose	—	15–30 mg/kg
Capreomycin	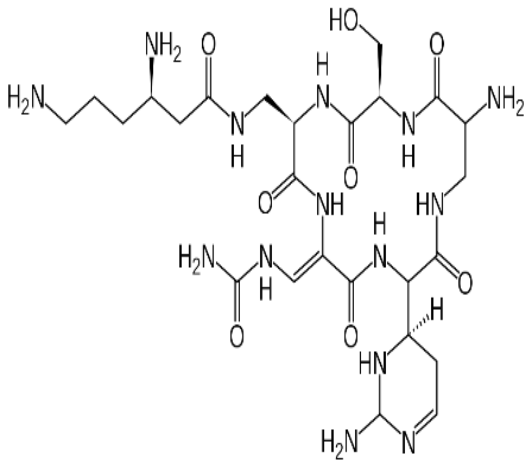	Adult (maximum)	D	D	D
		Children (maximum)	15–30 mg/kg/daily (1 g) as a single daily dose	—	15–30 mg/kg

p-Amino salicylic acid (PAS)	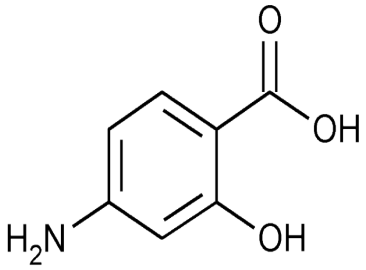	Adult	8–12 g/d in two or three doses	There are no data to support intermittent administration	There are no data to support intermittent administration
		Children	200–300 mg/kg/d in two four divided doses	There are no data to support intermittent administration	There are no data to support intermittent administration
Levofloxacin	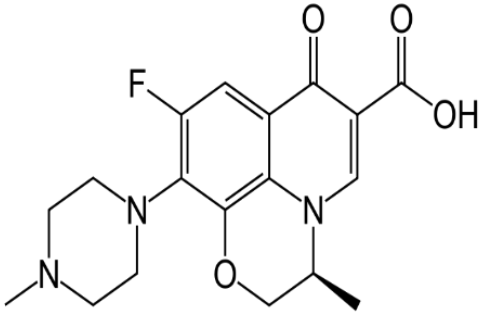	Adult	500–1,000 mg daily	There are no data to support intermittent administration	There are no data to support intermittent administration
		Children	C	C	C
Moxifloxacin	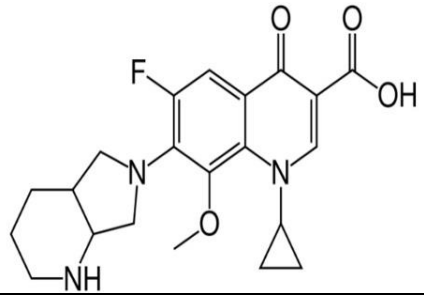	Adult	400 mg daily	There are no data to support intermittent administration	There are no data to support intermittent administration

		Children	A	A	A
Gatifloxacin	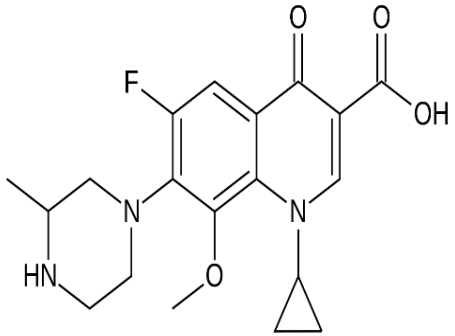	Adult	400 mg daily	There are no data to support intermittent administration	There are no data to support intermittent administration
		Children	B	B	B

Table 1.3: Doses[E] of antituberculosis drugs for adults and children[F]

A The long-term (more than several weeks) use of moxifloxacin in children and adolescents has not been approved because of concerns about effects on bone and cartilage growth. The optimal dose is not known

B The long-term (more than several weeks) use of gatifloxacin in children and adolescents has not been approved because of concerns about effects on bone and cartilage growth. The optimal dose is not known.

C The long-term (more than several weeks) use of levofloxacin in children and adolescents has not be approved because of concerns about effects on bone and cartilage growth. However, most experts agree that the drug should be considered for children with tuberculosis caused by organisms resistant to both INH and RIF. The optimal dose is not known.

[D] Dose: 15 mg/kg per day (1 g), and 10 mg/kg in persons more than 50 years of age (750 mg). Usual dose: 750–1,000 mg administered intramuscularly or intravenously, given as a single dose 5–7 days/week and reduced to two or three times per week after the first 2–4 months or after culture conversion, depending on the efficacy of the other drugs in the regimen.

[E] Dose per weight is based on ideal body weight. Children weighing more than 40 kg should be dosed as adults.

[F] For purposes of this document adult dosing begins at age 15 years.

Table 1.4: Suggested ethambutol doses, using whole tablets, for adults weighing 40–90 kilograms

	Weight (kg)*		
	40–55	56–75	76–90
Daily, mg (mg/kg)	1.000 (18.2-25.0)	1.500 (20.0-26.8)	2.000† (22.2-26.3)
Thrice weekly, mg (mg/kg)	1.500 (27.3-37.5)	2.500 (33.3-44.6)	3.000† (33.3-39.5)
Twice weekly, mg (mg/kg)	2.000 (36.4-50.0)	3.000 (40.0-53.6)	4.000† (44.4-52.6)

* Based on estimated lean body weight. † Maximum dose regardless of weight.

1.5 Aim

The aim of this study was to develop novel biosensors with potential applications for the sensitive detection of first line anti-TB drugs, isoniazid, pyrazinamide, rifampicin, ethambutol and streptomycin in various pharmaceutical samples using biosensor based electrochemical techniques and integration of its inclusion in next generation bio sensing platforms. The objectives of this study are outlined.

1.6 Objectives

a) Synthesis and characterization of titanium oxide, copper oxide, iron oxide and zinc oxide nanomaterials.
b) Fabrication of glassy carbon electrode with potent electrode modifiers whose applicability as electro catalysis agent towards anti-TB drugs investigation.
c) Optimization of cyclic and differential pulse voltammetric experimental conditions i.e. scan rates, deposition time, pH and pulse amplitude.
d) The performance of the developed electrochemical methods was examined using real pharmaceutical samples.
e) Validation studies including: accuracy, sensitivity, selectivity and precision for the developed methods were tested by running standards and their quantification.
f) The usage of new generation materials like graphene oxide and multiwalled carbon nanotubes with enzyme immobilization on glassy carbon electrode gives a new dimension to electrochemical investigation and development of biosensors for first line anti-TB drugs.

1.7 Electrochemical and biosensors techniques

The literature review shown that only spectrometric methods and few electrochemical methods are available for the first line anti TB drugs, with no described enzyme immobilized biosensors work for first line anti TB drugs. Moreover, in this regard our laboratory (Chokkareddy et al., 2017) recently reported an enzyme immobilized biosensor for the detection of isoniazid (INZ) in various pharmaceutical samples. This biosensor showed good limit of detection and limit of quantification values, viz., 0.0335 μM and 0.1118 μM, respectively. In addition, a unique cytochrome c immobilized glassy carbon electrode was constructed for the determination of pyrazinamide (PZM) in different pharmaceutical samples. From the measured DPV results, the limit of detection and limit of quantification of the developed sensor were calculated, and found to be 0.0038 μM and 0.0129 μM respectively. Rifampicin was determined by the coenzyme q immobilized biosensor and the studied linearity range (2-20 μM) showed a limit of detection of 0.032 μM, 0.413 μM and limit of quantification of 1.069 μM, 1.258 μM for anodic peaks I and peaks II respectively. A novel horseradish peroxidase fabricated nanocomposite electrochemical biosensor was described for the detection of ethambutol (ETB) in various pharmaceutical samples. Under the optimized conditions, the DPV technique gave good limit of detection and limit of quantification values of 0.0214 μM and 0.6713 μM respectively. A facile cytochrome c modified nanocomposite electrochemical biosensor was developed for the determination of streptomycin (STN) in various pharmaceutical samples. The developed biosensor showed good limit of detection and limit of quantification values i.e. 0.0028 μM and 0.5628 μM respectively. Finally, to construct the several biosensors with many nanomaterials and biomolecules such as graphene oxide, multiwall carbon nanotubes, metal oxide nanoparticles, horseradish peroxidase, cytochrome c and coenzyme q were used.

1.7.1 Nanomaterials

Nanoscience has the significant potential to develop a sensor, especially electrochemical biosensors for food quality. The selectivity, sensitivity and limit of detection ranges are dynamic parameters for the development of electrochemical biosensors. Therefore, the selectivity, sensitivity of the sensor method essentially depend on the active surface area of the electrode, and the area of the electrode which interacts with the analytes. Through increasing the surface area of the electrode, many nanomaterials such as graphene oxide, carbon nanotubes, fullerenes and metal oxide nanoparticles. These nanoparticles have been introduced to the field of electrochemical sensors ad these nanoparticles have gained extensive recognition. In current years, a widespread variety of nanoparticles with various properties were useful to the fabrication of electrochemical biosensors (Unruh et al., 1996). Nanoparticles show unique physical, chemical and electronic properties that are different from those of bulk materials. This is partially connected with the fact that surface to volume ratio deviations occur with a change in particle size. A high percentage of surface atoms are present in many size-dependent phenomena. High surface area is a significant feature of nanosized and nanoporous materials, which can be exploited in numerous potential industrial applications, such as separation science and catalytic processing, due to enhanced chemical reactivity (Chikama et al., 2008). Nanoparticles can provide larger surface-to-volume ratios due to their small size which have at least one dimension 100 nm or less, which increases the performance of the electrochemical biosensors. Hence the nanomaterials can be nanoscale in one dimension (e.g. surface films), two dimensions (e.g. strands or fibres), or three dimensions (e.g. particles).

They can exist in fused, single, aggregated or agglomerated forms with tubular, spherical, and irregular shapes. According to Siegel (Chikama et al., 2008), nanostructured materials are classified as zero dimensional (0D), one dimensional (1D), two dimensional (2D) and three dimensional (3D) nanostructures **(Figure1.7)**.

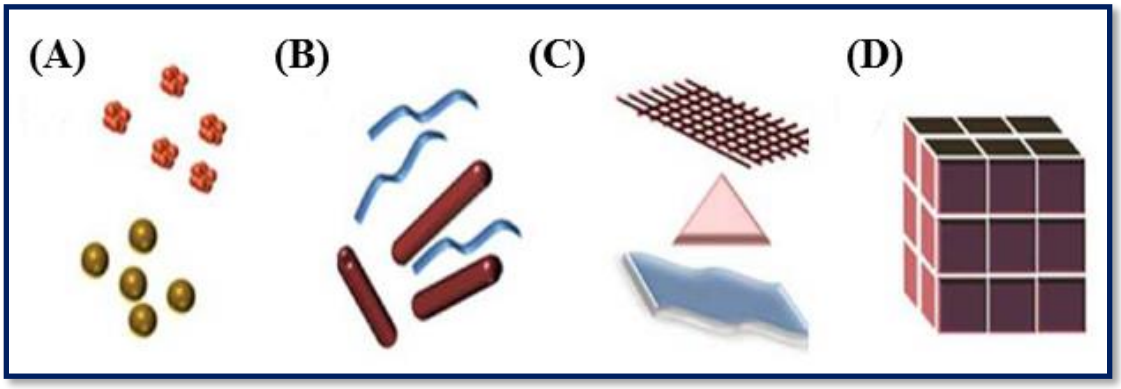

Figure 1.7: Classification of Nanomaterials (A) Zero D spheres and clusters, (B) 1D nanofibers, wires, and rods, (C) 2D films, plates, and networks, (D) 3D nanomaterials

Many kinds of nanoparticles are used in the modification of biosensors as well as metal nanoparticles (Ag, Cu, Au, Pd, Pt and Ru), metal oxide nanoparticles (ZnO, TiO_2, CeO_2 and Al_2O_3), semiconductor nanoparticles and even combined nanoparticles. Furthermost recent studies exhibited that biosensors composed of nanoparticles generated simple and accurate measurements, which offer exciting novel chances for the improvement of biosensors. Therefore, in this work metal oxide nanoparticles (TiO_2, CuO, Fe_3O_4 and ZnO) were used to fabricate the electrodes.

1.7.2 Metallic nanoparticles (MNPs) (Ag/Cu NPs)

Metallic nanoparticles have fascinated scientists for a long period and are now heavily used in the filed of medical, chemical, engineering and biomedical sciences. It is synthesized in two methods i.e. chemical and physical methods (Burda et al., 2005). Moreover, MNPs are prepared directly from the parent metals, metal salts are used as initial materials monitored by the reduction steps which in the case of chemical methods (Murphy et al., 2008, Dreaden et al., 2012). The utmost significant aspect of these NPs are for the stabilization and to avoid aggregation. Furthermore, the NPs in various cases ligands conjugated with thiol (-SH) and amine ($-NH_2$) functional groups were used to co-ordinate the NPs strongly to avoid the formation of bulk NPs (Love et al., 2005). Silver nanoparticels (AgNps) were used to deteemined the pencillin (Sistani et al., 2014), nitrocompounds (de Lima et al., 2014), quercetin (Yola et al., 2014) and caffeic acid (Golabi and Zare, 1999). The copper nanoparticle in the modification of sensors to determine the D-amino acid (Lata et al., 2013), neotame (Bathinapatla et al., 2015), glucose (Razmi and Mohammad-Rezaei, 2013) pyrazinamide (Rajasekhar et al., 2017) and glycerol (Arévalo et al., 2017).

1.7.3 Metal oxide nanoparticles (TiO_2, Fe_3O_4 and ZnO NPs)

Metal oxide nanoparticles have huge research importance in current years, due to their significant properties i.e. high catalytic activity and large surface area. TiO_2, Fe_3O_4 and ZnO NPs are semiconductors with a band gap energy of 3.0 eV, 3.33 eV and 3.36 eV at room temperature. Metal oxide nanoparticles morphology and size was based on the content of the precursors used in the preparation of the nanoparticles (Park and Blackstone, 2010). Initial use of TiO_2 NPs for

sensor applications was pioneered, Gnanasekaran et al., described a preparation and characterization of TiO_2 quantum dots for photocatalytic application (Gnanasekaran et al., 2015).

In this work TiO_2 NPs were synthesized from titanium tetra chloride, 25 mL of $TiCl_4$ was made up to a 100 mL with deionized water in a volumetric flask, and then placed in an ice cold bath. Likewise, 13 g of urea was dissolved in another 250 mL volumetric flask with deionized water. The urea solution was then slowly added to the contents of $TiCl_4$, and then subjected to heating at 110 °C on a hot plate, with a magnetic stirrer for about 30 min. After the completion of the reaction, a white colloidal solution was obtained. The colloidal solution was then centrifuged at 1000 revolutions per minute for 15 min. After centrifugation of the product, the residue was washed repeatedly with deionized water, and then dried at 60 °C for 3-4 h. The newly formed TiO_2NPs were then stored in the refrigerator at 4 °C, for further use.

Iron oxide nanoparticles are widespread in nature and it is present in the lithosphere and hydrosphere (as pollutants) in the atmosphere. Many methods have been used to synthesize iron oxide nanoparticles and include coprecipitation, polyol method, sonolyis and flow-injection methods (Fievet et al., 1989). ZnO NPs have significant properties such as larger surface area and higher catalytic activities. The size and morphology of ZnO NPs depends on the content of the precursors used in the synthesis of these NPs. Furthermore, ZnO NPs have many sensor applications, Srinivas Rao et al., reported a synthesis and characterization of the ZnO NPs. In this study ZnO NPs were synthesized from $ZnCl_2$, 8.17 g of $ZnCl_2$ (0.4 M) was dissolved in 150 ml ethanol. This solution was kept under constant stirring using the magnetic stirrer to completely dissolve the zinc chloride for 45 min. In another vessel 4.48 g (0.8 M) of KOH was dissolved in 100 ml of ethanol and it gave an aqueous ethanol solution of KOH. The complete

dissolution of $ZnCl_2$ was taken into a beaker and the 0.8 M KOH solution was added dropwise under constant magnetic stirring for 2 h. The beaker was sealed and the solutions were then allowed to settle for overnight. The solution was then separated carefully and centrifuged for 5 min, and thereafter the precipitate was removed. Furthermore, the precipitated ZnO nanoparticles were washed with deionized water several times and dried at 50 °C in an oven. Due to the drying the $Zn(OH)_2$ is completely converted in to ZnO (Rao and Rao, 2015). Balgobind et al., reported a biosensor, based on that ZnO NPs was used for the determination of aspartame in food and beverage samples (Balgobind et al., 2016).

1.7.4 Carbon nanotubes

Carbon nano tubes (CNTs) are discovered in the year 1991, and these incredible structures have unique chemical, fascinating electronic, magenetic and mechanical properties. CNTs are as the name implies hollow tubes that generally have a diameter in nano range and length in μm range made out of carbon (Monthioux and Flahaut, 2007). Moreover, CNTs show good metallic, semi conducting and have largest elastic modules with a hollow core (Ajayan and Zhou, 2001). The primary methdod to produce CNTs was with an arc discharge process but today many techniques to produce CNTs exist with varying physical properties as a result. Nowadays CNTs are prepared by chemical vapor deposition (CVD), and laser evaporation methods. CNTs are classified into two types: singlewalled carbon nanotubes (SWCNTs) and multiwalled carbon nanotubes (MWCNTs). SWCNTs was made by developing of a single graphite sheet into a tube which results in a cylindrical nano structure with a large aspect ratio, and these have up to 1000 GPa in tensile strength (Yu et al., 2000). Graphene layers that create the CNTs can be rolled in

different angles, so called chiral angles, which affect properties such as conductivity. MWCNTs have several graphene sheets with inter layer spacing of 3.4 Å, as shown in **Figure1.8**.

A **B**

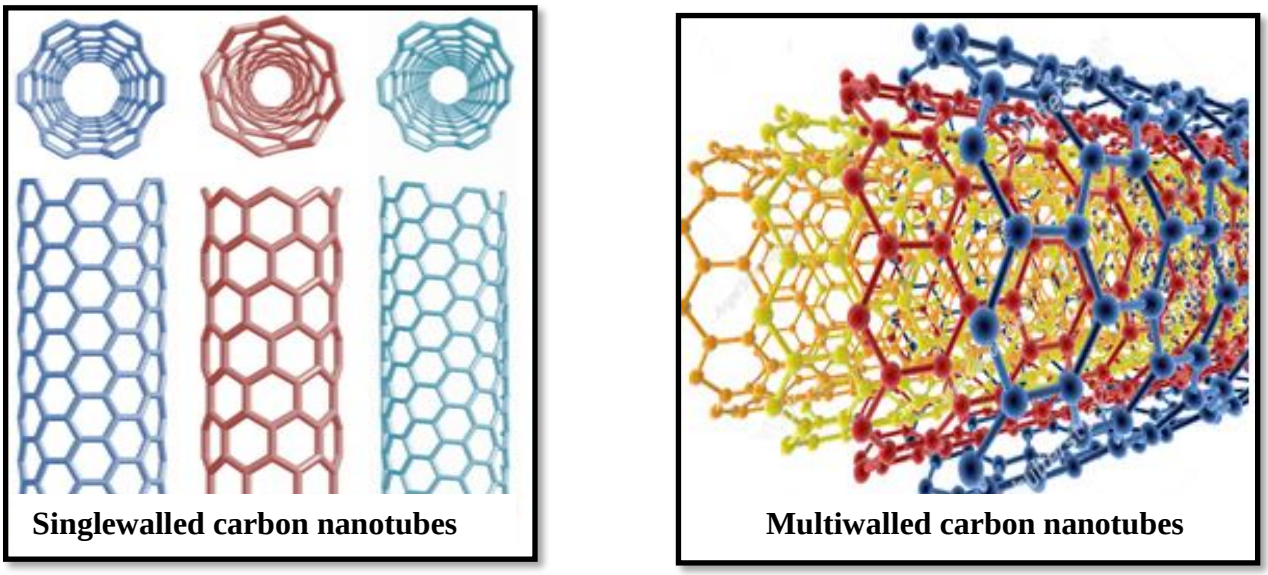

Figure 1.8: Structures of carbon nanotubes

In addition MWCNTs are thought to be conductive and for this reason it is very probable that one of their many layers has been conducting at chiral angles (Pugno, 2006). Due to their unique properties, CNTs are used as nanomaterials in various fields. MWCNTs have a unique physical and chemical properties i.e. large surface area in the 3D arrangements, high electrical conductivity, significant mechanical strength, and possess interesting electrochemical properties which can be used for the preparation of electrochemical sensors (CNTs-ECS). Furthermore, CNTs based electrochamical sensors show good limits of detection, high sensitivty, low over voltage and rapid electrode kinetics. Hence, in this study MWCNTs were used for the

construction of elctrochemical biosensors for the detection of isoniazide (INZ), pyrazinamide (PZM), rifampicin (RIF) and streptomycin (STN).

1.7.5 Graphene oxide (GO)

Graphene was first identified in 2004 by Prof. Novoselov and Prof. Geim in Manchester (UK), to whom the Nobel Prize was then assigned in 2010 for their studies on the structure and properties of graphene. Graphene oxide (GO) is a superior electrode material for biosensors and electrochemical sensors due to its nano scaled dimensions and unique properties, such as high electrical conductivity (550 S cm^{-1}), good electrochemical stability and high surface to volume ratio with theoretical specific surface area of 2630 m^2 g^{-1}, the GO has been the object of several studies for many different applications. GO has both sp^2 - and sp^3 -hybridized carbon atoms in the hexagonal ring-based carbon networks. The generally accepted model, described by Lerf and Klinowski, was a nonstoichiometric structure **(Figure 1.9)** in which the carbon plane is decorated with hydroxyl and epoxy (1,2-ether) functional groups. GO is highly hydrophilic because of the rich oxygen containing groups (hydroxyl, carboxyl, carbonyl and epoxide groups) on basal planes and edges of carbon atoms (Benvidi et al., 2017, Liu et al., 2015). The large surface area and high electrical conductivity of GO usually causes an increase of background currents which become the primary limiting factor for trace analyte detection. GO and metal oxides nanoparticles showed good catalytic properties, which make them suitable for acting as electronic wires to enhance the electron transfer between the analyte and electrode surfaces. Furthermore, it was described that some carbon materials including MWCNTs, SWCNTs and fullerenes which might be isolated in water the aid of GO through π-π interactions (JiaJ, 2014,

Man et al., 2014). Hence, in this work GO was used for the fabrication of electrochemical biosensors for the detection of ETB.

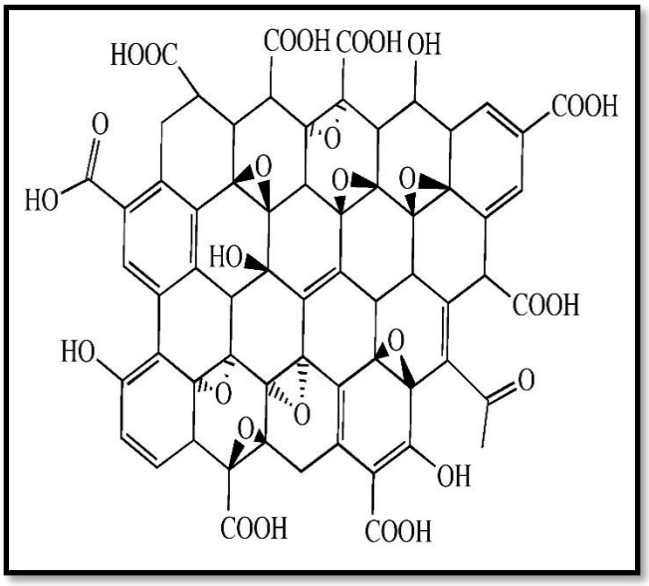

Figure 1.9: Chemical structure of graphene oxide

1.7.6 Horseradish peroxidase (HRP)

Horseradish peroxidase enzyme (HRP) found in horseradish (*Armoracia rusticana*) is a robust perennial herb cultivated in extreme sections of the world mostly for the cooking value of its roots. HRP containes 308 amino acid resdues and the sequence of order was explained by Welinder in 1976 (Veitch, 2004). HRP contains the elementary isoenzyme having a molecular weight of 44 kDa. HRP is a extremely water soluble heme protein, with a solubility of H_2O of not less than 100 µg/mL or more than 10 mg/mL solutions. In addition, HRP contains with other hemes peroxidases which are brightly coloured specially below the near-ultraviolet light regieon (Hu et al., 2008).

This property of heme peroxidases make them suitable for attaching to "transparent" proteins so that they can be seen under various wavelengths. HRP definitely one of the most suitable and significant enzymes used in a wide-ranging variety of bioassays. It is also regularly used for secondary determination of reagents in various biotechnological applications, as well as immunohistochemical analysis (Lee et al., 2008) and enzyme-linked immunosorbent assays (ELISAs) (Bertrand et al., 2004), blot analysis (Prusiner et al., 1990), *in-situ* hybridization (Conte-Perales et al., 2011), immuno sensors (Lee et al., 2008), electrochemical sensors, and DNA biosensors. Furthermore, the reduced form of HRP can be chemically reoxidized by H_2O_2. Generally, direct electron transfer among HRP and an electrode is difficult because the active sites of HRP are extremely buried in a thick protein shell, and because the huge distance between the active sites and the electrode surface will slow down the electron transfer process. Electron transfer via a mediator i.e. metal oxide nanoparticles and nanoparticles, though is more effective for establishing an electrical connection between the redox centers and the electrode. The three dimensional and chemical structures are shown in **Figure 1.10**.

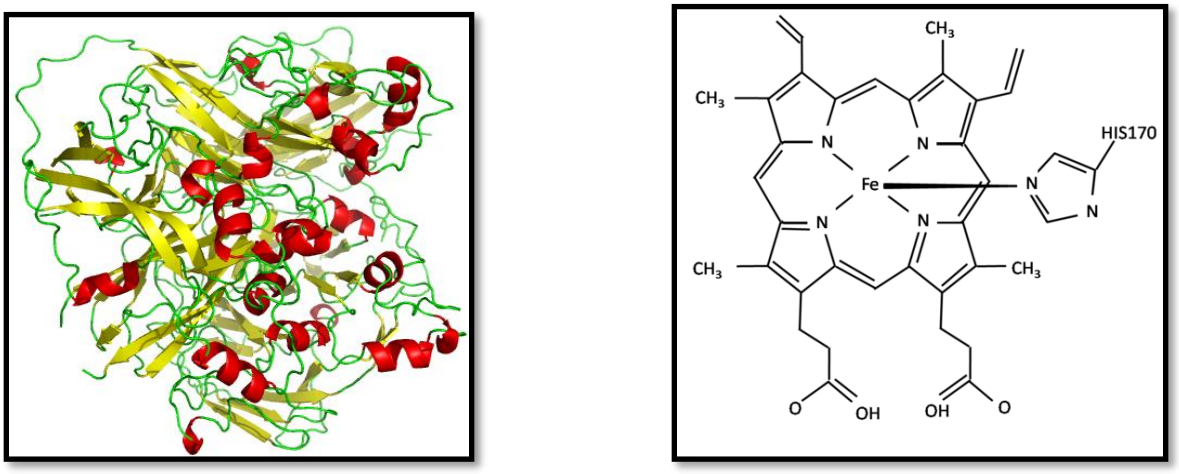

Figure 1.10: Three dimensional and chemical structures of horseradish peroxidase

HRP shows more affinity for coupling with the nanocomposite for electrochemical transduction due to the presence of amino groups in the HRP enzyme. In addition, HRP has good catalyzing properties, as well as a strong oxygenation nature for oxidization of a wide variety of organic substrates (Ahirwal and Mitra, 2009) . Furthermore, HRP immobilized with a nanocomposite results in the formation of a biosensor with high stability and good efficiency. Therefore, HRP was used for the construction of a biosensor based on HRP-TiO_2NPs-MWCNTs modified glassy carbon electrode for detection of isoniazid.

1.7.7 Coenzyme Q

Coenzyme Q (Co en-q) also known as ubiquinone-10, 2,3-dimethoxy-5-methyl- 6-decaprenyl-1, 4-benzoquinone, Co Q_{10}, was first isolated, characterized by Festenstein in 1955 and it was recognized in 1957 by Crane that this multiple functional in mitochondrial respiratory chain. The complex structure of Co en-q was determined by Wolf in 1958 (Festenstein et al., 1955, Wolf et al., 1958). Co en-q is a fat-soluble vitamin with a solubilty of $\geq$ 1mg/mL (solubility $\geq$95%) and dissolution rate. It is readily soluble in organic solvents and lipids but essentially insoluble in water. The structures of Co en-q are shown in **Figure 1.11**.

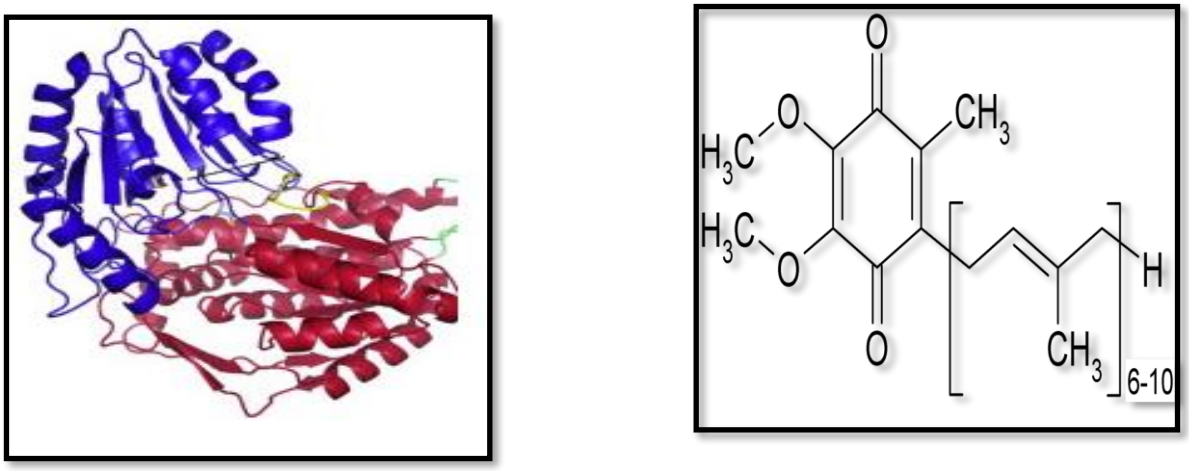

Figure 1.11: Three dimensional and chemical structures of Coenzyme q

Co en-q is a physiologically significant composite with applications as an antioxidant in the treatment of cardiovascular disorders such as hypertension, angina pectoris, and congestive heart failure. In the early period, the idea of Co en-q spreading and synthesis was attributed exclusively to the inner mitochondrial membrane. This appeared to be sensible, then the only known function at this time was transferring electrons from complexes I and II to complex III in the mitochondrial electron transfer system (Mitchell, 1975). In addition, the biological functions of Co en-q serve an important role in energy biosynthesis in the form of ATP, stabilization of mitochondrial enzymatic complexes, free radical detoxification, binding to the permeability conversion pore, and the function of mitochondrial uncoupling proteins. Additionally, the electrochemical properties of Co en-q has attracted attention due to its participation in a variety of antioxidant reactions (Schultz and Chan, 2001). This facilitates the fast transfer of electrons from RIF to the electrode surface and leads to the enrichment of electroactivity of the fabricated sensor. Furthermore, it also generates electrophilic sites which increase the sensitivity and limits

of detection of the fabricated electrode. Hence, Co en-q was used as a biomolecule to construct Co en-q-Fe_3O_4NPs-MWCNTs on the glassy electrode for determination of rifampicin.

1.7.8 Cytochrome c

Cytochrome c (Cyt c) is a low mass, water soluble protien related with the inner membrane of the mitochondrion. Cyt c is a extremely conserved with a molecular weight of approximately 12 kDa protein containing of a single 104 amino acid peptide with a single heme group, which is covalently attached to Cys^{14} and Cys^{17} (Cai et al., 1998). The solubility of Cyt c is approximately 100 g/L. Cyt c is a vital link in the electron transport chain through which cells achieve the controlled "burning" of glucose and capture abundant quantities of that released energy by storage in ATP, the cells main energy distribution molecule (Hüttemann et al., 2011). It transfers one electron among various electron transport complexes fixed in the internal membrane (Dormeshkin et al., 2016). The major role of cytochrome c is to transfer electrons from complex III (QH2-cytochrome c reductase) to complex IV (cytochrome c oxidase) in the respiratory chain and occurs in the mitochondria of vertebrates (Tafani et al., 2002, Zhao et al., 2003). Cyt c enzyme structures are shown in **Figure 1.12**.

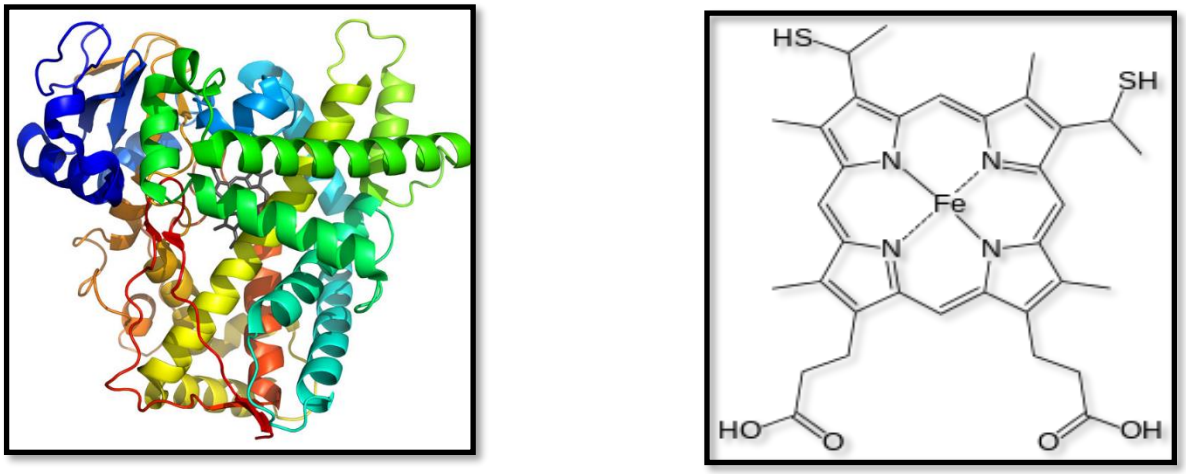

Figure 1.12: Three dimensional and chemical structures of Cytochrome c

The Cyt c reacts with several organic and inorganic radicals (Koppenol and Butler, 1984) and due its unique electron transfer property, it can be used as a potential biomaterial to construct an electrochemical biosensor. It generally carries an electron and is responsible for a redox mechanism in cellbiology as well. Hence, cytochrome c was also used as one of the electrode coating materials in the present investigation to determine the PZM and in order to increase the electrochemical sensing ability of the developed biosensor.

CHAPTER 2

LITERATURE REVIEW

This chapter deals with an in-depth literature review of the anti-tuberculosis (TB) drugs, isoniazid (INZ), pyrazinamide (PZM), rifampicin (RIF), ethambutol (ETB) and streptomycin (STN). The electroanalytical chemistry has played an important role in the different scientific areas and industrially based research, such as the analytical determination of anti TB drugs mechanisms with the background electrolyte.

2.1 Electrochemical detection of isoniazid and mechanism action of isoniazid

Isoniazid is a synthetic derivative of nicotinic acid compound also known as isonicotinylhydrazide and it was first prepared in 1912. The pyridine ring and the hydrazine group are essential components of isoniazid chemical structure **(Figure2.1)**. Isoniazid act as an antibiotic and it has many anti-microbial properties. The anti TB activity of this complex was first described in 1952 during the search for more potent products of nicotinamide. Isoniazid is the one of the most widely used first line anti TB agents, the activation of isoniazid produces oxygen derivative free radicals (hydrogen peroxide, superoxide and peroxynitrite) and organic free radicals that prevent the formation of mycolic acids of the bacterial cell wall, causing DNA damage and successively the death of the bacillus (Timmins and Deretic, 2006, Johnsson et al., 1995). While its mechanism of action is still unclear, isoniazid appears to block the production of mycolic acids, major components of the mycobacterial cell wall (Bernardes-Génisson et al., 2013). This agent is only active against actively developing mycobacteria because, as a pro-drug, it requires activation in subject to the mycobacterial species. The stimulated form of isoniazid is

a covalent complex with an inh-A (Acyl carrier protein) and KasA, a β-ketoacyl carrier protein synthetase (Suarez et al., 2009, Timmins et al., 2004), which easily blocks the mycolic acid synthesis and kills the *mycobacterium tuberculosis* as shown in **Figure 2.2**.

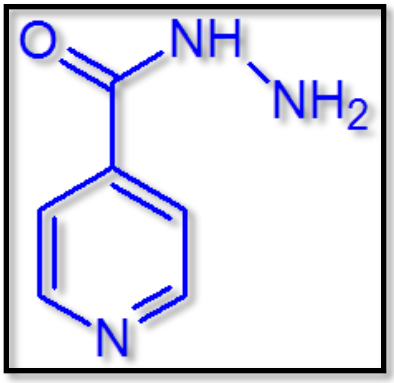

Figure 2.1: Chemical structure of isoniazid

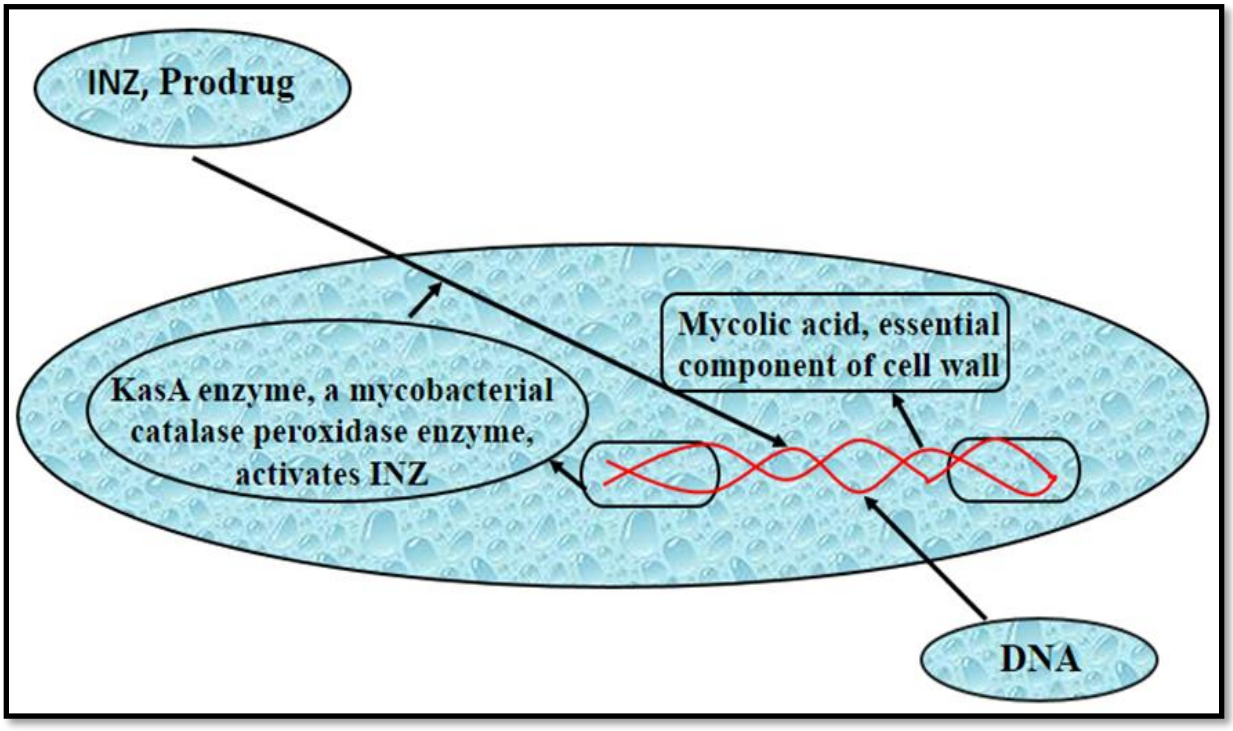

Figure 2.2: Isoniazid prodrug mechanism with DNA

Bergamini et al., 2010 have developed a very sensitive voltammetric method based on screen printed carbon electrode (SCE) modified with poly-L-histidine for the determination of isoniazid in human urine. The limit of detection was found to be 2.5×10^{-7} mol L^{-1} for square wave voltammetry (SWV), 5.0×10^{-7} mol L^{-1} for linear sweep voltammetry (LSV) and 1.7×10^{-7} mol L^{-1} for differential pulse voltammetry (DPV) (Bergamini et al., 2010). Yan et al., 2015 described the use of a glassy carbon electrode fabricated with poly (sulfosalicylic acid) (PSA) and carboxylated graphene (CG) nanocomposite for the simultaneous electrochemical analysis of INZ and uric acid (UA). For the mixture containing isoniazid and UA, the peak potentials were separated from each other. The DPV peak currents at PSA/CG/GCE responded linearly to the INZ concentration from 0.05-15 μM and UA concentration from 0.02-15 μM respectively with the detection limits of 12 nM for both INZ and UA (Yan et al., 2015).

Shahrokhian et al., 2007 studied the electrochemical response of isoniazid by cyclic voltammetry (CV) and differential pulse voltammetry (DPV) at a carbon paste electrode modified by multiwall carbon nanotubes (MWCNTs). In the potential range between 0.0 to 1.30 V (vs. Ag/AgCl), the isoniazid showed a peak at 0.84 V. Under the optimized conditions, the DPV potential ramp of 0.0-1.0 V was applied with the concentration range of 1×10^{-6}-1×10^{-3} M and the detection limit was found to be 5×10^{-7} M (Shahrokhian and Amiri, 2007). A novel efficient electrocatalytic oxidation and selective determination of isoniazid by Fe $(tmphen)_3^{2+}$ exchanged Nafion modified electrode was established by Azad and coworkers. The GC/Nf/Fe $(tmphen)_3^{2+}$ electrode, is very sensitive for isoniazid and it showed well defined oxidation peak, which can be used as electrochemical signal for isoniazid determination. The developed sensor showed a very low detection limit of 13 μM and wide linear range from 50-20,000 μM (Azad

and Ganesan, 2012). The electrochemical behaviour of isoniazid was investigated at a Fe/Al layered double hydroxide fabricated on glassy carbon electrode. Isoniazid showed a poor electrochemical response at the bare GCE; however, a Fe/Al-layered double hydroxide fabricated on a glassy carbon electrode can directly enhance the electrochemical response of isoniazid when applying CV and DPV without any mediator. The DPV current has a linear relationship with the isoniazid concentration in the range of 4.9-650.0 μM, with a correlation coefficient of 0.993. The limit of detection was found to be 4 μM (Asadpour-Zeynali et al., 2016). Zhu et al., 2015 studied the electrocatalytic response of the electrochemically reduced graphene oxide (ERGO) modified glassy carbon electrode towards isoniazid by CV and DPV. Compared with a bare glassy carbon electrode, the peak current had obviously increased, and the peak potentials were shifted. Under the optimum parameters, the DPV peak current is linear to the concentration of isoniazid in the range of 0.09-100 μM, and the limit of detection is 15 nM (Zhu et al., 2015).

Dass et al., 2014 have developed a graphene oxide (GO) and poly-L-arginine (PAG) modified glassy carbon electrode for the voltammetric determination of isoniazid, pyrazinamide and buspirone hydrochloride (BPH) simultaneously. The fabricated electrode showed an effective catalytic reaction to the oxidation of isoniazid, pyrazinamide, and BPH with good stability and reproducibility. The limit of detection values were found to be 2.59, 3.28 and 3.54 μM, for INZ, PYZ and BPH respectively (Devadas et al., 2014). The electrochemical behaviour of isoniazid on Fe/Al-layered double hydroxide (Fe/Al-LDH) modified glassy carbon electrode was studied by Asadpour-Zeynali and coworkers. The Fe/Al-LDH coated electrode showed excellent electrocatalytic reduction activity for isoniazid. The calibration curve is linear in the ranges of 4.9-770 μM and 4.9-650 μM with limit of detections of 7.0 and 4.0 μM for amperometric

techniques, and differential pulse voltammetry, respectively (Asadpour-Zeynali et al., 2015). A novel Au nanoparticle decorated silicate network for the amperometric sensing of isoniazid has been constructed by Jena and coworkers. The Au nanoparticles are chemo absorbed onto the thiol functional groups of the silicate network and their size was enlarged by hydroxylamine seeding. The silicate network was highly sensitive (4.03 ± 0.01 nA/nM) and it linearly responds to the isoniazid up to the concentration of 0.1-1mM and the limit of detection was found to be 0.1 nM (Jena and Raj, 2010).

You et al., 1999 have established a sensitive sensor for the detection of methyl hydrazine, isoniazid and hydrazine by capillary electrophoresis with a 4-pyridyl hydroquinone self-assembled micro disk platinum electrode. The reaction for methyl hydrazine, isoniazid and hydrazine are linear over 3 orders, detected concentration and magnitude of 0.2-400 mM, 0.5 mM-2 mM, and 0.2-400 mM with correlation coefficients of 0.9991, 0.9982, and 0.9998, respectively. The modified electrode shows highly stable catalytic capability for the analytes which can be detected even at 0.0 V in capillary electrophoresis (CE)/electrochemical detection (EC) (You et al., 1999). Xia et al., 2005 have reported a gold electrode for the electrochemical determination of isoniazid by using cyclic and differential pulse voltammetry. An irreversible anodic peak appeared at 20.3V vs SCE of isoniazid in 0.5 M NaOH (Yun Xia and Ya Hu, 2005). The electrochemical performance and detection of isoniazid at carbon ionic liquid electrode fabricated with palladium nanoparticles was carried out by Absalan and coworkers. Electrocatalytic oxidation of isoniazid at this electrode was studied in phosphate buffer solution using cyclic voltammetry. The linear relationship between anodic peak current and isoniazid concentration in the ranges of 5.0×10^{-6} to 1.0×10^{-6} mol L^{-1} isoniazid with a detection limit of

4.7×10^{-6} mol L^{-1}. The fabricated electrode revealed good properties like enhanced sensitivity, stability and reproducibility (Absalan et al., 2016).

A novel voltammetric technique was established for the detection of isoniazid using nafion ordered mesoporous carbon modified electrode by Yan and coworkers. Under the optimized experimental conditions, the peak current was linear to the concentration of isoniazid 1.0×10^{-6} M to 3.7×10^{-4} M at + 0.20 V vs. Ag/AgCl. The fabricated sensor has shown good sensitivity 0.031 µM and the limit of detection 8.4×10^{-8} M (Yan et al., 2011). Cheemalapati et al., 2013 have reported an electrochemically reduced graphene oxide (ERGO) fabricated on glassy carbon electrode for the voltammetric sensing of isoniazid. The ERGO modified GCE has greater electrocatalytic activity towards isoniazid than GO and bare GCE. The linear range for isoniazid has been found to be 2 µM to 70 µM with a limit of detection of 0.17 µM and the sensitivity of the proposed sensor towards isoniazid was found as 3.987 µA $\mu M^{-1} cm^{-2}$ (Cheemalapati et al., 2013). Chen et al., 2012 developed functionalized multiwalled carbon nanotubes (f-MWCNTs) fabricated on glassy carbon electrode for the amperometric determination of isoniazid. The f-MWCNTs film fabricated GCE showed good peak current for isoniazid among the various carbon nanomaterials, which is approximately 7.11 times greater than that obtained with only MWCNTs film (Chen et al., 2012). A screen-printed carbon electrode (SPCE) fabricated with silver hexacynaoferrates (NPAg-HCF), as flow injection analysis was developed for the detection of isoniazid by P.R. de Oliveira and coworkers. The catalytic response for the SPCE/NPAg-HCF electrode observed for isoniazid determination, was confirmed by the increase in the current of the $Ag_3K[Fe^{II}(CN)_6]$/ $Ag_3[Fe^{III}(CN)_6]$ redox couple at the electrode surface which was proportionally related to the INZ concentration. The linear concentration range

obtained in this study was 5.0×10^{-6} to 5.0×10^{-4} mol L^{-1} with a detection limit of 2.6 µ mol L^{-1} (Oliveira et al., 2012).

Miloglu et al., 2016 have developed a voltammetric sensor based on poly (3, 4-ethylenedioxythiophene)-modified gold electrode for the determination of isoniazid. The electrocatalytic performance measurements of this composite electrode toward oxidation of isoniazid exhibited an increase of 4-folds in oxidation peak densities, compared to the bare gold electrode. The variation of concentration of isoniazid also showed good linear relationship with the oxidation peak current in the range of 0.05-2 µM, with correlation coefficient of 0.9998 (Demirkaya-Miloglu et al., 2016). Lima et al., 2016 have proposed a novel electrochemical method for the detection of isoniazid based on 2, 3-dichloro-5, 6-dicyano-*p*-benzoquinone and reduced graphene oxide immobilized in Nafion membrane. Under the optimized conditions the fabricated sensor showed a wide linear range for isoniazid from 0.5 to 380 µmol L^{-1} with correlation coefficient of 0.999 (Lima et al., 2016). A gold-platinum core shell nanoparticle modified glassy carbon electrode was fabricated and the electrochemical behaviour of isoniazid was studied using CV and DPV by Gowthaman and coworkers. Compared with bare GCE, the Au/PtNPs/GCE exhibit good enhancement effects on the electrochemical oxidation of isoniazid. The amperometric current response was increased linearly while increasing the concentration of INZ from 50×10^{-9} to 100×10^{-6} M with a correlation coefficient of 0.998, and the limit of detection was found to be 26×10^{-9} M (Gowthaman et al., 2016).

A rapid and sensitive voltammetric sensor based on the oxidation of isoniazid was developed using poly (amidosulfonic acid) fabricated on glassy carbon electrode by Yang and coworkers. The oxidation of isoniazid gave a well-defined, pH dependent peak. The linear relationship between anodic peak current and isoniazid concentration in the range of 5.0×10^{-8}-1.0×10^{-5} M and limit of detection 1.0×10^{-8} M was obtained (Yang et al., 2008). Thionine immobilized on multiwalled carbon nano tubes involving a carbon paste electrode was successfully used for the simultaneous determination of ascorbic acid (AA) and acetaminophen (AC) in the presence of isoniazid by Shahrokhian and coworkers. The electrochemical response of AA, AC and isoniazid were investigated by cyclic voltammetry and differential pulse voltammetry. The electrochemical response of the fabricated electrode was analyzed by observing the CV at various potential sweep rates. The calibration curves for AA, AC and isoniazid ranged from 1.0×10^{-6} to 1.0×10^{-4}, 1.0×10^{-7} to 1.0×10^{-4} and 1.0×10^{-6} to 1.0×10^{-4} M respectively (Shahrokhian and Asadian, 2010).

The voltammetric behaviour of INZ in presence of surface active agents at poly (3, 4-ethylenedioxy thiophene) (PEDOT) fabricated electrode was studied by CV, LSV and EIS by Atta and coworkers. The presence of surfactant in the medium plays a key role in the electrostatic attraction and repulsion of isoniazid towards the polymeric surface at different pH values. The linear response obtained for isoniazid was in the range of 0.1 to 8 μmol L^{-1} and 10 to 100 μmol L^{-1} with correlation coefficients of 0.999 and 0.998, detection limits 32 nmol L^{-1} and 45 nmol L^{-1}, respectively (Atta et al., 2011). Majidi et al., 2006 have developed a voltammetric method for the detection of isoniazid using overoxidizied polypyrrole (OPPy) fabricated GCE. The OPPy modified GCE showed good catalytic activity towards the oxidation of isoniazid and

overall four electrons are involved in this electro oxidation. The diffusion coefficient of 3.6×10^{-6} cm^2 s^{-1} for isoniazid was also estimated using chronoamperometry study. It has been shown that using the OPPy-modified electrode, isoniazid can be determined by amperometry technique with limit of detection of 3.15×10^{-6} M (Majidi et al., 2006). Electrochemical behaviour of isoniazid at the mercury film silver based electrode was investigated by Szlosarczyk and coworkers. Compared with bare GCE, the mercury film silver based electrode remarkably enhanced the anodic peak current of isoniazid. The calibration graph obtained is linear from 5 nM up to 500 nM and the limit of detection is 4.1 nM (Szlósarczyk et al., 2012).

Yao et al., 1999 developed a simple ion-selective piezoelectric (ISP) sensor for the determination of isoniazid in body fluids. The concentration range obtained from 6×10^{-8} to 2×10^{-7} and the percent recovery was 98% to 102% respectively (Yao et al., 1999). Milan-Segovia et al., 2007 reported a high-performance liquid chromatography (HPLC) method for simultaneous determination of isoniazid and acetylisoniazid (AcINZ). The effluent was monitored by UV detection at 290 nm and the concentration range obtained was 0.5-15 µg mL^{-1}. The limit of detection for isoniazid and AcINZ were 0.24 and 0.12 µg mL^{-1} respectively (Milán-Segovia et al., 2007). Xiaomeng et al., 2011developed a HPLC method for the determination of isoniazid and isonicotinic acid and the UV detection wavelength was set at 261 nm. The linear concentration ranges from 10-1000 µg/mL^{-1} and 2-24 µg/mL^{-1} respectively, the average recoveries were 99.57% and 98.96% respectively (Xiaomeng et al., 2011). Dutt et al., 1964 reported a spectrophotometric method for the determination of isoniazid in excess p-amino salicylate with the recovery ranging from 100% to 109 % for INZ (Dutt and Chua, 1964). Stets et al., 2013 simultaneously determined isoniazid and RIF in urine and various pharmaceutical

samples. The concentration ranged from 8 to 57 mgL^{-1} for RIF and 1.5 to 7 mgL^{-1} for isoniazid with the recoveries ranging from 92 to 119% (Stets et al., 2013). Shetty et al., 2012 reported a spectrophotometric determination isoniazid. The linear range obtained was from 2-22 µg mL^{-1}, with the detection limit of 1.5 μgmL^{-1} (Shetty et al., 2012). Swamy et al., 2014 reported an HPLC/UV method for the determination of isoniazid in the presence of the Folin-Ciocalteu reagent in Na_2CO_3. The concentration ranged from 0.5-10 μgmL^{-1} and the limit of detection and limit of quantification achieved with this method was 0.03 and 0.09 μgmL^{-1} (Swamy et al., 2014). Sabitha et al., 2010 reported a reverse phase high performance liquid chromatography (RP-HPLC) method for the determination of isoniazid in plasma. The average recovery rate was 99.21% with a relative standard deviation of 3.74% (Sabitha et al., 2010).

Wen et al., 2014 developed a spectrophotometric determination of isoniazid in various pharmaceutical samples by Silicomolybdenum blue. The concentration range from 1.968 to 27.55 µg/mL and correlation coefficient was 0.9995 (Wen and Tu, 2014). Khuhawar et al., 2016 reported a capillary gas chromatographic determination of isoniazid in various pharmaceuticals and blood by precolumn derivatization with trifluoroacetylacetone. The linear calibration ranges for isoniazid were determined to be 2.5-25 µg/mL, with a detection limit of 62.5 pg, respectively (Khuhawar and Zardari, 2006). Cao et al., 2012 developed a liquid chromatography-mass spectrometry (LC-MS/MS) method for the simultaneous analysis of isoniazid and acetylisoniazid in human plasma with recoveries ranging from 73.58% to 103.86% (Cao et al., 2012). Pinzauti et al., 1974 reported a potentiometric determination for isoniazid, phenelzine and dihydralaine in the presence of chloramine-T with recovery percentage are 100.05 ± 0.44 % (Pinzauti et al., 1974).

Ali Karimi et al., 2009 proposed a method for the simultaneous spectrophotometric determination of isoniazid and hydrazine using an H-point standard addition method and partial least squares. The concentration ranged from 0.5-3.0 µg/mL^{-1} and the limit of detection was found to be 0.06 µg/mL^{-1} (Karimi et al., 2009). Scardi et al., 1957 reported a new colorimetric method for the determination of isoniazid in biological fluids with the recoveries of 99.5% to 102% (Scardi and Bonavita, 1957). Almani et al., 2013 developed a spectrophotometric determination of isoniazid from pharmaceutical samples using natural aldehyde with concentration ranging from 0.5-2.5 µg/mL, and the relative standard deviation was 0.2%-1.5% (Almani et al., 2013).

Satyanarayana et al., 2014 developed a voltammetric sensor based on MWCNTs-chitosan nano composites. The concentration ranges obtained were from 0.014-0.411 µg/mL^{-1} and the limit of detection was found to be 7.5 ng mL^{-1} (Satyanarayana et al., 2014). Iriminescu et al., 2016b reported a simultaneous determination of isoniazid and drifampicin (DRIF) by using the micellar electro kinetic chromatography technique. The concentration ranged from 5 – 100 µg/mL with the limit of detection and limit of quantification 4.59 and 15.32 µg/mL for isoniazid and 4.47 and 14.91 µg/mL for DRIF, respectively (Iriminescu et al., 2016b). Demirkaya-Miloglua et al., 2016 developed a new voltammetric method for the determination of isoniazid by using the poly (3, 4-ethylenedioxythiophene) (PEDOT) modified gold electrode. In this study concentration range was found to be 0.05-2 µM, with a limit of detection and limit of quantification of 0.014 µM and 0.043 µM respectively (Demirkaya-Miloglu et al., 2016). Asadpour-Zeynali et al., 2017 developed a voltammetric sensor for the detection of isoniazid at a poly eriochrome black T (EBT) modified GCE. The linear concentration range obtained for the developed sensor was in

the range 8.0×10^{-6} to 1.18×10^{-3} M and 2.90×10^{-5} to 1.67×10^{-3} M with a limit of detection of 6.0 µM and 16.4 µM respectively (Asadpour-Zeynali and Baghalabadi, 2017). Smith et al., 1999 reported a HPLC method for the simultaneous determination of isoniazid, RIF and PZM from plasma with detection limits of 0.05 µg and the recovery percentages are 90% for RIF, PZM and 70% for INZ respectively (Smith et al., 1999). Guermouche and Guermouche, 2004 developed a solid-phase extraction and HPLC technique for the determination of isoniazid and acetylisoniazid (AcINZ) in serum, and the recoveries ranged from 87.2 to 96.1% for isoniazid and 87.2 to 93.7% for AcINZ (Guermouche and Guermouche, 2004). Florence Oga et al., 2010 determined isoniazid in various pharmaceutical samples using HPLC and UV methods with recoveries ranging from 97.4% to 106% (Oga and Enoche, 2010).

Hassan AL-Ameri et al., 2010 have developed a highly sensitive electrochemical method for determination of isoniazid in various pharmaceuticals. A sensitive linear voltammetric response for isoniazid was obtained in the concentration range of 0.05-0.40 $\mu g.mL^{-1}$ with a limit of detection and quantification of 0.05 and 0.12 $\mu g.mL^{-1}$ (S.A. Hassan 2010). Mahjoub et al., 2016 reported a HPLC method for the simultaneous determination of the isoniazid, PZM in plasma using C_{18} column and the recoveries obtained were 91% (RSD 3.64%) for PZM and 96.28% (5.4%) for isoniazid respectively (Mahjoub et al., 2016). Agbokponto et al., 2014 reported a (LC-MS/MS) method for the determination of isoniazid and the recoveries ranged from 92.8% to 108.8% (Agbokponto et al., 2014). Zheng et al., 2001 developed a new flow-injection electro generated chemiluminescence (ECL) for the determination of isoniazid by using the luminol. The concentration range of 4.0×10^{-8} to 8.0×10^{-6} mol/L and with a limit of detection of 2.8×10^{-8} mol/L (Zheng et al., 2001).

Barsoum et al., 2008 described a HPLC method for the simultaneous determination of isoniazid and RIF from pharmaceutical samples and biological fluids. The recovery average was 99.86% for isoniazid and 99.02% for RIF (Barsoum et al., 2008). Gowda et al., 2002 developed a spectrophotometric method for the determination of isoniazid in pharmaceutical formulation with recovery percentages of 101.53% (Gowda et al., 2002). Agbokponto et al., 2014 developed a sensitive liquid chromatography coupled with mass spectrometry for the determination of isoniazid in biological samples, with detection limits of 5 ng/mL (Agbokponto et al., 2014). Hsu and Ho, 1989 described a HPLC method for the simultaneous determination of isoniazid and AcINZ in a rabbit blood. The recovery percentages are 97.6 ± 2.7 for INZ and 104.6 ± 3.6 respectively (Hsu and Ho, 1989).

Bhandari et al., 2012 reported a HPLC method for the detection of isoniazid in rat plasma, brain, liver and kidney. The concentration range from 250 ng/mL to 25,000 ng/mL and the limit of detection was 150 ng/mL and limit of quantification was 200 ng/mL respectively (Bhandari, 2012). Hakkimane et al., 2017 described a RP-HPLC method for the determination of isoniazid and simultaneous determination of anti-tuberculosis drug isoniazid and RIF, with a detection limit and limit quantification of 0.03 μg/mL and 0.12 μg/mL respectively (Hakkimane and Guru, 2017).

A survey of the reported literature for the separation and detection of isoniazid in various pharmaceutical samples show that most of the analytical work has been performed with high-performance liquid chromatography (HPLC). Bhandarl et al., reported an enhanced HPLC method for the quantitative determination of isoniazid with average recovery of 92% and the

limit of detection was found to be 150 ng/mL (Bhandari, 2012). Seifart et al., reported simultaneous preparative HPLC extraction method for the analysis of isoniazid, acetylisoniazid and hydrazine in pharmaceuticals. The linear calibration curves in the range 10-400 ng/mL for hydrazine and 1-25 µg/mL for the isoniazid and acetylisoniazid (Seifart et al., 1995). Khuhawar et al., 2002 reported HPLC method for the detection of isoniazid, PZM, RIF and separated in YMC-ODS column. The detection limits were 0.11 ng, 0.2 ng and 13 ng/injection (5µL) for INZ, PZM and RIF respectively (Khuhawar and Rind, 2002).

2.2 Electrochemical detection of pyrazinamide and mechanism action of pyrazinamide

Pyrazinamide (PZM) is a nicotinamide equivalent compound and illustrated in **Figure 2.3**. It generally acts as a bacteriostatic agent. Pyrazinamide was first chemically manufactured in 1936 but its anti-tuberculosis nature was not predictable untill 1952 (Dalmer et al., 1934). Pyrazinamide action against mycobacteria was conducted in animal models only, after that succeeding synthesis of nicotinamide analogs and direct testing in the mouse model TB infection without in vitro testing leads to the identification of pyrazinamide as a most active agent (Yeager et al., 1952). Pyrazinamide was mainly used as a second line TB drug for the resistance of *mycobacterium tuberculosis,* due its hepatic toxicity caused by high dosage of pyrazinamide. In 1970s McDermott and colleagues worked on the impressive mouse studies and they confirmed high sterilizing activity of pyrazinamide in combination with INZ (Dessau et al., 1952). The mechanism action of pyrazinamide is unknown, pyrazinamide and its analog, 5-chloro-PZM is believed to prevent the fatty acid synthetase I (FASI) enzyme of *mycobacterium tuberculosis* (Zimhony et al., 2000, Ngo et al., 2007). Pyrazinamide diffuses into the granuloma of *mycobacterium tuberculosis*, where the TB enzyme pyrazinamidase (PZase) converts PZM to the active form pyrazinoic acid. Pyrazinamide was more active in acidic nature (pH 5-6), the pyrazinoic acid gradually leaks out and changes to the protonated conjugate acid (Zhang et al., 1999, Heifets et al., 2000). The protonated conjugate acid easily diffuses the *mycobacterium tuberculosis* and accumulates the bacteria. Pyrazinoic acid also binds to the ribosomal protein S1 (RpsA) and inhibits the translation, which easily describes the ability of the drug to kill latent mycobacteria (Shi et al., 2011) as illustrated in **(Figure 2.4)**.

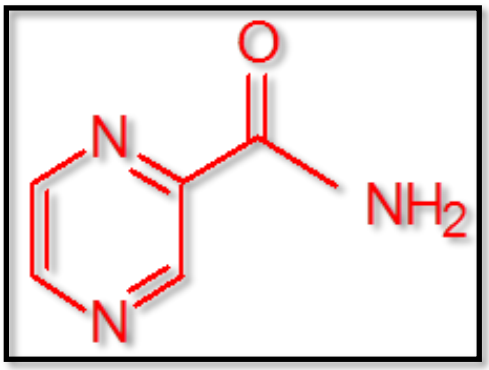

Figure 2.3: Chemical structure of pyrazinamide

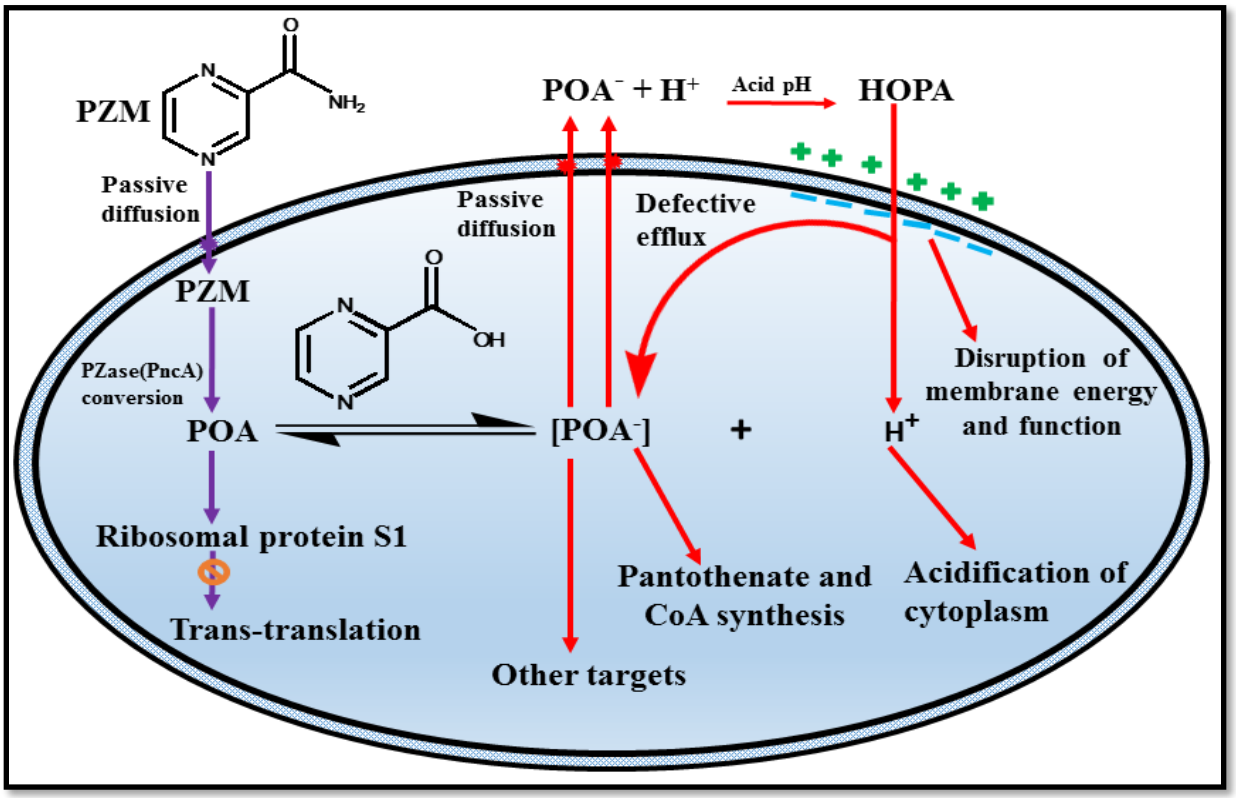

Figure 2.4: Mechanism of action of pyrazinamide

Pyrazinamide enters tubercle bacilli by passive diffusion, where it is converted to POA by PZase/nicotinamidase encoded by the *pncA* gene. POA then reaches the cell surface through passive diffusion and a weak (deficient) efflux mechanism. At acid pH, the protonated POA (HPOA) enters the cell in a pH-dependent manner by passive diffusion and then accumulates to high levels intracellularly, and then kills by multiple mechanisms including disruption of membrane energy production, inhibition of trans-translation, possibly inhibition of pantothenate and CoA biosynthesis, and other as yet unidentified mechanisms.

Multiwalled carbon nanotubes (MWCNTs) and graphene oxide (GO) hybrid nanocomposite on a glassy carbon electrode were successfully used for the selective determination of pyrazinamide (PZM) by Mani and coworkers. The oxidation potential of pyrazinamide is shifted to less negative potentials due to the high catalytic activity of MWCNTs and GO. The DPV technique has been followed for the detection of pyrazinamide in the potential range of -0.4 to -1.2 V and the following parameters of 50 mV for pulse amplitude, 0.05 ms for pulse width and 200 ms for pulse period was used for this (Mani et al.,) study. The fabricated electrode shown a good linearity range for pyrazinamide from 37.5-1800 μM range with a concentration coefficient of equation R^2 to 0.990. The low detection limit (S/N = 3) for pyrazinamide was found to be 5.54 μM (Mani et al., 2015). A rapid, sensitive and simple electrochemical method was investigated by Cheemalapati et al., 2014a for the determination of pyrazinamide at poly-L-methionine/reduced graphene oxide modified electrode by differential pulse voltammetry in human blood plasma and urine samples. The electrocatalytic response of analyte at PMET/ERGO/GCE film was measured using both cyclic voltammetry and differential pulse voltammetry. The prepared PMET/ERGO/GCE film exhibits excellent DPV response towards

pyrazinamide and the reduction peak current increased linearly with respect to pyrazinamide concentration in the linear range between 0.4 μM to 1129 μM with a sensitivity of 0.266 μA μM^{-1} cm^{-2} (Cheemalapati et al., 2014a). The electrochemical response of pyrazinamide at the graphene-zinc oxide nanocomposite fabricated carbon paste electrode (GNS-ZnO-CPE) has been investigated by Kalambate and coworkers, using cyclic voltammetry by sweeping potential from -0.3 to -1.3 V. Under the optimized parameters, the oxidation peak current was linear to the pyrazinamide concentration over the range of 1.5×10^{-7} to 4.0×10^{-4} M, with a detection limit of 4.31×10^{-8} M (Kalambate et al., 2016).

A ploy (glycine) fabricated glassy carbon electrode was constructed by Ferraz and coworkers et al., and used as a highly sensitive tool for the determination of pyrazinamide (PZM) at trace level. It has been shown that from cyclic voltammetry and differential pulse voltammetry, poly (Gly)/GCE results in a redox reaction of pyrazinamide in 0.1 mol L^{-1} phosphate buffer solution at pH 7.5, and produces a sharp anodic peak at – 0.85 V, with cathodic peak at -0.8 V respectively. Square wave voltammetry optimized conditions showed a linear response of pyrazinamide concentrations in the range from 0.47 to 6.15 μmol L^{-1}, with a detection limit of 0.035 μmol $L^{-1}$and a limit of quantification of 0.12 μmol L^{-1} (Ferraz et al., 2016). Dass et al., 2014 developed a high sensing graphene oxide (GO)/poly-arginine-modified (PAG) electrode for the simultaneous electrochemical determination of buspirone (BPH), isoniazid (INZ) and pyrazinamide (PZM) drugs. The proposed GO/PAG/GCE sensor has a wide linear range of 20 to 1400 μM for INZ, 25 to 900 μM for BPH and 25 to 1600 μM for PZM, respectively. The low limit of detection values was found as 2.59, 3.54 and 3.28 μM respectively, for INZ, BPH and PZM (Devadas et al., 2014).

A novel voltammetric sensor was modified by Bergamini and coworkers, which was based on screen printed carbon electrode (SPCE) fabricated with poly-L-histidine. The electrochemical behaviour of the SPCE was studied by linear sweep (LSV), cyclic, square-wave (SWV), differential pulse (DPV) voltammetry and electrochemical impedance spectroscopy. The limit of detection of 1.0×10^{-7} mol L^{-1}, 2.5×10^{-7} mol L^{-1} and 5.0×10^{-7} mol L^{-1} were estimated from DPV, SWV and LSV determination respectively (Bergamini et al., 2013). Mani et al., 2015 developed a simple electrochemical method for detection of pyrazinamide by using the cyclic voltammetry and differential pulse voltammetry. The bare GCE was fabricated with multiwalled carbon nanotubes (MWCNTs)/graphene oxide (GO) composite. The response of pyrazinamide is linear over the concentration range from 37.5-1800 µM, with the limit of detection found to be 5.54 µM. The fabricated electrode has shown good stability and sensitivity of 0.038 µA μM^{-1} cm^{-2} (Mani et al., 2015).

Sidwaba et al., 2014 reported that a novel biosensor for the detection of pyrazinamide was prepared with nanocomposites of multiwalled carbon nanotubes (MWCNTs), polyanilino (PANI) and cytochrome P450 3A4 (CYP3A4) electrochemically deposited on a glassy carbon electrode. The biosensor showed good sensitivity of 7.80 µA/µg mL^{-1} pyrazinamide and the linear range was 4.92-160 ng/mL (Sidwaba et al., 2014). Chenna et al., 2011 reported a spectrophotometric determination of pyrazinamide in various pharmaceuticals. PZM has absorbance maximum at 269 nm and the linearity range was found to be 2-16 µg/mL (Chenna et al., 2011). Prasanthi et al., 2015 developed a HPLC method for the simultaneous estimation of pyrazinamide, INZ and RIF in human plasma. The limits of detection and limit of quantification for pyrazinamide were found to be 0.5 and 1.6 µg/ml, for INZ 0.6 and 1.8 µg/mL, and for RIF

0.13 and 0.4 µg/mL respectively (Prasanthi et al., 2015). Glass et al., 2007 reported a HPLC method for the simultaneous determination of pyrazinamide, isoniazid and rifampicin in fixed dose combination using artificial neural networks. The correlation coefficient was 0.9998 for pyrazinamide, 0.9999 for both isoniazid and rifampicin respectively (Glass et al., 2007). Conte et al., 2000 described a HPLC method for the determination of pyrazinamide in human plasma, Bronchoalveolar Lavage Fluid (BLF), and Alveolar Cells (AC) and the recoveries of 95.3% – 108.9% respectively (Conte et al., 2000) .

Kaka reported a HPLC method for the determination of pyrazinamide in rat plasma with a limit of detection of 0.5 µg/mL (Kaka et al., 1994). Krishna et al., 2012 developed an HPLC/MS technique for the analysis of pyrazinamide in human plasma samples. The linear over the range of 0.935 µg/mL to 60.408 µg/mL with a precision of < 9.86% (Krishna et al., 2012). Chellini et al., 2015 developed a HPLC method for the simultaneous determination of pyrazinamide, rifampicin, ethambutol and isoniazid. ETB detection was performed at 210 nm and RIF, INZ and PZM were detected at 238 nm and the correlation coefficient was 0.9911 for RIF, 0.9936 for INZ, 0.9915 for PZM and 0.9906 for ETB respectively (Chellini et al., 2015). Revankar et al., reported a facile and sensitive HPLC method for the analysis of pyrazinamide in human plasma. The concentration range of 2000-5000 ng and the limit of detection was found to be 0.2 mg (Revankar et al., 1994). A fast isocratic HPLC method was reported by Mehmedagic and coworkers, for the analysis of pyrazinamide in rat urine with a LOD of 300 µg/L for PZM (Mehmedagic et al., 1997).

Brouard et al., 1985 reported an HPLC method for the analysis of pyrazinamide in biological fluids. The concentration ranged from 50-800 µg/mL with recoveries ranging from 91% and 92%, respectively (Brouard et al., 1985). An improved HPLC/MS method was reported by Wu et al., by evaluating pyrazinamide from the rat blood, brain and bile. The concentration ranges from 0.5-10 µg mL^{-1} and the recovery percentages ranging from 13.3 ± 0.9 to 80.6 ± 1.5% respectively (Wu et al., 2004). Allen et al., 1953 developed a UV method for the determination of pyrazinamide in blood and urine and an the absorption wave length of 460 µm (Allen et al., 1953). Khuhawar et al., 2005 developed an HPLC method for the determination of INZ, pyrazinamide, and indomethacin (IM) in pharmaceutical preparations. The linear calibration plots were obtained between 6.2 and 30.8 µg mL^{-1}, between 10.7 and 64.08 µg mL^{-1} for (IM) and 1.4 and 5.5 µg mL^{-1} for INZ (Khuhawar et al., 2005).

Dhal et al., 2009 developed a new validation RP-HPLC method for simultaneous determination of pyrazinamide, isoniazid, and rifampicin and pyridoxine hydrochloride in pharmaceutical formulations. The limit of detection and limit of quantification were 0.036, 0.063, 0.059, 0.043 µg mL^{-1} and 0.11, 0.19, 0.018 and 0.13 µg mL^{-1} for pyrazinamide, INZ, RIF and pyridoxine hydrochloride respectively (Dhal and Sharma, 2009). Kurniati et al., 2016 developed a simultaneous determination for pyrazinamide, INZ, ETB and RIF in 4FDC tablets by FTIR spectrophotometry in combination with multivariate calibration. The optimized wavenumber range for the detection of 1714-2756 cm^{-1}, 433-873 cm^{-1}, 1552-2970 cm^{-1} and 433-1552 cm^{-1} for RIF (Kurniati et al., 2016).

Maaboud et al., 2013 developed a novel spectrofluorometric determination of pyrazinamide, INZ, ETB and RIF in their pure and pharmaceutical dosage forms by quenching effect on the fluorescence of NBS-phenothiazine product. The limit of detections were 0.029, 6.39×10^{-3}, 0.139 and 0.180 µg mL^{-1} respectively in pharmaceuticals (Mohamed et al., 2013). Salfinger et al., 1988 developed a radiometric method for the determination of pyrazinamide MICs for mycobacterium tuberculosis at different pHs (Salfinger and Heifets, 1988). Reena et al., 2013 reported an calorimetric method by using the vitro drug susceptibility testing of pyrazinamide, in this method the drug susceptibility tests are routinely performed before initiating multidrug drug resistant tuberculosis treatment (Reena and Shanthi et al., 2013).

Muchlisyam et al., 2002 reported a second derivative spectrophotometric method for the detection of pyrazinamide, rifampicin and isoniazid in combined pharmaceutical forms. The recovery percentages for pyrazinamide obtained was 99.84 % with relative standard deviation (RSD) = 1.39%, RIF was 100.95% with RSD = 0.415% and INZ returned 99.88% with RSD 1.318% (Muchlisyam et al., 2002). Martin et al., 2006 reported a new rapid and simple colorimetric method for the determination of pyrazinamide resistance in mycobacterium tuberculosis using nicotinamide (Martin et al., 2006). Simioni et al., 2017 have reported a nondiamond based voltammetric sensor for the detection of pyrazinamide and linear concentration range from 7.9×10^{-7} to 4.9×10^{-5} mol L^{-1}, with a limit of detection of 2.2×10^{-7} mol L^{-1} (Simioni et al., 2017). Zosiwe, 2015 developed an electrochemical sensor for the determination of pyrazinamide at a Cytochrome P450 2E1/Nickel-poly (propylene imine) composite fabricated on a platinum electrode. The linear range for pyrazinamide was from 0.01 nM to 0.12 nM with a detection limit of 0.00114 nM (Zosiwe, 2015).

Rote and Sharma, 1997 developed a simple method for the simultaneous detection of pyrazinamide, isoniazid and rifampicin by using a first derivative techniques on UV spectrophotometry. The UV adsorption of the pyrazinamide, isoniazid and rifampicin was 268.8 nm, 262.2 nm and 254 nm respectively (Rote and Sharma, 1997). Calleri et al., 2002 reported a simple RP-LC method for the simultaneous determination of pyrazinamide, INZ and RIF in various pharmaceuticals. The recovery percentages are 98.51% for PZM, 98.55% for INZ and 98.56% for RIF respectively (Calleri et al., 2002). Zhifeng et al., 2010 developed a sensitive HPLC method for the determination of pyrazinamide, INZ, RIF and Acetylisoniazid (AcINZ) simultaneously with the detection limits of 0.014, 0.023, 0.054 and 0.009 μg mL^{-1} for PZM, INZ, RIF and AcINZ respectively (Zhifeng et al., 2010).

Pullan et al., 2016 developed a method related to the influence of the growth rate on pyrazinamide action in mycobacterium tuberculosis insights for early bacterial activity. Three different phases of drug responses could be distinguished for both slow growing (69.3 h MGT) and fast growing (23.1 h MGT) bacilli (Pullan et al., 2016). Mulyani et al., 2016 reported a HPLC and UV methods for the determination of pyrazinamide in human plasma with the limit of quantification and limit of detection values are 27.672 and 2.532 μg/mL, respectively (Mulyani et al., 2016). Lacroix et al., 1988 reported HPLC techniques for the detection of pyrazinamide and Allopurinol (AL). In this method the pharmacokinetics of pyrazinamide and its metabolites were studied in six healthy human volunteers, in a cross-over design, after a single oral dose of pyrazinamide alone and, in a second trial, after the same dose together with all (Lacroix et al., 1988).

Allana et al., 2017 reported a polymorphism in the pyrazinamide and pncA gene. The results were found to be 96% of extensively drug resistant, 70% pncA gene multidrug resistant mycobacterium tuberculosis isolates from Georgia and South Africa (Allana et al., 2017). Sturkenboom et al., 2015b reported a LC-MS/MS for the quantification of pyrazinamide, isoniazid and ethambutol in various serum samples. The linear calibration curves in the range of 2-80 mg/L for PZM and 0.2-8 mg/L for INZ and ETB respectively (Sturkenboom et al., 2015b).

2.3 Electrochemical detection of rifampicin and mechanism action of rifampicin

Rifamycins are a family of antibiotics, with the first agent rifamycin V synthesized in 1957 in the Dow- lepetit research laboratories (Milan, Italy) from the soil mold amycolaptis rifamycinica. Most of these are new species produced a new class of molecules with high antibiotic activity, except rifamycin B which has a practically inactive nature for some of the bacterial infections (Sensi, 1983). In 1959, to obtain more stable semisynthetic products, a new molecule with high efficiency and excellent tolerability was produced and named as rifampicin. Rifampin was released in 1967 and is the most commonly used rifampicin in dermatology. Rifampicin has a critical structure, it has flat naphthalene rings and several of the OH groups are essential for activity **(Figure 2.5)**. The mechanism action of rifamycins inhibit the enzyme RNA polymerase and prevents the RNA syntheses which in turn prevents the protein synthesis (Zumla et al., 2014, Lönnroth et al., 2015). RIF is a bacterial drug that kills growing, metabolically active bacilli, as well as bacilli in the inactive phase, during which metabolism is reduced. When RIF is used in combination with pyrazinamide, tuberculosis treatment duration can be reduced to six months. Moreover, the rifampicin inhibits gram-positive bacteria and it mainly works by binding non-covalently to DNA and RNA polymerase. The DNA dependent and RNA polymerase in eukaryotic cells are unaffected, since the drug binds to a peptide chain not present in the mammalian RNA polymerase (Levin and Hatfull, 1993, Wehrli, 1983). The mechanism action is illustrated in **Figure 2.6**.

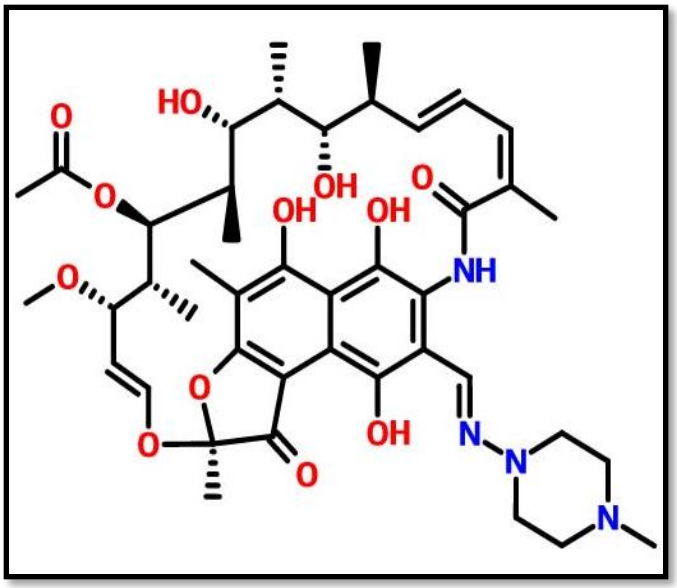

Figure 2.5: Chemical structure of rifampicin

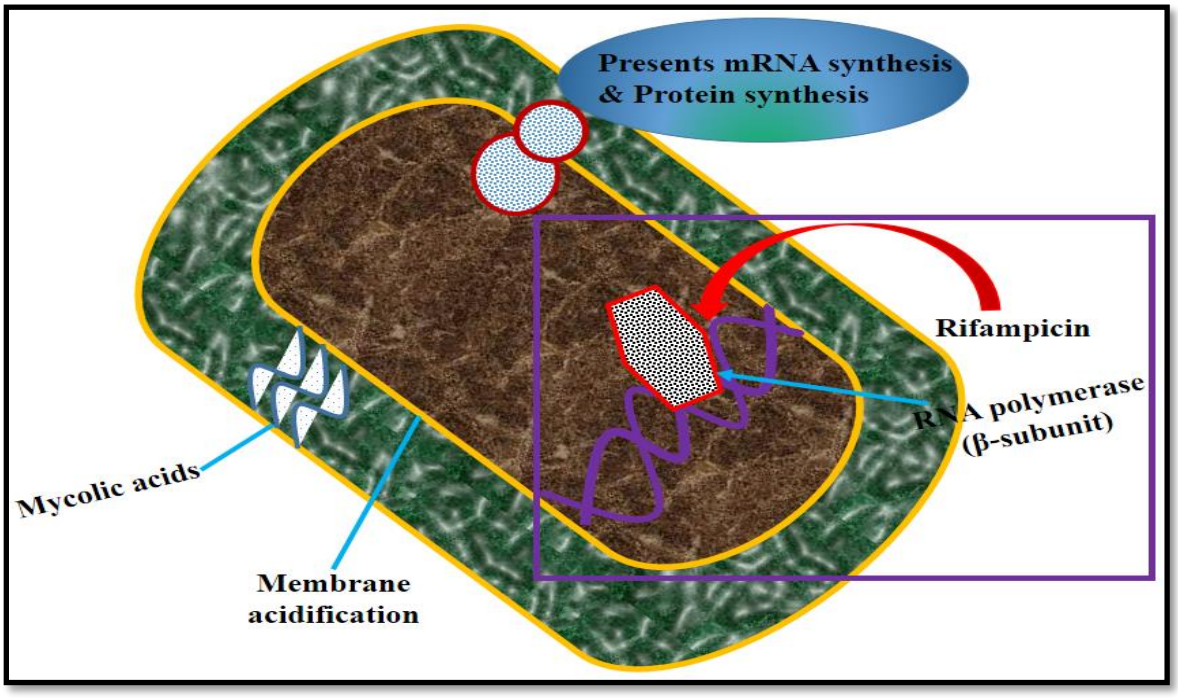

Figure 2.6: Mechanism of action of rifampicin

The electrochemical behaviour of rifampicin (RIF) on the cyclodextrin based sensor was fabricated on platinum electrode (pyrrole electropolymerization) and investigated by Lomillo and coworkers (Lomillo et al., 2015). RIF was deposited on the surface of the modified electrode through complex formation and quantified amperometrically. The linear range of three calibrations were made with 10 additions comprising 50 µL each of a 6.0×10^{-4} mol L^{-1} and the average limit of detection was found to be 1.69×10^{-6} mol L^{-1} (Alonso Lomillo et al., 2005). A chemically amplified cytochrome P450-2E1 coated on gold electrode was prepared by Ajayi and coworkers, for electrochemical determination of rifampicin. The electrochemical behaviour of RIF on Au/PVP-AgNPs/PANSA/EG-CYP2E1 fabricated gold electrode was explored using cyclic voltammetry, differential pulse voltammetry, electron impedance spectroscopy and steady state amperomerty under aerobic conditions. The linear range 2-14 µM and detection limit was estimated to be 0.05 µM, while a sensitivity of 1.4 µA/µM was determined from the calibration curve (Ajayi et al., 2014).

Hassan et al., 1997 described a novel potentiometric membrane sensor for the potassium ion based on the use of rifampicin as a neutral ionophore. The linear and stable potential response with near Nernstian slope of 56.7 ± 0.2 mV $decade^{-1}$ are obtained over the concentration range $1 \times 10^{-1} - 3 \times 10^{-5}$ M K^+. The detection limit is 0.3 µg ml^{-1} K^+, the response time is 10–30 s and the working pH range is 4–11 (Hassan et al., 1997). Oswald et al., 2011 developed a LC-MS/MS method for the simultaneous determination of clarithromycin, rifampicin and their main metabolites in horse plasma. The validation studies were performed at low and high concentration ranges for all analytes, and the results were found to be 2.5-25 for the low and 25-250 ng/mL in pharmaceuticals (Oswald et al., 2011). Mansilla et al., 2001 developed a classical

partial least squares and modification for the novel hybrid linear analysis regarding the simulations spectrophotometric determination of rifampicin, pyrazinamide and isoniazid. The concentrations ranges were 0-15 mg/mL for the rifampicin, pyrazinamide and 0-10 mg/mL for isoniazid. The limit of detection was found to be 0.40, 0.45 mg/mL for rifampicin, pyrazinamide and 0.91 mg/mL for isoniazid (Espinosa-Mansilla et al., 2001). Girousi el al., 2004 developed a DNA fabricated carbon paste electrode for the determination of RIF by using the cyclic voltammetry and differential pulse voltammetry. The limit of detection was found to be 0.25×10^{-7} M (Girousi et al., 2004).

Liang et al., 2007 reported a method for the analysis of rifampicin with electrochemiluminescense (ECL) in various pharmaceutical samples and human urine. The ECL intensity was linear with RIF concentration in the range of 1.0×10^{-7} to 4.0×10^{-5} mol L^{-1} and limit of detection was found to be 3.9×10^{-8} mol L^{-1} (Liang et al., 2007).

A horseradish peroxidase enzyme based biosensors was developed for the determination of RIF by Lomillo and coworkers, the concentrations ranged from 5.88 to 54.07 µmol dm^{-3} and the limit of detection was found to be 5.06×10^{-6} µmol dm^{-3} (Alonso Lomillo et al., 2003). Oldfield et al., 1986 developed a HPLC method for the measurement of rifampicin and 25-desacetylrifamicin in biological fluids. The rifampicin concentration ranges from 1.8 to 10.7 mg/L (Oldfield et al., 1986). Rastgar et al., 2014 developed a method for the determination of rifampicin by using the nickel hydroxide nanoparticles and reduced graphene oxide nanosheets film on the GCE. The fabricated electrode showed two oxidation peaks at 0.08 V and 0.069 V. The linear dynamic range was obtained from 0.006 to 10.0 µmol L^{-1} and 0.04 to 10 µmol L^{-1}, with a limit of

detection of 4.16 nmol L^{-1} and 2.34 nmol L^{-1} considering peaks I and II, respectively (Rastgar and Shahrokhian, 2014). De Velde et al., 2009 proposed a method for the simultaneous determination of rifampicin and clarithromycin in human plasma by using the HPLC-MS technique. The calibration curves were linear in the range of 0.10 to 10 mg/L for clarithromycin and 0.20 to 5.0 mg/L for rifampicin (de Velde et al., 2009). Zeynali et al., 2010 proposed a method for the simultaneous detection of rifampicin and INZ by using the differential pulse polarography. The calibration graph was linear in the range of 6×10^{-8}–10^{-4} M and 10^{-7} to 10^{-4} M for INZ and RIF (Asadpour-Zeynali and Soheili-Azad, 2010). Hammam et al., 2004 developed an electrochemical determination of isoniazid and rifampicin by using the cyclic voltammetry and square wave voltammetry. The limit of detection and limit of quantification was found to be 5×10^{-8} and 1.7×10^{-7} M for rifampicin and 6.1×10^{-8} and 1.7×10^{-7} M for INZ (Hammam et al., 2004).

Benetton et al., 1998 reported a visible spectrophotometric and first derivative UV spectrophotometric determination of rifampicin and INZ in various pharmaceutical samples. The absorbance of the rifampicin was at 475 nm and the recoveries were 99.03% for RIF and 100.01% for INZ (Benetton et al., 1998). Mohamed et al., 2005 reported an UV spectrophotometric method for the determination of rifampicin and INZ with the concentration ranges from 2.5 to 12.5 µg/mL and 5 to 25 µg/mL with good linearity and the limit of detection was found to be 0.70 and 0.26 µg/mL for INZ and rifampicin respectively (Mohamed et al., 2005). Walash et al., 1993 reported a spectrophotometric determination of rifampicin in the presence of 3-formyl rifampicin and rifamoin quinone. The percentage recoveries ranged from 99.33 ± 0.63 % to 100.2 ± 0.44% (Walash et al., 1993). Hahn et al., 2001 reported an electrochemical determination of rifampicin by using the differential pulse polarography

technique. The rifampicin concentration ranged from 1.0×10^{-7} M to 2.0×10^{-7} M yielded a straight line with a correlation coefficient of 0.9996 and the detection limit was found to be 1.0×10^{-8} M (Hahn and Shin et al., 2001). Sriram Siddhartha et al., 2012 reported a HPLC method for the determination of rifampicin in human plasma. The linearity range was 0.31-25.48 µg/mL and recovery percentages are 90.07 % (Siddhartha et al., 2012). liu et al., 2008 reported a HPLC method using a C_{18} column which was developed for the detection of rifampicin, rifamycin SV (SV), 3-formylrifamycin SV (3-FR), rifampicin quinone (RQ) and rifampicin N-oxide (RNO). The limit of quantification was 0.2 µg/mL, limit of detection was 1 µg/mL and the recovery percentages ranging 99.7% to 100.5% (Liu et al., 2008).

Calleja et al., 2004 reported an HPLC method for the determination of rifampicin in human plasma and tissues. The average recoveries were found to be 83% and 95%, with relative standard deviation (RSD) were below 15% (Calleja et al., 2004). Gowda et al., 2014 described an HPLC method for the determination of rifampicin in urine and plasma. The linear concentration ranged from 2.5 to 80 µg mL^{-1} for urine and 0.25 to 15 µg mL^{-1} for plasma. The limit of quantification were found to be 1.0 and 2.5 µg mL^{-1}, limit of detection was 0.1 and 0.25 µg mL^{-1} for plasma and urine respectively (Gowda and Nandibewoor, 2014). Tatarczak et al., 2005 reported an HPLC method for the determination of rifampicin in complex pharmaceutical preparations and serum with the average recoveries of 91.4% and 98.97% respectively (Tatarczak et al., 2005). Louveau et al., 2016 described an HPLC method coupled with UV detector for the detection of rifampicin in human plasma, rifampicin was identified at a wavelength of 335 nm with a lower limit of quantification of 0.05 mg/L in human plasma (Louveau et al., 2016). Yong et al., 2008 developed a new chemiluminescence technique for the detection of rifampicin by Peroxomonosulfate-Cobalt (II) and obtained detection limit of 7×10^{-9}

g/mL and the relative standard deviation was 2.7% for 6×10^{-9} g/mL for rifampicin (Ma et al., 2008). Shah el al., 1992 reported a HPLC method for the determination of rifampicin and isoniazid with the detection being obtained at 254 nm (Shah et al., 1992). Allanson et al., 2007 developed a HPLC-UV method for the determination of rifampicin in human plasma and blood spots. The limit of quantification obtained was 1.5 µg/mL in blood spots and 0.5 µg/mL in plasma (Allanson et al., 2007). Goicoechea et al., 1999 reported an multivariate spectrophotometric determination of rifampicin, pyrazinamide and isoniazid in various tablet preparations with the recoveries are 99.9% for rifampicin, 100.4% for pyrazinamide and 104.7% for isoniazid respectively (Goicoechea and Olivieri, 1999).

Panchagnula et al., 1999 reported an HPLC method for the determination of rifampicin and its metabolites in the presence of PZM and INZ. The metabolite values were found to be 86% and 79% in urine and plasma respectively (Panchagnula et al., 1999). Benetton et al., 1998 developed a first derivative UV spectrophotometric method for the detection of rifampicin and INZ with recovery percentages of 99.03% for rifampicin and 100.01% for INZ (Benetton et al., 1998). Argekar et al., 1996 reported an HPLC method for the determination of rifampicin, pyrazinamide and isoniazid with the average recovery percentages of 97.98% for RIF, 100.01% for PZM and 101.74% for INZ respectively (Argekar et al., 1996). Swart et al., 1992 reported an HPLC method for the determination of rifampicin in plasma. The calibration curves were linear at least 20 µg/mL and the limit of quantification was 0.16 µg/mL(Swart and Papgis, 1992). Finkel at al., 1971 reported a fluorometric and microbiological array for the determination of rifampicin in serum levels in dogs. The maximum fluorescence was measured at 480 nm, with an excitation wavelength of 370 nm, and the limit of detection was found to be 0.1 µg/mL (Finkel et al., 1971).

Li et al., 2005 developed flow chemiluminescence with artificial neural network calibration method for the determination of rifampicin and isoniazid with the limit of detection 0.005 $\mu g/mL^{-1}$ for RIF, 0.03 $\mu g/mL^{-1}$ for INZ respectively (Li et al., 2005). Kisa et al., 2003 reported FASTPlaqueTB-RIF for determination of rifampicin resistance in Mycobacterium tuberculosis complex isolates with the accuracy of 94.3% (Kisa et al., 2003). Kumari et al., 2015 developed an RP-HPLC method for the determination rifampicin and isoniazid in various pharmaceutical formulations with recovery percentages of 99.56 % for RIF and 99.83 % for INZ. The limit of quantification was 1.75 µg/mL for both INZ and RIF, and the limit of detection was 0.5 µg/mL for both RIF, INZ respectively (Kumari et al., 2015).

Daneshgar et al., 2009 have developed dysprosium hydroxide nanowires modified electrode for the determination of rifampicin in human urine and capsules by adsorptive square wave voltammetry. The limit of detections were 5.0×10^{-10} M and 8.0×10^{-10} M respectively (Daneshgar et al., 2009). Marta Boffito et al., 2002 reported a HPLC method for the simultaneous detection of rifampicin and Efavirenz (EFA) in plasma with recoveries of 96% for RIF and 97.5% for EFA (Boffito et al., 2002). Shah et al., 2015 developed chemometric assisted spectrophotometric methods for the simultaneous determination of rifampicin and Piperine (PIP) in bulk and capsule with recovery percentages of 101.31% for RIF and 98.57% for PIP respectively (Shah et al., 2015). Jansson et al., 2014 reported an a comparison of two assays for molecular determination of rifampicin resistance in clinical samples from patients with Buruli Ulcer Disease, with a lower limit of detection of 100 to 200 copies of the targeted sequence (Jansson et al., 2014).

Umapathi et al., 2010 developed RP-HPLC method for the determination of rifampin quinone (RIF Q) and hydrazone with the recoveries of 99.95% for RIF Q and 99.39% for hydra zone (Umapathi et al., 2010). Ravi Shankar et al., 1998 developed a method for the detection of rifampicin bulk and marketed samples by simple UV method with the obtained recovery percentages from 98 to 100% (Ravi Shankar 1998). Iriminescu et al., 2016a reported a micellar electronic chromatography method for the simultaneous determination of rifampicin and isoniazid, with the limit of detection 4.59 µg/mL for INZ and 4.47 µg/mL for RIF (Iriminescu et al., 2016a). Mariana Tilinca et al., 2017 reported an UV method for the determination of rifampicin and isoniazid, the determinations were made at 263 nm for RIF and 290 nm for INZ respectively (Tilinca et al., 2017).

Chatterjee et al., 2015 reported a fluorescence method for the detection of residual rifampicin in urine via quenching of gold nanoclusters, and the obtained sensitivity range from 0.5 to 823 µg/mL, with the limit of detection of 70 ng/mL (Chatterjee et al., 2015). Tian Gan et al., 2015 have developed a sensitive sensor for the determination of rifampicin using a hollow manganese oxide mesoporous silica oxide (Mn_3O_4 SiO_2) core-shell nanohybrid as sensitive material and the limit of detection was evaluated to be 10.8 nM (Gan et al., 2015). Khamar et al., 2012 reported a spectrophotometric method for the simultaneous determination of rifampicin Piperine (PIPE) in their combined capsule dosage, and the recoveries ranged from 98.36% to 99.23% for RIF, 98.91% to 99.53% for PIPE (Khamar and Patel, 2012). Liu wei et al., 2002 reported a chemiluminescence method for the determination of rifampicin with the detection limit of 7×10^8 g/mL (Wei et al., 2002). Lutfullah et al., 2011 developed a UV method for the determination rifampicin in soil samples and the limit of detection obtained was 0.20 $\mu g/mL^{-1}$ (Sharma et al., 2011).

Lachau et al., 1992 developed a UV method for the determination of rifampicin in human albumin and serum. The RIF bound and unbound fractions were determined at 473.5 nm and 475.8 nm respectively (Lachau et al., 1992). Balbao et al., 2010 reported a stir bar-sorptive extraction and high-performance liquid chromatography-UV detection (SBSE/HPLC-UV) method for therapeutic drug monitoring of rifampicin in plasma samples with the recoveries ranging from 75%-80% (Balbao et al., 2010). Fathalla et al., 2013 developed a micellar HPLC method for the simultaneous determination of rifampicin and linezolid (LNZ) with the resulting limits of detection of 0.65 and 1.40 $\mu g/mL^{-1}$ (Fathalla et al., 2013). Anusha et al., 2014 reported a RP-HPLC method for the determination of rifampicin and isoniazid with a recovery of 101% for RIF, 100% for INZ and the detection limit of 9.58 µM for RIF, 2.88 µM for INZ (Anusha and Sreedevi et al., 2014). Negi et al., 2009 described a *RPO* B gene for the detection of rifampicin resistance by SSCP and Sensitivity, specificity were calculated as 90.90% and 100% respectively (Negi et al., 2009).

2.4 Electrochemical detection of ethambutol (ETB) and mechanism action of ETB

Ethambutol (ETB) has been shown to enhance therapeutic activity in experimental tuberculosis infection in guinea pigs and monkeys (Karlson, 1961a, Karlson, 1961b). Discovered in 1961, ethambutol is an antibacteriostatic agent that is most usually used in combination with additional drugs in the treatment of tuberculosis. Ethambutol also used as part of a combination regimen in the therapy of *Mycobacterium avium complex* (MAC), *Mycobacterium bovis* (MB) and *Mycobacterium marinum* (MM) infections in patients with concomitant infection with human immunodeficiency virus (HIV) (Namdar et al., 2005, Forbes et al., 1962). The chemical structure of ethambutol is showed in **Figure 2.7**. The mechanistic action of ethambutol is not clear but it is bacteriostatic against actively growing tuberculosis bacilli. It works by blocking the formation of the cell wall, mycolic acids attach to the 5-hydroxyl groups of D-arabinose residues of arabinogalactan and mycolyl-arabinogalactan-peptidoglycan complex in the cell wall (Shi et al., 2007, Ramakrishnan et al., 1972). Ethambutol interrupts arabinogalactan synthesis by inhibiting the enzyme arabinosyl transferase. Due to the disruption of the arabinogalactan synthesis, the formation of this complex is prevented and leads to increased permeability of the cell wall (Musser, 1995, Ramaswamy et al., 2000). The mechanistic action of ethambutol is generally bactericidal, and the drug can penetrate the human cell membranes to exert its fatalistic effect. The mechanism action showed in **Figure 2.8**.

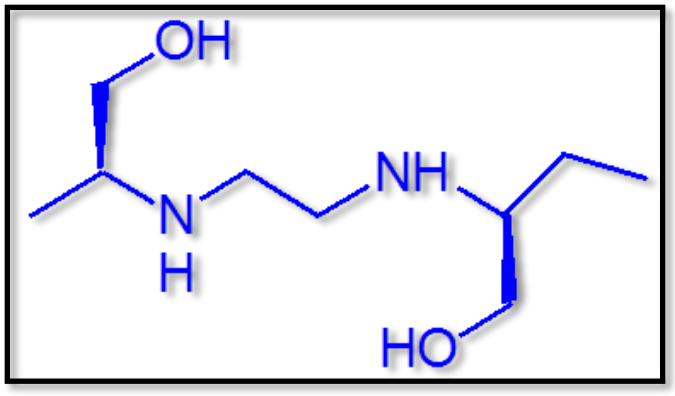

Figure 2.7: Chemical structure of ethambutol

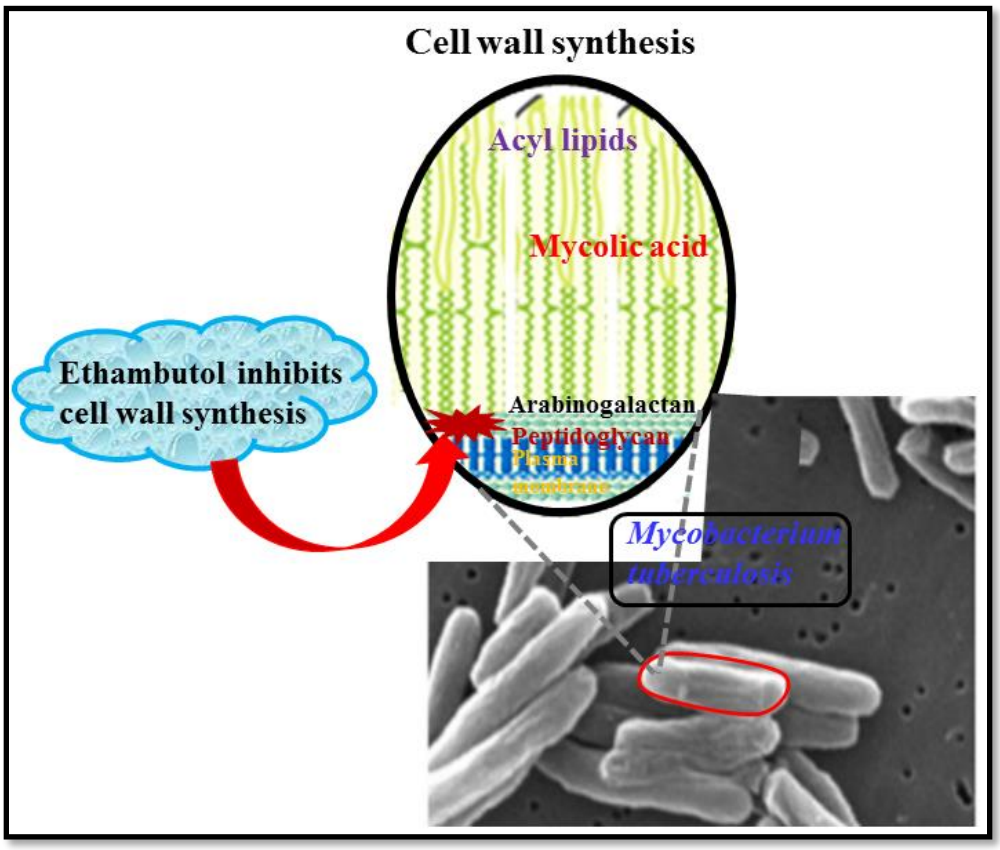

Figure 2.8: Mechanism of action of ethambutol

Da Silv et al., 2010 reported a capillary electrophoresis (CE) method for the separation of ethambutol (ETB) and its main products. The concentration range studied was from 100 to 500 µmol/L, and the detection limit was found to be 23.5 and 78.3 µmol/L, the sensitivity was 1.26 × 10^{-4} V min µmol/L (da Silva et al., 2010). Gupta et al., 2003 developed potentiometric sensor based on plasticizer in poly (vinyl chloride) (PVC) for the determination of ethambutol. The concentration ranges from 7.94 × 10^{-6}-1.0 × 10^{-1} M with a slope of 29.9 ± 0.2 mV (Gupta et al., 2003). Couto et al., 2016 described a voltammetric sensor for the determination of ethambutol based on the nafion and MWCNTs. Several concentrations of ethambutol were analyzed at the surface of Nafion/MWCNT-SPCEs and the calibration curve over a range of 0.028 to 0.28 mg/µL was obtained, and the detection limit was found to be 8.4 × 10^{-4} mg/µL and 2.8 × 10^{-2} mg/µL respectively (Couto and Quinaz, 2016).

Perantoni et al., 2011 reported a flow injection analysis of ethambutol using the graphite-paraffin composite electrode. The linear response for the technique was extended up to a 1.5 mmol/L^{-1} ethambutol solution with a detection limit of 0.1 mmol/L^{-1} (Bellei Perantoni et al., 2011). Ngece et al., 2011 developed a biosensor for the determination of ethambutol based on the silver nanoparticles (AgONPs), poly (8-anilino-1-napthalene Sulphonic acid) (PANSA) and cytochrome P450-2E1 (CYP2E1). The concentration ranges from 2-12 µM and the limit of detection was found to be 0.7 µM and the sensitivity was 1.125 µA/µM (Ngece et al., 2011). Shao et al., 2008 developed an electrochemical method for the detection of ethambutol using a glassy carbon electrode fabricated with MWCNTs. The concentration of ethambutol in the range 8.0× 10^{-6} to 2.5×10^{-4} mol L^{-1} and the limit of detection was found to be 7.6 × 10^{-7} mol L^{-1} (Shao et al., 2008).

Mohamed et al., 2015 described a UV method for the quantification of ethambutol with a detection limit of 0.82, 2.64 and 15.5 µg mL^{-1} at 250, 348 and 521nm respectively (Mohamed et al., 2015). Lima et al., 2015 developed an electrochemical method for the determination of ethambutol in aqueous medium using a gold microelectrode. The concentration range from 5.0 × 10^{-5} to 2.0 × 10^{-3} mol L^{-1} and the limit of detection and limit of quantification was found to be 4.73× 10^{-5} mol L^{-1} and 1.57 × 10^{-4} mol L^{-1} respectively (Lima et al., 2015). Rageh et al., 2015 reported a UV method for simultaneous determination of the ethambutol, isoniazid, rifampicin and pyrazinamide. ETB was determined by UV detection at 250 nm, and then INZ, RIF and PZM were derivatised and detected at 270 nm. The correlation coefficients ranged from 0.991-0.9998 with a detection limit of 18.14 to 94.34 ng/band for all the drugs (Rageh et al., 2015).

Cheemalapati et al., 2014b developed a voltammetric sensor for the simultaneous determination of ethambutol, isoniazid, pyrazinamide and hydralazine hydrochloride (HDH). The concentration range 10 – 150 µM of each analyte and the limit of detection was found to be 9.61, 6.93, 5.13 and 5.66 µM and the limit of quantification was found to be 29.15, 21.05, 15.56 and 17.18 µM respectively (Cheemalapati et al., 2014b). Song et al., 2007 reported a HPLC/MS method for simultaneous determination of the first line anti TB drugs using C_{18} reverse phase column, and the limit of detection and limit of quantification was found to be 0.01-0.5 µg/mL and 0.05-1.0 µg/mL respectively (Song et al., 2007). The HPLC technique was used by M. Yan and coworkers, for the determination of ethambutol, the linear concentrations were obtained in the range of 20-120 µg/mL and the limit of detection and limit of quantification was found to be 0.2 µg/mL and 1 µg/mL respectively. The average recovery of the samples at three levels is 99.8% (Yan et al., 2007).

Gurumurthy el al., 2004 developed a HPLC method for the determination of ethambutol in various pharmaceutical samples and biological fluids. The concentration ranged from 50-400 µg/ml and the limit of detection was found to be 25 µg/mL (Gurumurthy et al., 2004). Chenevier et al., 1998a proposed a HPLC/UV method for the determination of ethambutol in plasma. The quantification of ETB in plasma was achieved at 200 nm and the limit of detection was found to be 0.2 µg/mL (Chenevier et al., 1998a). Breda et al., 1996 developed a HPLC method for the determination of ethambutol in human plasma and urine. The concentration ranged from 10-1500 ng/mL for plasma and 10-500 µg/mL for urine. The limit of quantification was found to be 10 ng/mL for plasma and 10 µg/mL for urine (Breda et al., 1996).

Conte et al., 2002 determined ethambutol in human plasma, bronchoalveolar lavage (BAL) fluid and alveolar cells (AC) by HPLC-MS detection with detection limits of 0.05 µg/mL for plasma and 0.005 µg/mL for the BAL and AC (Conte et al., 2002). Jiang et al., 2002 reported a HPLC/UV method for the determination of ethambutol and achieved a limit of detection 0.0006 mg/mL and limit of quantification 6 µg/mL (Jiang et al., 2002). Shewiyo et al., 2012 reported a reversed phase high performance thin layer chromatography (RP-HPTLC) method for the simultaneous determination of ethambutol, isoniazid, pyrazinamide and rifampicin. The ethambutol was derivatized and detected at a VIS wavelength of 450 nm, whilst INZ, PZM and RIF were detected at 280 nm (Shewiyo et al., 2012). De Oliveira Neves et al., 2012 developed a near infrared spectroscopy (NIRS) and HPLC methods for the simultaneous determination of ethambutol, isoniazid, rifampicin and pyrazinamide. The NIRS range was 1100-2500 nm for all analytes and the correlation coefficient for the HPLC determination versus predicted values (NIRS) ranged from 0.88 to 0.98 (de Oliveira Neves et al., 2012).

Chen et al., 2005 reported a liquid chromatography (LC) and MS methods for simultaneous determination of the ethambutol and isoniazid in human plasma. The linear concentration range of 10.0-5000 ng/mL was obtained for each analyte using 100 µL plasma. The recoveries were in the range of 53.2 to 4298 ng/mL for INZ and 54.5 to 4689 ng/mL (Chen et al., 2005). Ragonese et al., 2002 reported a CE method for determination of ethambutol in various pharmaceutical samples. The concentration ranges from 25 mbar for 3 S to 50 mbar for 10 S and the coefficient of variation obtained was 0.82% (Ragonese et al., 2002). The HPLC technique was used by Ayyappan and coworkers, for the simultaneous determination of ethambutol and isoniazid. The detection wave length was 254 nm and the linear concentration range obtained was 0.25-1500 µg/mL, the limit of detection was found to be 0.083 µg/mL (Ayyappan et al., 2011).

Cheneviera et al., 1998b reported a HPLC method for the determination of ethambutol in plasma. Intra- and inter-day variabilities were lower than 5.2 and 7.6%, respectively. The limit of quantitation achieved was observed as 0.2 µg/mL (Chenevier et al., 1998b). Jadaun et al., 2007 developed a method for the determination of ethambutol MICs for mycobacterium tuberculosis (MTB) and mycobacterium avium isolates. MTB showed 96.7% sensitivity, 98.0% accuracy and 100% specificity (Jadaun et al., 2007). Mack et al., 1981 described a gas chromatographic-mass spectrophotometric method for the determination of ethambutol in human plasma, with detection limits of 36 ng (Holdiness et al., 1981). Ying Wu et al., 2011 developed a fluorescent probe method for the detection of ethambutol with detection limit of 1.7 ng mL^{-1} (Wu et al., 2011). Ming yan et al., 2007 reported a HPLC method for the determination of ETB-HCL with the recovery percentage of 99.8% (Yan et al., 2007).

Sayanna et al., 2010 developed a spectrophotometric method for the determination of ethambutol in pure and pharmaceutical samples using triphenyl methane dynes with a limit of detction of 0.51 µg mL^{-1} (Sayanna et al., 2010). Tabak et al., 1988 developed a gas chromatography method for the determination of ethambutol in air by using fluorophore. Ethambutol was quantified at levels as low as 12.5 µg/mL of extract (Tabak et al., 1988). Devani et al., 1990 reported a spectrophotometric method for the detection of ethambutol and beers law was obeyed in the range 1-14 mg/mL with the relative standard deviation (RSD) 0.43% (Devani and Shah, 1990). Suzuki et al., 1991 described a HPLC method for the determination of ethambutol in plasma and the determined range was 0.18-18 nmol/mL, with a relative standard deviation of 1.88-3.39% (Suzuki et al., 1991).

Sampath et al., 2011 developed a LCMS/MS method for the determination of ethambutol in human plasma with recovery of 100% (Sampath et al., 2011). Faria et al., 2011 reported a spectrophotometry method for the analysis of ethambutol by copper complexation in various pharmaceuticals with the recovery range of 100.9%-104.0%, and the detection limit of 0.8 mgL^{-1} (Adriana et al., 2011). Gupta et al., 2006 reported simultaneous determination of ethambutol and isoniazid resistance in clinical isolates of mycobacterium tuberculosis. 44.21, 24.73 and 14.21% of isolates were resistant to ethambutol at concentrations of 2, 4 and 6 µg/mL respectively (Gupta et al., 2006). Sivaram et al., 2015 described ultra-fast liquid chromatography – mass spectrometry method (UFLC-MS) method for the determination of ethambutol in human plasma, with a detection limit of 5.78 ng/mL (Sivaram et al., 2015). Sturkenboom et al., 2015a developed a LC-MS/MS method for the simultaneous determination of ethambutol, pyrazinamide and

isoniazid in serum, and obtained linear calibration curves in the range of 0.2-8 mg/L for ETB, INZ and 2-80 mg/L for PZM respectively (Sturkenboom et al., 2015a).

2.5 Electrochemical detection of streptomycin (STN) and mechanism action of STN

Streptomycin was first discovered by Albert Schatz in the year of 1943. It is a water-soluble aminoglycoside produced from the soil actinomycete *Streptomyces griseus*. It is mainly presented in the form of a sulphate salt of streptomycin (Syal et al., 2013). The chemical term of streptomycin sulphate is D-Streptamine, *O*-2-deoxy-2-(methylamino)-α-L-glucopyranosyl-(1→2)-*O*-5-deoxy-3-*C*-formyl-α-L-lyxofuranosyl-(1→4)-N,N^1-bis(aminoiminomethyl)-,sulphate (2:3) (salt). The molecular formula for streptomycin sulphate is $(C_{21}H_{39}N_7O_{12})_2$-$3H_2SO_4$ and the molecular weight is 1457.41 g mol^{-1}. Streptomycin was the primary antibiotic cure for TB, in 1952 Waksman has received the Nobel Prize for his discovery of streptomycin, the antibiotic active against TB. Furthermore, streptomycin is protein synthesis inhibitor and it binds to the small 16S rRNA of the 30S subunit of the bacterial ribosome, interfering with the binding of formyl-methionyl-tRNA to the 30S subunit. The microbial mechanism effects of the streptomycin was not fully understood (Cooksey et al., 1996).The chemical structure is shown in **Figure 2.9**.

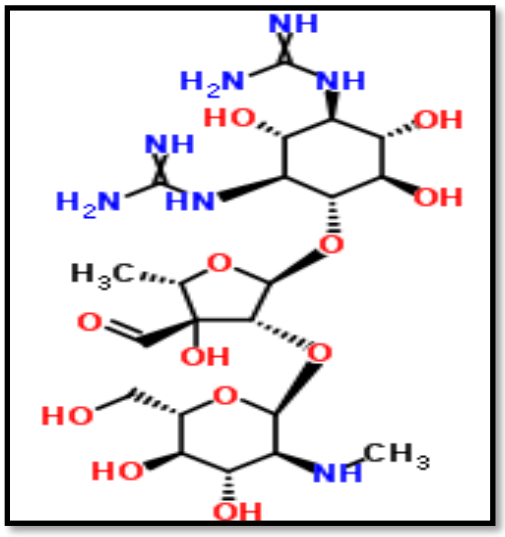

Figure 2.9: Chemical structure of streptomycin

In addition that the streptomycin causes a structural conversion which interferes with the recognition site of codon-anticodon interaction resulting in misreading of the genetic message conceded by messenger RNA (mRNA) (Spies et al., 2008, Bartlett et al., 2000). The mechanism of inhibition of protein synthesis by streptomycin is schematically shown in **Figure 2.10**.

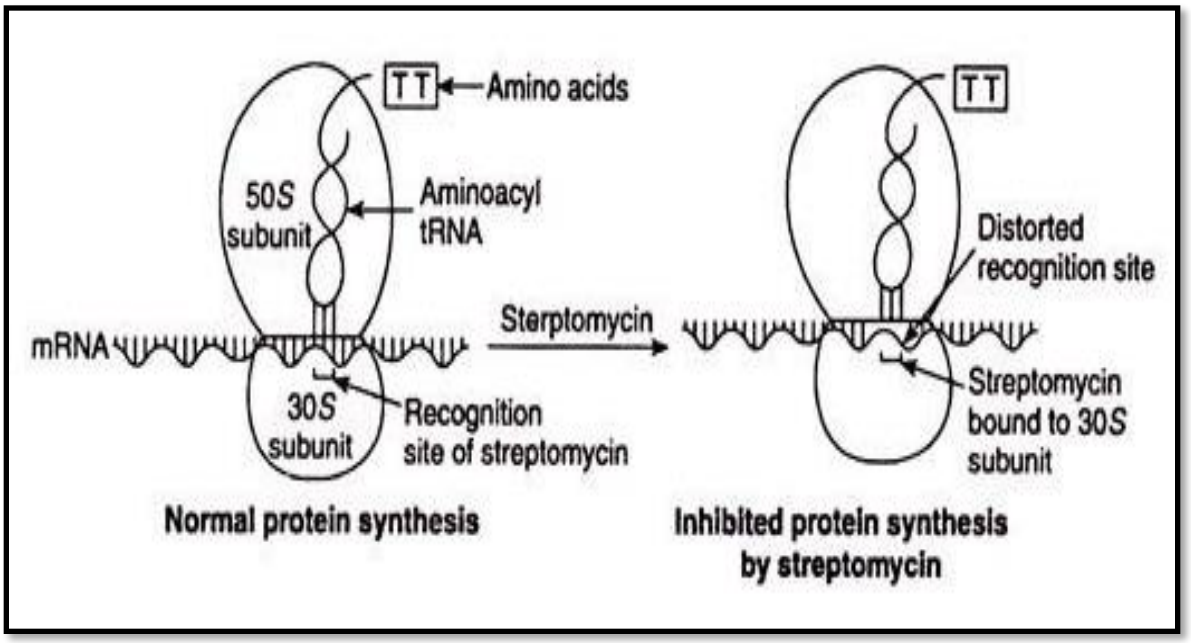

Figure 2.10: Schematic illustration of protein synthesis inhibition by streptomycin (Adapted from- Streptomycin: Discovery, Structure and Mechanism, Antibiotics)

Ototoxicity and nephrotoxicity are related with streptomycin administration. Vestibular dysfunction is more mutual than hearing damage. Renal toxicity occurs less frequently than with kanamycin or capreomycin. Hearing and renal function must be observed in patients receiving streptomycin. In addition, some low-level streptomycin resistance seems to be produced by

increased efflux as efflux pump inhibitors caused increased sensitivity to streptomycin, while the exact mechanism remains to be identified (Spies et al., 2008).

Boxer et., 1947 developed a calorimetric sensor for the determination of streptomycin in urine and broth and recovery percentages ranging from 76.5 to 87.5 % respectively (Boxer et al., 1947). Baxter et., 2001 reported an optical immunobiosensor for the detection of streptomycin in whole milk, with a detection limit of 4.1 ng/mL (Baxter et al., 2001). Yin et al., 2016 described an electrochemical aptasensor for the highly sensitive determination of streptomycin. Under the optimized conditions, the variations in the signals were linear with the concentration of STN in the range of 0.05-300 ng mL^{-1}. In this study with a low detection limit of 0.036 ng mL^{-1} was observed (Yin et al., 2016). Hanko et al., 2007 reported an anion-exchange chromatography with electrochemical detection method for simultaneous determination of streptomycin and dihydrostreptomycin (DSTN). The linear range for STN was 1.5-106 µM (20 µL), with R^2 = 0.9976, and the limit of detection and limit of quantification were 0.6 and 2 pmol STN respectively (Rohrer et al., 2007).

Hanko et al., 2010 described a high performance anion-exchange chromatography with pulsed amperometric detection (HPAE – PAD) method for the determination of streptomycin and the recoveries were in the 82.6 ± 0.6% (n=4) and 92.9 ± 0.6% (n=4) for the 10 and 41 µM concentrations respectively (Hanko and Rohrer et al., 2010). Que et al., 2013 reported an electrochemical method for the determination streptomycin with a limit of detection of 7.0 pg mL^{-1} and recoveries ranging from 82 – 124.2 % (Que et al., 2013). Fedorchuk et al., 2005 reported a voltammetry technique for the simultaneous determination of streptomycin and azithromycin in various pharmaceutical samples. The linear concentration range from 5.0 to 50.0

µg/L with the limit of detection of 3.2×10^{-11} M for STN and 1.84×10^{-10} M for Azithromycin respectively (Fedorchuk et al., 2005).

Wen et al., 2017 have developed a sensitive voltammetric sensor for the determination of streptomycin using a glassy carbon electrode modified with electro polymerized poly (pyrrole- 3-carboxy acid) and electrochemically reduced graphene oxide. Under optimized conditions, the sensor for streptomycin shows two linear ranges that cover the 2 to 80, and the 80 to 1000 nM concentration range and the limit of detection was found to be 0.5 nM (Wen et al., 2017). Ramezani et al., 2017 reported an optical and electrochemical aptasensor for the sensitive detection of streptomycin in blood serum and milk samples. The designed electrochemical aptasensor showed high selectivity towards STN with a limit of detection as low as 11.4 nM (Ramezani et al., 2017). Liu et al., 2013 developed an electrochemical method for the determination of streptomycin residues in various food samples. The catalytic currents increased linearly with the STN concentration in the range of 0.05-20 ng mL^{-1}, with a detection limit of 10 pg mL^{-1} (Liu et al., 2013).

Danesh et al., 2016 described a novel electrochemical aptasensor for the sensitive determination of streptomycin, based on exonuclease I (Exo I), complimentary strand of aptamer (CS), arch-shape structure of aptamer (Apt)-CS conjugate and gold electrode. The designed electrochemical aptasensor showed high selectivity toward streptomycin with a limit of detection as low as 11.4 nM (Mohammad Danesh et al., 2016). Leech et al., 1990 have reported ruthenium oxide modified glassy carbon electrode for detection of STN and relative antibiotics in various samples. Standard calibration graphs for streptomycin and neomycin yielded slopes of 4.43 and 0.08 nA μM^{-1} over the linear ranges of 1.5×10^{-6}-2.5×10^{-4} and 1×10^{-5}-2×10^{-3} M, respectively.

The detection limits of 1.5, 6.0 and 10 µM were found for STN, novobiocin and neomycin, respectively (Leech et al., 1990).

Liu et al., 2011 reported a facile and simple electrochemical immunoassay for ultrasensitive detection of streptomycin residues in various food samples. The linear range from 0.05 – 50 ng mL^{-1} and with a detection limit of 5 pg mL^{-1} (Liu et al., 2011). Emrani et al., 2016 developed a colorimetric and fluorescence quenching aptasensors for the determination of streptomycin in blood serum and milk samples based on double stranded DNA and gold nanoparticles. The concentration ranged from 0 to 4000 nM for both samples with a detection limit of 73.1 nM and 47.6 nM respectively (Emrani et al., 2016). Wang et al., 1986described a voltammetric sensor for the determination of streptomycin residues and related antibiotics and with a detection limits of 7 × 10^{-10} M for STN, 2.5 × 10^{-9} M for novobiocin and 1.3 × 10^{-8} M erythromycin respectively (Wang and Mahmoud, 1986).

Adams et al., 2000 reported a LC method for the determination of streptomycin and the concentration rages from 0.5 to 10 % with a detection limit of 0.100 µg and limit of quantification of 0.250 µg (Adams et al., 2000). Amen et al., 1995 reported a spectrophotometric method for the determination of streptomycin in various samples with a detection limit of 0.1 µg/mL (Aman et al., 1995). Horie et al., 2001 developed a liquid chromatography-electrospray mass spectrometry (LC-ESI-MS) for the determination of streptomycin and dihydro-streptomycin. The recoveries of streptomycin and dihydrostreptomycin from swine and bovine muscle fortified at 0.2 µg/g were 73.2 to 82.6 %, and the detection limits were 0.01 µg/g for both drugs (Horie et al., 2001). Huang et al., 2014 reported HPLC-MS method for the determination of streptomycin. The average recovery percentages ranges from 76.8 % to 100.3 % and with a limit of detection 5 µg/kg, and limit of quantification 10 µg/kg respectively (Huang et al., 2014).

Arrowood et al., 1991 reported a gas chromatography method for the determination of streptomycin in various pharmaceutical formulations and the relative standard deviation was ± 1.3 % (Arrowood et al., 1991). Nese et al., 1959 reported a method for the detection of streptomycin in various parts of the TB lungs (Nese and Omland, 1959). Bohm et al., 2012 reported a LC-MS/MS method for the determination of streptomycin and dihydrostreptomycin in honey samples. The recoveries ranges from 97% to 101 % with RSD values of 16.4 and 20.8 % respectively (Bohm et al., 2012). Bohm et al., 2010 developed a LC-MS/MS method for the detection of streptomycin in apple samples. The average recovery rate was 101-105 % with relative standard deviation of 4.1-11.4 % and the limit of quantification was found to be 2 $\mu g/kg^{-1}$ (Bohm et al., 2010).

Kurosawa et al., 1985 used a HPLC technique for the detection of streptomycin in serum samples. STN was added to serum at the level of 20.0 µg/mL and its concentration was determined to be 18.9 µg/mL with the coefficient of variation of 2.07 % (n = 5) (Kurosawa et al., 1985). Granja et al., 2009 developed a LC-MS method for the detection of streptomycin in honey samples. The recoveries of streptomycin from honey fortified at 2.5, 10, 15 and 20 $\mu g\ kg^{-1}$ levels are around 100 %. The detection limit and detection capability of streptomycin was 3 $\mu g\ kg^{-1}$ and 4.7 $\mu g\ kg^{-1}$ respectively (Granja et al., 2009). Kowalski et al., 1999 developed a capillary electrophoresis method for the determination of streptomycin in egg yolk. The average recovery percentages are 71.8 % ± 6.6 % with the relative standard deviation ranging from 2.0 $\mu g\ g^{-1}$ to 13.9 7 $\mu g\ g^{-1}$ respectively (Kowalski et al., 1999). Edrington et al., 2002 reported a determination of MICs of streptomycin for resistant salmonella isolates in swine and poultry using a micro-broth dilution system, MIC testing was carried out with the sensititre susceptibility system for streptomycin, which uses a microwell concentration gradient of 16 to 800 µg/mL.

Results indicated that >80 % of the swine isolates had MICs of ≤ 64 μg/mL, while 51 % of poultry isolates exhibited MICs of ≥128 μg/mL (Edrington et al., 2002). 1974 Hurtubise et al., developed an atomic adsorption spectrophotometry for the detection of streptomycin in disodium edetate dihydrate. The average percent recovery ranged from 94 % to 100 %, with a detection limit of 4 μg/g respectively (Hurtubise, 1974). Ghoulipour et al., 2011 described an ion exchange-high-performance thin-layer chromatography (IE-HPTLC) for the determination and separation of streptomycin in various biological fluids. The recovery percentages are 97.9 % and the relative standard deviation was < 0.94 %. The limit of detection and limit of quantification were found to be 2.4 and 12 ng respectively (Ghoulipour et al., 2011).

Do et al., 2015 developed a liquid chromatograph tandem mass spectrometer (LC-ESI-MS/MS) method for the determination of streptomycin in kiwi fruit. The average streptomycin recoveries (6 replicates each sample) were in the range of 94.8%-110.6% with relative standard deviations of < 10%. The linearity of the concentration range of 0.01-5.0 mg/kg using a matrix-matched calibration gave R^2 = 0.9995. The limit of quantification was found to be 0.01 mg/kg (Do et al., 2015). Edder et al., 1999 reported a solid phase extraction and LC method for the detection streptomycin in various food samples. The analytical recoveries were 86-94 %, with relative standard deviation of 0.4-3.5 % (n = 2 or 3) (Edder et al., 1999). Pramer et al., 1962 reported a determination of streptomycin in soil and the effect of soil colloidal material on its activity and with the recovery percentages are 100 % (Pramer and Starkey, 1962). Olitzki et al., 1952 described the most probable numbers (MPN) method for the determination streptomycin – fast cells in brucella cultures and their variability in growing and ageing cultures. The method showed that there exist differences in the numbers of resistant cells in different strains, and that in cultures originating from the same colony variations occur (Olitzki et al., 1952). Gerhardt et

al., 1994 developed a LC method for the determination of streptomycin and dihydrostreptomycin in animal tissue. The recoveries were 61.1% (coefficient of variation 7.3%) for STN and 55.3% (coefficient of variation, 8.2%) for dihydrostreptomycin. The detection limits were 10 ppb for STN and 20 ppb for dihydrostreptomycin (Gerhardt et al., 1994). Maria et al., 2002 developed a simple and rapid HPLC method for the simultaneous determination of benzylpenicillin potassium, streptomycin sulphate and related substances in Ascomicin in a veterinary use ointment. The recovery percentages are 99.1-101.8 % for benzylpenicillin potassium and 98.0 – 100.6 % for streptomycin sulphate (Maria et al., 2002).

Wang et al., 2013 reported a highly reliable and accurate indirect competitive enzyme-linked immunosorbent assay (icELISA) for the detection of streptomycin in animal-derived foods. The recoveries for all samples at five levels (15, 30, 120, 300, 600 ng g^{-1}) ranged from 71.32 % to 106.94 %. The coefficients of variation of intra- and inter-assays were below 14% and the limit of detection was found to be 0.24 ng mL^{-1} (Wang et al., 2013). Duda et al., 1973 described a spectrophotometric method for the determination of streptomycin and the absorbance was measured at 415 nm against a blank run with water instead of sample. The molar extinction coefficient of streptomycin was 17.6×10^3 in the assay (Duda et al., 1973). Drummond et al., 1951 reported the effect of heat on streptomycin and paraaminosalicylic acid (PAS) in TB culture medium and recoveries obtained when the concentration of streptomycin was 1000 mg/mL. Averaged 95.1±7 .1 % for 12 samples, and 95.6±4.9 % for 11 samples for a concentration of 500 mg/mL. The recoveries of PAS added to the liquid medium were carried out using dilutions of 0.5, 1.0 and 10.0 mg/% PAS. On a series of seven determinations, the mean percentage recoveries were 94.1± 4.9 % for the 0.5 mg/% concentration, 97.0 ± 5.0 % for a series of twelve of the 1.0 mg/% concentration and 99.2 ± 48 % for a series of 6 determination of

the 10.0 mg/% concentration (Drummond et al., 1951). Verma et al., 2012 developed a colorimetric method for evaluating streptomycin sulphate loaded with solid lipid nanoparticles (STN-SLNs) and the total drug content and entrapment efficiency of STRS-SLNs was estimated to be 89.0 % ± 1.2 % and 60.0 % ± 2.1 % (n=6) respectively. In addition the method was also evaluated for determining streptomycin in spiked human plasma samples with mean recovery of 89.1% ± 4.7 (Verma et al., 2012).

Cara et al., 2013 reported a thermal degradation of streptomycin residues in honey samples by using the HPLC method and the average recovery percentages were 9.06 to 98.12 % (Cara et al., 2013). Siddiqui et al., 2014 developed kinetic spectrophotometric method for the quantitate analysis of streptomycin and the limit of detection of initial rate method and fixed time method was obtained to be 0.011 µM and 0.50 µM, respectively while limit of quantitation upon calculation came out to be 0.032 µM and 1.5 µM for initial rate and fixed time absorbance difference methods, respectively (Raza Siddiqui et al., 2014). Mitic et al., 2006 reported the determination of streptomycin in a pharmaceutical sample based on its degradation by hydrogen peroxide in the presence of copper (II). The calibration graph is linear in the ranges 1.94-15.48 µg/cm^3 and 0.15-1.94 µg/cm^3 (Mitic et al., 2006). Demirci et al., 2013 reported a structural basis for streptomycin induced misreading of the genetic code and the crystal structures display a significant local distortion of 16S ribosomal RNA induced by streptomycin, including the crucial bases A1492 and A1493 that participate directly in codon recognition (Demirci et al., 2013). Frugeri et al., 2014 developed a spectrophotometric flow injection analysis for the detection of streptomycin in veterinary sample. The linear range of 60 up to 1000 mg L^{-1}, the limit of detection was found to be 18 mg L^{-1} and sampling rate of 36 readings per hour (Frugeri et al., 2014). Mao et al., 2013 described a synchronous fluorescence determination of

streptomycin in biological fluids with CdTe/CdSe quantum dots as fluorescence probe. The good linear relationship between the fluorescence intensity and the streptomycin concentration was obtained in the range 1.0 to 10 µmol L^{-1}, with a correlation coefficient of 0.9971 and the detection limit was found to be 25 nmol L^{-1} for STN (Mao et al., 2013). Benveniste et al., 1970 developed an enzymatic adenylylation of streptomycin and spectinomycin by R-Factor-resistant escherichia coli (Benveniste et al., 1970).

Ullah et al., 2012 described a simple and rapid HPLC method for the estimation of streptomycin sulphate. The flow rate was 1.0 mL/min; the separation was done by using C-18 column and detected by UV-Visible detector at 240 nm. The retention time was within 2.62-2.63 min. Standard curves were linear over the concentration range of 0.01 to 2 µg/L and the extraction recovery of STN was within 96 and 103 % (Ashad et al., 2012). Kurosawa et al., 1985 reported a HPLC method for the determination of streptomycin in serum samples and the concentration range are 5-50 µg/mL. STN was added to serum at the level of 20.0 pg/mL and its concentration was determined to be 18.9 pg/mL with a coefficient of variation of 2.07 % (n = 5) (Kurosawa et al., 1985). Whall et al., 1981 developed a HPLC method for the determination of streptomycin and dihydrostreptomycin and the method employs a microparticulate reversed-phase column (PBondapak Cis, LiChrosorb RP-18 or Ultrasphere Ion Pair), and a mobile phase composed of 0.02 M sodium hexanesulfonate and 0.025 M tribasic sodium phosphate in acetonitrile-water (8:92, v/v) at pH 6.0 with detection by ultraviolet absorbance at 195 nm (Whall et al., 1981). Kubo et al., 1986 reported a reversed phase ion pairing liquid chromatography for the determination of streptomycin in different serum samples and the recovery percentages are 100.0 ± 0.3 % (Kubo et al., 1986). Granados et al., 2007 reported an HPLC method for the determination of streptomycin and its putative ototoxic derivative, streptidine, in blood serum

samples. The average recovery of streptomycin and streptidine was ≥ 91.5 %, and the linearity was R^2 ≥ 0.99. The intraday and interday precisions were ≤ 9.7 and ≤1 0.6 %, respectively (Granados and Meza, 2007).

Okayama et al., 1988 developed a HPLC method for the detection of streptomycin in meat using ninhydrin as a postcolumn labelling agent and the average recovery of streptomycin added to chicken meat at the level of 2 µg/g was 66.7 %. The detection limit of STN was 0.5 µg/g (Okayama et al., 1988). Hormazhal et al., 1995 described a new HPLC ion paring and postcolumn derivatization method for the determination of dihydrostreptomycin in various milk samples. The lower limit of quantification was 25 ng/mL and the limit of detection close to 15 ng/mL. The recovery of dihydrostreptomycin sulphate varying from 82.6 to 82.8 % (Hormazábal and Yndestad, 1995). Abbasi et al., 1998 reported an HPLC method for the determination of dihydrostreptomycin in kidney, muscle and milk samples. The fluorescence response was linear from 25-2000 µg L^{-1} of injected analyte. The detection limits were 10 µg kg^{-1} for milk and 15 µg kg^{-1} for muscle and kidney and the analyte recoveries were on average 93% for milk, 70% for kidney and 75% for muscle (Abbasi and Hellenäs, 1998).

De Oliveria et al., 2009 developed a new LC – atmospheric pressure chemical ionization (APCI)-tandem mass spectrometry (MS–MS) for the determination of streptomycin and dihydrostreptomycin residues in various milk samples. The method presented adequate linearity with correlation coefficients above 0.99 for both analytes in the dynamic range of 50–400 µg/kg, and average accuracies between 84-110 %. The limit of detection and limit of quantifications were, respectively, 25 µg/kg and 50 µg/kg for both analytes (de Oliveira et al., 2009). Horie et al., 2004 reported a liquid chromatography–electrospray ionization-mass spectrometry (LC/ESI-MS) method for the simultaneous determination of streptomycin and dihydrostreptomycin in

honey samples. The recoveries of both drugs from honey fortified at a level of 0.1 µg/g was 85.8–89.1%, with high precision. The limits of quantification of the drugs in honey were 0.01 µg/g (signal-to-noise ratio >10) (Horie et al., 2004).

CHAPTER 3

MATERIALS AND METHODS

All materials and methods used in the investigations is outlined in this chapter. The general method for the synthesis of nanomaterials and also fabrication of the electrodes is also described. Moreover, this chapter deals with the preparation of general reagents and use of instrumentation, followed by the general procedure for the analysis of the pharmaceutical formulations and real samples.

3.1 Instrumentation

Voltammetric measurements were carried out with a 797 VA Computrace system with version 1.3.1 software from Metrohm (Herisau, Switzerland). A three-electrode system comprised of a platinum wire which served as a counter electrode, Ag/AgCl (3.0 M KCl) acted as a reference electrode and the fabricated GCE was used as the working electrode. All solutions were filtered before analysis using a 0.45 μM pore size cellulose acetate filter medium. All the solutions examined by electrochemistry were primarily purged with nitrogen gas for 15 minutes. A combined Thermo Gravimetric Analysis (TGA) and Differential Scanning Calorimetry (DSC) 1SF model 1346 with STAR^e software version 9.20 (Mettler Toledo, Columbus, Ohio, USA) instrument was used for the thermogravimetric characterization of the bio nanocomposite. The morphologies and characterizations were done with transmission electron microscopy (TEM) model JEM 2100 equipped with a Lab6 emitter, Max Oxford instrument for TEM analysis (JEOL Inc., Peabody USA). Fourier transformation infrared (FTIR) characterization was performed on a Varian 800 FTIR scimitar series (by SMM instruments, Durban, South Africa).

The X-ray diffractions were performed with a Philips PW1710 X-Ray Diffraction Spectrometer (XRD). An ultrasonic bath (Labcon model 5019 U) was used to prepare nanomaterial suspensions. A (CRISON digital micro pH 2000) pH meter was used for the preparation of the buffer solutions. Deionized water was provided by the Aqua MAXTM-basic 360 system.

3.1.1 Reagents

Sodium hydroxide, sulphuric acid, disodium hydrogen phosphate, sodium dihydrogen phosphate, titanium tetra chloride, urea, N, N-dimethyl formamide (DMF), copper (II) chloride pentahydrate, copper sulphate, ethanol (99.9%), $FeCl_2.4H_2O$, zinc chloride, uric acid, glucose, sodium chloride, glutamic acid, folic acid, sucrose, potassium bromide, ferrous sulphate, nickel nitrate, potassium sulphate, potassium hydroxide and acetic acid were purchased from Capital Lab Supplies (Durban, South Africa). Pure analytical grade of isoniazid, pyrazinamide, rifampicin, ethambutol, streptomycin and MWCNTs (O.D.-L 6-9 nm-5 μM) were purchased from Sigma Aldrich (Durban, South Africa). The 99.9% purity of nitrogen gas was supplied by AFROX (Durban, South Africa). Deionized water was produced from an aqua MAXTM-basic 360 series water purification system supplied by Trilab Support (Durban, South Africa). Alumina powder ≤ 3 μM was supplied by Metrohm (Durban, South Africa). All reagents and samples were prepared with deionized water filled in vials using disposable syringes and filtering through a 0.45-μm pore size, with 25-mm diameter syringe filters containing cellulose acetate as filter medium (supplied from Anatech Instruments (Pty) Ltd. Durban, SA) before analysis.

3.1.2 Preparation of stock and standard solutions

A stock solution of Isoniazid (INZ 1 M) was prepared by weighing an appropriate amount in a 10 mL volumetric flask and diluted with deionized water. 0.1 mM pyrazinamide standard solution was prepared quantitatively by weighing an equivalent amount in a 10 mL volumetric flask and diluted with deionized water. 1 M Rifampicin stock solution was prepared in a 10 mL volumetric flask by dissolving an equivalent amount in deionized water. 0.1 mM Ethambutol standard solution was made by dissolving an appropriate amount in a 10 mL volumetric flask and diluted with deionized water. A stock solution of streptomycin (STN 1 M) was prepared by balancing an appropriate amount in a 10 mL volumetric flask and diluted with deionized water. Bovine heart Cytochrome C, Horseradish peroxidase and Co enzyme Q were prepared as, 0.066 g of each Cyt C, HRP and Co en-q dissolved in 10 mL volumetric flask with 0.1 M phosphate buffer solution respectively. A 0.1 M phosphate buffer solution was prepared by dissolving a desirable amount of disodium hydrogen orthophosphate and sodium dihydrogen phosphate with suitable amount of deionized water in 250 mL volumetric flask and the desired pH was adjusted with 0.02 M H_2SO_4 or 0.1 M NaOH. All the working standard, stock and buffer solutions were kept in to the refrigerator at 4 $^{\circ}$C for stability.

3.2 Preparation methods for nanocomposites

3.2.1 Preparation and modification of glassy carbon electrode with HRP-TiO_2NPs MWCNTs for isoniazid analysis

The method for the synthesis of TiO_2NPs was modified from the previously reported method (Strushkevich et al., 2011). 25 mL of $TiCl_4$ was made up to a 100 mL volumetric flask with deionized water, in an ice cold bath. Likewise, 13 g of urea was dissolved in another 250 mL volumetric flask with deionized water. The urea solution was then slowly added on to the contents of $TiCl_4$, and then subjected to heating at 110 °C on a hot plate, with magnetic stirrer for about 30 min. After the completion of the reaction, a white colloidal solution was obtained. The colloidal solution was centrifuged at 1000 revolutions per minute with rotational centrifugal force for 15 min. After centrifugation of the product, the residue was washed repeatedly with deionized water, and then dried at 60 °C for 3-4 hours. The newly formed TiO_2NPs was then stored in the refrigerator at 4 °C, for further use. Prior to modification, the bare GCE was polished with alumina slurry on a wet polished cloth and then further washed with deionized water followed by electrochemical cleaning by cycling at a potential range of - 0.1 to + 0.7 V for 20 cycles in acidified distilled water. This process allowed the removal of any chemisorbed or physisorbed materials from the surface of the electrode. A total of 5 mg of MWCNTs was dissolved in 5 mL of DMF and thereafter kept for ultrasonification for about 30 min at 50 °C. The suspension was used for the modification of the GCE. Further, 10 mg of MWCNTs and 10 mg of TiO_2NPs were dissolved in 10 mL of N, N-dimethyl formamide (DMF) followed by ultrasonification for about 1 h, to form a stable black suspension of MWCNTs-TiO_2NPs. This was then used for the modification of the GCE. The MWCNT modified GCE and MWCNT-TiO_2NPs modified GCE were prepared by dropping 5 µL of MWCNT suspension onto the

cleaned electrode, which was then dried for 10 min at 50 °C (Bhajanthri et al., 2016). The HRP enzyme was immobilized on the MWCNT-TiO_2NPs nanocomposite fabricated on the surface of GCE. The MWCNT-TiO_2NPs-HRP-GCE sensor was fabricated by dropping 5 µL of the HRP solution onto the surface of the MWCNT-TiO_2NPs-GCE. The modified electrode was dried and then stored in the refrigerator at 4 °C (Hua et al., 2011). The fabricated electrode was now ready for use.

3.2.2 Preparation and modification of glassy carbon electrode with Cyt c-CuONPs-MWCNTs for pyrazinamide analysis

The CuONPs were synthesized according to the previous report (Aparna et al., 2012) with slight modification. 1.59 g of $CuSO_4$ was dissolved in 150 mL of deionized water to prepare 0.2 M $CuSO_4$. This initially appeared as a green coloured solution, and to this 1 mL of acetic acid was added. In another vessel 8 g of NaOH was dissolved in 25 mL of deionized water to get 8 M NaOH. In a dropwise manner, NaOH was added to the $CuSO_4$ solution with continuous stirring and was subjected to heating at 90 ^oC. This gave a black coloured precipitate immediately. The precipitate was then centrifuged, repeatedly washed 4 to 5 times with deionized water and oven dried at 60 ^oC for 3 hours. This powder was further used for the characterization of CuONPs. The bare GCE surface was initially treated with alumina slurry on a wet polishing pad and washed with deionized water, followed by ultra-sonication with an equal amount of ethanol and deionized water for about 15 min. There after the GCE was followed by electrochemical cleaning procedure with cycling at a potential range of – 1.4 to 0.1 V for 20 cycles in deionized water with 2 to 5 drops of concentrated nitric acid. This process allowed the removal of any chemisorbed or physisorbed materials from the electrode surface. 0.25 g of MWCNTs were then dispersed into 5 mL of DMF, the resulting mixture was sonicated for 30 min at 50 ^oC, to give a

black suspension. The resulting mixture was used for the coating of MWCNTS on the GCE. Equal quantities (0.30 g) of pure MWCNTs and CuONPs were dispersed into a 10 mL of DMF, the resulting mixture was sonicated for 60 min at 50 ^{o}C resulting in the formation of a black suspension. Thereafter, the GCE was immobilized in two different stages. In the first stage 5 µL of CuONPs-MWCNTs paste was coated on the surface of the bare GCE and dried at 50 ^{o}C for 15 min, whilst in the second stage the modified GCE was cooled at room temperature and then dipped in to the 1 mg mL^{-1} Cyt c solution for 7-10 h at 4 ^{o}C (Bathinapatla et al., 2015). It was then dried at room temperature for another 10 min. Cyt c was successfully adsorbed on the surface of MWCNTs-CuONPs coating, as a result fully fabricated Cyt c-CuONPs-MWCNTs-GCE was formed.

3.2.3 Preparation and modification glassy carbon electrode with Co en-q-Fe_3O_4NPs-MWCNTs for rifampicin analysis

According to previous literature (Kahani and Yagini, 2014) with slight modification, 1.21 g (0.03 M) of $FeCl_2.4H_2O$ was dissolved in a 250 mL volumetric flask with deionized water. The 4 g (1 M) NaOH was dissolved in another 100 mL volumetric flask with deionized water. Further, 150 mL of $FeCl_2.4H_2O$ was taken into the 500 mL beaker and then slowly added to 50 mL of the 1 M NaOH and then subjected to heating at 100 ^{o}C on a hot plate for about 30 min, with continuous stirring. After the completion of the reaction the reaction mixture turned into a black coloured precipitate from the original wine red colour. The precipitate was then washed several times with deionized water and filtered with Whatman-1 filter paper and thereafter dried at 50 ^{o}C for 2 hours. The newly formed Fe_3O_4NPs were kept in a refrigerator for further use. Prior to use, the GCE was polished with an alumina slurry to obtain a mirror like surface, there after washed with deionized water and sonicated with ethanol and deionized water (50:50) to remove the alumina

particles on electrode surface. It was finally rinsed with deionized water and dried in an oven. 0.10 mg of MWCNTs was dissolved in 4 mL of N, N-dimethyl formamide (DMF) and then subjected to ultra-sonication for 30 min, finally resulting in a black suspension. This suspension was used for the modification of GCE. Thereafter, 0.20 mg Fe_3O_4 and 0.20 mg of MWCNTs were dispersed into 5 mL of N, N-dimethyl formamide (DMF) and ultra-sonicated for 1 hour to give a black suspension. The resulting dispersion (5 µL Fe_3O_4-MWCNTs) was dropped to the surface of the GCE and then kept for drying in an oven at 50 ^oC for about 10 min (Wang et al., 2016). The electrode was then cooled to room temperature and thereafter 2 µL of Co en-q enzyme was added, and the coated electrode then left undisturbed at 4 ^oC for about 15 min for the complete enzyme immobilization process to occur, finally resulting in the Co en-q-Fe_3O_4NPs-MWCNTs-GCE.

3.2.4 Preparation and modification glassy carbon electrode with HRP-ZnONPs-RGO for ethambutol analysis

ZnONPs was prepared according to the previous report (Rao and Rao, 2015) with slight modification 8.17 g of $ZnCl_2$ (0.4 M) was dissolved in 150 mL ethanol. This solution was kept under constant stirring using the magnetic stirrer for 45 min to completely dissolve the zinc chloride. In another vessel 4.48 g (0.8 M) of KOH was dissolved in 100 mL of ethanol to give an aqueous ethanolic solution of KOH. The completely dissolved $ZnCl_2$ solution was put into a beaker and the 0.8 M KOH solution was added dropwise under a constant magnetic stirrer for 2 h. The beaker was then sealed and the solution allowed to settle overnight. The solution was then separated carefully and centrifuged for 5 min, and thereafter the precipitate was removed. Furthermore, the precipitated ZnO nanoparticles were washed with deionized water several times and oven dried at 50 °C. Due to the drying, the $Zn(OH)_2$ was completely converted in to ZnO.

The bare GCE was carefully polished to a mirror like finish with 0.3 μM alumina powder. It was then rinsed with deionized water, followed by successive sonication in 1:1 ethanol and deionized water for 15 min respectively. For preparing HRP-ZnONPs-RGO-GCE, 30 mg ZnONPs and 30 mg RGO were dispersed into 15 mL of N, N-dimethyl formamide (DMF) followed by ultra-sonication for about 90 min, resulting in a homogeneous suspension of ZnONPs-RGO. 5.0 μL of ZnONPs-RGO suspension was coated onto the surface of the GCE and dried in the oven at 50 ºC for 10 min (Balgobind et al., 2016). Thereafter ZnONPs-RGO-GCE was dipped into HRP solution for 1 h and kept undisturbed at 4°C for about 30 min in order to fully complete enzyme immobilization, and then allowed to dry in ambient temperature for 10 min. The resulting electrode was noted as HRP-ZnONPs-RGO-GCE. For comparison, a similar procedure was used to prepare the ZnONPs-RGO-GCE and RGO-GCE. Finally, HRP-ZnONPs-RGO-GCE was used for the electrochemical measurements.

3.2.5 Preparation and modification glassy carbon electrode with Cyt c-ZnONPs-MWCNTs for streptomycin analysis

ZnONPs was prepared according to the previous report (Rao and Rao, 2015) with slight modification and 8.17 g of $ZnCl_2$ (0.4 M) was dissolved in 150 mL ethanol. This solution was kept under constant stirring using the magnetic stirrer to completely dissolve the zinc chloride for 45 min. In another vessel 4.48 g (0.8 M) of KOH was dissolved in 100 mL of ethanol to give an aqueous ethanol solution of KOH. The complete dissolution of $ZnCl_2$ was allowed to occur in a beaker and the 0.8 M KOH solution was then added dropwise under constant magnetic stirring for 2 hours. The beaker was now sealed and the solution was allowed to settle overnight. The solution was then separated carefully by centrifuging for 5 min, and thereafter the precipitate was removed. Furthermore, the precipitated of ZnO nanoparticles were washed with deionized water

several times, and then oven dried at 50 °C. Due to the drying the $Zn(OH)_2$ was completely converted in to ZnO. A glassy carbon electrode (GCE, 3 mm diameter, Metrohm) was polished with 0.3 μM aluminium slurry and rinsed thoroughly with deionized water. The GCE electrode was individually washed by ultrasonic agitation for 5 min in ethanol and then deionized water. The electrode was then dried under nitrogen gas flow. Thereafter, 0.20 mg of MWCNTs was dissolved in 5 mL of N, N-dimethyl formamide (DMF) and then kept for ultra-sonication for 60 min, resulting in the formation of black suspension, which was used for the fabrication of the GCE. In addition, 0.40 mg ZnONPs and 0.40 mg of MWCNTs was dispersed into 20 mL of DMF by ultra-sonication for 1 hour to give a black suspension. Then, 10 μL ZnONPs-MWCNTs was dropped on to the polished electrode and kept for drying in an oven at 50 ^oC for about 15 min. The prepared ZnONPs-MWCNTs-GCE was cooled to room temperature and stored at 4 °C in refrigerator before use. In the determination process, the sensor was dipped in Cyt c enzyme solution for 20 min. 30 μL 0.6 mg/mL Cyt c was subsequently dropped on the electrode surface for 30 min incubation time. The electrode was then dried at ambient temperature for 15 min to obtain the fabricated electrode Cyt c-ZnONPs-MWCNTs-GCE.

3.3 Preparation of drug sample solutions

3.3.1 Isoniazid solution

Commercially-available INZ tablets (100 mg) were purchased from the local pharmacy. The samples (tablets) were used to evaluate the realistic performance of the MWCNT-TiO_2NPs-HRP-GCE. Ten tablets were taken into a mortar and crushed to a fine powder with pestle. A 0.1 mM INZ tablet sample solution was prepared by dissolving the appropriate amount of powder sample in a 10 mL volumetric flask and adding 10 mL of phosphate buffer solution. Finally, real sample analysis was carried out with 0.1 mM INZ by the DPV technique via the standard addition method.

3.3.2 Pyrazinamide solution

The proposed electrochemical sensor was used to examine its performance towards the determination of pyrazinamide (PZM) in real pharmaceutical formulated samples. PZM tablets (400 mg and 500 mg) were purchased from the local pharmacy. Randomly 15 tablets of PZM were selected, accurately weighed and finely grounded with mortar and pestle. An appropriate quantity of PZM was then weighed and carefully transferred into a 50 mL volumetric flask, along with 40 mL of 0.1 M phosphate buffer solution (pH 7.0) followed by 30 min ultra-sonication. In this analysis, quantitative determination of pharmaceutical samples was carried out by the standard addition method via the DPV technique.

3.3.3 Rifampicin solution

Tablet samples containing rifampicin (RIF) were purchased from the local pharmacy (Ebsar-2 Ds, R-Cin 600). The fabricated sensor was tested to determine the RIF concentration in

commercialized tablets via following procedure. 5-10 tablets were weighed and ground as a finely powdered sample. A 50 mg tablet sample was transferred into a 100 mL volumetric flask and dissolved in phosphate buffer solution. The resulting mixture was sonicated for 40 min. The analyses were performed via the standard addition method in DPV technique.

3.3.4 Ethambutol solution

Commercially available tablets (fifteen), each containing 300 mg and 500 mg of ethambutol (ETB), were completely powdered with mortar and pestle. Average weight of five tablets was determined transferred into a 50 mL standardized volumetric flask, to which 50 mL of deionized water was added and ultra-sonicated for 60 min. The resulting mixture was successively filtrated with Whatman (No 1) filter paper and the concentration of the samples was diluted and made equal to the working concentration range. The concentration of ETB in the pharmaceutical formulations were determined by the DPV, using the calibration curve plot.

3.3.5 Streptomycin solution

The detection of streptomycin in commercially accessible formulation: tablet 1 containing 300 mg streptomycin per tablet, tablet 2 and 3 containing 500 mg streptomycin per tablet. The pharmaceutical samples were made by the following process:

Five tablets were crushed in a mortar pestle and to the usual weight for tablet, and then the mass of homogeneous powder was transferred into a 25 mL volumetric flask, and diluted with phosphate buffer (pH 7.0). The obtained solution was submitted to ultra-sonication for 60 min, in order to complete the dissolution, and then filtered with Whatman Filter Paper No.1. Furthermore, an appropriate aliquot amount of the solution was added to the supporting electrolyte in the voltammetric cell and analyzed directly by differential pulse voltammetry.

3.4 Electrochemical measurements for biosensors

10 mL of the 0.1 M of phosphate buffer solution with pH 7.0 was added into the electrochemical cell in which the bare electrode or fabricated electrode was immersed prior to the electrochemical measurements. The cell was purged with nitrogen gas for 5 min to remove dissolved oxygen. To optimize the back ground current readings, several cyclic sweeps were carried out. The analyte sample was added into the electrochemical cell and stirred at 1000 rpm. An aliquot of the analyte solutions was introduced into the electrochemical cell, and the pre-concentration time, stirring was stopped and a 10 s equilibration period was allowed for the solution to become inert. The cyclic voltammetry and differential pulse voltammetry were recorded using the bare or the fabricated working electrode by scanning the potential towards the positive direction, and sweeping was done at an optimum scan rate of 0.01 Vs^{-1} in DPV mode. After each measurement, the working electrode was removed from the system and rinsed with deionized water.

CHAPTER 4

THEORETICAL FRAME WORK OF ELECTROCHEMICAL BIOSENSORS

4.1 Electrochemistry in combination with corresponding biosensor techniques

A biosensor is an analytical device, comprise two components: a bioreceptor and a trans-ducer. The main principle of a biosensor, the analytical device which translates a biological response into an electrical signal **(Figure 4.1)**. Biosensors are extremely valuable devices for determining a wide spectrum of analytes including gases, ions, organic compounds and bacteria.

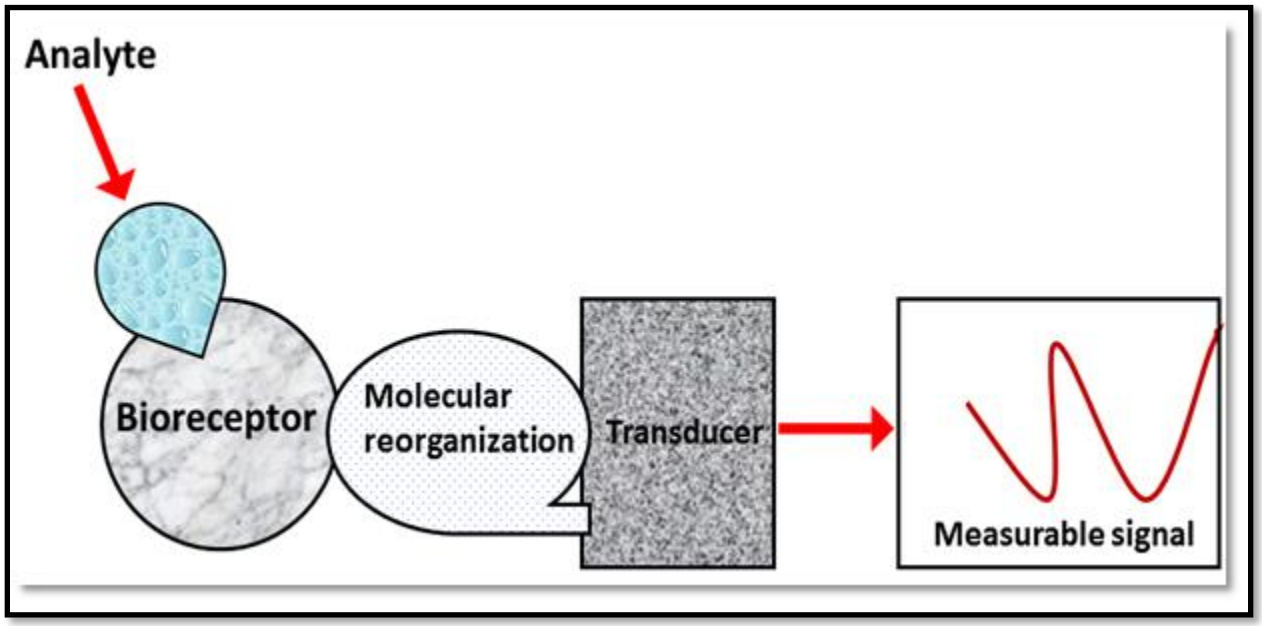

Figure 4.1: Conceptual diagram of the biosensing principle

The initial experiment to mark the origin of biosensors was carried out by Leland C. Clark in the 1960s (Clark and Lyons, 1962). Biosensors have been widely used in two primary areas such as environmental monitoring and biological sensing with a wide variety of applications. A biosensor typically operates a bio-recognition site (e.g., an enzyme, a protein, an antibody), electronic system which contain a signal amplifier, display and processor (Shah and Wilkins, 2003). A transducer should be able to convert the biorecognition into a quantifiable signal, and is classified in to three sections (1) optical measurements (2) electrochemical and (3) mass-sensitive measurements. The significant part of a biosensor is the transducer which makes use of a physical change accompanying the reaction illustrated in **Figure 4.2**.

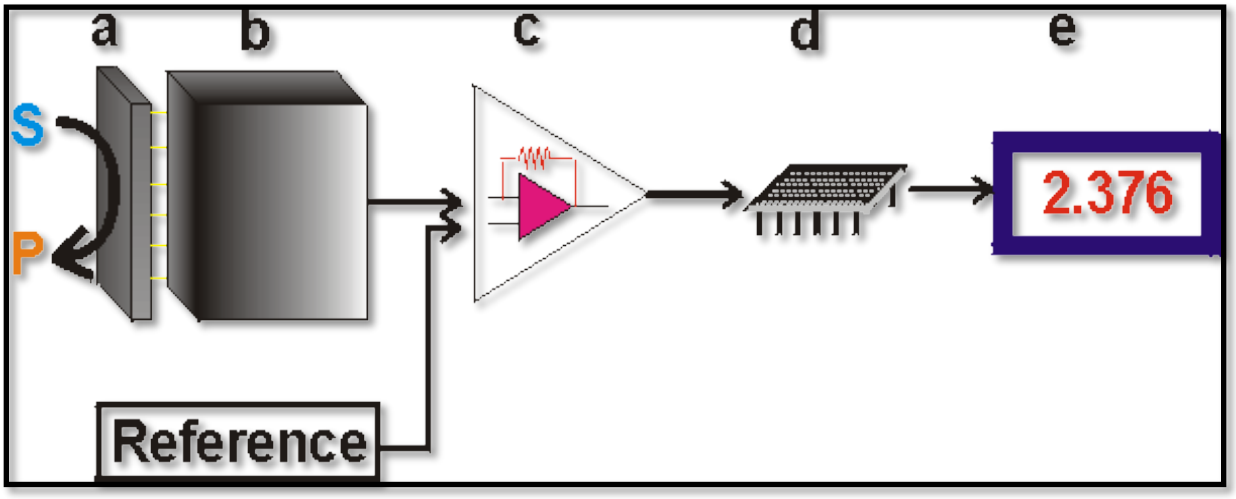

Figure 4.2: Schematic illustration showing the main components of a biosensor. The biocatalyst (a) converts the substrate to a product. This reaction is determined by the transducer (b) which converts it to an electrical signal. The output from the transducer is amplified (c), processed (d) and displayed (e) (Sabr, 2016)

4.2 Bioreceptor

The bioreceptor is a biomolecule that identifies the target analyte whereas the transducer converts the recognition event into a measurable signal. Moreover, many types of bioreceptors are used nowadays and the main types include enzyme bioreceptors and cellular bioreceptors.

4.2.1 Enzyme bioreceptor

Enzymes are macromolecular biological substances generally used as bioreceptors based on their precise binding abilities as well as their catalytic activity. Additionally, most enzymes are used to make building blocks of body such as amino acids and proteins (Yaghi et al., 1998). These enzymes require another chemical component called a cofactor, which are either organic compounds (heme and flavin) or inorganic ions (Cu^{2+}, Zn^{2+}, Ni^{2+}, Fe^{2+}) and a coenzyme (ATP, NADPH and NADH). Finally, enzymes provide good catalytic activity and allow for much lower detection limits than would be obtained with common binding techniques (Sherigara et al., 2003). In this present work, horseradish peroxidase, cytochrome c and coenzyme q enzymes were used as enzyme bioreceptors to construct the enzyme based biosensor for the determination of first line anti TB drugs.

4.3 Interfacial electrochemistry

Current improvements in the arena of material science and characterization techniques have blossomed ‘Electrochemistry’ as a multidisciplinary branch acquired from Physics, Biology, Chemistry and Chemical Engineering. Furthermore, the conversion of Electrochemistry from 18^{th} century to the present stage is attributed to the thermodynamic, kinetic and quantum mechanical study possible at the ‘surface’ mutually to the experimentalist and theoretician. Electrochemistry is the branch of chemistry that employs electrochemical methods to get

information related to the amounts, environments of chemical species and properties (Bard and Faulkner, 2001). Electrochemical determination is another extensively used transduction technique in biosensors and associated to optical techniques, it is very sensitive, shows sufficient selectivity, good accuracy, and precision and easy to operate (Rüdel et al., 1996, Tobalina et al., 1999).

According to Isaac Maurits Kolthoff electroanalytical chemistry is defined as the application of electrochemistry to analytical chemistry. It is better to study electroanalytical chemistry as that area of analytical chemistry and electrochemistry in which the electrode is used as a probe, to measure approximately that directly or indirectly involves the electrode (Plambeck, 1982). Electroanalytical methods are one of the best known analytical techniques due to the following advantages:

a) Relatively low cost of equipment and wide spectrum of analytes (especially drug samples)

b) Low detection, determination limits and high sensitivity.

c) Possibility of furnishing results in real time or close to real time.

d) Selectivity resulting from the choice of electrode material

e) Relative simplicity, rapidity.

f) Application as miniaturized sensors where other sensors may not be useful.

4.4 Classification of electroanalytical methods

Electroanalytical chemistry involves a group of quantitative analytical techniques that are based upon the electrical properties of the solution (Kissinger and Heineman, 1996). There are basically three types of electroanalytical measurements:

1) Coulometry

2) Potentiometry

3) Amperomerty and Voltammetry

4.4.1 Coulometry

Coulometry is an electroanalytical method for measuring an unknown concentration of an analyte in solution by totally changing the analyte quantitively from one oxidation state to another oxidation state. Coulometry is classified into two methods: **controlled-potential coulometry**, in which we apply a constant potential to the electrochemical cell, and **controlled-current coulometry**, in which we pass a constant current through the electrochemical cell **(Figure4.3)** (Kauffmann and Vire, 1993).

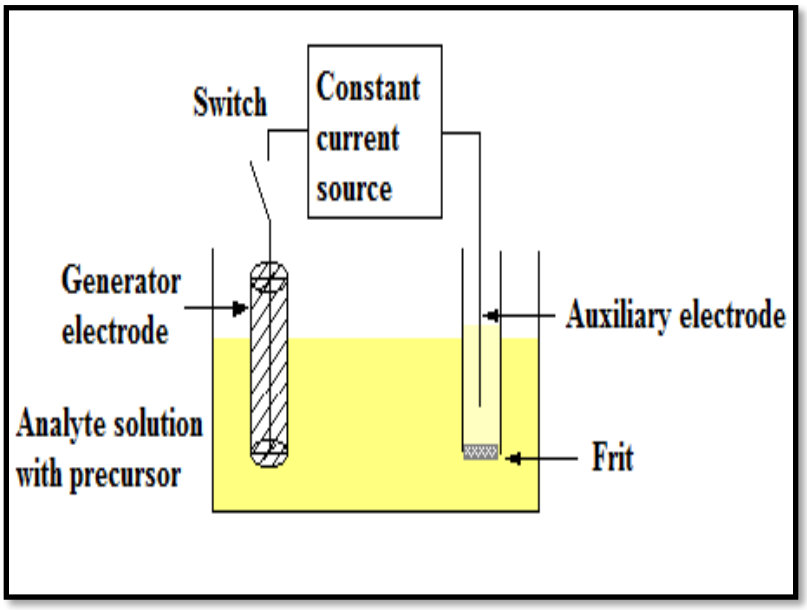

Figure 4.3: Schematic of a coulometric cell used for coulometric titration (Chemicool, 2017)

Coulometric study is an application of Faraday's first law of electrolysis and the extent of the chemical reaction at an electrode is directly proportional to the amount of electricity passing through the electrode (Lingane, 1958). During an electrolysis process, the total charge Q, in coulombs, passing through the electrochemical cell is proportional to the absolute amount of analyte by Faraday's law

$$Q = nFN_A \tag{4.1}$$

where n is the number of electrons per mole of analyte, F is Faraday's constant (96487 C mol^{-1}), and N_A is the moles of analyte. A coulomb is equivalent to an ampere per sec, and when passing a constant current i, the total charge is

$$Q = i\, t_e \tag{4.2}$$

where t_e is the electrolysis time. If the current varies with time, as it does in controlled-potential coulometry, then the total charge is **(Figure 4.4)**

$$Q = \int_0^{t_e} i\,(t)dt \qquad (4.3)$$

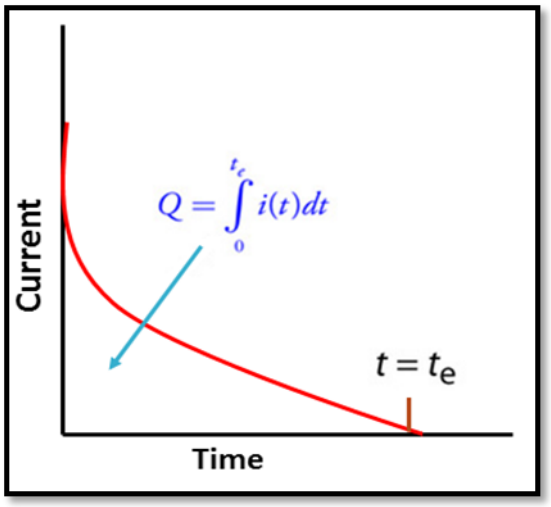

Figure 4.4: Current versus time for a controlled-potential coulometric analysis. The measured current is shown by the red curve. The integrated area under the curve is the total charge (Harvey, 2017)

4.4.2 Potentiometry

In the potentiometry method, the potential of an electrochemical cell is measured below the static circumstances because no current flows while measuring solutions potential and its composition remains unaffected. In potentiometry the data on a composition of the sample is obtained through the potential appearing among two electrodes **(Figure 4.5)** and the current path between the two electrodes can be of high resistance (Andreescu and Marty, 2006). In the year of 1889, the Nernst equation was developed and helped in connecting an electrochemical cells potential to the concentration of electroactive species in the cell. Potentiometric determinations are based upon

measurements of electrochemical cells under zero current, where the Nernst equation governs the operation of potentiometry.

$$E_{cell} = E^0_{cell} - (RT/nF)\ InQ \quad (4.4)$$

where, E_{cell} = cell potential under non-standard conditions (V)

E^0_{cell} = cell potential under standard conditions

R = universal gas constant (8.341 J mol-K)

T = temperature (K)

n = no of moles of electrons exchanged in the electrochemical reaction (mol)

F = Faraday constant 96500 Coulombs/mol

Q = reaction quotient

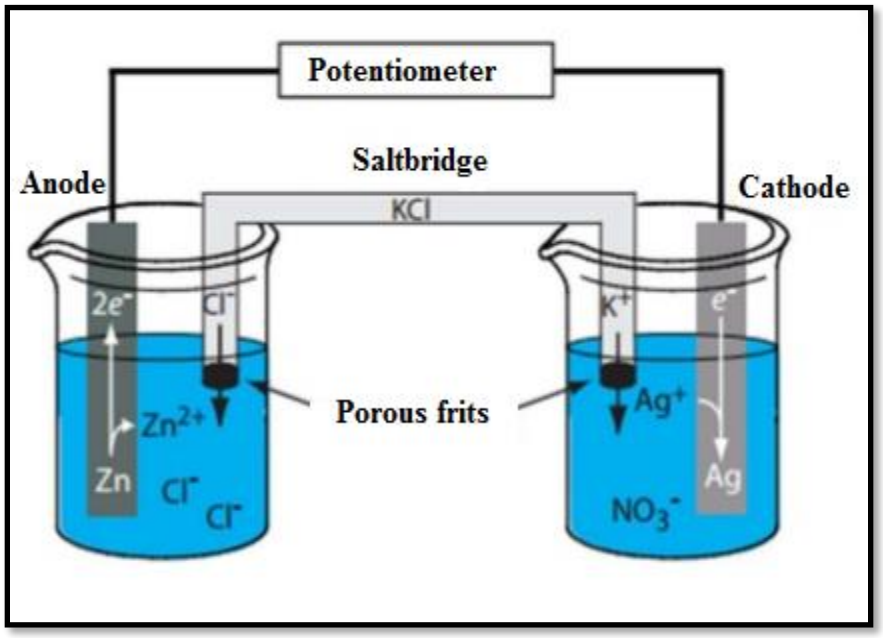

Figure 4.5: Schematic illustration of an electrochemical cell used for potentiometric measurement (Harvey, 2002)

Potentiometric analysis is classified into two analytical techniques: direct potentiometry and potentiometric titrations. In direct potentiometry, the cell potential is determined and correlated to the activity or concentration of the different chemical species. In potentiometric titration, the variation in cell potential is observed as a function of the volume of reagent added (Wang, 2002).

4.4.3 Voltammetry/Amperometry

The polarography method was established in 1922 by the Czechoslovakia chemist Jaroslav Heyrovsky and he received the Noble Prize in 1959. From his development of polarography, voltammetry was also developed and now it becomes one of the important branches in the field of electroanalysis. The primary voltammetric techniques experienced many difficulties, making

them less ideal for repetitive analytical use (Lubert and Kalcher, 2010). However, in the 1960s and 1970s substantial advances were made in all areas of voltammetry (methodology, instrumentation and theory), which improved the sensitivity and extended the range of analytical methods. The mutual characteristic of all voltammetric techniques is that, they include the application of a potential (E) to an electrode and then monitoring the resulting current (i) flowing through the electrochemical cell. In various cases, the applied potential is varied, or the current is monitored over a period of time (t). Hence, all voltammetric methods can be defined as function of E, i, and t. They are measured as active methods because the applied potential forces a modification in the concentration of an electroactive types at the electrode surface by electrochemically oxidizing or reducing it (Galus, 2015). The analytical advantages of the several voltammetric methods contain outstanding sensitivity with a very large useful linear concentration range for both organic and inorganic species. The techniques normally used are voltammetry, potentiometry, coulometry, polarography and conductometry (Eggins, 2008, Ronkainen et al., 2010, Heyrovský, 1956). The sensitivity limits of common electroanalytical techniques are shown in the **Table 4.1**. Moreover, the literature survey for the last 25 years shows that polarography and voltammetry have been used in the inorganic, physical, and organic field, mostly for the pharmaceutical and biological applications. Voltammetric techniques are also useful for the determination of compounds of pharmaceuticals and, when coupled with HPLC, they are active tools for the analysis of complex mixtures. Amperometry is also a voltammetric technique, which is based on the measurement of current at a fixed operating potential. If this potential is suitably selected then the magnitude of current is directly proportional to the concentration (Scholz, 2011). The electrochemical sensors use amperometric measurements for the current resulting from the reduction or oxidation of an electroactive

species in a biochemical reaction. In this study, amperometric devices were used to measure the current-voltage relation and is outlined below.

Table 4.1: Sensitivity limits of electroanalytical methods

Serial number	Techniques	Sensitivity limits/M
1	AC polarography, Thin layer coulometry	10^{-4} to 10^{-5}
2	Chronocoulometry, Classical polarography	10^{-5} to 10^{-6}
3	Derivative polarography, Square wave polarography, Linear sweep voltammetry, Chemical stripping analysis	10^{-6} to 10^{-7}
4	Differential pulse polarography, Amperometry, Conductivity	10^{-7} to 10^{-8}
5	Anodic stripping with hanging mercury drop electrodes	10^{-8} to 10^{-9}
6	Anodic stripping with thin film electrodes or solid electrodes	10^{-9} to 10^{-10}

4.4.3.1 Voltammetric methods and theoretical characteristics

Many voltammetric techniques are produced commercially for the determination of definite species that are of curiosity in industry and research. The methods used in the voltammetry were illustrious from each other by the potential function that is applied to the working electrode to drive the electrochemical reaction, and by the material used as the working electrode. The voltammetric techniques are classified into many types, some of these are listed below:

- Staircase Voltammetry (SV)
- Linear Sweep Voltammetry (LSV)
- Cathodic Stripping Voltammetry (CSV)
- Square Wave Voltammetry (SWV)
- Normal Pulse Voltammetry (NPV)
- Anodic Stripping Voltammetry (ASV)
- Fast Scan Cyclic Voltammetry (FSCV)
- Cyclic Voltammetry (CV)
- Differential Pulse Voltammetry (DPV)

Staircase Voltammetry (SV) was introduced about thirty years ago as a digital counterpart to the widely used Linear Sweep Voltammetry. In SV, the potential sweep is a sequence of steps and the current was measured at the end of each potential change (Markovic et al., 1997).

Linear Sweep Voltammetry (LSV) is a voltammetric technique where the current at working electrode is measured while the potential among the working electrode and reference electrode is swept linearly in time. LSV involves applying a linear potential sweep to the working electrode (modified electrode) while monitoring at the same time the current flowing in the circuit. Here the signal generator produces a voltage step from E_i to E_f and a potentiostat spread on this potential wave to the electrode under study. Finally, the scan direction can be negative or positive and in principle, the sweep rate can possess at any constant value.

$$\text{Sweep rate} = dE/dt \tag{4.5}$$

Cathodic Stripping Voltammetry (CSV) is a voltammetric method for the quantification of specific ion species and metal species form their reduction current. CSV was parallel to the trace analysis process of anodic stripping voltammetry, except that for the electroplating step, the potential is held at an oxidizing potential, and the oxidized species are stripped from the electrode by sweeping the potential positively (Yaacob et al., 2014, Hrabánková et al., 1969). Furthermore, the stripping step can be also linear, square wave, staircase or pulse.

Square Wave Voltammetry (SWV) was introduced by Barker in the year of 1957. SWV is superimposed on the potential staircase sweep and SWV employs scan rate up to 1 V/sec or faster, allowing much quicker determinations (Author, 1957). Reduction or oxidation of species is registered as a peak or through in the current signal at the potential at which the species begins to be oxidized or reduced (Christie et al., 1977). In the SWV method, the peak potential occurs at the $E_{1/2}$ of the redox couple because the current is symmetrical around the potential.

In **Normal Pulse Voltammetry (NPV)** the cell current resulting from a series of ever large potential pulse are compared with the current at a constant 'baseline' voltage. The potential is varied using pulses of increasing amplitude and the current is tested after each voltage pulse (Aoki and Osteryoung, 1980). Another type of pulse voltammetry is square wave voltammetry, which can measured a different type of differential pulse voltammetry in which equivalent time is consumed at the potential of the ramped baseline, and potential of the superimposed pulse.

Anodic Stripping Voltammetry (ASV) technique was used for the quantitative determination of specific ionic species. The increasing use of the ASV method is due to its ability to simultaneously determine some elements at concentration levels ranging down to the tiny parts per billion range with relatively inexpensive instrumentation (Švancara et al., 2010). The analyte concentration is electroplated on the working electrode during an oxidized from the electrode during the stripping step and deposition step. The current is measured during the stripping step (Barón-Jaimez et al., 2013). The oxidation of the species is registered as a peak in the current signal at the potential at which the species begins to be oxidized. The stripping step can be also square wave staircase, linear, or pulse.

Fast Scan Cyclic Voltammetry (FSCV) was established by Julian Millar and colleagues in London in the early 1980s. FSCV is a linear sweep voltammetric method in which the background subtracted voltammogram gives additional information about the electroanlyzed species with high scan rate up to 1×10^6 Vs^{-1} (Alkire et al., 2008, Holze, 2009). It is a comparatively fast technique which has been accelerated by many orders of magnitude to provide progressive resolution in subsecond time typically recorded every 100 ms, but the fast scan rate decreases the signal to noise ratio.

Cyclic Voltammetry (CV) was primary reported in 1938 and theoretically defined by Radies and later it has been established for the estimation of charge transfer mechanisms. CV is a very important amperometric technique that allows one to scan the potential of working electrode either in cathodic or anodic directions and observe peaks due to reduction or oxidation of the reactions. The electrode system in CV is dictated by the nature of the medium as well as the process being calculated. CV is a simple voltammetric method and provides a great deal information about electrochemical behaviour of the analyte. Moreover, in recent years several voltammetric methods has been established for the measurement of electrode reactions. The unique features of CV are its ability to produce a potentially reactive species and then to study it directly by reversal, so providing an electrochemical overview for a reaction system.

The main advantages of cyclic voltammetry are:

- The wide applicability of electrode materials and relatively low-cost instrumentation.
- Greater flexibility in setting up scan limits and reversal conditions and highly developed theory.
- An essential ability for highlighting the chemical conditions between various electroactive species present in the voltammogram.
- A direct estimation of electrode reversibility is provided, because the potentials at which oxidation and reduction occur are observed directly within range.
- A wide variety of five orders of magnitude in scan rates is possible.

Cyclic voltammetry responses can be calculated in three ways depending on the analyte response of such reversible, irreversible and quasi reversible reactions.

(i) Cyclic Voltammetry with reversible system

The system is defined as "reversible" when the electrode kinetics is considerable faster than the rate of diffusion. The Nernst equation is the ultimate boundary condition for a reversible reaction:

$$\frac{[Ox]_{x=0}}{[Red]_{x=0}} = \exp\left[\frac{nF}{RT}\,(E - E^0)\right] \tag{4.6}$$

This equation (4.7) can be rewritten as

$$\mathrm{E} = E^0 + \frac{RT}{nF}\ln\frac{[Ox]_{x=0}}{[Red]_{x=0}} \tag{4.7}$$

Where $[X]_{x=0}$ is the concentration of analyte at the electrode surface

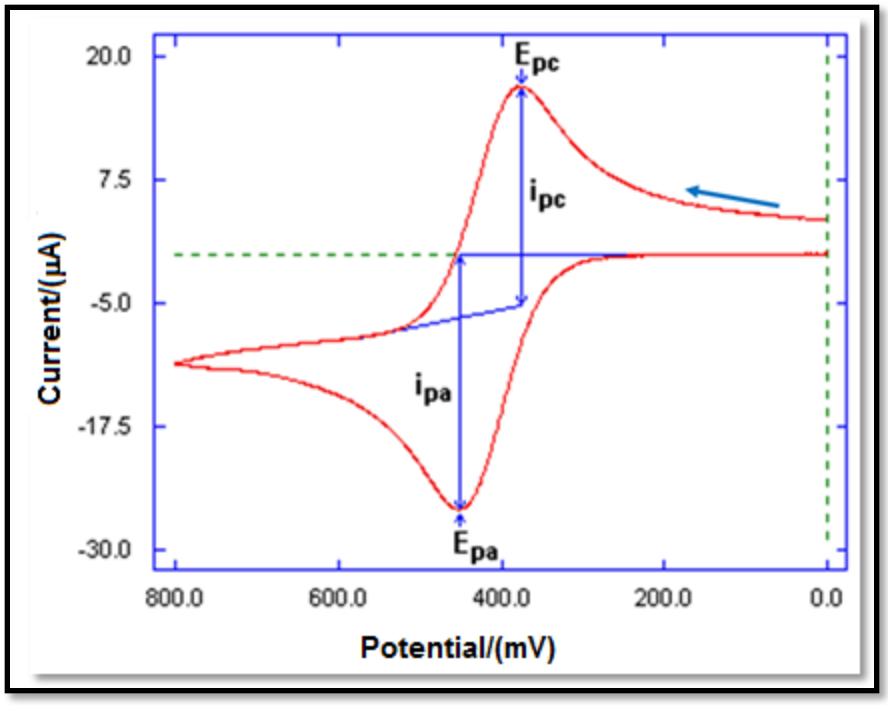

Figure 4.6: A reversible system. The arrow shows the direction of the initial scan (Basi, 2017)

Figure 4.6 indicates that the electron transfer mechanism is reversible i.e. the system primarily undergoes oxidation followed by reduction. The equation for peak current in linear sweep voltammetry at 298 K is (Eqn 4.8)

$$i_{pa} = 2.69\ x10^5 A C_0 n^{3/2} {D_R}^{1/2} v^{1/2} \quad (4.8)$$

Where $i_{pa}$the anodic peak current in amperes, A is the surface area of the electrode in cm^2, C_0 is the concentration in mol cm^{-3}, n is the number of electrons transferred, D_R is the diffusion coefficient in $cm^2\ s^{-1}$, and V is the scan rate in V s^{-1}.

Peak potential of E_p is given below (Eqn 4.9)

$$E_p = E^0 - 1.109 \frac{RT}{nF} \quad (4.9)$$

If the peak is broad, the peak potential could be difficult to analyse, hence sometimes it is easy to calculate the potential at $i_{p/2}$, named half-peak potential, $E_{p/2}$ can be calculated using Eqn 4.10

$$E_{p/2} = E^0 + 1.109 \frac{RT}{nF}$$

$$\therefore \quad E_p - E_{p/2} = 2.20 \frac{RT}{nF} \quad (4.10)$$

Moreover, the peak potential (E_p) is independent of the scan rate (v) and the peak current (i_p) is proportional to $v^{1/2}$.

(ii) Cyclic voltammetry with irreversible systems

The system is defined as “irreversible” when the electrode kinetics are slower than the rate of diffusion. For an irreversible system (those with slow electron exchange), the individual peaks are reduced in size and widely separated. **Figure 4.7** shows a characteristic response where the peak extreme clearly shifts with the applied voltammetric scan rate. Totally irreversible systems are quantitatively characterized by a shift in the peak potential with scan rates. The shape of the voltammogram mostly depends upon the mechanism of the electrode process. Cyclic voltammetry can provide information about the number of electrons transferred in each peak. The analytical criteria for two important systems are discussed and others are presented in **Table 4.2**.

Table 4.2: Analytical criteria for the charge transfer reactions

System	Analytical criteria
(a) Reversible $Ox + ne^- \rightleftharpoons Red$	E_p is independent of; $E^o = (E_p^a - E_p^c)/2$ $E_p^c - E_p^a$ = (59/n) mV at 25° C and is independent of ν; $ip/\nu^{1/2}$ is independent of ν; i_p^a/i_p^c is unity and independent of ν Wave shape is independent of ν
(b) Quasi reversible $Ox + ne^- \rightleftharpoons Red_{(low\ \nu)}$ $Ox + ne^- \rightarrow Red_{(high\ \nu)}$	E_p shifts with ν $E_p^c - E_p^a$ may approach (60/n) mV at low ν but increases as ν increases $i_p/\nu^{1/2}$ is nearly only for α = 0.5
(c) Irreversible $Ox + ne^- \rightarrow Red$	No current response in reverse scan E_p shifts cathodically by (30/αn) mV per ten-fold increase in ν The wave shape is determined by α and is independent of ν
(d) Preceding reversible chemical reaction $Z \underset{k_b}{\overset{k_f}{\rightleftharpoons}} Ox \overset{ne^-}{\rightleftharpoons} Red$	E_p shifts anodically with an increase in ν $i_p/\nu^{1/2}$ decreases as ν increases
(e) Following reversible chemical reaction $Ox + ne^- \rightleftharpoons Red \underset{k_b}{\overset{k_f}{\rightleftharpoons}}$	E_p shifts cathodically with an increase in ν $ip/\nu^{1/2}$ virtually constant with ν i_p^a/i_p^c decreases from unity as ν increases
(f) Charge transfer with catalytic regeneration $Ox + ne^- \rightleftharpoons Red + Z$ k_c	E_p shifts anodically by a maximum of (60/n) mV $i_p/\nu^{1/2}$ increases at low values of ν and becomes independent in higher ν i_p^a/i_p^c is unity
(g) Following irreversible dimerization reaction $Ox + ne^- \rightleftharpoons Red$ $2Red \xrightarrow{k_d} Z$	E_p shifts cathodically by (20/n) mV per tenfold increase in ν and per tenfold decrease in initial concentration, C^*_{ox} $ip/\nu^{1/2}$ decreases a maximum of 20% from low to high ν i_p^a/i_p^c increases with ν and decreases as C^*_{ox} increases.

Furthermore, the Nernstian boundary condition is replaced by a kinetic boundary condition when equilibrium is not engaged at the electrode surface as shown in Eqn 4.11

$$\frac{i}{FA} = D_0 \left[\frac{\partial C_0(x,t)}{\partial_x}\right]_{x=0} = k_f\,(t)\; C_0\,(0,\,t) \qquad (4.11)$$

Where k_f is the rate constant for reduction

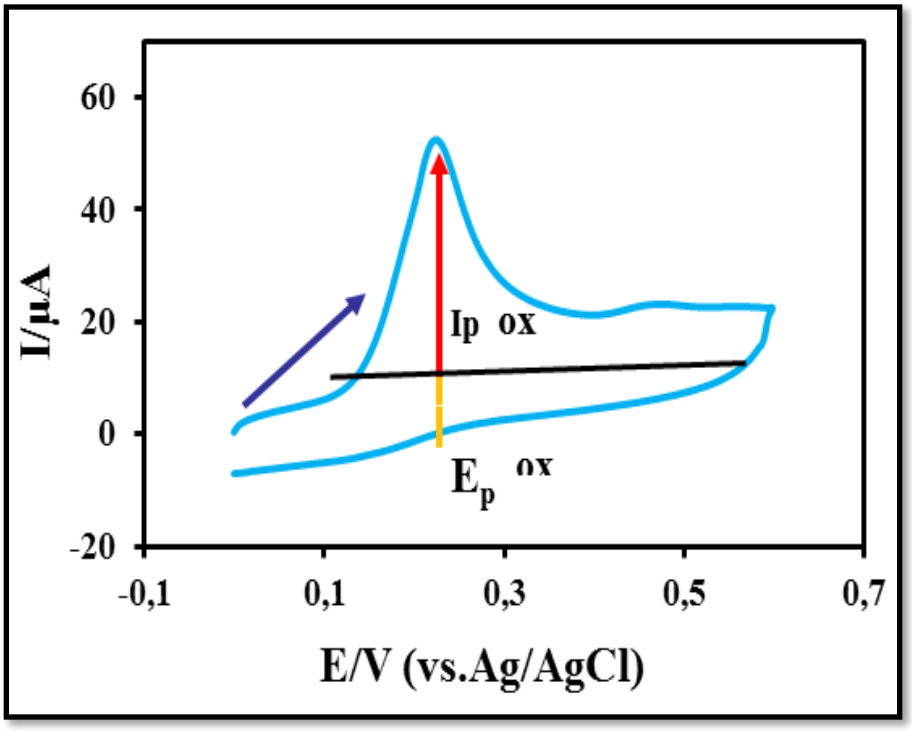

Figure 4.7: An electrochemically-irreversible voltammogram. The numerical values illustrated are dimensionless values of current and potential. The arrow indicates the direction of the initial scan (Chokkareddy, 2017)

In irreversible systems, the peak potential appears at higher potentials, accurately beyond E_0 value, due to the small amounts. Hence, a bigger overpotential is being requested to lead the reduction. The peak current for irreversible systems (at 298 K) is given by Eqn 4.12,

$$i_{pa} = 2.99\ x10^5 AC_0\alpha^{1/2}{D_R}^{1/2}v^{1/2} \quad (4.12)$$

Where $i_{pa}$the anodic peak current in amperes, A is the surface area of the electrode in cm^2, C_0 is the concentration in mol cm^{-3}, n is the number of electrons transferred, D_R is the diffusion coefficient in $cm^2\ s^{-1}$, and V is the scan rate in $V\ s^{-1}$.

The peak potential for irreversible system is given below

$$E_p = E^0 - \frac{RT}{\propto F}\left[0.780\ +\ \ln\ \frac{D_0^{1/2}}{k_0} + (\frac{\propto Fv}{RT})^{1/2}\right] \quad (4.13)$$

$$E_p - E_{p/2} = \frac{1.857\ RT}{\alpha F} \quad (4.14)$$

Accordingly, for a totally irreversible system, E_p depends on the scan rate, variably (for reduction) in a negative direction by 30 mV at 298 K (or 1.15RT/αF) for each tenfold increase in the scan rate (v).

(iii) Cyclic voltammetry with quasi-reversible systems

Quasi-reversible system was developed by Matsuda and Aybe for reactions that show electron-transfer kinetic limitations. These systems are transitional state between reversible and irreversible systems as shown in **Figure 4.8**.

Used for the one-step, one electron case,

$$Ox + e^- \underset{K_b}{\overset{K_f}{\rightleftharpoons}} Red$$

The resultant boundary condition is given by Eqn (4.15)

$$D_0 = \langle \frac{\partial C_0(x,t)}{\partial_x} \rangle_{x=0} = k^0 \, e^{-af\,[E(t) - E_0]} \{C_0\,(0, t) - C_R\,(0, t)\, \boldsymbol{e^f}^{[E(t) - E_0]}\} \quad (4.15)$$

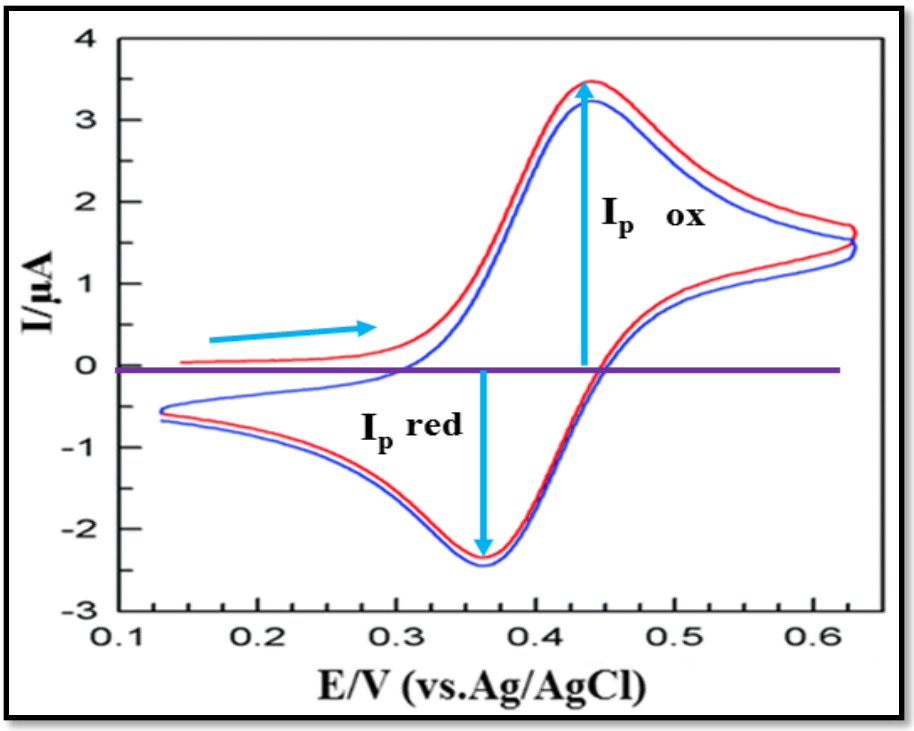

Figure 4.8: Cyclic voltammogram of a quasi-reversible system. The numerical values shown are dimensionless values of current and potential. The arrow indicates the direction of the initial scan (Song, 2016)

Current is given by Eqn 4.16

$$i = FAD_0^{1/2}C_0 f^{1/2} \nu^{1/2} / \Psi(E) \quad (4.16)$$

Where, $f = F/RT$, Ψ (E) is a function of the quasi-reversible system, A is the area in cm^2, D_0 is the diffusion coefficient in cm^2s^{-1}, C_0 is the concentration in mol cm^{-3} and ν is the scan rate in Vs^{-1}.

$$\Delta = \frac{k_0}{D_0 1/2\left(\frac{F^{1/2}}{RT}\right)\nu^{1/2}}$$

When $\Delta > 10$, the behaviour approaches that of a reversible system.

The values of i_p, E_p and $E_{p/2}$ depends on Δ and α. The peak current is given by

$$i_p = i_p\,(\mathrm{rev})\ K\,(\Delta, \alpha)$$

Where, i_p (rev): is the reversible i_p value. For a quasi-reversible reaction, i_p is not proportional to $\nu^{1/2}$. The peak potential is given by an integral equation which is solved using numerical methods. A Nernstian, quasi-reversible, or totally irreversible behaviour depends on the Δ and on the scan rate employed.

Electrochemical cell contains of the sample dissolved in a solvent, an ionic electrolyte, and three electrodes: working electrode (WE), reference electrode (RE) and counter electrode (CE). The main working principle of cyclic voltammetry is that the applied potential is measured against the RE, while the CE closes the electrical circuit for the current to flow. Furthermore, the obtained measurements are plotted as current vs voltage, also known as a voltammogram and also ascertain a meaningful chemical reaction. Hence, the critical influence of the scan rate is very significant because the extent of a scan must provide appropriate time for a specific chemical reaction. Additionally, the varying scan rates showed equivalent results and also varied for example, with an increase in the scan rate the oxidation and reduction peak potentials slowly move to the right and left sides with a steady increase and decrease in the oxidation and reduction peak currents. The developed biosensors depend mainly on the size and shape of the voltammogram for a given compound, and depends not only on the scan rates and the electrode surface, but also depends on the catalyst (enzymes or nano materials) concentration.

Differential pulse voltammetry/polarography is the most commonly used voltammetric technique and it is equivalent to normal pulse voltammetry in that the potential is also scanned with a series of pulses. It is similarly well appropriated for reversible and irreversible systems and showed high sensitivity. The digital instruments indicate staircase shaped signals and increase through the direct potential, to which small square wave pulses with a constant potential (pulse amplitude) are useful in periodic series. The DPV varies from normal pulse voltammetry (NPV) because each potential pulse is fixed, of small amplitude (10 to 100 mV), and is superimposed on a slowly shifting base potential. In the pulse mode current is measured at two points for each pulse, the first point just before the application of the pulse and the second at the end of the pulse time. The difference amongst the current measurements is plotted against the through potential and produces peak-shaped polarograms, as the difference in current is the largest for the potential modifications around the half-wave potential as shown in **Figure 4.9**.

According to the Ilkovich equation

$$i_p = \frac{n^2F^2}{4RT} AC_0 \Delta E_A \sqrt{\frac{D}{\pi t_p}} \qquad (4.17)$$

In reversible electrode processes, the peak height i_p in the DP polarograms is proportional to the analyte concentration C_a and is determined by the amplitude ΔE_A of the square wave pulses as well as by the pulse time t_p among other factors (Gumede, 2008). Moreover, the detection limit for determinations by differential pulse voltammetry is like that for square wave polarography at about 10^{-7} - 10^{-8} mol/L; but, the decrease in sensitivity resulting from irreversibility is lower.

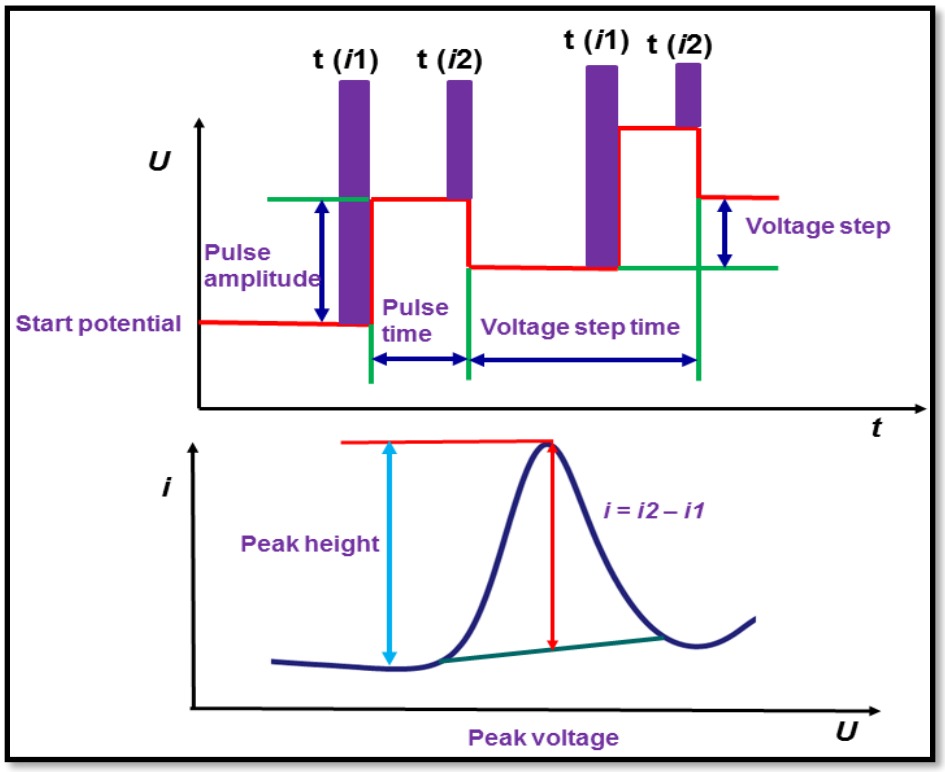

Figure 4.9: A typical DPV measurement process whereby the current is measured twice at each mercury drop, before each pulse and at the end of the pulse time. The difference between the measurements is plotted against the direct potential and produces peak-shaped polarograms, as the change in current is the largest for the potential alterations in the region of the half-wave potential. Typical current-potential curve expected for a DPV measurement (Kerman, 2007)

4.4.4 Three electrode system

Figure 4.10 shows the three-electrode system. Here the working electrode or modified electrode is used to study the redox reactions of the compounds. Reference electrode, whose high potential stability is constant enough so that it can be occupied as the reference standard against which the potentials of the additional electrodes present in the cell can be measured. There are various reference electrodes that are used, the simplest is when the reference electrode is used as a half

cell to develop an electrochemical cell. Generally used reference electrodes are the silver-silver chloride electrode (Ag/AgCl/4M KCl, e = 0.222 V) or the calomel electrode (Hg/HgCl/KCl). Auxiliary or counter electrode, which serves as a basis for electrons so that current can be passed from the external circuit through the cell. The regular material for cell construction is Pyrex glass for reasons both of prominence and general chemical inertness. The working electrode can be provided the transduction component in the biochemical reaction, while the counter electrode creates a connection to the electrolytic solution therefore that a current can be applied to the working electrode. These electrodes would be chemically and conductively stable. Hence, gold, platinum, carbon (e.g. graphite) and silicon composites are generally used, depending on the analyte.

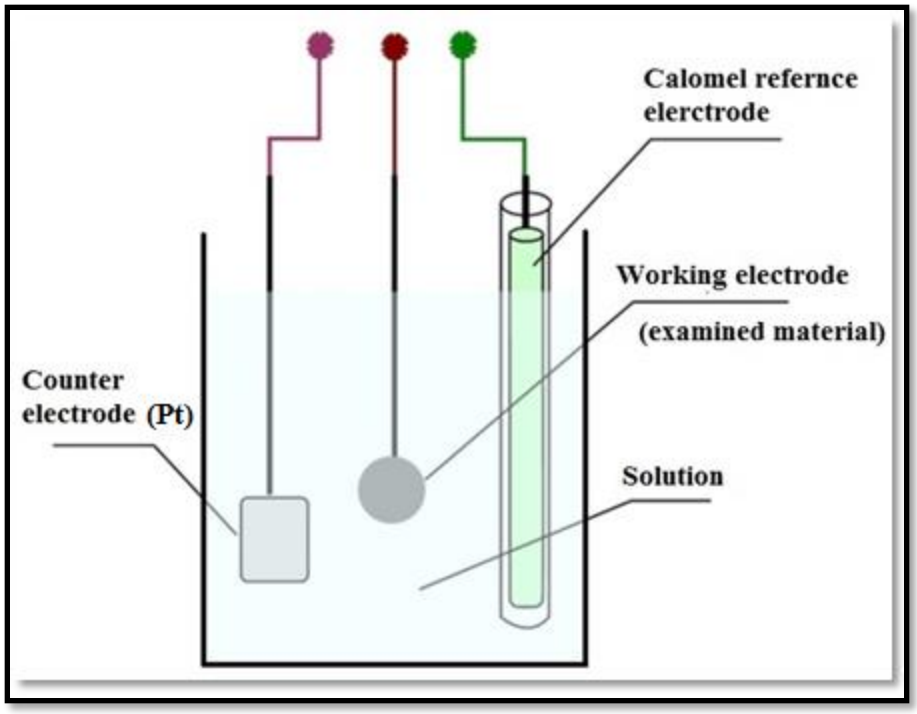

Figure 4.10: A typical electrochemical cell consists of three electrode systems (Roy, 2017)

4.4.4.1 Metal electrodes (Au and Pt)

Metal electrodes are the critical interface between a stimulating or measuring device, and the entity to be measured or stimulated. Electricity flows through wires by electron flow. It flows through tissue or fluid by ion flow, and to produce an ion from an electron, a chemical reaction is necessary. Nobel metals like gold and platinum have generally been used as electrode substrates. Noble metal electrodes can offer very promising electron transfer kinetics and an extensive anodic potential range and cathodic potential window of these electrodes is usually controlled due to the low hydrogen overvoltage. Furthermore, the establishment of surface oxide or adsorbed hydrogen layers may lead to high background currents, which powerfully move the kinetics of the electrode reaction. To avoid this problem, a pulse potential cycle must be done before the electrochemical experiments (Johnson and LaCourse, 1990). **Figure 4.11** shows the gold and platinum electrode.

Figure 4.11: Gold electrode and platinum electrode

Gold electrodes act equally to platinum, but have limited usefulness in the positive potential range due to the oxidation of its surface. They has been very useful, but the modification electrodes containing surface structures known as self-assembled monolayers (SAMs) (Baś et al., 2006). Further metals, such as nickel, silver and copper are also used as electrode materials due to the specific applications, such as the determination of carbohydrates or amino acids in basic medium (copper and nickel) and of sulphur or cyanide compounds (silver). In addition, many alloy electrodes like platinum–ruthenium and nickel–titanium electrodes have also been described, which are frequently used for the preparation of fuel cells, due to their bifunctional catalytic mechanism.

4.4.4.2 Carbon electrodes

The carbon compounds have been widely used as electrode substrates to make several electrodes. Due to the soft properties of carbon, such as wide-ranging potential window, rich surface chemistry, low background current and comparative chemical inertness these electrode surfaces can easily be renewable for electron exchange. Carbon is a passive electrode material, carbon is useful for both oxidation and reduction in both aqueous and nonaqueous solutions. Many forms of carbon have been used to make suitable electrodes including pyrolytic graphite (a high density, highly oriented form of graphite), spectroscopic-grade graphite (usually impregnated with ceresin or paraffin wax), graphite isolated in epoxy resin or silicone rubber carbon paste (spectroscopic-grade graphite mulled in sufficient Nujol to form a stiff paste), and vitreous or glassy carbon electrode.

4.4.4.3 Vitreous or glassy carbon electrode

Vitreous carbon can also be formed as a foam. It is then called reticulated vitreous carbon (RVC). This foam was first established in the year of 1960s as a thermally insulating, microporous glassy carbon electrode material **(Figure 4.12)**. Glassy carbon is an electrically conductive and gas impermeable material, highly resistant to chemical attack and obtainable in pure state. From the previous studies, it was realised that glassy carbon electrode materials synthesized at high heat-treatment and shows good electrochemical activity. Glassy carbon electrode is prepared by controlled heating program of a pre-modeled polymeric (phenol-formaldehyde) resin body up to 3000 °C.

Figure 4.12: Glassy carbon electrode

The structure of glassy carbon involves thin, tangled ribbons of cross-linked graphite-like sheets. Because of its high density and small pore size, no saturated procedure is required. Moreover, a surface pre-treatment is frequently employed to create active and reproducible glassy-carbon

electrodes and to improve their analytical performance, glassy carbon electrode is polished using alumina in the form of polishing cloth or powder, which stimulates it in electron transfer reactions. The electrode should then be rinsed with deionized water before use. This behaviour has been thoroughly examined using electrochemical as well as other microscopic techniques

Glassy carbon electrode advantages

- High resistivity to heat and chemicals
- Excellent thermal and electrical conductivity
- Little or no contamination on its fine impermeable structure
- Absolute gas impermeability like glass and light weight and high mechanical strength

4.4.4.4 Rotating disc electrode (RDE)

The partial anodic potential of mercury electrodes has excluded their utility for monitoring oxidizable compounds. Hence, solid electrodes with extended anodic potential windows have attracted substantial analytical interest **(Figure 4.13)**. Of the various different solid materials that can be used as working electrodes, the ones most often used are platinum, carbon and gold. Nickel, Silver and copper can also be used for specific applications. The solid electrodes can be rotating or stationary, generally in a planar disk configuration. Such electrodes contains of a short cylindrical rod of the electrode material surrounded in a tightly fitting tube of an shielding material (Teflon, KelF etc.) It is critical to avoid crevices among the sleeve and the electrode materials, and thus to avoid solution creeping (and an increase in background response). Electrical interaction is made at the final face and the RDE provides an effective and

reproducible mass transport and hence the analytical measurement can be made with precision and high sensitivity.

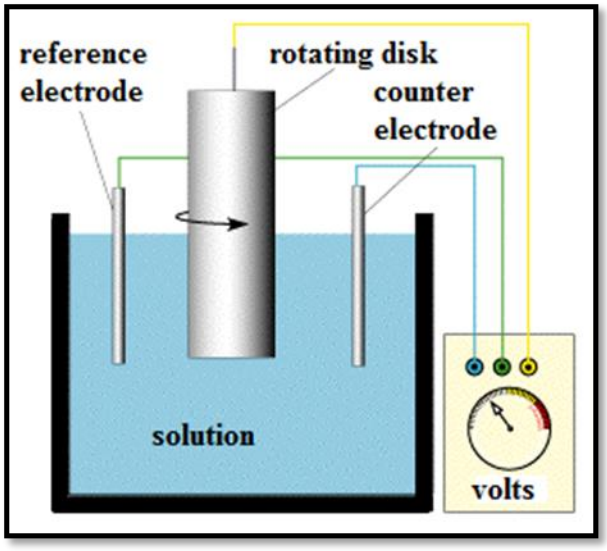

Figure 4.13: Graphical illustration device of rotating disc electrode (University of Cambridge, 2017)

4.4.4.5 Chemically modified electrodes (CMEs)

An active area of investigation in electrochemistry is the development of electrodes formed by chemical modification of many conductive substrates. Such electrodes have been tailored to accomplish a wide-range of functions. The deliberate modification of electrode surfaces can thus meet the needs of several electro-analytical problems, and may form the basis for new analytical application and different sensing devices (Msagati and Ngila, 2003). Moreover, there are many ways in which CMEs can advantage analytical applications. These include acceleration of preferential accumulation, electron-transfer reactions. Such steps can impart higher sensitivity, selectivity, or stability to electrochemical devices. Several significant applications, such as

precise release of drugs, electrochromic devices, electro combination, and corrosion protection, should also benefit from the rational design of electrode surfaces. One of the utmost significant properties of CMEs is their capability to catalyze the oxidation or reduction of solute types that exhibits high over voltages at unmodified surfaces. Thus, CMEs play a vital role in reducing the high overvoltage essential for the voltammetric detection of analyte without its main interferences. Moreover, the most important analytical use for such electrodes is as analytical sensors selective for specific species or functional groups. Many substrates such as Multiwalled Carbon Nanotubes (MWCTs), Reduced graphene oxide (RGO), Titanium oxide nanoparticles (TiO_2NPs), Iron oxide nanoparticles (Fe_3O_4NPs) Polymer films, Metalloporphyrins, Calixarenes etc. are used for the modification of electrode surfaces. For the present investigation, the modification methods adopted are MWCTs, RGO based modification, and TiO2NPs based modification and enzyme immobilization.

4.5 Supporting electrolyte

The supporting electrolyte is an inert soluble ionic salt added to the solvent, usually in 10-fold or 100- fold excess over the concentration of the species being calculated. The inertness meant here is the ability to avoid oxidation or reduction at the indicating or reference electrode, while the electrochemical measurements are being made. Additionally, there are three functions of the supporting electrolyte. Firstly, it transmits most of the ionic current of the cell since its concentration is much higher than that of the other species in solution. Thus, it helps to complete the circuit of the electrochemical cell and retain the cell resistance at a low value. Secondly, it keeps a constant ionic strength. This is essential because the structure of the interphase region should not change significantly if a reaction arises here.

A stable structure is formed on the electrolyte side by adding a high concentration of an inert salt. Thirdly, migration current detected is reduced by the presence of excess of ions that are not electrochemically active at the potentials in use, because they can carry an ionic current without permitting its change into electronic, and hence net or measured, current at the electrodes.

CHAPTER 5

RESULTS AND DISCUSSION

Electrochemical characterization and detection of isoniazid, pyrazinamide, rifampicin, ethambutol and streptomycin

This chapter deals with the results initiate from the experimental part of the electrochemical work. The experimental work is mainly divided into two sections, viz., nanocomposite electrochemical sensor for the determination of the isoniazid, pyrazinamide, rifampicin and ethambutol, and the development of horseradish peroxidase (HRP) based biosensor for the determination of isoniazid (INZ) and streptomycin (STN), cytochrome c (Cyt c) modified biosensor for the detection of pyrazinamide (PZM) and streptomycin (STN), coenzyme q (Co en-q) based biosensors for the determination of rifampicin (RIF), as well as HRP based biosensor for the detection of ethambutol (ETB) are discussed.

5.1 Nanocomposite voltammetric sensor for the determination of isoniazid

In this work HRP was immobilized on the glassy carbon electrode using titanium oxide nanoparticles (TiO_2NPs) and anchored with multiwalled carbon nanotubes (MWCNTs). MWCNTs facilitate the electron transfer among the electroactive species and electrode, while N, N dimethyl formamide was used as a dispersing reagent for the carbon nanotubes (Ra et al., 2005). Furthermore, TiO_2NPs were added onto the MWCNTs and immobilized with HRP to produce other electro catalytic sites and substantially increase the sensitivity, and limit of detection of the fabricated electrode. To the best of our knowledge this is the first electrochemical attempt using MWCNT-TiO_2NPs-HRP-GCE for the determination of isoniazid.

5.1.1 Characterization of the MWCNT-TiO_2NPs-HRP-GCE

The MWCNT-TiO_2NPs-HRP-GCE was characterized using FT-IR, X-ray diffraction (XRD), transmission electron microscopy (TEM), and thermogravimetry (TGA) techniques. FT-IR was performed to assess characteristic stretching variations for synthesized TiO_2NPs. **Figure 5.1A** reveals the presence of a sharp peak at 523 cm^{-1} indicating the presence of Ti-O stretching vibrations. A well-defined sharp peak appeared at 1403 cm^{-1}, indicating the Ti-O-Ti stretching vibrations. The peak at 1163 cm^{-1} is responsible for C-O stretching (Azad and Ganesan, 2012).

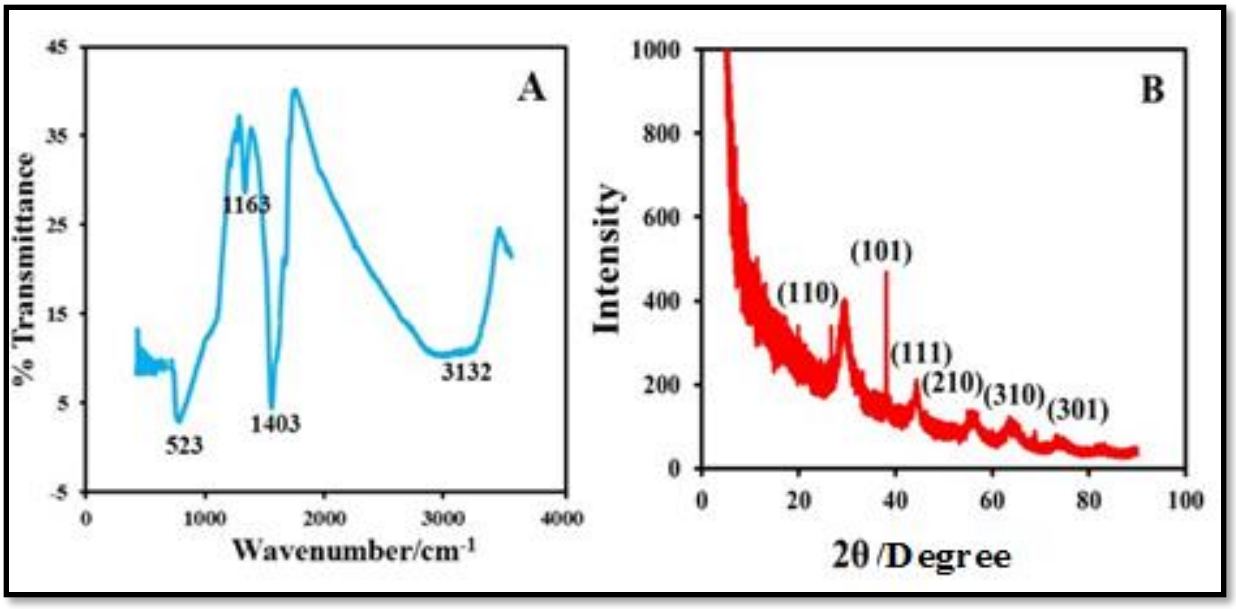

Figure 5.1: (A) Fourier transform infrared spectroscopic (FT-IR) characterization of titanium oxide nanoparticles (TiO_2NPs). (B) X-ray diffraction (XRD) image of TiO_2NPs

In addition, peaks at 3132 cm^{-1} were attributed to the presence of O-H stretching. **Figure 5.1B** shows the XRD data, with Miller indices (101,110, and 111) attributed to the body-centred cubic, crystalline nature of the TiO_2NPs. The broad diffraction peaks are an indication of the nano-size of the crystalline compound. The experimental XRD pattern obtained agrees with the 2θ peak at 25.4° and confirms the TiO_2 anatase structure (Asadpour-Zeynali et al., 2016). The strong diffractions at 25° and 48° were also attributed to TiO_2NPs in the anatase phase (You et al., 1999). The above evidence confirmed the presence of synthesized TiO_2NPs.

Figure 5.2A is the TEM image of the TiO_2NPs, which clearly indicates the spherical shape geometry of TiO_2NPs with an average diameter of 25 nm. **Figure 5.2B** shows TEM of pure MWCNTs as having tubular network-like structures. **Figure 5.2C** clearly shows the adherence of TiO_2NPs on the surface of the MWCNTs. **Figure 5.2D** shows the thermogravimetric curves of pure MWCNTs, TiO_2NPs and MWCNTs-TiO_2NPs. The TGA curve of MWCNTs (black line in **Figure 5.2D** denoted by i) exhibited definite mass loss at 570 °C, which may possibly be due to the carbon oxidation. The TGA curve of TiO_2NPs which one showed nearly flat characteristics with minor mass loss observed before 100 °C, and this may be due to loss of water, whereas at 400 °C this may signify loss of nitrogen content. The TGA curve of MWCNTs-TiO_2NPs also showed slight mass loss in two stages around at 100 °C and 250 °C, respectively; this may be due to the evaporation of the solvent. Beyond this temperature, the composite was highly stable due to the dispersion of TiO_2NPs on the surface of MWCNTs. The graphical illustration of the electrochemical oxidation of INZ at HRP-TiO_2NPs-MWCNTs-GCE is shown in **Scheme 5.1**.

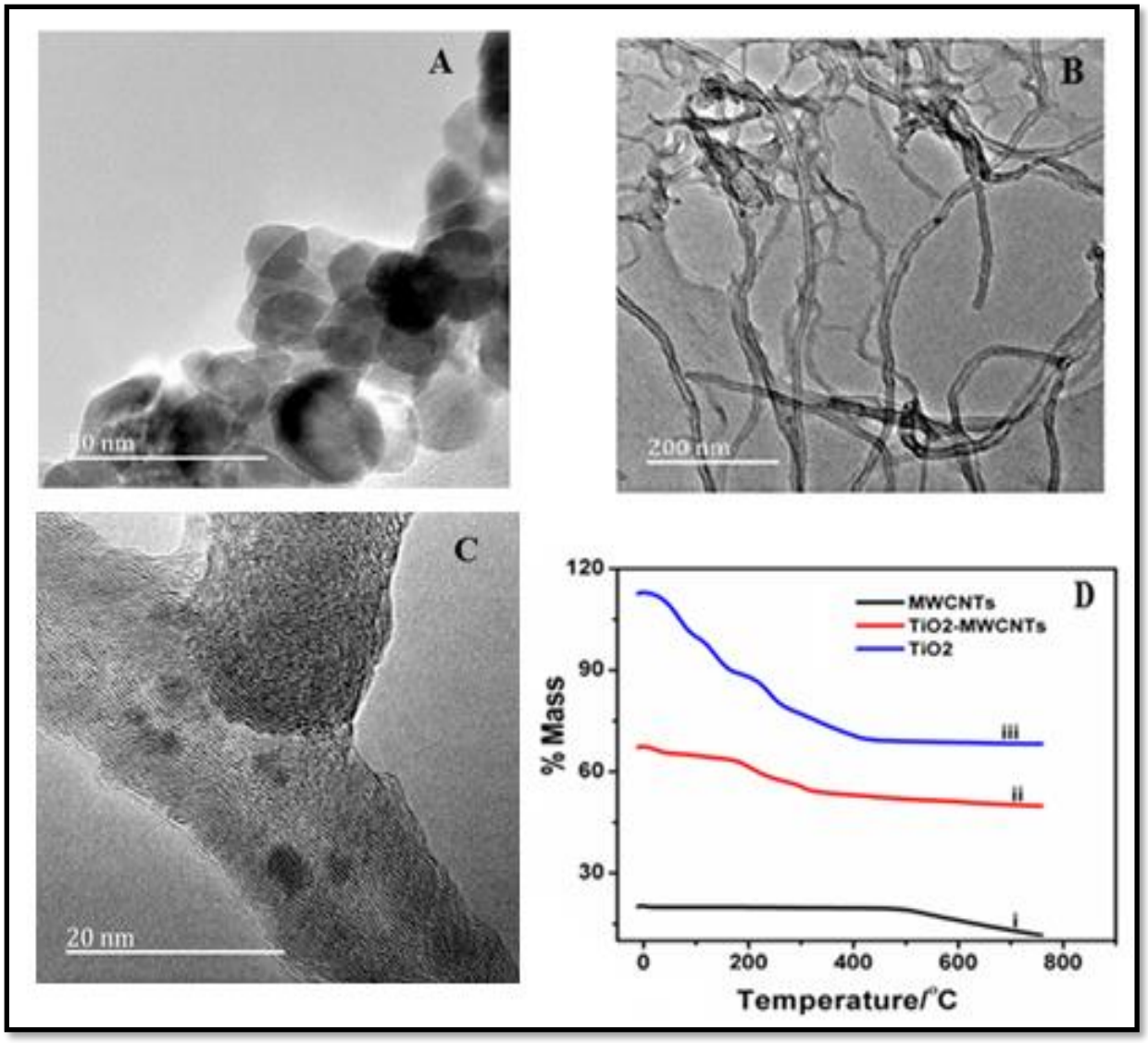

Figure 5.2: (A) Transmission electron microscopy (TEM) image of TiO_2NPs (B) Pure multiwalled carbon nanotubes (MWCNTs) (C) MWCNTs-TiO_2NPs (D) Thermogravimetry (TGA) curves for: (i) MWCNTs; (ii) MWCNTs-TiO_2NPs; and (iii) TiO_2NPs

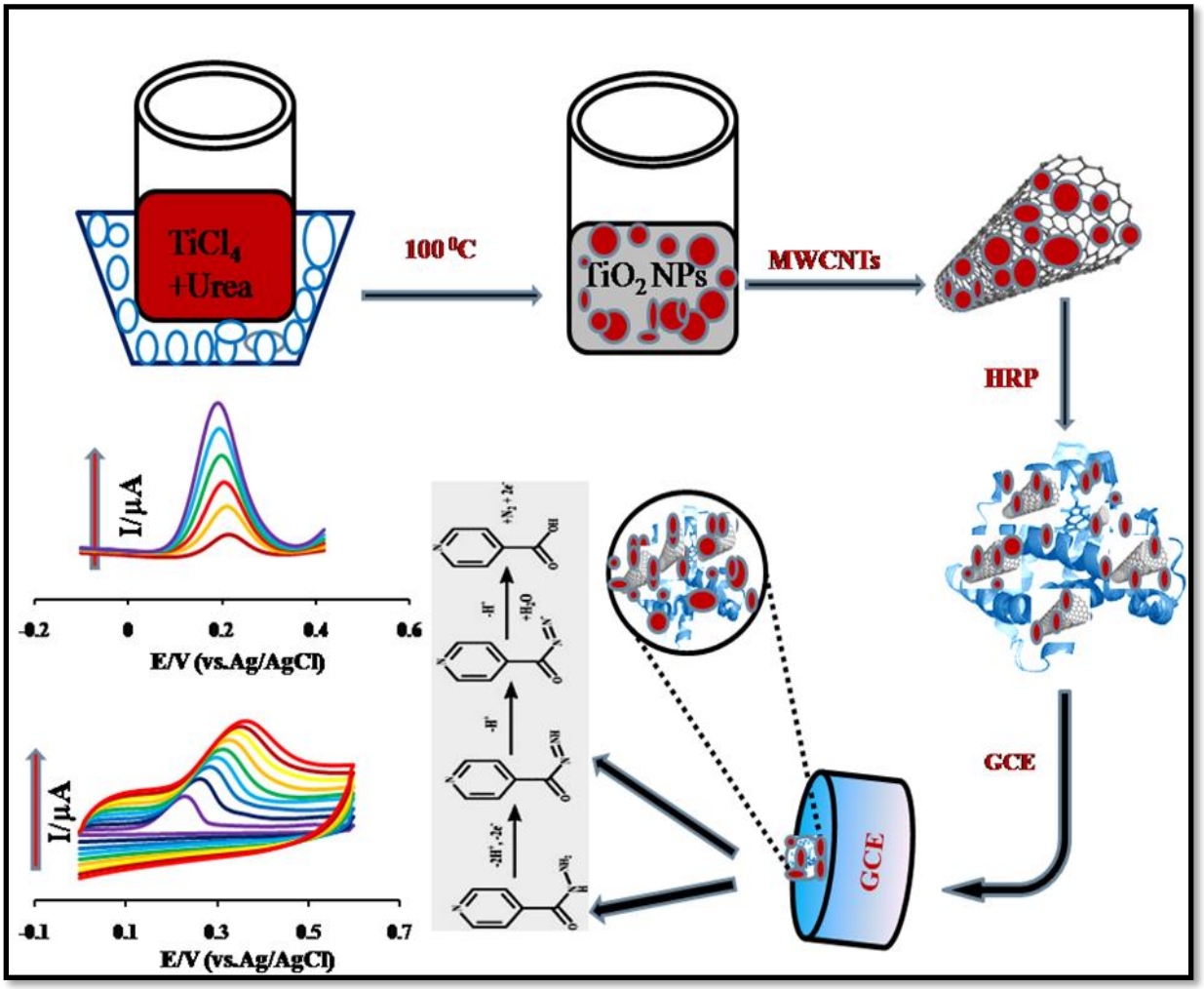

Scheme 5.1: Graphical illustration of electrochemical oxidation of isoniazid at HRP-TiO_2NPs-MWCNTs-GCE

5.1.2 Method Optimization

The effect of pH played an important role in the electrochemical signal amplification of isoniazid. The effect of pH with peak current was studied in the range of 3.0–10.0. As the pH increases, peak currents gradually increase until pH 7, and then decrease beyond pH 7. The changes in the anodic peak currents and peak potentials responses were monitored by varying the

pH **(Figure 5.3B)**. According to the obtained results from Figure 5.3B, the anodic peak current of INZ reaches a maximum at pH 7, and decreases beyond pH 7. Due to this observation, a pH of 7 was selected as optimum for the entire study. In addition, the effect of deposition time was also monitored from 30 to 150 s **(Figure 5.3C)**. Based on the results obtained, deposition time with 120 s was selected as optimum deposition time for the present study. Further, the most effective parameter, notably, scan rate, was examined in the range of 0.1 to 1.0 $V \cdot s^{-1}$. The results obtained showed that 0.9 $V \cdot s^{-1}$ was the optimum potential scan rate. The effect of incubation temperature was also tested with the activity of HRP immobilized on the surface of the MWCNT-TiO_2NPs-GCE. The anodic peak current response was observed with different incubation temperatures ranging from 5 to 50 °C **(Figure 5.3D)**. The fabricated MWCNT-TiO_2NPs-HRP-GCE showed maximum peak currents at 30 °C. Therefore, 30 °C was selected as the optimum temperature for the experiment. At 5-30 °C the increase in current responses of the modified sensor was due to the increase in the activation energy of the reaction. Higher than 30 °C, the current responses were decreased due to enzyme denaturation. The enzyme reaction rate increases as the incubation temperature increases up to an optimum temperature, and after that the enzyme activity declines rapidly. Moreover, the immobilized enzyme shows no changes at the optimum temperature when compared with free enzyme. The enzyme incubation time is also an important parameter in the method optimization, and was monitored from 5 to 25 min at room temperature, whilst the corresponding current responses were measured. **Figure 5.4** shows the current responses gradually increased with sustained enzyme incubation time. The enzyme-fabricated electrode showed good peak current response at 15 min. Based on the current response and adsorption equilibrium of the enzyme, 15 min was selected as the optimum incubation time for

the entire study. After 15 min, the current response gradually decreased with prolonged incubation time.

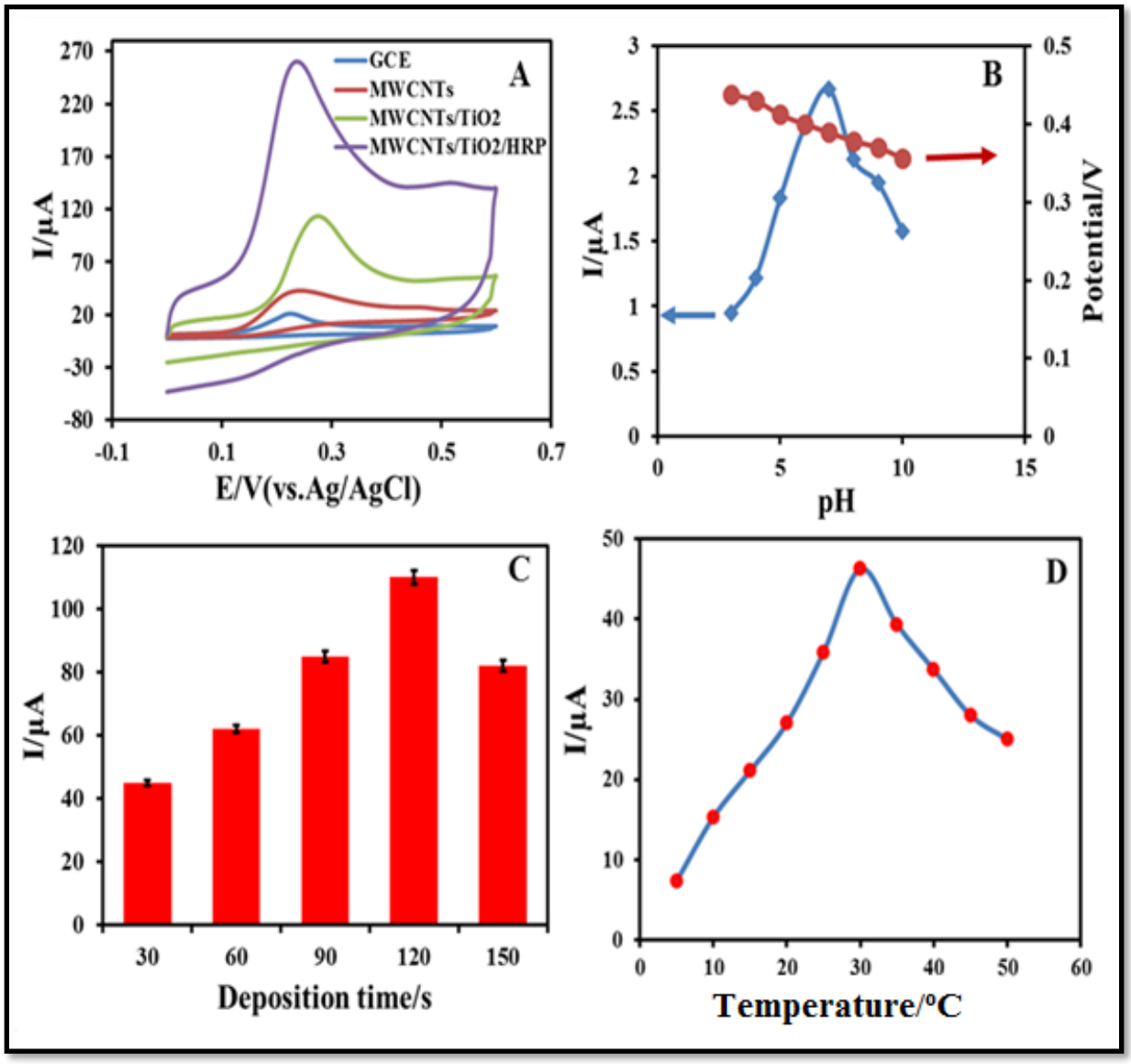

Figure 5.3: (A) Cyclic voltammograms of 0.1 mM isoniazid (INZ) with: (1) a bare glassy carbon electrode (GCE); (2) MWCNT-GCE; (3) MWCNT-TiO_2NPs-GCE; and (4) MWCNT-TiO_2NPs-horseradish peroxide (HRP)-GCE. (B) Peak potential and peak currents response with pH at 3.0, 4.0, 5.0, 6.0, 7.0, 8.0, 9.0 and 10.0. respectively (C) Peak

current responses vs. different deposition times of 30, 60, 90, 120 and 150 s. (D) Effect of temperature on the current response of the MWCNT-TiO$_2$NPs-HRP-GCE

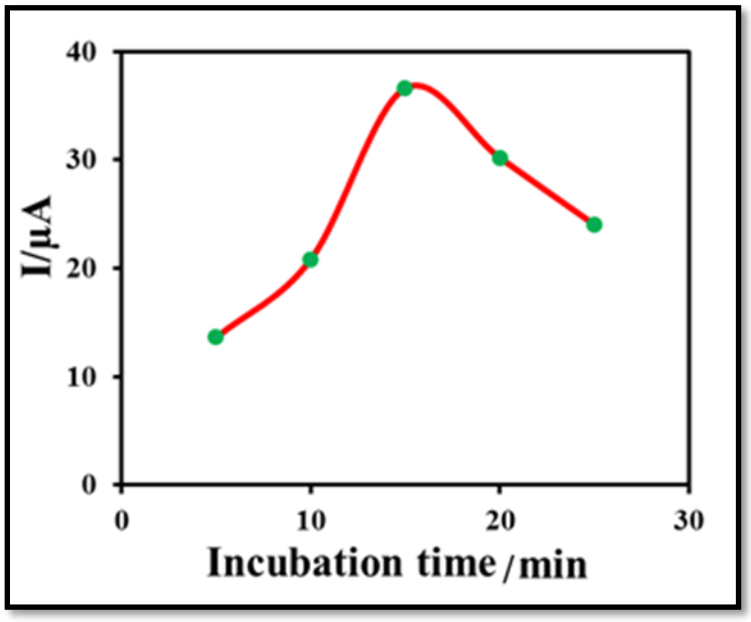

Figure 5.4: The effect of the enzyme incubation time on the current responses of the modified electrode

5.1.3 Electrochemical Behaviour of INZ on the MWCNT-TiO$_2$NPs-HRP-GCE

The MWCNT-TiO$_2$NPs-HRP-GCE was electrochemically analysed by CV and DPV techniques. The modified electrode surface area calculation was justified by using the Randles–Sevick (Chen et al., 2012) as in the following equation: (5.1).

$$i_{pa} = 2.69 \times 10^5 A C_0 n^{3/2} {D_R}^{1/2} v^{1/2} \quad (5.1)$$

where i_{pa} is the anodic peak current, A is the surface area of the electrode, C_0 is the concentration of INZ, n is the number of electrons transferred, D_R is the diffusion coefficient,

and v is the scan rate. Based on Equation (5.1), the MWCNT-TiO_2NPs-HRP-GCE and GCE surface areas were calculated and found to be 19.32 and 3.14 mm^2, respectively. This indicated that the MWCNT-TiO_2NPs-HRP-GCE sensor was exhibiting approximately a six-fold increase in surface area over the GCE. This implies that the fabricated sensor provides a high surface area for INZ to undergo electrochemical oxidation (Devadas et al., 2015a) **(Scheme 5.2)**.

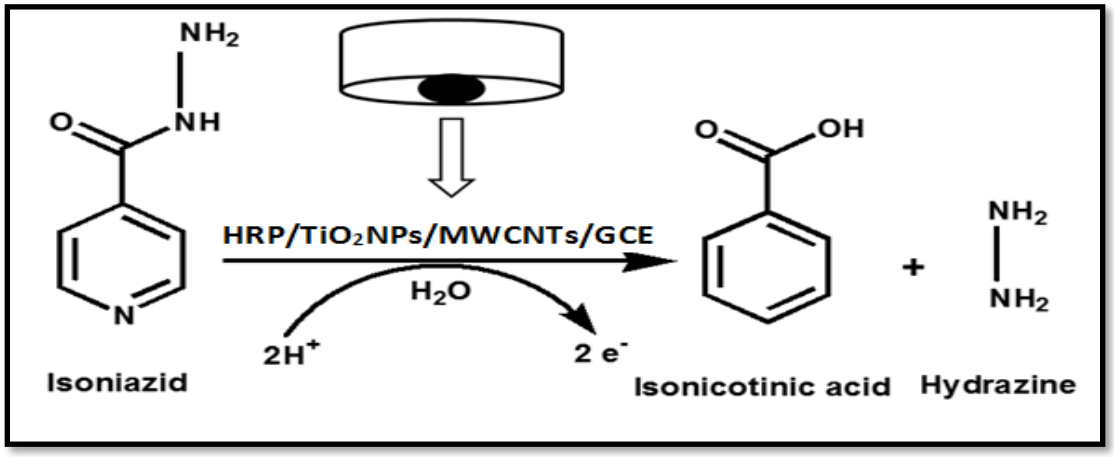

Scheme 5.2: Electrochemical oxidation mechanism of INZ with the MWCNT-TiO_2NPs-HRP-GCE

The electrochemical sensing ability of the MWCNT-TiO_2NPs-HRP-GCE was compared with the bare GCE, MWCNTs and MWCNTs-TiO_2NPs **(Figure 5.3A)**. The potential scale was monitored in the range of −0.1 to +0.7 V for the appearance of anodic peak. The GCE exhibited a much lower current of 25 µA, while the MWCNT-GCE and MWCNT-TiO_2NPs-GCE showed good current responses of 56 µA and 110 µA, respectively. The final MWCNT-TiO_2NPs-HRP-GCE showed much greater peak current response of 200 µA **(Figure 5.5A)**. **Figure 5.5B** shows the linear relationship between log i_{pa} and log v, and it is suggested the diffusion of INZ at the surface of the MWCNT-TiO_2NPs-HRP-GCE can be expressed by the following equation (5.2).

$$\log i_{pa} = 0.7841 \log v + 1.5351 \quad (5.1)$$

Figure 5.5C shows that the oxidation of INZ at the MWCNTs-TiO_2NPs-HRP-GCE is similar to the diffusion-controlled process owing to the linear relationship between anodic peak current and the square root of the scan rate. The fitted regression line can be expressed as i_{pa} = 0.2642 $v^{1/2}$ + 0.2891; R^2 = 0.9822. This clearly indicates the outstanding performance of the MWCNT-TiO_2NPs-HRP-GCE compared to the other three electrodes.

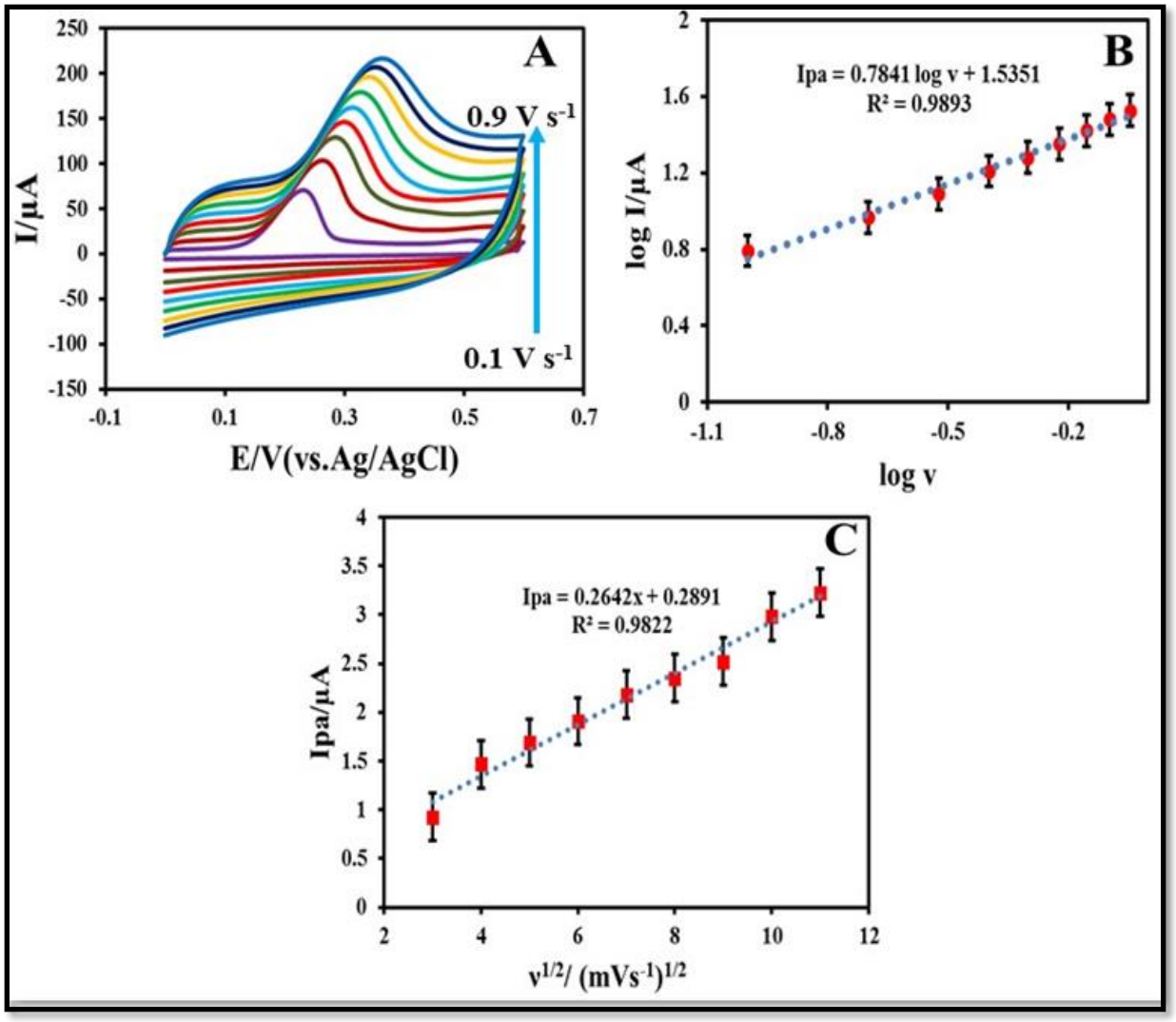

Figure 5.5: (A) Cyclic voltammograms of 0.1 mM of INZ at scan rates of 0.1, 0.2, 0.3, 0.4, 0.5, 0.6, 0.7, 0.8 and 0.9 V·s^{-1}. (B) Graph of (log anodic peak current) versus log (scan rate) for 0.1 mM INZ in 0.1 M phosphate buffer solution (PBS; pH 7.0) with different scan rates for the MWCNT-TiO$_2$NPs-HRP-GCE. (C) Linear plot of (anodic peak current) against the square root of the scan rate (n = 5, average standard deviation)

5.1.4 Quantitative Analysis of INZ

DPV was carried out with a 0.5 to 5 μM solution of INZ, via the standard addition method. The MWCNT-TiO_2NPs-HRP-GCE gave a well-defined anodic peak at 0.2 V (vs. Ag/AgCl) with the optimized working parameters (scan rate of 0.09 V s^{-1}, deposition time 120 s, pulse amplitude 0.050 V, voltage step 0.00935 V, voltage step time 0.1 s and pulse time 0.040 s). It was shown that as the concentration of INZ was increased, the anodic peak currents gradually increased **(Figure 5.6)**.

A calibration graph was plotted for the concentration of INZ against anodic peak currents. The obtained regression equation (i_{pa} =12.22 c + 0.375) showed a good correlation coefficient of R^2 = 0.998 for DPV. The limit of detection (LOD) and limit of quantification (LOQ) were calculated based on signal to noise ratios by using the Equations (5.3) and (5.4). In terms of the instrument signal, it is important in determining the smallest signal that is distinguishable from the background (baseline) noise.

$$\text{LOD} = (3 \times \text{SD/Slope}) \quad (5.2)$$

$$\text{LOQ} = (10 \times \text{SD/Slope}) \quad (5.3)$$

where SD is the standard deviation of the peak currents for three different runs and slope of the calibration curve. The limit of detection and limit of quantification for INZ is 0.0335 μM and 0.1118 μM, respectively. The comparison of the current fabricated sensor method with the previous methods (Chen et al., 2012, Azad et al., 2015, Cheemalapati et al., 2014a, Wei et al., 2016, Gnanasekaran et al., 2015, Thamaphat et al., 2008, Absalan et al., 2016, Ghoneim et al., 2003, Yun Xia and Ya Hu, 2005) used in the determination of INZ is listed in **Table 5.1**. It is

evident that the current method reported showed lower LOD and LOQ values for the determination of INZ compared to previous reports.

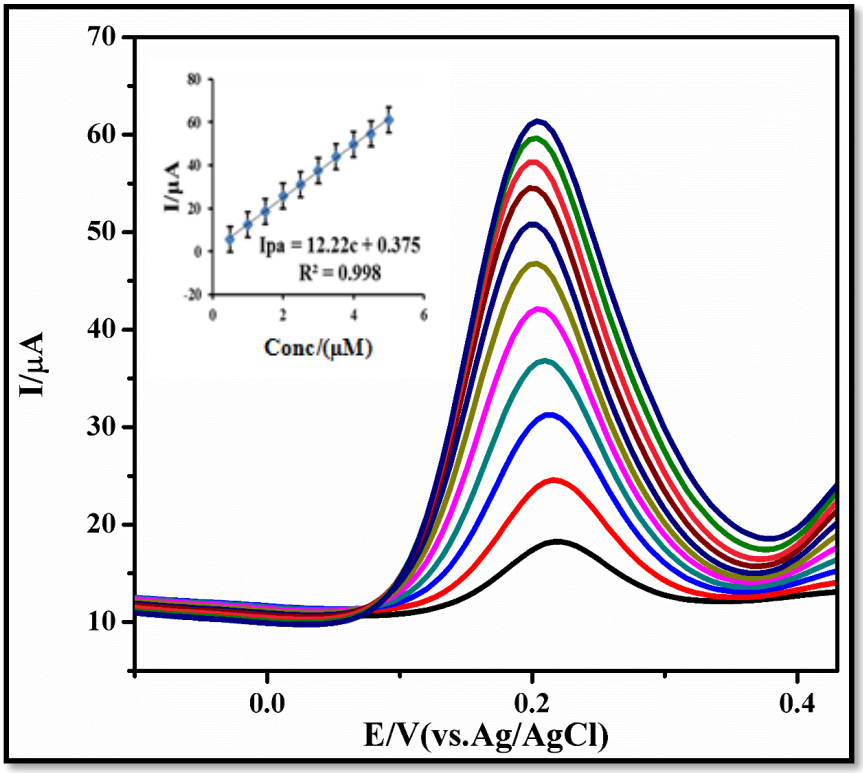

Figure 5.6: Differential pulse voltammetric (DPV) response of 0.5 to 5 µM INZ with the MWCNT-TiO_2NPs-HRP-GCE at pH 7.0, scan rate: 0.09 V s^{-1}, deposition time: 120 s, pulse amplitude: 0.050 V and pulse time: 0.040 s. (Inset calibration plot) (n = 5, average SD)

Table 5.1: Comparison of some characteristics of previously reported modified electrodes with the current MWCNT-TiO_2NPs-HRP-GCE study

Electrode	Technique	Detection Limits/(µM)	Linear Range/(µM)	Buffer and pH	References
Nf/Fe/GCE [a]	CV	13.00	50–20,000	Na_2SO_4 (9)	(Bergamini et al., 2010)
LDH/GCE [b]	DPV	4.00	4.9–770	BR (9)	(Yun Xia and Ya Hu, 2005)
4-pyridyl hydroquinone SAM/platinum electrode [c]	CV	20.0	-	PBS (7.2)	(Absalan et al., 2016)
poly-L-histidine/SPE [d]	DPV	0.50	-	PBS (7)	(Ghoneim et al., 2003)
Gold electrode [e]	DPV	0.09	-	NaOH (13.6)	(Cheemalapati et al., 2013)
PdNP/CPE [f]	CV	0.47	-	PBS (7)	(Chen et al., 2012)
Hanging mercury drop electrode [g]	SWADCS	1.18	-	BR (5.5)	(Cheemalapati et al., 2014a)
GO/GCE [h]	LSV	0.17	2–70	PBS (7)	(Azad et al., 2015)
F-MWCNT/GCE [i]	CV	0.27	1–70	AB (4)	(Wei et al., 2016)
Rh/GCE [j]	CV	13.00	70–130	PBS (7)	(Gnanasekaran et al., 2015)
Bentonite clay/GCE [k]	LSV	0.80	-	Na_2SO_4 (13.5)	(Thamaphat et al., 2008)
MWCNT-TiO_2NPs-HRP-GCE	DPV	0.03	0.5–5	PBS (7)	Present work

[a] Nf/Fe/GCE—Nafion on iron-coated GCE; [b] LDH/GCE—layered double hydroxide-coated GCE; [c] 4-pyridyl hydroquinone SAM/platinum electrode-4-pyridyl hydroquinone self-assembled monolayer-coated platinum electrode; [d] poly-L-histidine/Screen printed electrode (SPE)-poly-L-histidine coated on a SPE ; [f] PdNP/CPE—palladium nanoparticle-coated CPE; [h] GO/GCE—graphene oxide-coated GCE; [i] F-MWCNT/GCE—functionalized multi-wall carbon nanotube-coated GCE; [j] Rh/GCE—rhodium nanoparticle-coated GCE; [k] bentonite clay/GCE—bentonite clay-modified GCE; SWADCS—square-wave adsorptive anodic stripping

voltammetry; LSV—linear sweep voltammetry; CPE—carbon paste electrode; SPE—screen-printed electrode; CV—cyclic voltammetry; PBS—phosphate buffer solution.

5.1.5 Repeatability and Stability

The repeatability efficiency of the proposed sensor was examined with 0.1 mM INZ solution using DPV under the optimized parameters. After each determination, the used fabricated electrode underwent five to six sweeps in 0.1 M phosphate buffer solution (pH 7.0), to remove any adsorbents and yield a reproducible electrode surface. The peak current response of INZ was determined with five electrodes under the same conditions. From the five parallel determinations, the Relative Standard Deviation (RSD) of INZ determination was found to be 4.12%. Based on the results, the proposed sensor showed good repeatability. The long-term stability of the sensor was tested after 80 days. When not used, the sensor was stored at 4 °C. The stability studies were carried out with the MWCNT-TiO_2NPs-HRP-GCE for the detection of INZ. This study was carried out in two batches. In the first batch, the stability of the modified electrode was observed from day 1 to day 40, in terms of electrochemical signalling. It was observed that for 40 days, the average electrochemical signal was found to be 91%. In the second batch, the stability study was carried out for an additional 40 days with the same materials and electrode. Interestingly, it was now observed that the electrochemical signal was found to be 87%. This implies only 4 % of the electrochemical signal decreased. These results indicate that the fabricated electrode showed good repeatability and long-term stability.

5.1.6 Interference Studies

To evaluate the selectivity ability of the developed sensor, interference studies were also performed for INZ with coexisting compounds like uric acid, glucose, and ascorbic acid. In this analysis, the peak current for INZ was recorded (Ip_1). The excess amount of the potential interferent species was added to the mixture and DPV was recorded (Ip_2). The tolerance limit was defined as the maximum concentration of the interfering components that caused an error less then ±5% (Ip_1/Ip_2 = 95–105%). In addition, the influence of some common ions such as Fe^{3+}, Al^{3+}, Cl^{-}, Na^{+}, and K^{+} were studied and the results obtained indicated that these ions have no significant influence on the determination of INZ **(Table 5.2)**.

Table 5.2: The influences of some anions, cations and important biological substances on the peak current of 0.1 mM INZ with the MWCNT-TiO_2NPs-HRP-GCE

Interferents	Concentration/(μM)	Signal Change (%)
Ascorbic acid	250	4.03
Uric acid	250	1.24
Glucose	500	0.34
Fe^{3+}	500	0.81
Al^{3+}	500	1.27
Cl^{-}	500	0.67
Na^{+}	500	2.01
K^{+}	500	1.35

5.1.7 Real Sample Analysis

Commercially-available INZ tablets (100 mg) were purchased from the local pharmacy. The samples (tablets) were used to evaluate the realistic performance of the MWCNT-TiO_2NPs-HRP-GCE. Approximately ten tablets were taken into a mortar and crushed to fine powder with pestle. A 0.1 mM INZ tablet sample solution was prepared by dissolving the appropriate amount of powder sample in a 10 mL volumetric flask and adding 10 mL of PBS. Finally, real sample analysis was carried out with 0.1 mM INZ by the DPV technique via the standard addition method. The results with respect to the analytical performances of the MWCNT-TiO_2NPs-HRP-GCE obtained were then tabulated **(Table 5.3)**. The two pharmaceutical samples showed good RSD values (1.69 and 1.98) with an excellent percentage of recovery (99.2% and 98.9%). This indicates that the developed sensor exhibited good recovery capability towards INZ in various pharmaceutical samples.

Table 5 3: Determination of INZ in various pharmaceutical samples using the developed sensor (n = 5)

Declared Amount Tablet (mg)	Found (mg)	Recovery (%)	Relative Standard Deviation (RSD) (%)	Added (mg)	Found (mg)	Recovery (%)	RSD (%)
Sample 1 (100 mg)	99.2	99.2	1.69	20	19.3	96.5	0.32
Sample 2 (100 mg)	98.9	98.9	1.98.	10	9.5	95.0	0.79

5.2 Development of Cyt c-CuONPs-MWCNTs fabricated glassy carbon electrode for the detection of PZM

In this present work cytochrome c (Cyt c) immobilized on copper oxide nanoparticles (CuONPs) decorated multiwalled carbon nanotubes (MWCNTs) were explored to in terms of fabrication on glassy carbon electrode. Physically MWCNTs contain several layers of graphite superimposed and rolled in on themselves to form a tubular shape and high surface area. Cyt c is generally used to modify the electrodes to promote direct electron transfer for biosensors and bio fuel cells (Zhao et al., 2012). The presence of CuONPs on the surface of MWCNTs gave a higher surface to volume ratio to immobilize higher quantity of Cyt c on the electrode surface. Furthermore, Cyt c was strongly adsorbed onto the surface of the fabricated electrode and showed an enzyme-like activity of the redox reaction of PZM. Finally, CuONPs-MWCNTs nanocomposite were applied for the detection of PZM and showed good sensitivity and detection limits.

5.2.1 Characterization of Cyt c-CuONPs-MWCNTs-GCE

The Cyt c-CuONPs-MWCNTs-GCE hybrid electrode was characterized by TEM, TGA, XRD and FTIR. FT-IR spectra were recorded for the CuONPs in the range of 400-4000 cm^{-1} **(Figure 5.7A)**. The two characteristic bands observed at 509 cm^{-1} and 604 cm^{-1} can be assigned to the CuONPs (Kshirsagar et al., 2015). For the range from 605-660 cm^{-1} no other IR active mode was observed in CuONPs (Ramesh et al., 2012). Moreover, the peak at 871 cm^{-1} was responsible for =C-H bending, 1122 cm^{-1} for C-O stretching, 1629 cm^{-1} for C = C stretching, 2195 cm^{-1} for –C ≡ C – stretching, and 3396 cm^{-1} for O-H stretching vibrations respectively (Dodoo-Arhin et al., 2012). The XRD scan for the CuONPs is shown in **(Figure 5.7B)**. The XRD peaks confirmed that the formation of CuONPs from each precursor was in a monoclinic phase, no other impurity peaks were observed in the XRD pattern. According to previous literature the XRD pattern

exhibits two main diffractions at 2θ = 36.6º (110) and 2θ = 38.8º (111) and these were ascribed to the formation of the CuONPs in face centered cubic (FCC) and monoclinic crystal lattice respectively (Morales et al., 2004, Ethiraj and Kang, 2012).

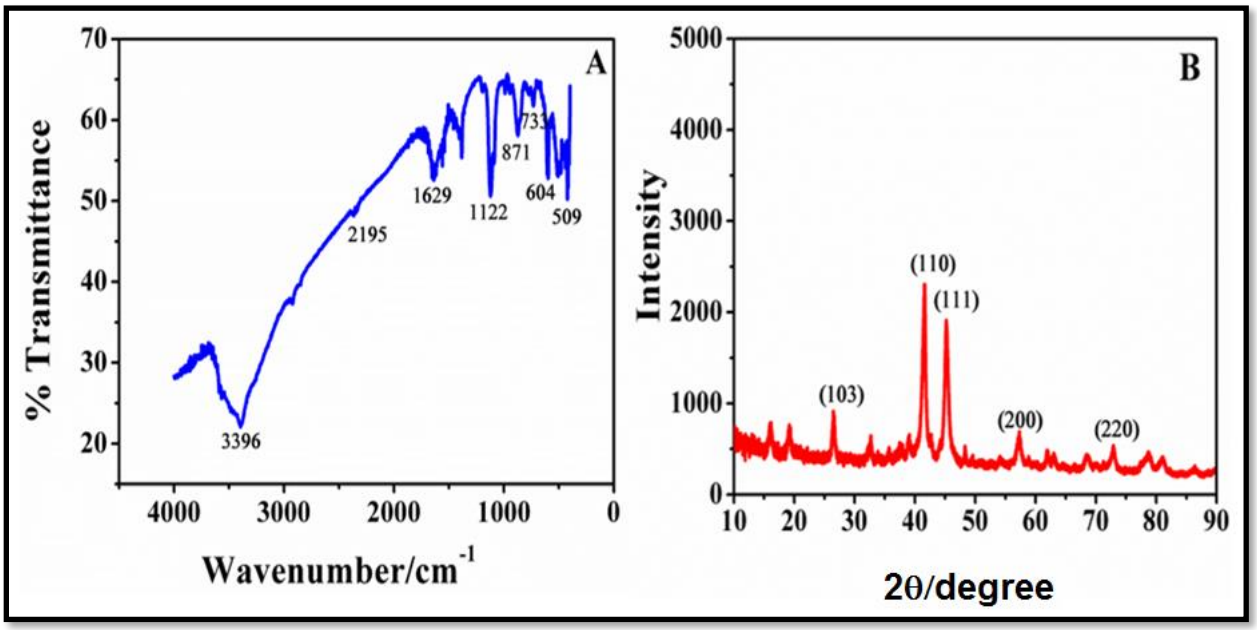

Figure 5.7: (A) FT-IR characterization of CuO NPs (B) XRD image of CuO NPs

Figure 5.8A-D shows the transmission electron microscopic images of pure MWCNTs, CuONPs and CuONPs-MWCNTs. **Figure 5.8A** shows the morphological structure of pure MWCNTs with tube like structure whilst **Figure 5.8B** shows the CuONPs which are almost spherical in shape and have average diameters varying between 3-7 nm. **Figure 5.8C** indicates the TEM image of MWCNTs decorated with CuONPs. The CuONPs and MWCNTs nano composites stability and thermal behavior was investigated by thermo gravimetric analysis (TGA). **Figure 5.8D** show the TGA curves for MWCNTs (i), CuONPs (ii) and CuONPs-MWCNTs (iii). MWCNTs showed one major decrement in the mass around 570 °C. The TGA curve of CuONPs shows loss of mass in two steps. In the first step it loses minor mass at 100 °C due to evaporation

of water, whereas in the second step mass losses occur at above 400 °C and can be attributed to the removal of organic moieties. Finally, the CuONPs decorated on the MWCNTs show different TGA curves, and it loses minor mass at below 600 °C, due to the evaporation of some organic moieties (Seifart et al., 1995, Gou et al., 2008).

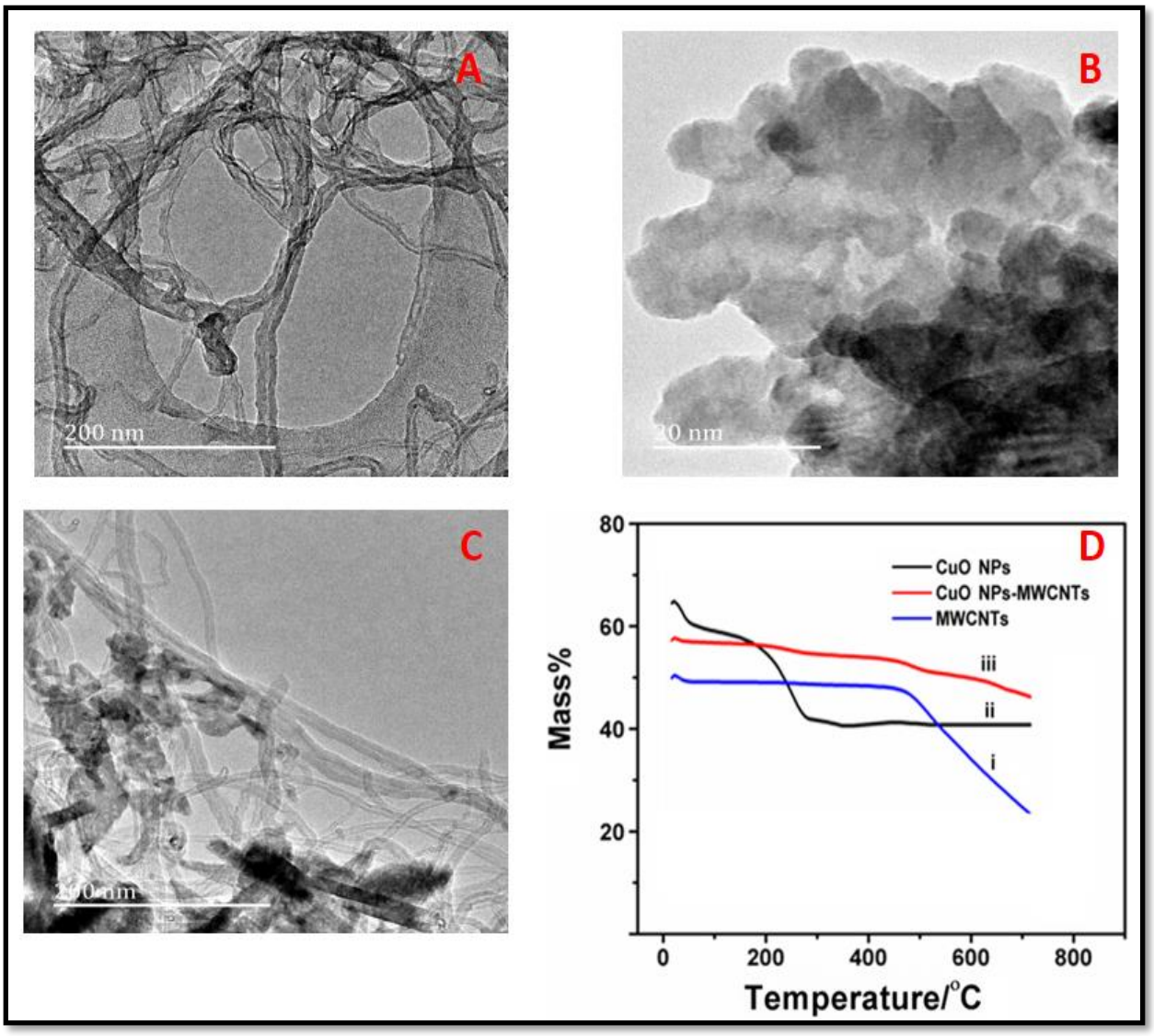

Figure 5.8: (A) TEM image Pure MWCNTs (B) CuONPs (C) CuONPs-MWCNTs (D) TGA curves for (i) MWCNTs, (ii) CuONPs and (iii) CuONPs-MWCNTs

5.2.2 Electrochemical behaviour of PZM at Cyt c-CuONPs-MWCNTs-GCE

The electrochemical behavior of PZM was evaluated with 0.1 M PBS (pH 7.0) at different electrodes. PZM generally undergoes an electrochemical reduction reaction at the electrode surface and converts pyrazinamide to pyrazinoic acid (Nxusani et al., 2012). In this reaction, two electrons and three protons are involved in the hydroxylation process. They are responsible for the generation of reduction peaks at the electrode surface, **(Figure 5.9)**. The graphical representation of electrochemical redox mechanism of PZM at Cyt c-CuONPs -MWCNTs-GCE is illustrated in **Scheme 5.3**.

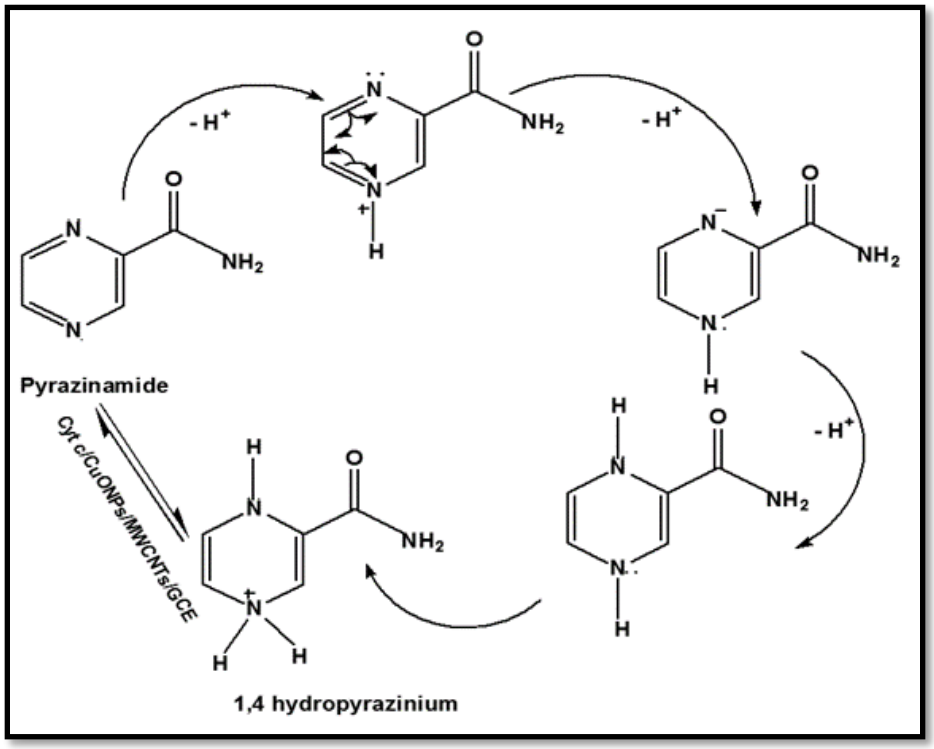

Figure 5.9: Proposed electrochemical reaction of PZM at Cyt c-CuONPs-MWCNTs-GCE

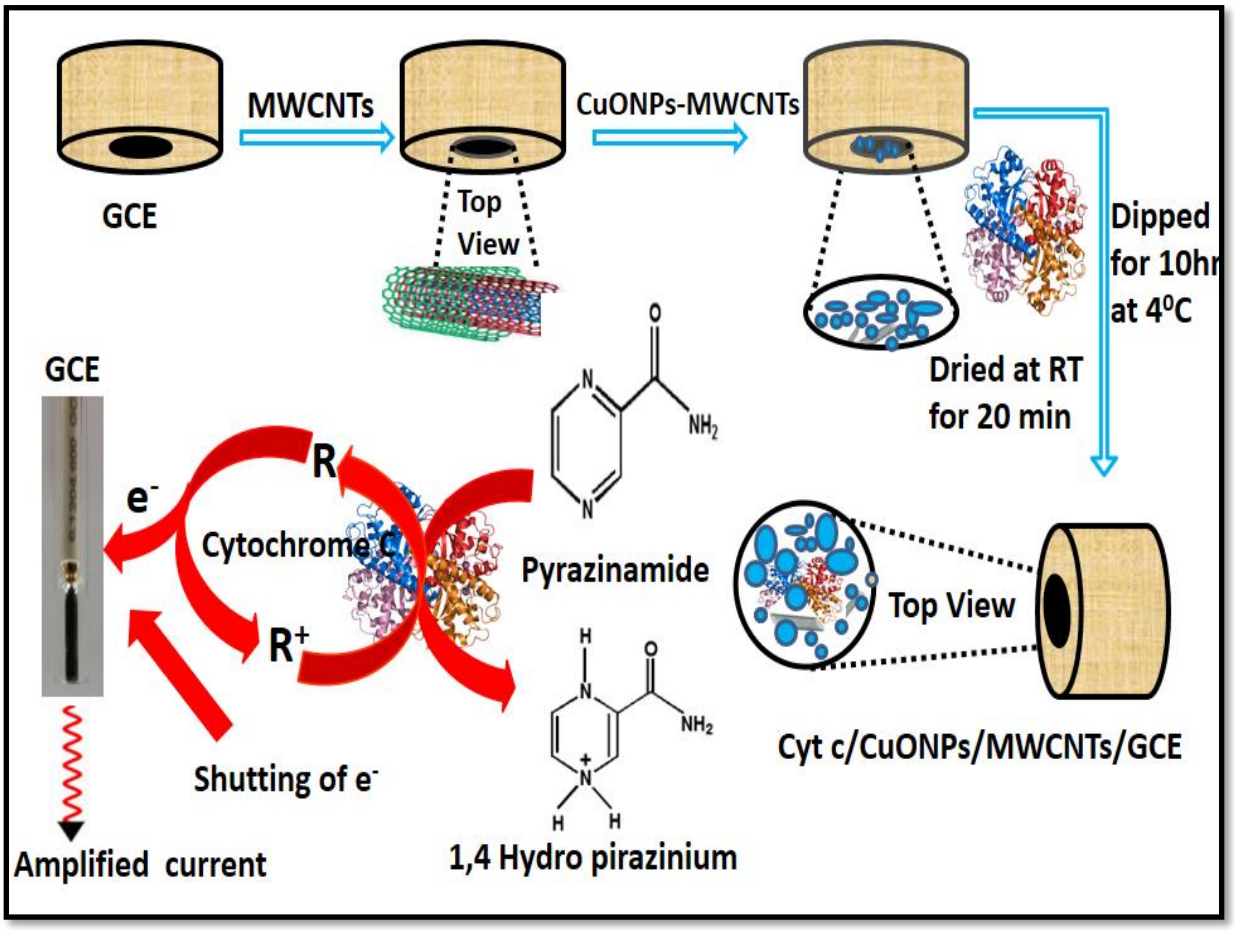

Scheme 5.3: Graphical representation of electrochemical redox mechanism of PZM at Cyt c-CuONPs -MWCNTs-GCE

The Cyt c-CuONPs-MWCNTs-GCE demonstrated the good current response against PZM. The increasing anodic and cathodic currents for the different modified electrodes were calculated by using the Randles-Sevick equation (Bhajanthri et al., 2016).

$$i_{pa} = 2.69 \times 10^5 A\, C_0\, n^{3/2}\, {D_R}^{1/2}\, v^{1/2} \qquad (5.5)$$

In the Randles-Sevick equation i_{pa} is the anodic peak current, C_0 is the concentration of PZM, A is the surface area of electrode, n is the number of electrons transferred, D_R is the diffusion coefficient and ν is the scan rate. The bare GCE anodic peak currents were used to calculate D_R. Further the surface area of the Cyt c-CuONPs-MWCNTs-GCE was calculated by using the diffusion coefficient value. The surface area of Cyt c-CuONPs-MWCNTs-GCE was calculated and found to be 15.23 mm^2, and for the bare GCE it was 3.14 mm^2. The obtained results reveal that the Cyt c-CuONPs-MWCNTs nanocomposite provides larger surface area on the GCE, and allows more PZM molecules to take part in the reduction mechanism. Cyt c is strongly adsorbed on the MWCNTs-CuONPs-GCE surface and it forms a monolayer. The Cyt c had two active sites, these active sites are capable of electron transfer. Among the two active sites of Cyt c, one binds with MWCNTs-CuONPs-GCE and the second active site binds with the PZM (Friedrich et al., 2004).

Figure 5.10A clearly shows the obtained CV curves for bare GCE, MWCNTs-GCE, MWCNTs-CuONPs-GCE and Cyt c-CuONPs-MWCNTs-GCE at an optimum scan rate of 50 mV s^{-1}. The CV measurements were done in the potential range of -1.4 to 0.1 V for all the electrodes. At the bare GCE, the anodic and cathodic peaks were obtained at the potentials of -0.75 V and -0.78 V with minor 25 μA currents responses. Under identical conditions, MWCNTs-GCE and CuONPs-MWCNTs show corresponding anodic and cathodic peaks at the potentials of -0.78 V, -0.81 V and -0.77 V, -0.80 V with modest currents of 145 μA and 780 μA respectively. Cyt c-CuONPs-

MWCNTs-GCE show corresponding peaks at -0.77 V and -0.80 V with extraordinary higher current responses (1600 μA). At ambient temperature Cyt c is stable and the denaturation temperature for Cyt c is 68.4 °C (Bagelova et al., 1997). Comparing all the fabricated electrodes and bare GCE, the Cyt c-CuONPs-MWCNTs-GCE showed the highest electrochemical responses towards PZM **(Figure 5.10D)**.

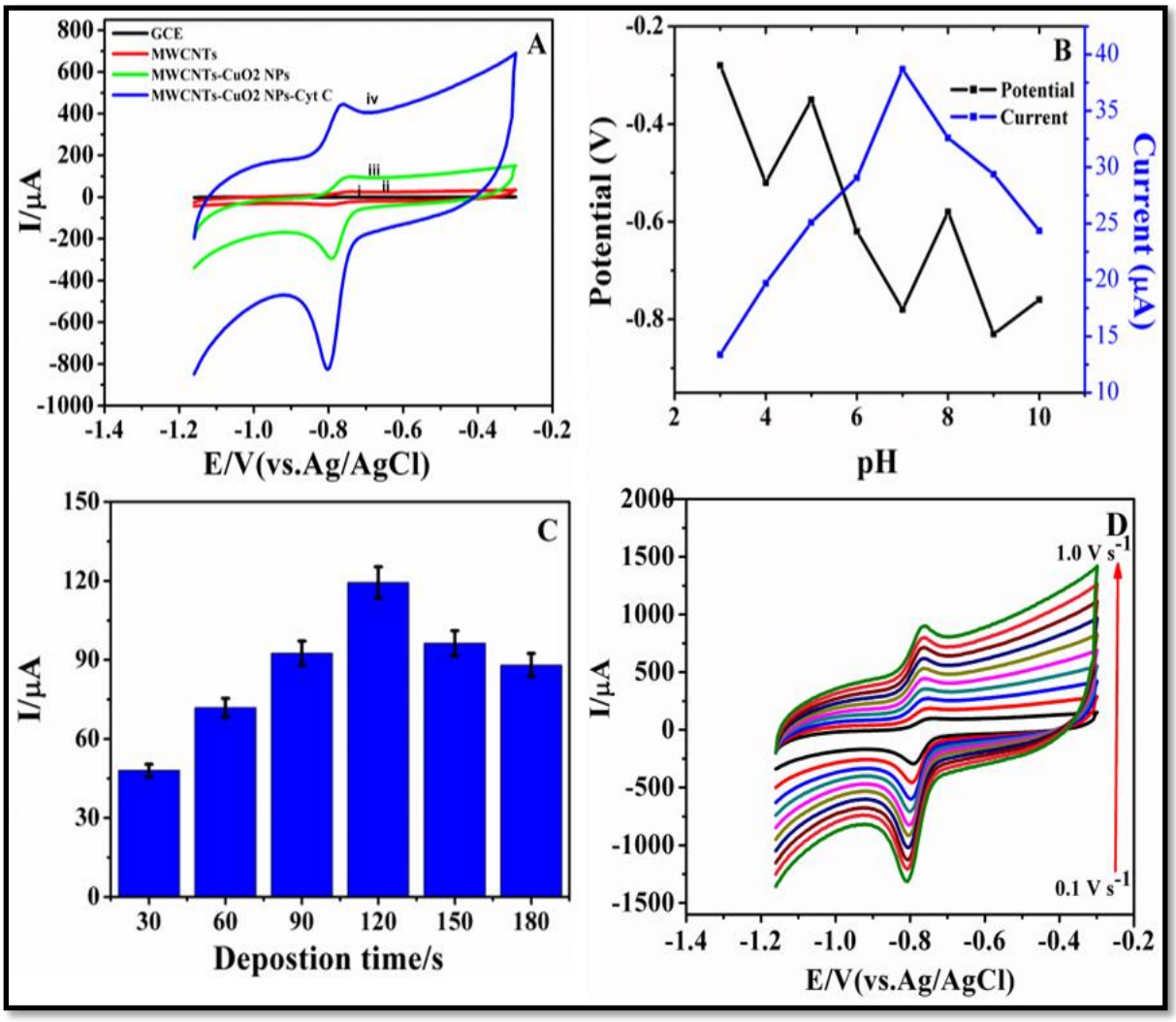

Figure 5.10: (A) Cyclic Voltammograms of 0.1 mM PZM at bare (i) GCE, (ii) MWCNTs-GCE (iii) CuONPs-MWCNTs-GCE, and (iv) Cyt c-CuONPs-MWCNTs-GCE. (B) Peak potential and current response with respect to change in pH (3-10) with 0.1 mM PZM. (C) Various deposition times (30, 60, 90, 120,150 and 180 s) on peak current. (D) Cyclic Voltammograms of PZM at various scan rates from inner to outer (10, 20, 30, 40, 50, 60, 70, 80, 90 and 100 V s^{-1}.)

5.2.3 Method Optimization

pH is the most significant factor that plays a key role in the determination of the analyte of interest chiefly in electrochemical investigations. In order to optimize the pH for the present study, various buffer solutions with pH ranges 3-10 were examined. **Figure 5.10B** clearly shows the effect of pH on the peak currents and potentials of PZM. The anodic peak currents gradually increase with the increase in the pH 3-10. Moreover, the maximum peak current response was observed at pH 7, after that the peak currents are decreased because the electrode surface has become saturated. Hence the pH 7.0 was taken as optimum value for the duration of the experimental work.

The deposition time was studied for the range **(Figure 5.10C)** 30-180 sec. The peak currents increase steadily with increase in the deposition time from 30 s to 120 s. A longer deposition time was favoured for the adsorption of a higher number of PZM molecules on the electrode surface. After 120 s the peak currents were decreased, because the electrode surface was now saturated. Hence a deposition time of 120 s was used for further analysis. The effect of the scan rate was studied further in order to investigate the nature of the surface coated electrode. The CV experiment was performed with PZM at a concentration of 0.1 mM and the redox electrochemical responses were investigated between 10 to 150 mV s^{-1}. The anodic peak currents and cathodic peak currents increase linearly with the square root of the scan rates, and the diffusion controlled oxidation and reduction process occur at Cyt c-CuONPs-MWCNTs-GCE. The dependence of the anodic peak currents and cathodic peak currents ratios on the scan rate is different from unity, and this ratio was increased as the scan rate was increased. Based on these results, a scan rate of 50 mV s^{-1} was chosen as optimum, and used in this work.

5.2.4 Quantitative analysis of pyrazinamide

The DPV method was employed with Cyt c-CuONPs-MWCNTs-GCE for quantification of PZM. The working parameters viz., pulse time 0.045 s, potential range -1.1 to -0.6 V, and pulse amplitude 0.055 V, were used for this study. The Cyt c-CuONPs-MWCNTs-GCE fabricated electrode shows one reduction peak at -0.80 V with higher currents at pH 7.0. The peak currents for PZM increases linearly with an increase in the concentration of PZM (3 to 30 μM) as shown in **Figure 5.11**. The calibration curve obtained by plotting peak current verses concentration of PZM is shown as an insert in **Figure 5.11**. The linear equation and correlation coefficient was found to be i_{pa} =2.249 c + 2.930 (R^2 = 0.994). Furthermore, the limit of detection (LOD) and limit of quantification (LOQ) was calculated according to the ratio of (3σ)/b and (10σ)/b respectively, where b is the slope of the calibration curve, and sigma is the standard deviation values from the five voltammetric runs for the blank electrode. The LOD and LOQ were found to be 0.0038 μM and 0.0129 μM respectively. Furthermore, the LOD and LOQ values were compared with the previous reports **(Table 5.4)**, and reveal the high performance of the developed sensor towards PZM.

Table 5.4: Comparison of electrochemical performance of the developed sensor with previous reports

Electrode	Method	LOD	Buffer & pH	References
SPCE/EPH	DPV& SWV	68 μM	PBS (1.0)	(Bergamini et al., 2013)
GO/PAG/GCE	CV & DPV	3.28 μM	PBS (7.0)	(Devadas et al., 2015b)
PMET/ERGO/GCE	CV & DPV	0.16 μM	PBS, (7.0)	(Cheemalapati et al., 2014b)
Poly(Gly)/GCE	CV & DPV	0.035 μM	PBS (7.5)	(Simioni et al., 2017)
GNS/ZnO/CPE	CV & DPV	0.0431 μM	BRS (7.0)	(Kalambate et al., 2016)
Poly (L-Cys)/GCE	CV& SWV	0.113 μM	BRS (1.0)	(Ferraz et al., 2016)
PARS/ GCE	CV & DPV	1.2 μM	HAc-NaA c (4.5)	
Cyt c-CuONPs-MWCNTs-GCE	CV & DPV	0.0038 μM	PBS (7.0)	This work

SPCE/EPH: screen printed electrode modified with poly-histidine prepared by histidine monomer electro polymerization; GO/PAG/GCE: graphene oxide and poly arginine poly-L-methionine modified GCE; GCE: glassy carbon electrode; CPE: carbon paste electrode; PMET/ERGO/GCE: poly L-methionine and reduced graphene oxide modified GCE; Poly (Gly)/GCE: poly L methionine modified GCE; GNS/ZnO/CPE: graphene zinc oxide modified CPE; Poly (L-Cys)/GCE: Poly-L-cysteine (Poly(L-Cys)) modified glassy carbon electrode; PARS/ GCE: A poly-alizarin red S modified glassy carbon electrode: Cyt c-CuONPs-MWCNTs-GCE: cytochrome c enzyme, copper dioxide, multi wall carbon nanotubes modified GCE.

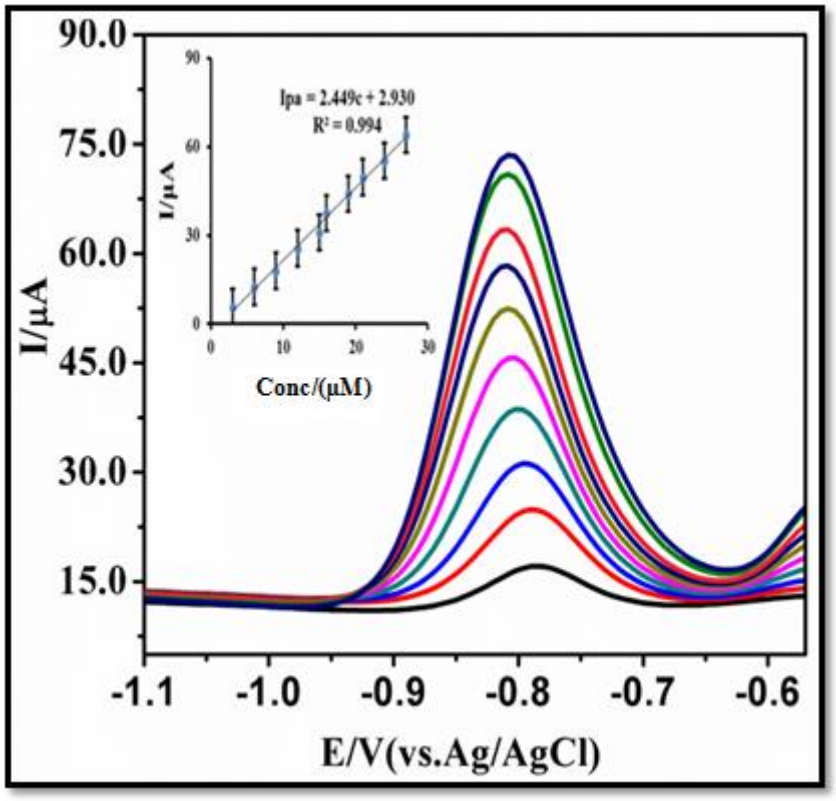

Figure 5.11: DPV response of 3 to 30 µM of PZM at Cyt c-CuONPs-MWCNTs-GCE at pH 7.0; scan rate 0.015 V s^{-1}; deposition time 120 s; pulse amplitude 0.055 V; and pulse time: 0.045 s. (Insert calibration plot)

5.2.5 Application to real pharmaceutical samples

The real sample analysis is a most significant application to determine electrochemical behavior of the fabricated electrode towards the analyte. The commercial pharmaceutical samples were used to determine the electrochemical performance of the Cyt c-CuONPs-MWCNTs-GCE sensor. The obtained DPV results clearly shows the electrochemical enrichment of the PZM reduction peak. The developed sensor showed good percentages of recovery rates viz., 99.5 % and 98.2 % respectively, for the two different pharmaceutical samples. The recovery percentages are very close to the official monograph of PZM. (Not less than 90 % and not more than 110 % of PZM are contained in real labeled samples) (Jeba et al., 2015). The results are summarized in **Table 5.5**.

In order to evaluate the selectivity of the proposed sensor, interference studies were performed with the real pharmaceutical samples (Antib-4 and Rimstar 4-Fdc). These tablets have some common interferents like isoniazid, rifampicin and ethambutol in its composition. The maximum concentration of the interfering substance caused an error of less than ±5% towards the determination of PZM. This indicates the extremely high selectivity of the developed sensor towards the determination of PZM in real pharmaceuticals.

Table 5.5: Determination of PZM in different pharmaceutical samples using proposed sensor (n = 6)

Tablet Sample (mg)	Found (mg)	Recovery (%)	Added (mg)	Found (mg)	Recovery (%)
Sample1 (400 mg)	398.2	99.5	50	49.1	98.2
Sample 2 (500 mg)	491.3	98.2	50	48.4	96.8

*n= average determinations

5.2.6 Stability and reproducibility of Cyt c-CuONPs-MWCNTs-GCE

The stability and reproducibility of the Cyt c-CuONPs-MWCNTs-GCE were studied by using CV and DPV measurements with 0.1 mM PZM. The developed sensor was investigated by keeping the electrode in PBS (pH 7.0) for 15 days and then the CV was recorded and compared to the previous CV results. Based on the obtained results, the peak current decreased by 1.35 % for Cyt c-CuONPs-MWCNTs-GCE after 15 days. This indicates stability of the proposed sensor. The reproducibility of Cyt c-CuONPs-MWCNTs-GCE was measured by performing the analysis at different time intervals (10-50 days). The fabricated sensor was stored in the refrigerator at 4 ^{o}C, and after ten days the initial response of Cyt c-CuONPs-MWCNTs-GCE was 94 %, whilst after 50 days it decreases to 89.32 %. According to the results obtained, the fabricated electrode exhibits high stability and reproducibility.

5.3 Investigation of rifampicin (RIF) using Co en-q-Fe_3O_4NPs-MWCNTs-GCE

An electrochemical method has been developed for the voltammetric determination of RIF, at a glassy carbon electrode in the presence of MWCNTs and coenzyme q. MWCNTs are endowed with exceptionally high material properties, very close to their theoretical limits. A combination of these impressive properties enables a whole new variety of useful and beneficial applications. MWCNTs are polymers of pure carbon and can be reacted and manipulated using the rich chemistry of carbon. This provides opportunity to modify the structure and to improve solubility and dispersion, allowing innovative applications in various materials. Co en-q is a fat soluble, vitamin-like quinone present in the cell membranes, regulates metabolic pathways via redox signaling. Furthermore, Cyt c-CuONPs-MWCNTs-GCE shows high sensitivity and reproducibility in sensing of RIF.

5.3.1 Co en-q-Fe_3O_4NPs-MWCNTs-GCE characterization

The FTIR spectra of the Fe_3O_4NPs are shown in **Figure. 5.12A**. From the FTIR spectrum the band appeared at 580 cm^{-1} the peak associated with Fe-O presenting the tetrahedral side which can be attributed to Fe_3O_4 (Ahmad et al., 2009). The Fe_3O_4NPS can be seen by a strong absorption band at around 669 cm^{-1} which corresponds to the Fe-O absorption. The band at 1400 cm^{-1} indicates –C-H bending vibrations. The intense band at 1631 cm^{-1} is attributed to stretching of OH mode of H_2O (Shalaby et al., 2014). On the other hand, the peak at 2363 cm^{-1} showed strong stretching of O=C=O. The peak at 3438 cm^{-1} is attributed to the stretching vibrations of OH arising from hydroxyl groups from the water on Fe_3O_4NPs (Yan et al., 2016). **Figure. 5.12B** shows the x-ray diffraction pattern of the Fe_3O_4NPs. The Fe_3O_4NPs showed six specific peaks at 30.03º, 35.52 º, 43.02 º, 53.6 º, 68.25 º and 76.32 º, corresponding to (220), (311), (400), (511),

(440) and (622) respectively. The above strong diffraction intensities of the Fe_3O_4NPs reveals a the cubic spinal structure (Silva et al., 2013).

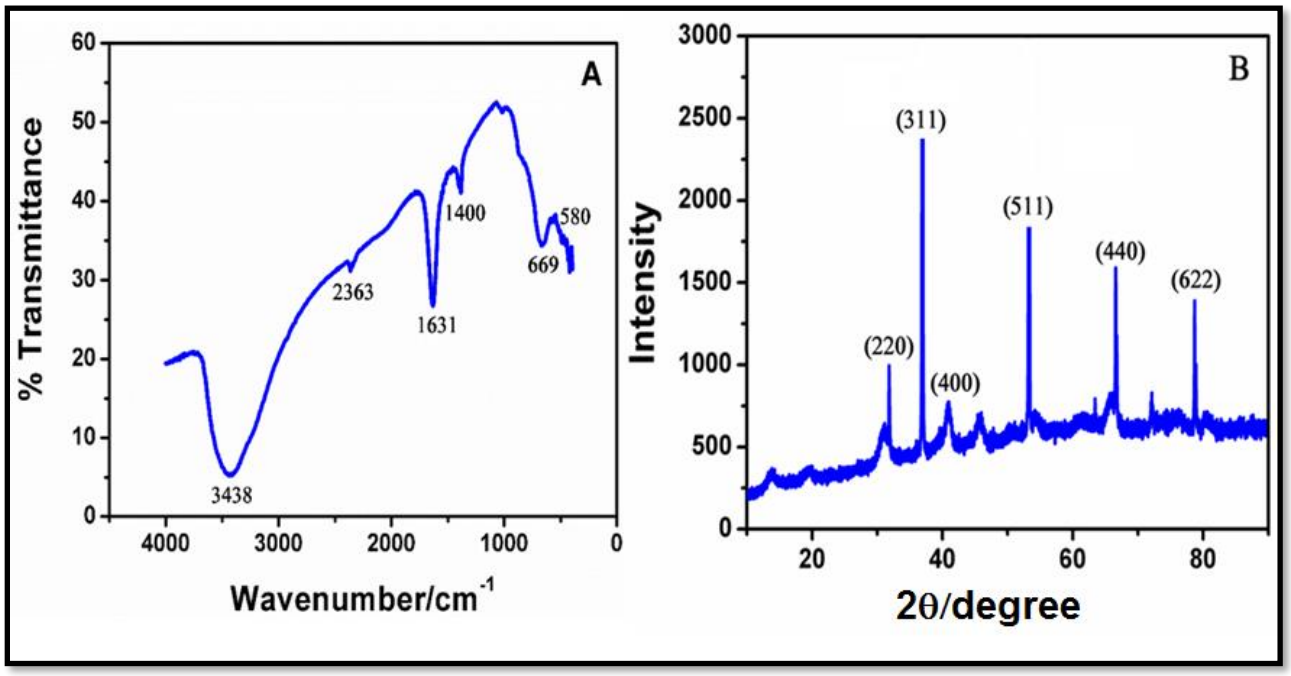

Figure 5.12: (A) FT-IR characterization of Fe_3O_4NPs. (B) XRD Image of Fe_3O_4NPs

Fe_3O_4NPs shows a very high intensive peak at 35.52 ^{o} (311) indicating that the nanoparticles are ultrafine in nature, single cubic phase and small crystallie size. Based on the Debye-Scherer formula (Ashour et al., 2016), the size of the Fe_3O_4NPs was also calculated and found to be approximately 15 nm in diameter.

$$d_{hkl} = \frac{0.9\,\lambda}{\beta\, Cos\, \theta} \qquad (5.6)$$

where β is the full width at half maximum value of XRD diffraction lines, λ is the wave length and θ is the half diffraction angle of 2θ. **Figure. 5.13A** denotes TEM image of the synthesized Fe_3O_4NPS. These nanoparticles are in rod like geometry and they are aggregated like a bunch.

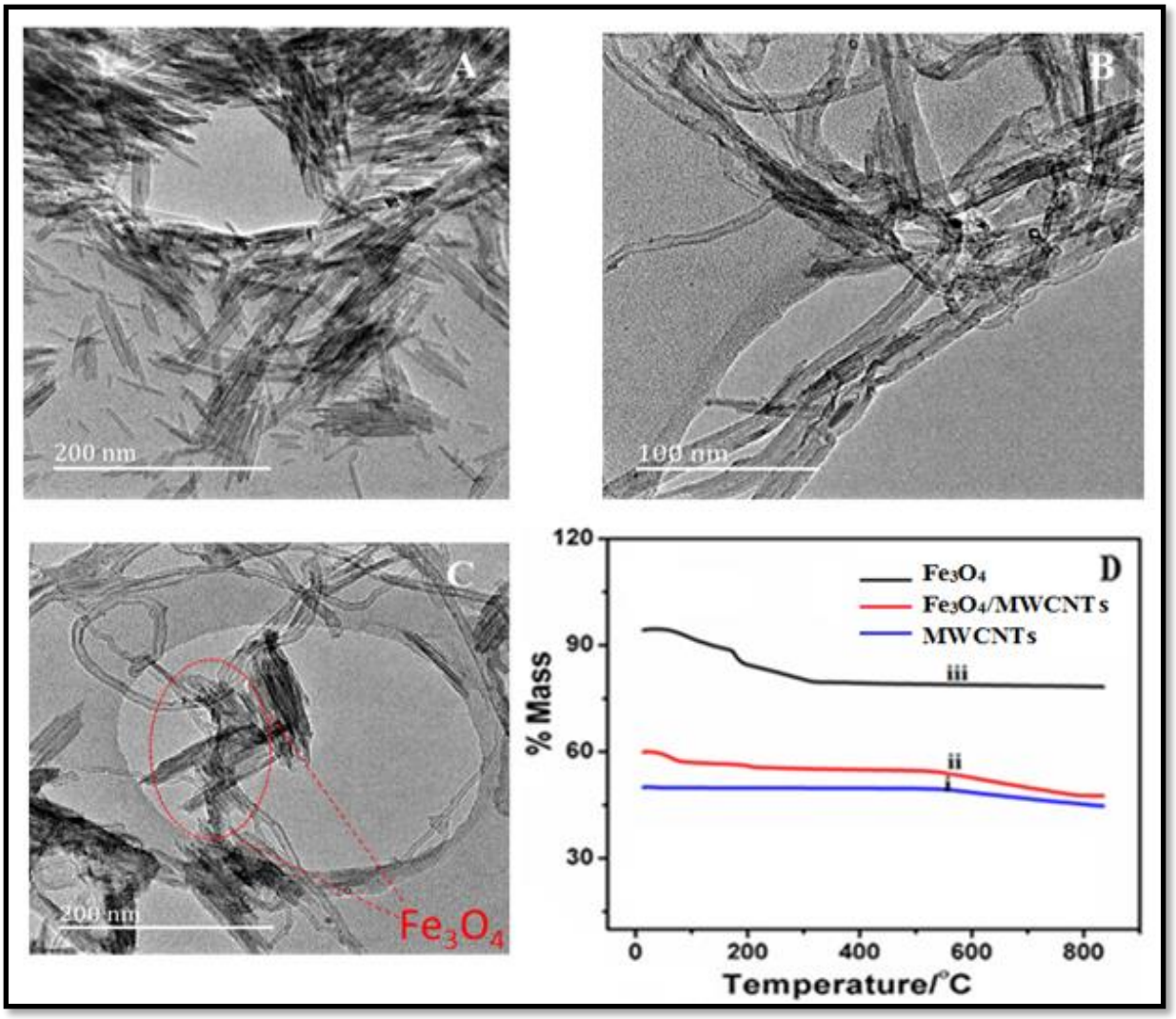

Figure 5.13: (A) TEM image Fe_3O_4NPs (B) Pure MWCNTs (C) MWCNTs-Fe_3O_4NPs (D) TGA curves for (i) MWCNTs (ii) Fe_3O_4NPs-MWCNTs and (iii) Fe_3O_4NPs

Figure. 5.13B clearly shows the tubular network like structure of MWCNTs. The **Figure. 5.13C** reveals the adherence of Fe_3O_4NPS on the surface of the MWCNTs. Furthermore, the thermo gravimetric analysis of the MWCNTs, Fe_3O_4NPs-MWCNTs and Fe_3O_4NPs are shown in **Figure. 5.13D**. The thermograms for pure MWCNTs are shown with definite mass losses at 570 °C due

to the carbon oxidation (black line **Figure. 5.13D**). The Fe_3O_4NPs-MWCNTs shows that the mass losses at below 300 °C due to the loss of residual water in the sample (Arsalani et al., 2010). On the other hand, the Fe_3O_4NPs loses minor mass at below 300 °C due to the evaporation of water. At 600 to 800 °C there is no significant mass loss, and this implies that there is only iron oxide at this range of temperature (Zhou et al., 2010).

5.3.2 Electrochemical behavior of fabricated electrodes

Figure. 5.14A shows the electrochemical behaviors of RIF on bare GCE (black line), MWCNTs-GCE (red line), Fe_3O_4-MWCNTs-GCE (blue line) and Co en-q-Fe_3O_4-MWCNTs-GCE (green line), investigated by cyclic voltammetry. The cyclic voltammograms of RIF showed two anodic peaks at + 0.1 V and + 0.7 V potentials. The bare GCE showed very low anodic peak currents 28 µA, whereas the MWCNTs-GCE and Fe_3O_4-MWCNTs-GCE showed 75 µA and 150 µA currents respectively. The Co en-q-Fe_3O_4-MWCNTs-GCE showed the higher peak currents (220µA) than the remaining modified electrodes **(Figure. 5.14B)**. It can be concluded that the Co en-q has actively participated in the high electron transfer between the RIF molecule and fabricated electrode. Moreover, a graph drawn between log V and log I_{pa} shows a linear relationship and can be expressed as I_{pa} = 0.6782 log V+ 2.6128 (R^2 = 0.9815, **Figure. 5.14C**). Simultaneously a graph was drawn between the anodic peak currents and square root of the scan rate ($\nu^{1/2}$), and the resulting linear equation can be express as I_{pa} = 0.2515 $\nu^{1/2}$ + 0.298 (R^2 = 0.9878) **(Figure. 5.14D)**. The results confirm that the diffusion controlled mechanism is usual for the overall electrochemical reaction of RIF at the fabricated electrode surface (Nicholson and Shain, 1964, Streeter et al., 2008, Xiao et al., 2009). According to these results, an improved electrocatalytic effect of RIF at the fabricated electrodes is due to the increased surface to volume ratio and electronic conductivity. The fabricated electrode surface area was calculated by

Randles-Sevick equation (Bhajanthri et al., 2016). The graphical illustration of electrochemical mechanism of RIF at Co en-q-Fe_3O_4-MWCNTs-GCE.

$$I_{pa} = 2.69\times10^5 \, A \, C_0 \, n^{3/2} D_R \, \nu^{1/2} \qquad (5.7)$$

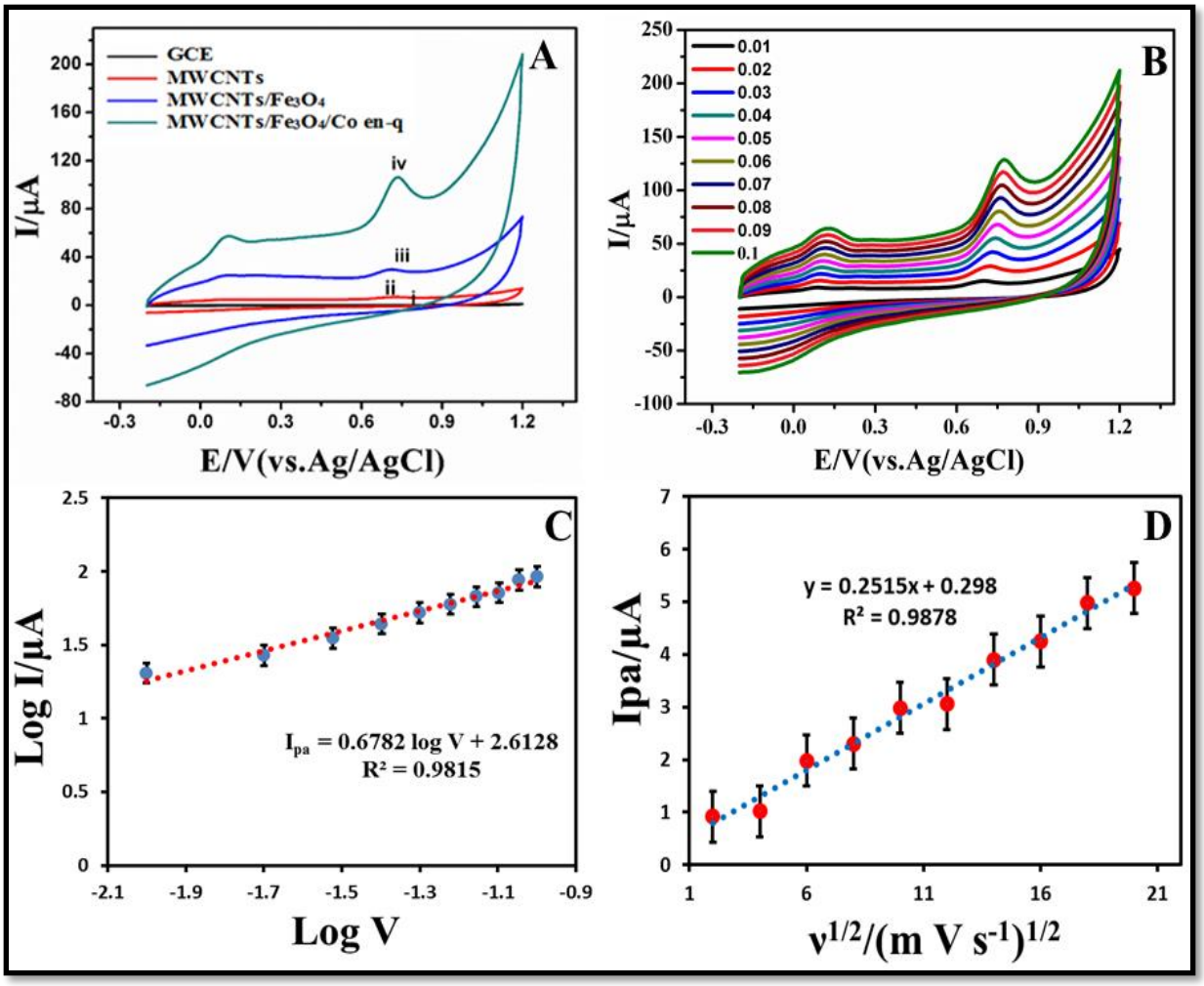

Figure 5.14: (A) Cyclic voltammograms of 0.1 mM RIF in 0.1M PBS (pH 7.5) (i) GCE, (ii) MWCNTs, (iii) MWCNTs-Fe_3O_4NPs-GCE, (iv) Co en-q-MWCNTs-Fe_3O_4NPs-GCE. (B) Cyclic voltammograms of 0.1mM RIF at scan rates 0.01, 0.02, 0.03, 0.04, 0.05, 0.06, 0.07, 0.08 0.09, and 0.1V s^{-1}. (C) Linear relationship of log (I_{pa}) and log (v) (D) The relationship between anodic peak currents (I_{pa}) vs square root of scan rate

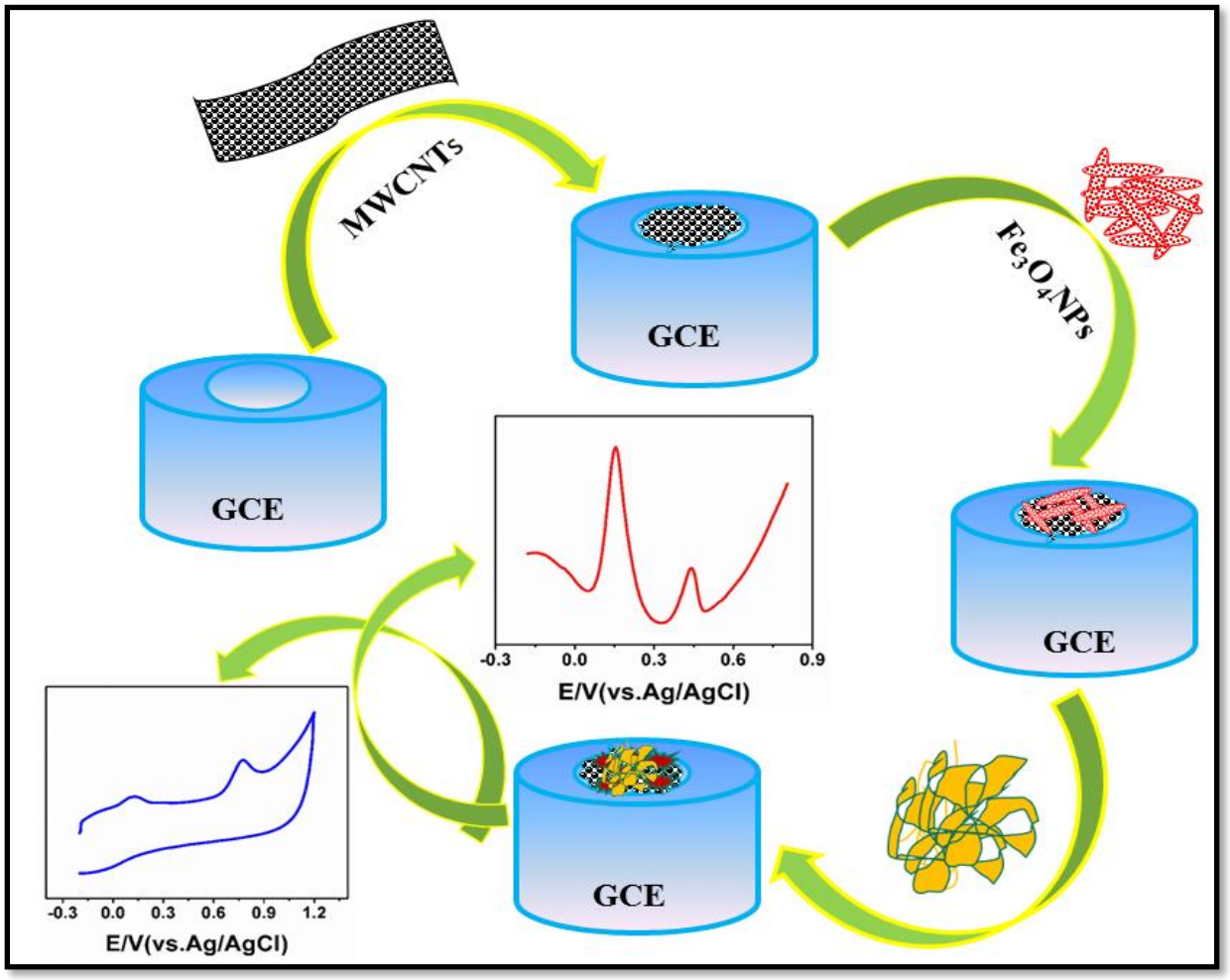

Scheme 5.4: Graphical representation of electrochemical redox mechanism of RIF at Co en-q-Fe_3O_4-MWCNTs-GCE

where I_{pa} denotes the anodic peak current, A the electrode area (A is surface area electrode, r_e is the radius of the rotating disc electrode, ($A=\pi r_e^2$)), C_o is the concentration of RIF, n is the number of electrons involved in the reaction, D_R is the analyte diffusion coefficient (cm^2/s), ν is scan rate ($V\ s^{-1}$). From the above equation, the fabricated electrode and GCE surface area was estimated to be 10.03 and 3.14 mm^2 respectively. The increased surface area and the presence of

adsorptive sites in Co en-q resulting in the significant increase of the anodic currents. This is due to the high density of active sites and the ketonic functional group in Co en-q, accelerating the electron transfer between fabricated electrode and RIF. Based on the obtained results this indicates that the Co en-q-Fe_3O_4-MWCNTs-GCE sensor surface area was approximately three times greater than the GCE surface, which is responsible for the high electrochemical oxidation of RIF **(Scheme 5.5)**.

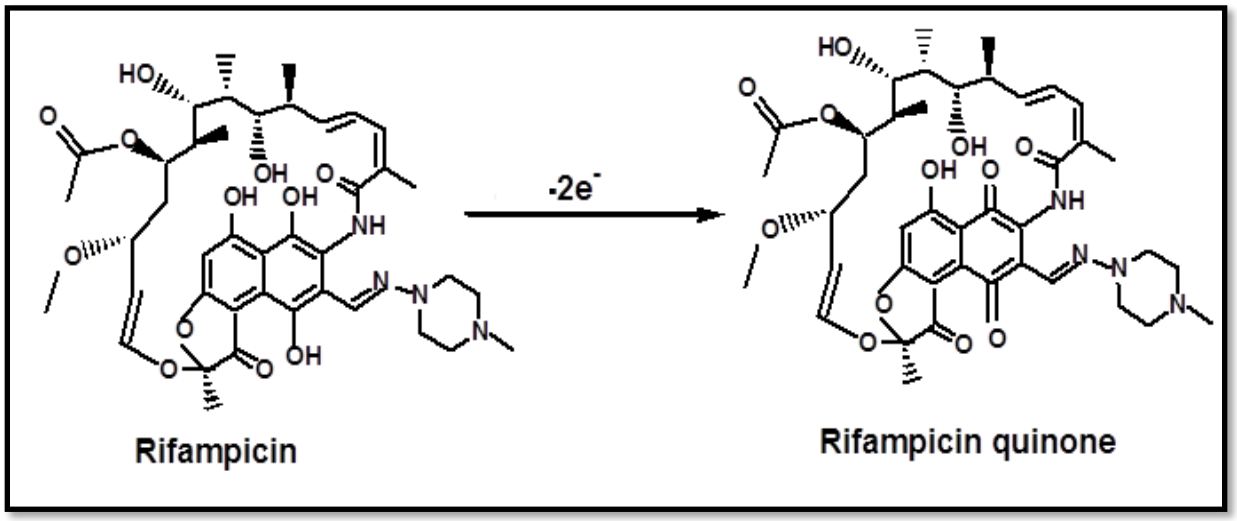

Scheme 5.5: Schematic illustration of the electro oxidation reaction of RIF leading to rifampicin quinone formation

5.3.3 Effect of Co en-q concentration on the sensor response

The CV study was performed in order to determine the optimum concentration of Co en-q within the range of 1.2 to 14 µg mL^{-1}. The anodic peak currents were gradually increasing with the increase in concentrations Co en-q, from 1.2 to 6 µg mL^{-1} **(Figure. 5.15)**. Beyond the concentration 6 µg mL^{-1} the current response decreased gradually. This is due to the steric

hindrance of more accumulation of enzyme on the surface of the electrode, leading to inhibition of the electronic communication between RIF and the fabricated electrode. The concentration of Co en-q was (6 µg mL^{-1}) selected as optimum for the present study.

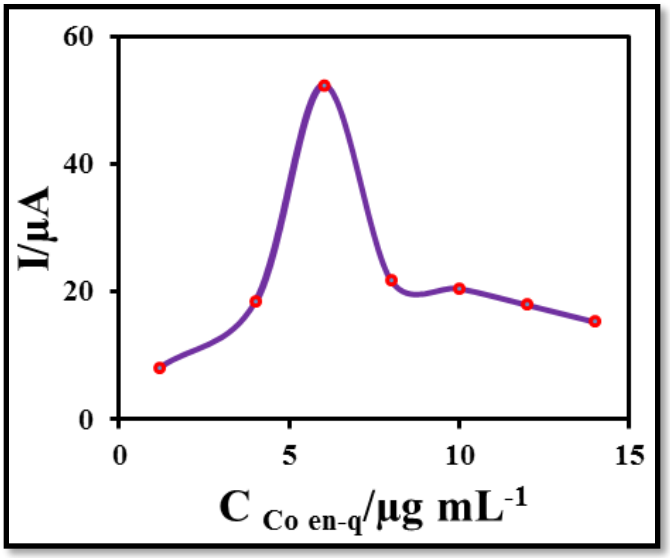

Figure 5.15: Effect of the Co en-q concentration on the response of the Co en-q-Fe_3O_4-MWCNTs GCE in 0.1 mM of RIF with PBS (pH 7.5) at ambient temperature

5.3.4 Influence of pH, scan rates and deposition time

The electrochemical oxidation of RIF basically depends upon the range of the supporting electrolyte pH, because it effects of the responses of peak currents and peak potentials. **Figure. 5.16A** shows the electrochemical sensing abilities of modified electrode in the pH ranges from 2.5 to 9.5. The RIF gave well-defined anodic peak with high current response at pH 7.5, beyond pH 7.5 the peak current responses gradually decreased. According to these results pH 7.5 was choosen as optimum pH. Additionally, the relationship between peak potentials and pH values were plotted and shown in **Figure. 5.16B**.

The linear regression equation obtained in **Figure. 5.16B**, E_p (V) = - 0.0688 pH + 0.8579 with correlation coefficient with R^2 = 0.9877 was approximately equal to the previously reported regression equation E_p (V) = -0.0591 pH + 0.3296 with R^2 = 0.9897 (Asadpour-Zeynali and Mollarasouli, 2017, Rastgar and Shahrokhian, 2014). Based on the above results it is evident that two electrons were involved in electrode oxidation process. **Figure. 5.14B** shows the effect of scan rates ranges from 0.01 to 0.1 mVs^{-1} on the current response of RIF at the fabricated electrode. It can be seen that by increasing the scan rates, the anodic peak currents increase linearly with maximum peak current 0.1 m V s^{-1}. Thus 0.1 m V s^{-1} was used as an optimum scan rate for this study. It was possible to calculate current efficiency of RIF at electrode deposition process based on the polarization curves **(Figure. 5.16C)**. The effect of deposition time was also monitored from 30 to 150 s at scan rate of 0.1 mV s^{-1} at pH 7.5 resulted in a deposition potential of -0.187 V. The current responses were maximum at 90 s, thus it is preferred as optimum deposition time for the entire study **(Figure. 5.16D)**.

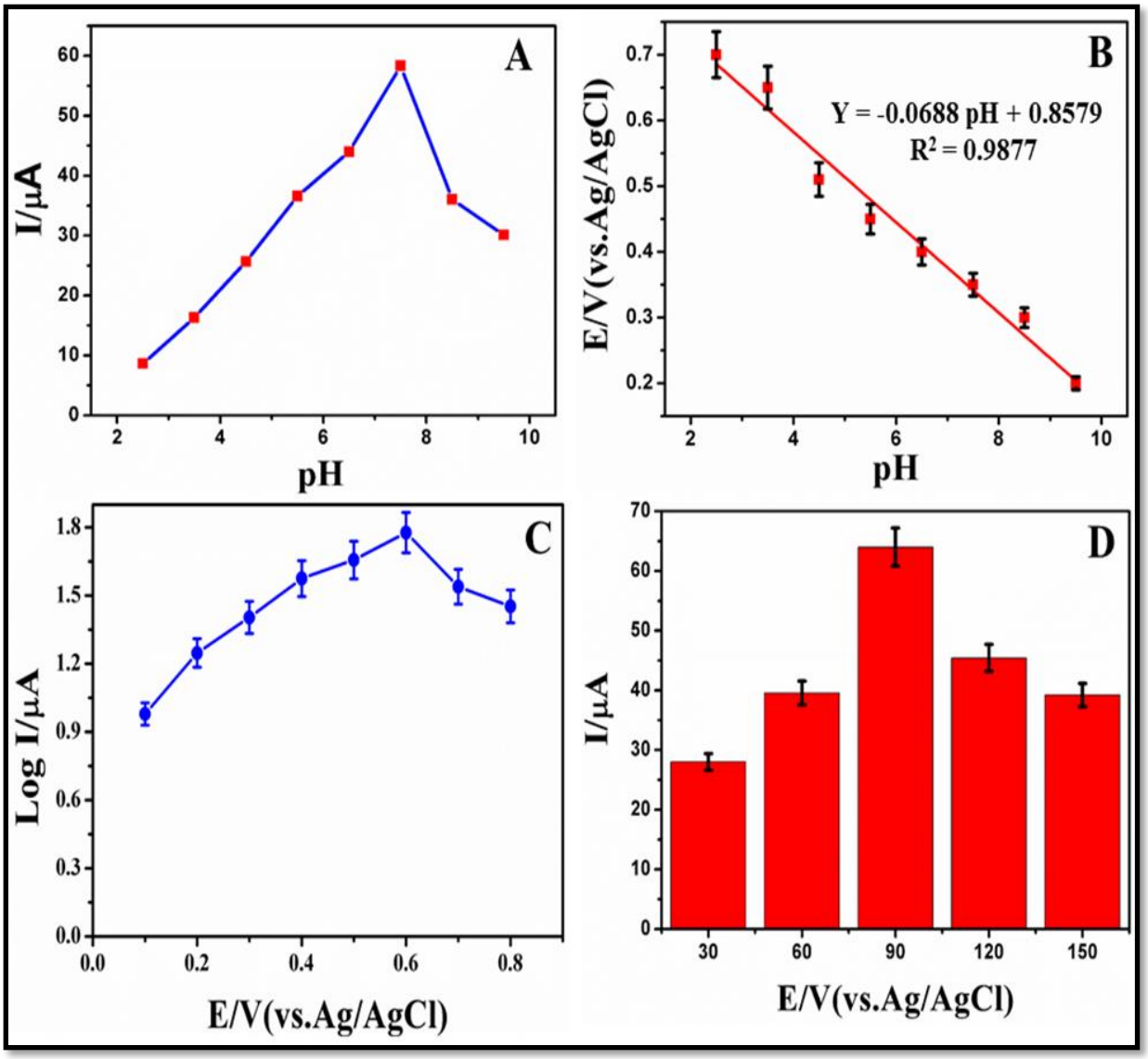

Figure 5.16: (A) Peak potential and peak currents response with pH ranges 2.5, 3.5, 4.5, 5.5, 6.5, 7.5, 8.5, and 9.5. (B) Peak potentials and pH (C) Polarization curve of Co en-q- Fe_3O_4-MWCNTs-GCE. (D) Peak current responses vs different deposition time ranges 30, 60, 90, 120 and 150 s

5.3.5 Determination of sensitivity of the developed sensor

DPV was used to evaluate the sensitivity of the fabricated sensor towards RIF. The working method parameters (scan rate 0.1 V s^{-1}, deposition time 90 s, pulse amplitude 0.050 mV and pulse time 0.040 s) were employed for the differential pulse voltammetric determination. The peak current responses on the concentration of RIF were obtained in the linear range 2 to 20 µM. The calibration curves are linear over the concentration ranges from 2 to 20 µM for DPV. The calibration curve was then plotted for the concentration of RIF versus peak currents **(Figure. 5.17)**.

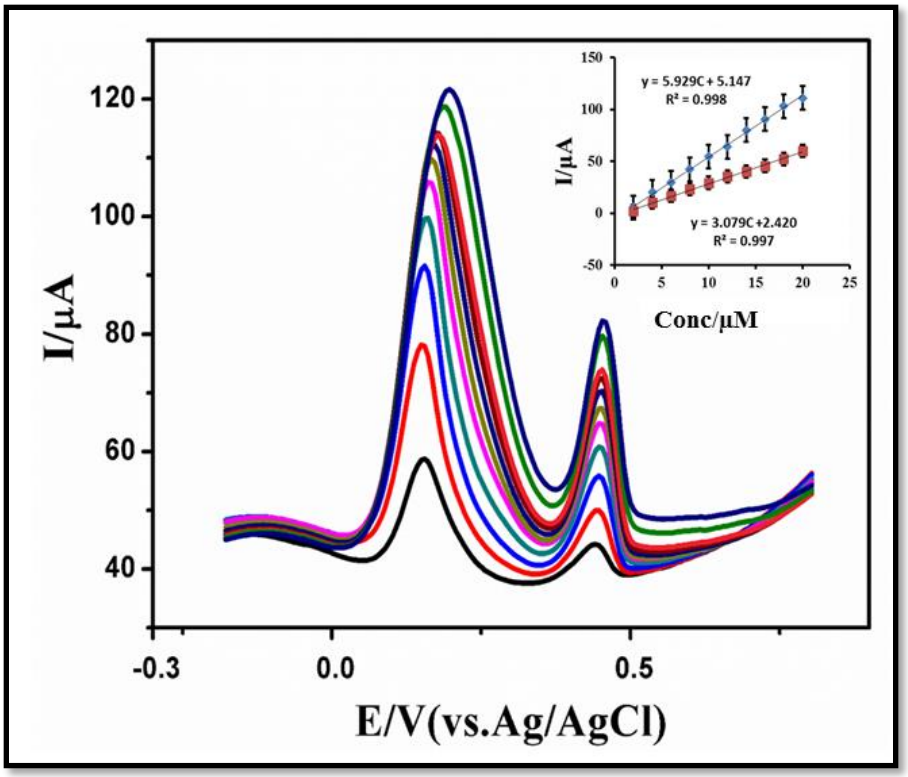

Figure 5.17: DPV recorded at Co en-q-Fe_3O_4NPs-MWCNTs-GCE at different concentrations of RIF (2–20 µM), inset: plot show for linear dependence of I_{pa} versus RIF. (Conditions for DPV pH: 7.5, accumulation time: 90 s, accumulation potential: 0.1Vs^{-1}, pulse amplitude: 0.050 V, pulse time 0.040 s)

Table 5.6: Comparison of some characteristics of modified electrodes with Co en-q-Fe_3O_4NPs-MWCNTs-GCE

Electrode	Technique	LOD/ (μM)	Linear Range/ (μM)	Buffer/ pH	Reference
β-CD/PPY/Pt[1]	CA	1.69	10-50	PBS;7.06	(Lomillo et al., 2005)
AgNPs/PANSA/EGCYP2E1[2]	CV; DPV	0.05	2 - 14	PBS;7.4	(Ajayi et al., 2014)
CPE[3]	SWAdASV	0.05	0.1-6	PBS;7	(Pumera, 2009)
$Ni(OH)_2$–RGO–GCE[4]	LSV	2.34	0.004–10	PBS;7	(Lomillo et al., 2003)
Co en-q- Fe_3O_4NPs-MWCNTs-GCE[5]	CV; DPV	0.032	2-20	PBS;7	This work

β-CD/PPY/Pt- ß-cyclodextrin-polypyrrole coated on platinum electrode; Au/PVP-AgNPs/PANSA/EG-CYP2E1- Polyvinyl pyrrolidone/silver nanoparticles/poly (8-anilino-1-naphthalene sulphonicacid); CPE-Carbon paste electrode; $Ni(OH)_2$–RGO–GCE- Nickel hydroxide nanoparticles-reduced graphene oxide nanosheets coated on glassy carbon electrode; Coenzyme q/ Fe_3O_4NPs/MWCNTs/GCE-Coenzyme q- Fe_3O4 nanoparticles-multiwall carbon nanotubes coated on GCE; CA-chronoamperometry; CV-Cyclic voltammetry; DPV- Differential pulse polarography; SWAdASV- Square-wave adsorptive anodic stripping voltammetry; LSV-Linear sweep voltammetry; PBS-Phosphate buffer solution.

The linear regression equation can be expressed as I_{pa} = 5.929 C_{RIF} (μM) + 5.147 with correlation coefficient [(R^2 = 0.998) and I_{pa} = 3.079 C_{RIF} (μM) + 2.420 with correlation coefficient (R^2 = 0.997)] was determined by DPV. The limit of detection (LOD) and limit of quantization (LOQ) were calculated based on signal to noise ratios, by using the following equations:

$$LOD = \frac{3S_B}{b} \quad (5.8)$$

$$LOQ = \frac{10S_B}{b} \quad (5.9)$$

where S_B is the standard deviation of the blank solution for three different runs, and b is the slope of the calibration curve. The limit of detection and limit of quantification was found to be 0.032 µM, 0.413 µM and 1.069 µM, 1.258 µM for anodic peak I and peak II respectively. The results obtained indicated that the Co en-q-Fe_3O_4NPs-MWCNTs-GCE was an excellent biosensor for the sensitive determination of RIF. Compared to previous reports sensors comparison table **(Table 5.6)**.

5.3.6 Interference studies

The interference effect of the Co en-q-Fe_3O_4NPs-MWCNTs-GCE with 0.1 mM RIF was evaluated in the presence of some organic, inorganic, and some other foreign interfering molecules through DPV method. The inorganic interference ions like $SO4^{-2}$, Br^-, NO_3^-, Ni^{2+}, $Fe^{3+}$and K^+ do not interfere with electrochemical response of RIF. The real samples were also investigated with the possible interference of these pharmaceutical samples with RIF peaks. In addition, the organic interference like glutamic acid, uric acid and folic acid do not interfere with the current response (≤6%) when present in 0.1 mM concentration of RIF. Based on the current results, the fabricated electrode was successfully used for the quantification of RIF in PBS (pH 7.5) and the results of this study are summarized in **Table 5.7**.

Table 5.7: Effects of interferents on the anodic peak current responses for 0.1mM RIF at Co en-q- Fe_3O_4NPs-MWCNTs-GCE based electrochemical sensor

Interference species	Interferents/molar ratio of RIF	Responses ratio (%)
SO_4^{-2}	200	< 1.05
	400	< 2.09
Br^-	200	< 0.9
	400	< 1.06
NO_3^-	200	< 1.35
	400	< 2.49
Ni^{2+}	200	< 0.85
	400	< 1.79
Fe^{3+}	200	< 1.02
	400	< 2.89
K^+	200	< 0.95
	400	< 2.01
Glutamic acid	200	< 1.05
	400	< 2.09
Uric acid	200	< 1.25
	400	< 2.49
Folic acid	200	< 1.09
	400	< 3.01

5.3.7 Analytical performances of the modified sensor

The repeatability of the fabricated sensor performance was calculated by using the anodic currents generated by the various analyte concentrations taken 10 times in a day. In the following day responses of 10 different preparations of electrodes in 0.1 M RIF solution were again tested. It was found that the repeatability decreased less than 5% to original current responses. In order to investigate the stability of Co en-q-Fe_3O_4NPs-MWCNTs-GCE, the CV peak currents were measured in PBS with 0.1 M RIF, and was tested after 50 days. The current responses of the final biosensor remained at 80.25% of the initial response after 40 days as indicated in **Figure 5.18**.

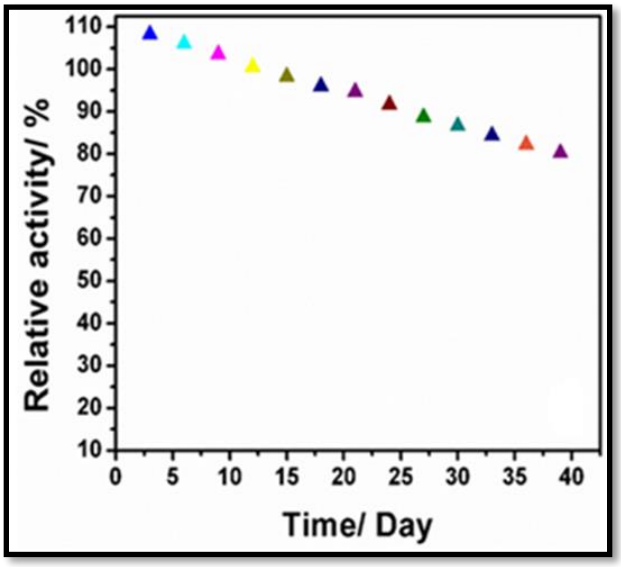

Figure 5.18: Stability for Co en-q-Fe_3O_4NPs-MWCNTs-GCE

5.4 Development of HRP-ZnONPs-RGO-GCE modified glassy carbon electrode for the determination of ethambutol (ETB)

In this study zinc oxide nanoparticles (ZnONPs), reduced graphene oxide (RGO) nanocomposite immobilized with horseradish peroxidase (HRP) on glassy carbon electrode. RGO is a single-to-few-atoms-thick planar sheet of carbon atoms arranged in a honeycomb two-dimensional lattice. It shows good electrical, thermal, optical properties and biocompatible properties. ZnO-RGO nanocomposite provides higher surface area, exhibited and enhanced electron responses in the fabricated electrode. Furthermore, HRP was strongly adsorbed on the surface of modified electrode and showed an enzyme activity for the electrochemical reaction of ETB. Hence, the exceptional properties of HRP-ZnONPs-RGO nano composite enhance electron transfer for the electro catalytic reaction of ETB and this nanocomposite was applied for the determination of ETB and found to exhibit good sensitivity with low detection limits.

5.4.1 Morphological and structural characterization of HRP-ZnONPs-RGO-GCE

Figure 5.19A shows the TEM image of ZnONPs, which are nearly spherical and monodispersed. TEM studies were carried out to find the exact particle size of ZnONPs. The TEM image shows that the particles diameter is approximately 35 nm and matched with XRD data (AbdElhady, 2012, Taunk et al., 2015). The obtained **Figure 5.19B** shows the TEM image of RGO, the sheets consist of few layers, each fixed with a wrinkled structure due to sheet folding (Ortolani et al., 2012, Zhang and Feng, 2010). **Figure 5.19C** shows the TEM of the ZnONPs-RGO, which clearly shows the ZnO nanoparticles agglomerated and distribute homogeneously on the RGO sheet. Our study revealed that such a complex lends itself as a potential precursor for ZnONPs synthesis through thermal decomposition. TGA analyses of the ZnONPs, RGO and ZnONPs-

RGO were carried out from room temperature to 800 °C. **Figure 5.19D** revealed the TGA curves for a typical precursor, at 200 °C the ZnONPs losses high rate of mass due to the evaporation of water absorbed on the surface (Mohamed et al., 2015), and the maximum mass losses occurs at 375 °C also indicating a high rate of degradation of ethyl alcohol into volatile combustible products (Khalil et al., 2014). RGO exhibits one clear step of weight losses below 150 °C, and this relates to the losses of water molecules (Loryuenyong et al., 2013). Furthermore, the ZnONPs-RGO shows minor weight losses below 100 °C due to the release of moisture, and a reliable loss of weight at 200 °C may be attributed to desorption of moisture and solvents (Becheri et al., 2008).

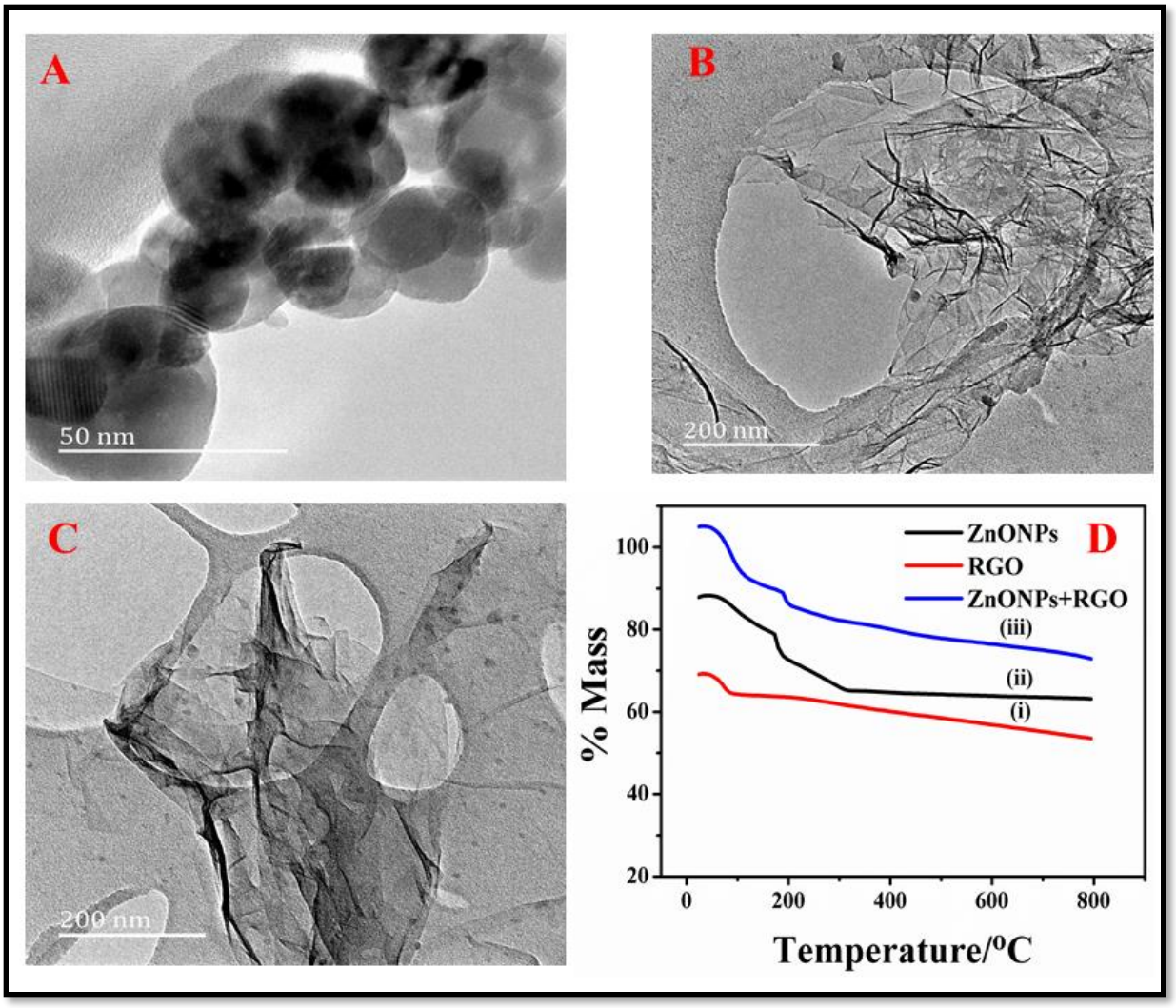

Figure 5.19: (A) TEM image of Pure ZnONPs (B) RGO (C) ZnONPs-RGO (D) TGA curves for (i) RGO (ii) ZnONPs (iii) ZnONPs-RGO

FT-IR studies were carried out in order to determine the purity and nature of the metal oxide nanoparticles. The metal oxide nanoparticles generally give adsorption bands in the fingerprint region below 1000 cm^{-1} arising from inter atomic vibrations. ZnONPs mainly show adsorption bands at 440 – 500 cm^{-1} which are indicative of Zn-O stretching (Becheri et al., 2008). The peaks at 2350 and 3450 cm^{-1} specify the presence of C = O and – OH residues, which may be due to the atmospheric moisture and CO_2 respectively (Becheri et al., 2008, Zak et al., 2011). The peaks which are located at 2937 and 2885 cm^{-1} are due to the symmetric and asymmetric C-H bonds respectively (Zak et al., 2011). The XRD pattern of the synthesized ZnONPs are shown in **Figure 5.20**.

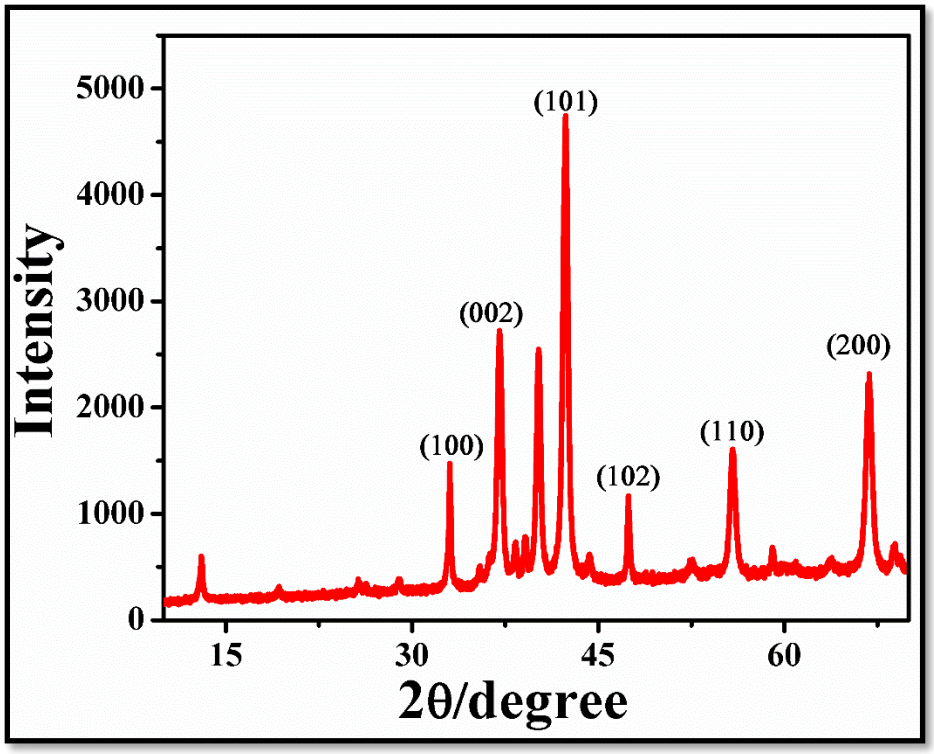

Figure 5.20: XRD image of ZnONPs

The diffraction peaks are located at 32.85° (100), 38.23° (002), 42.36° (101), 47.62° (102), 56.35° (110), and 64.38° (200) respectively. Moreover, the peak intensity is narrow and sharp, it conforms the quality of the ZnONPs with excellent crystallinity. The diffraction peaks of the ZnONPs obtained correspond to the specific hexagonal wurtzite structure (Khalil et al., 2014, Talam et al., 2012). The crystallites undergo a reorientation with the (002) orientation being favoured, while the (100) peak intensity decreases. The nanoparticles sizes also calculated by using the Debye-Scherer formula.

$$d = \frac{0.89\lambda}{\beta cos\theta} \tag{5.10}$$

where 0.89 is Scherer's constant, d is the average grain size, θ is the Bragg diffraction angle, λ is the wave length of X-rays and β is the full width at half maximum of the diffraction peak corresponding to plane (101).

5.4.2 Electrochemical characterization and effect of deposition time

The electrochemical behaviour of ETB on the bare GCE, RGO-GCE, ZnO-RGO-GCE and HRP-ZnONPs-RGO-GCE are shown in **Figure 5.21A**. The CV is used to examine the electron transmission process of the fabricated electrode. The CV performance of 0.1 mM ETB in 0.1 M PBS (pH 7.0) in the positive scan direction shows a quasi-reversible pair corresponding to redox reactions. The bare GCE shows an oxidation peak at -0.12 V and reduction peak -0.22 V with a redox peak separation of 14 µA, which may be attributed to the poor electrochemical activity on the bare GCE (Curve i). RGO-GCE and ZnO-RGO-GCE also show a reversible anodic and cathodic peak at -0.12 V and -0.22 V with 25 µA and 85 µA currents respectively. On the other hand, the HRP-ZnONPs-RGO-GCE gave rise to a sharp redox peak with a peak current of 130

µA. Moreover, the fabricated electrode provides an extremely large enhancement of the anodic and cathodic currents as observed. The kinetics of electron transfer for ETB improves remarkably at the fabricated electrode, here the HRP enzyme act as a good electron transfer agent between the electrode and analyte. **Figure 5.21D** shows the effect of deposition time from 30 - 150 s. The anodic and cathodic peak currents are increased proportionally with the time between 30 to 150 s. In addition, that the sensitivity was improved to provide a longer deposition time, and also increases the upper detection limits, due to the electrode surface becoming saturation in the high concentration region were observed. When the deposition time became longer than 60 s, the peak currents decrease gradually and this might be due to the working electrode surface saturation. Due to the consideration of increased sensitivity the optimized deposition time of 60 s was used throughout this experiment.

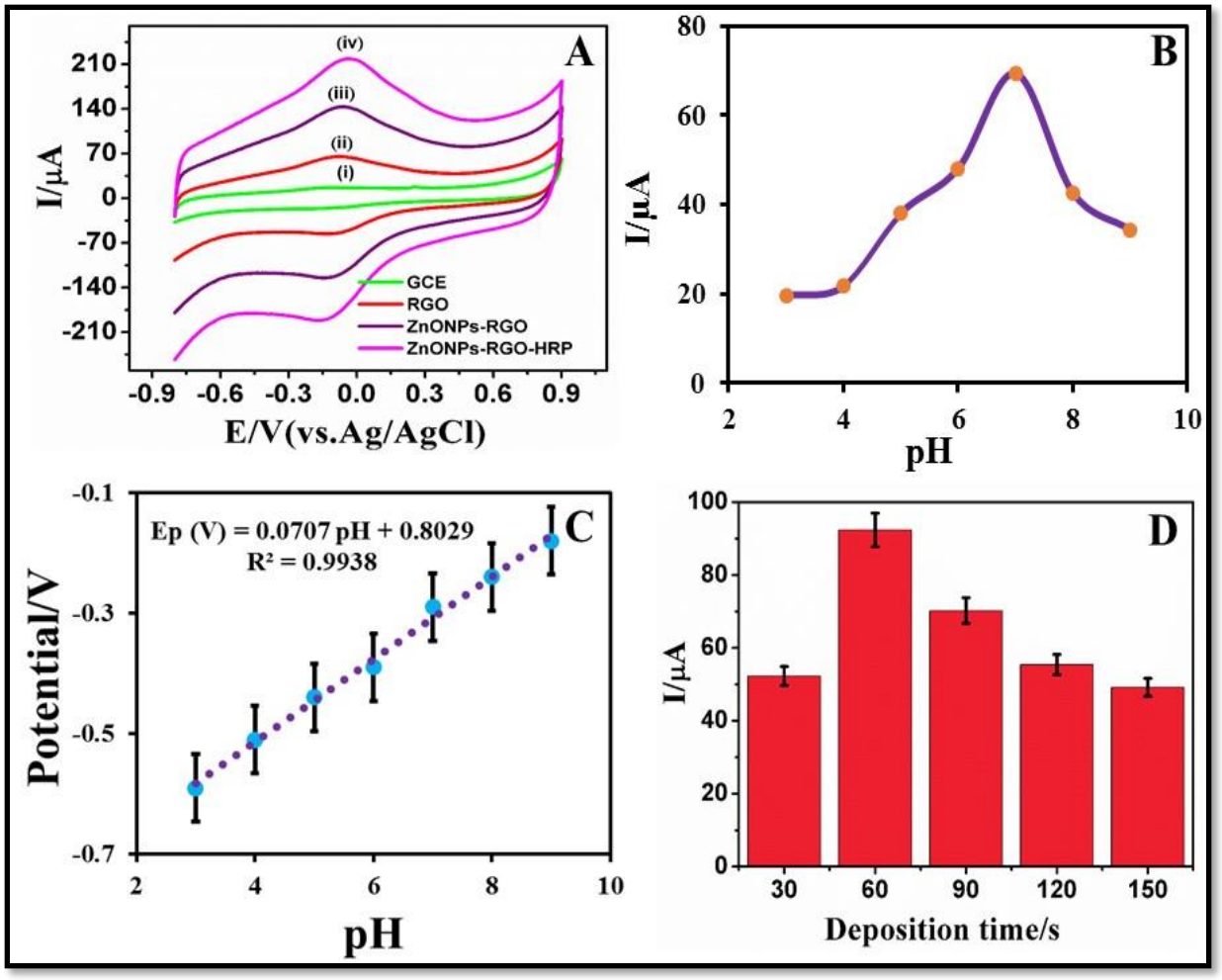

Figure 5.21: (A) Cyclic Voltammograms of 0.1mM ETB at bare (i) GCE, (ii) RGO-GCE (iii) ZnO NPs-RGO-GCE, and (iv) HRP-ZnONPs-RGO-GCE. (B) Peak potential and current response with respect to change in pH (3-9) with 0.1 mM ETB. (C) The plot of peak potential (Ep) of anodic wave versus pH (pH 3-9). (D) Various deposition times (30, 60, 90, 120, and 150 s) on peak current

5.4.3 Effect of pH on the electrochemical behavior of ETB at HRP-ZnONPs-RGO-GCE

The electrochemical redox reaction was influenced by protons in the electrode reaction process of ETB, and the effects of solution pH was investigated. The effect of pH on the current responses of HRP-ZnONPs-RGO-GCE towards 0.1 mM of ETB was investigated within the pH range of 3.0 to 9.0. **Figure 5.21B** shows that the oxidation peak currents are gradually increasing with the increased pH from 3.0 to 7.0. The phenomenon was attributed to the high concentration of protons in the solution. The anodic peak current of ETB reaches a maximum at pH 7.0. **Figure 5.21C** shows the peak potential E_{pc} shifts to higher negative potential when the pH is increased and obtained correlation coefficient is R^2 = 0.993. The HRP-ZnONPs-RGO-GCE showed electron transfer accompanied by an equal number of protons in the electrode reaction.

5.4.4 Effect of enzyme incubation time

The enzyme incubation time of the HRP-ZnONPs-RGO-GCE is an important parameter for the determination of ETB. The enzyme incubation time was investigated in the range from 5 to 25 min at room temperature, and then the corresponding response of currents were measured by the DPV. **Figure 5.22** shows that the current response increased gradually with prolonged incubation time and the maximum is attained at 15 min. When 15 min exceed, the peak current response gradually decreased with prolonged incubation time. This suggests that the fabricated electrode reached saturation point.

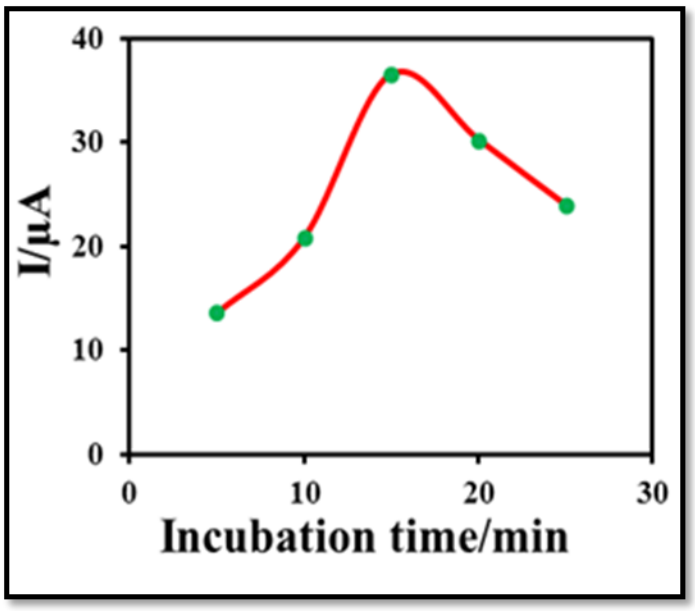

Figure 5.22: Effect of incubation time on the response of HRP-ZnONPs-RGO-GCE

5.4.5 Effect of scan rate variation on the electrochemical behaviour of ETB at HRP-ZnONPs-RGO-GCE

Figure 5.23A shows the effect of scan rate on the peak current and peak potential of ETB at HRP-ZnONPs-RGO-GCE. For this investigation, the electrochemical reaction of ETB at the HRP-ZnONPs-RGO-GCE was studied using cyclic voltammetry, at relatively low scan rate from 0.01 to 0.1 V s^{-1}, in the presence of 0.1 mM of PBS (pH 7.0). The anodic and cathodic peak currents of ETB at final sensor was proportional to the square root of the scan rate **(see Figure 5.23B)**, which indicates a diffusion controlled electrochemical reaction at HRP-ZnONPs-RGO-GCE.

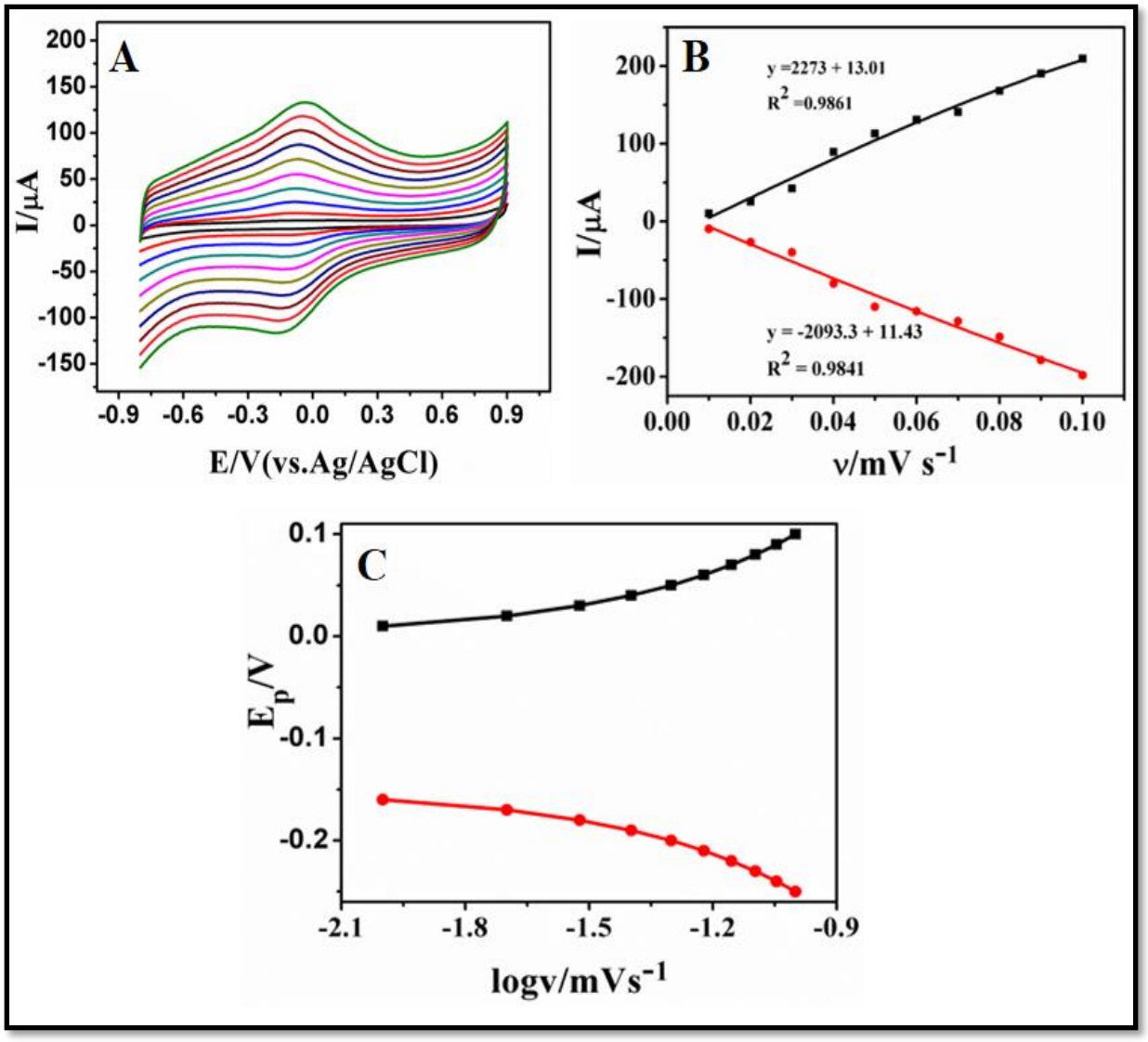

Figure 5.23: (A) Cyclic voltammograms 0.1 mM ETB on surface of HRP-ZnONPs-RGO-GCE at various scan rates; (1) 0.01, (2) 0.02, (3) 0.03, (4) 0.04, (5) 0.05, (6) 0.06, (7) 0.07, (8) 0.08, (9) 0.09 and (10) 0.1 mV s^{-1} in PBS buffer of pH 7.0. (B) Dependence of anodic and cathodic peak current on scan rate. (C) Variation of peak potential vs logarithm of the scan rates from 0.01 to 0.1 mV s^{-1}

The results indicate that the anodic and cathodic peak current increased with an increase in the scan rate. The regression equations are I_{pa} (μA) = 2273 + 13.01 v (R^2 = 0.9861) and I_{pc} (μA) = – 2093.3 + 11.43 v (R^2 = 0.9841), indicating electrochemical oxidation and reduction process of ETB at the HRP-ZnONPs-RGO-GCE. Based on the above results, it could be reasonably assumed that ETB was firstly absorbed on the surface of the electrode and then the electrode reaction occurs. Moreover, based on the laviron (Gowda and Nandibewoor, 2014) model, the electron transfer coefficient *α*, and the apparent heterogeneous charge transfer rate constant k_s, can be estimated from cyclic voltammetry using the deviation of the anodic and cathodic peak potentials as a function of the logarithm of scan rates. At high scan rates, this theory calculated a linear dependence of E_{pvs} and log v which can be used for the determination of kinetic parameters like *α* and k_s from the slope intercept plots shown in **Figure 5.23B**. The graph drawn for E_P against log *v* from CV of ETB at HRP-ZnONPs-RGO-GCE in PBS (pH 7.0) is shown in **Figure 5.23C**. From the graph values versus log *v* was give slightly curved lines with a slope. Based on the slope the cathodic peak equal to −2.3*RT*/*αnF*, and anodic peak equal to 2.3*RT*/ (1 − *α*) *nF*. The two peak values are substituted in the equation (5.11), the charge transfer coefficient *α* was found to be 0.63 and the electron transfer constant was estimated to be k_s = 2.93 s^{-1}.

$$\log k_s = \alpha \log(1-\alpha) + (1-\alpha) - \log\left(\frac{RT}{nFv}\right) - \alpha(1-\alpha)\left(\frac{nF\Delta Ep}{2.3RT}\right) \qquad (5.11)$$

where ΔE_P is ($E_{Pa} - E_{Pc}$), *α* is the transfer coefficient, *v* is the potential scan rate (V s^{-1}), k_s is the heterogeneous electron transfer rate constant (s^{-1}) and *R* indicate gas constant and *T* is temperature in kelvin. The electrochemical mechanism is indicated in **scheme 5.6**.

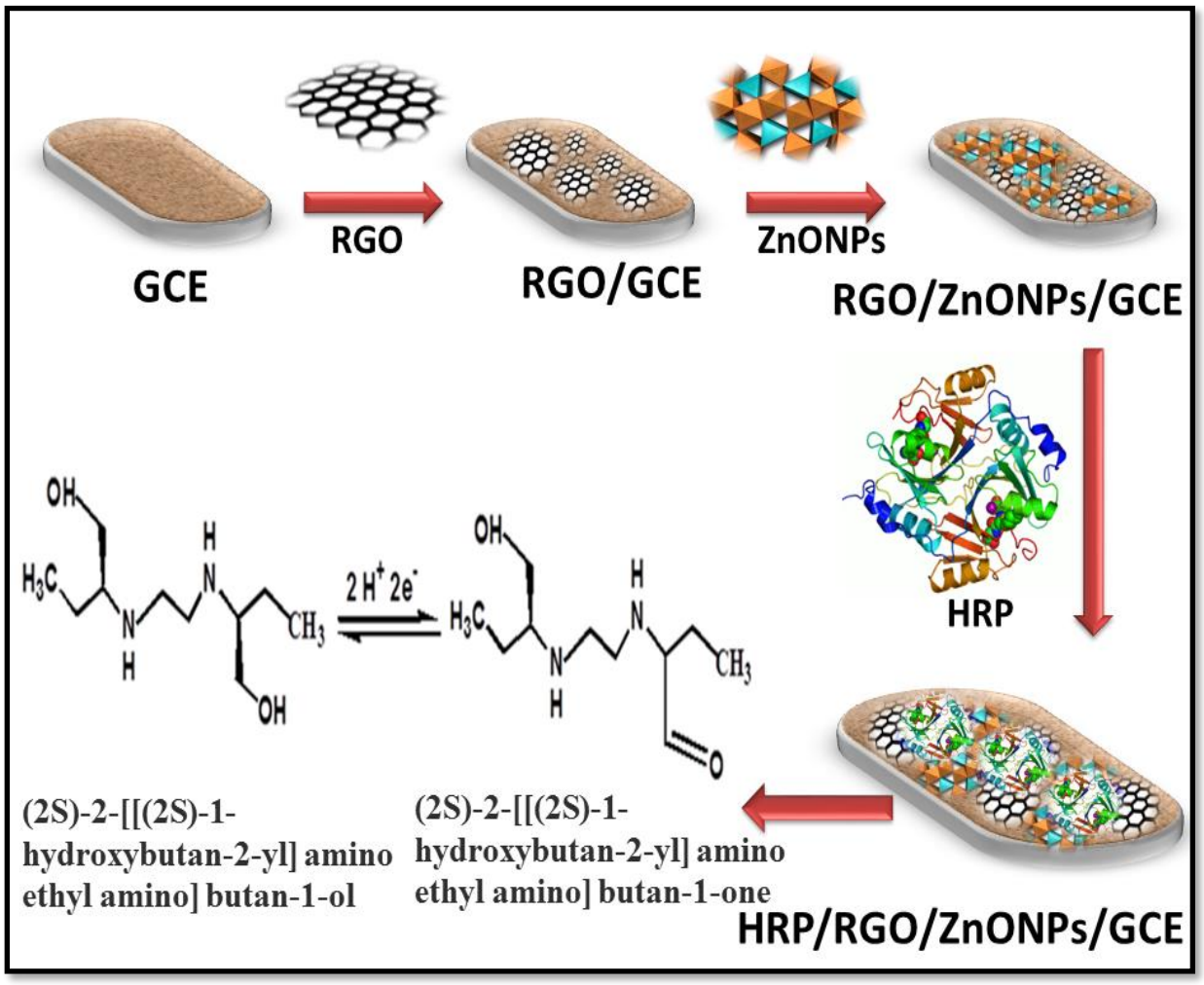

Scheme 5.6: Fabrication of GCE with nanocomposite and electrochemical mechanism for ETB

5.4.6 Reproducibility and stability studies

The electro chemical oxidation and reduction reactions of ETB at the HRP-ZnONPs-RGO-GCE were studied using the CV and DPV technique to evaluate the repeatability and reproducibility as these are critical parameters for the biosensor performance. Moreover, the reproducibility of the HRP-ZnONPs-RGO-GCE was estimated under the optimal experimental conditions based on current responses given by the 0.1 mM ETB which are three modified electrodes. The three electrodes are fabricated independently, the relative standard deviation (RSDs) was found to be 2.83 % of the HRP-ZnONPs-RGO-GCE. The repeatability of the biosensor was also examined by monitoring the current response to 0.1 mM ETB for five times. The RSD was 1.93 %, indicating a remarkable reproducibility of this fabricated electrode.

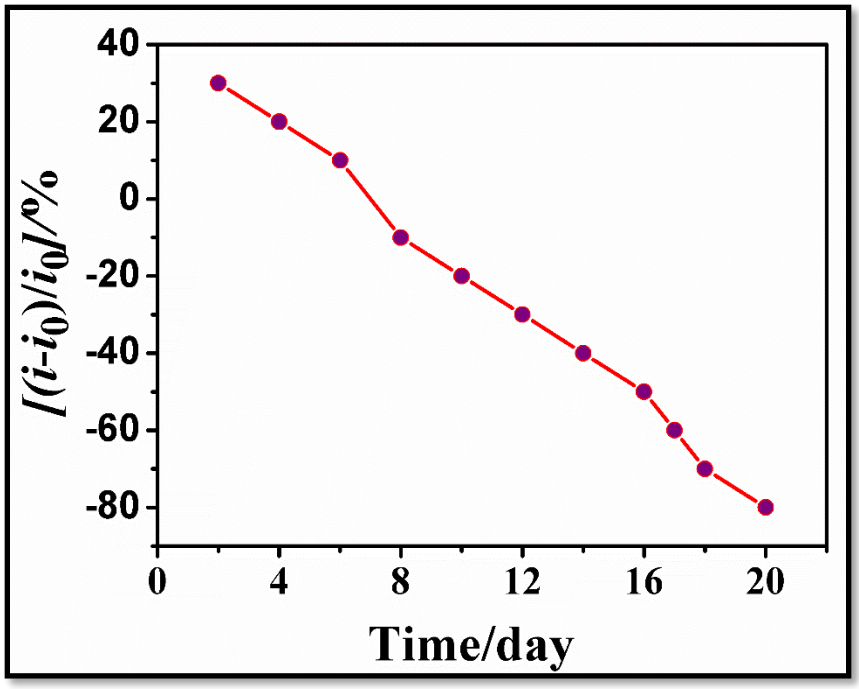

Figure 5.24: Stability of HRP-ZnONPs-RGO-GCE. Each data point of graph is based on measuring the DPV response of 0.1 mM of ETB in 0.1 M PBS at pH 7.0

In order to investigate the HRP-ZnONPs-RGO-GCE long term storage stability, the current response of 0.1 mM ETB was measured during a period of 20 days. The fabricated electrode was stored in 0.1 M PBS (pH 7.0) at 4 °C when not in use. **Figure 5.24** shows the stability response of the HRP-ZnONPs-RGO-GCE, where i_0 is the current response of the modified HRP-ZnONPs-RGO-GCE, i is the current response at any storage time, (i-i_0) is the change in the current response at any storage time. Initially the HRP-ZnONPs-RGO-GCE showed a good stability for five days, the current response being 84 %. Thereafter, an activity of 72 % was observed after 15 days and only 12 % of the current response decreased after 15 days. Based on the results the biosensor showed good long-term stability.

5.4.7 Calibration plots and detection limit

In order to develop a voltammetric procedure for the determination of ETB DPV technique was chosen, DPV is a rapid and effective electroanalytical technique with more advantages such as low detection limits, good sensitivity and selectivity against background currents, DPV was the chosen technique. The current – voltage analytical curve for the HRP-ZnONPs-RGO-GCE, and quantitative analysis of the 0.1 M concentration of ETB were performed by DPV, under the optimized experimental conditions. Moreover, with successive additions of the ETB, the peak currents increased linearly with increasing the concentration of ETB and the corresponding calibration curve is presented as an insert in the respective voltammograms shown in **Figure 5.25**. The calibration curves are linear over concentration ranges from 2 to 32 µM for DPV. Using HRP-ZnONPs-RGO-GCE the detection of ETB in the potential range of -0.5 to 0.0 V under optimal parameters of 0.052 V for pulse amplitude, 0.041 s for pulse time, scan rate of 0.015 V s^{-1} and deposition time 60 s was used for this study. It gave a well-defined peak at -0.2 V

(vs. Ag/AgCl) with good linearity and the linear regression equation was expressed as R^2 = 0.9818.

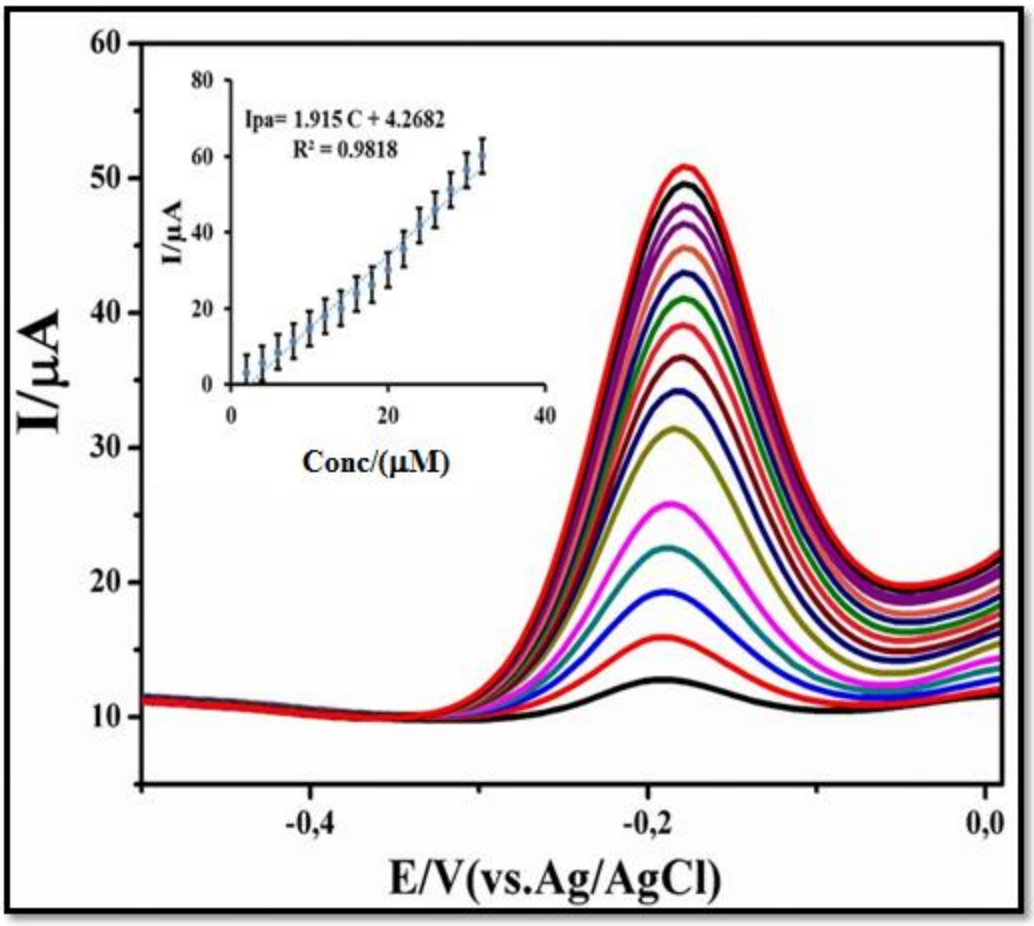

Figure 5.25: DPVs of HRP-ZnONPs-RGO-GCE obtained in a linear range of 2 to 32 µM of ETB in PBS (pH 7.0) at 0.015 mV s^{-1} scan rate. Insert plot shows the linear dependence of Ipa vs. [ETB]

The limit of detection (LOD) and limit of quantization (LOQ) was calculated by using the signal to noise method. A signal to noise ratio of three is generally accepted for estimating LOD and signal to noise ratio of ten is used for estimating LOQ.

$$DL = \frac{F \times SD}{b} \quad (5.12)$$

where DL is corresponded to 3 or 10 times of the noise level, F is the factor of 3.3 and 10 for DL, SD is the standard deviation of the blank, b is the slope of the regression curve. The limit of detection (LOD) and limit of quantification (LOQ) is 0.0214 µM and 0.6713 µM respectively. HRP-ZnONPs-RGO-GCE was compared with some other electrodes reported for ETB determination **(Table 5.8)**. The HRP-ZnONPs-RGO-GCE showed better LOD and LOQ values for ETB than the previously reported sensors.

Table 5.8: Comparison of some characteristics of modified electrodes with HRP-ZnONPs-RGO-GCE

Electrode	Technique	Detection Limit/µM	Buffer & pH	Reference
Carbon electrode [a]	FIA	100	NaOH (12)	(Bellei Perantoni et al., 2011)
Platinum electrode [b]	CE	24.2	Sodium tetra borate (8.03)	(Ngece et al., 2011)
Au-PVP-Ag-PANSA-CYP2E1 [c]	CV&DPV	0.7	PBS (7)	(da Silva et al., 2010)
Tyr-GCE [d]	CV&DPV	9.61	PBS (7)	(Cheemalapati et al., 2014c)
Gold microelectrode [e]	CV&SWV	4.73	Acetate (4.5)	(Lima et al., 2016)
Nafion-MWCNT-SPCE [f]	CV&SWV	8.4	CPBS (7.4)	(Couto and Quinaz, 2016)
HRP-ZnONPs-RGO-GCE	CV&DPV	0.0214	PBS (7)	This Work

FIA- Flow Injection Analysis, CE-Capillary electrophoresis, Au/PVP-Ag-PANSA/CYP2E1[c]- A silver Nanoparticle/Poly (8-Anilino-1-Naphthalene Sulphonic Acid), CV-Cyclic voltammetry, DPV-differential pulse voltammetry, Tyr/GCE-Tyrosine modified on glassy carbon electrode, SWV-Square wave voltammetry, Nafion/MWCNT-SPCE[f]-Nafion/multiwall carbon nanotubes modified screen printed carbon electrode, HRP/ZnONPs/RGO/GCE-Harsh radish peroxidase, zinc oxide, reduced graphene oxide modified glassy carbon electrode.

5.4.8 Interference studies

In order to evaluate the interference from the various reductive species existent in real samples, DPV was used with 0.1 mM ETB. The interference concentrations were added higher than those normally present in the real samples. Some of the organic compounds such as ascorbic acid, sucrose, glucose and some of the common ions such as Ca^{2+}, K^{+}, Cl^{-}, Ag^{+}, Br^{-}, Na^{+} and SO_3^{2-} had no influence on the determination of ETB. The tolerable interference concentration was taken as the measured signal variation which was approximately ±3. After the addition of varying concentration of each interferent the results are presented in **Table 5.9**. According to these results, they show that this HRP-ZnONPs-RGO-GCE has negligible interference effect for the determination of ETB.

Table 5.9: The influences of some anions, cations and important biological substances on the peak current of 0.1 mM ETB at HRP-ZnONPs-RGO-GCE

Interferents	Concentration of interferents/µM	Change in current responses/%
Ascorbic acid	50	-2.06
	100	-3.96
Sucrose	50	-1.32
	100	-2.03
Glucose	50	-1.28
	100	-2.62
Ca^{2+}	50	-0.36
	100	-0.65
K^{+}	50	-0.64
	100	-1.02
Cl^{-}	50	-1.20
	100	-2.01
Ag^{+}	50	-0.86
	100	-1.54
Br^{-}	50	-0.56
	100	-1.26
Na^{+}	50	-0.21
	100	-0.5
SO_3^{2-}	50	-0.76
	100	-1.36

5.4.9 Determination of ETB in pharmaceutical formulation

The real pharmaceutical sample preparations were described in the above section. In order to test the applicability of the proposed biosensor for the investigation of real pharmaceutical samples, the analysis of the ETB tablets (300 and 500 mg/tablet) were carried out by differential pulse voltammetry and the results are summarized in **Table 5.10**. The recovery percentages are varied in the ranged of 98.5–99.6%, which can be considered to be substantial, and these recovery

percentages are very close to the official monograph of ETB (A.M.I. Rageh et al., 2016). (Not less than 98 % and not more than 105 % of ETB are contained in real labeled samples).

Table 5.10: Determination of ETB in various pharmaceutical samples using HRP-ZnONPs-RGO-GCE (n=5)

Declared amount tablet (mg)	Found (mg)	Recovery (%)	RSD (%)	Added (mg)	Found (mg)	Recovery (%)	RSD (%)
Sample 1 (300 mg)	298.7	99.5	1.79	50	49.3	98.6	0.42
Sample 2 (500 mg)	498.2	99.6	1.98	100	98.5	98.5	0.89

n: average determination

5.4.10 Precision and accuracy

The proposed electrochemical biosensor repeatability (intra-day precision) was estimated by associating the standard deviations found from the peak area measurements. The standard deviation values varied from 0.58 to 0.98 for intra-day precision. Inter-day precision analysis was performed on five consecutive days and the obtained standard deviations were from 1.12 to 1.16, which show good precision for the proposed method. The standard deviation value obtained in this analytical technique compare very favourably with that obtained in the reference material (A.M.I. Rageh et al., 2016). Accuracy was estimated as a percentage of relative error

between the calculated mean concentration and added (spiked) concentration for ETB (Bias %). The values are shown in **Table 5.11**.

Table 5.11: Precision and accuracy study for the commercial dosage forms (n=5)

Sample Added/µM	Inter-day			Intra-day		
Tablet (Rimstar 4-Fdc brand)	Found[a]/ µM	Precision[b]/ (%)	Accuracy[c]/ (%)	Found[a]/ µM	Precision[b]/ (%)	Accuracy[c]/ (%)
3	2.98±0.03	0.58	0.66	3±0.03	1.12	0
5	5.01±0.04	0.76	0.20	4.98±0.04	1.14	0.40
8	7.97±0.06	0.98	0.37	8.02±0.06	1.16	0.25

[a] Mean ± standard error.
[b] Precision%: Relative standard deviation (RSD).
[c] Bias %: [(found-added)/added] ×100%.

5.5 Development of Cyt c-ZnONPs-MWCNTs fabricated on glassy carbon electrode for the detection of streptomycin (STN)

In this work cytochrome c (Cyt c) enzyme was used in the fabrication of the glassy carbon electrode with zinc oxide nanoparticles (ZnONPs) on the multiwalled carbon nanotubes (MWCNTs). MWCNTs enabled the electron transfer among the electroactive species and the electrode, while DMF was used as a dissolving reagent for the MWCNTs. In addition, the MWCNTs were anchored with ZnONPs to produce the extra electro catalytic sites, MWCNTs-ZnONPs nanocomposite enriched the thermal stability and activity of Cyt c over a wide pH range. Furthermore, Cyt c was strongly adsorbed on the surface of the fabricated electrode and showed an enzyme immobilization activity for electrochemical reduction of STN. Therefore, the unique properties of Cyt c-ZnONPs-MWCNTs nano composites improve the electron transfer for the electro catalytic reduction of STN, compared either with ZnONPs or MWCNTs. Likewise, the Cyt c-ZnONPs-MWCNTs nanocomposite substantially improved the detection of STN, and also showed good limit of detection, limit of quantification and sensitivity.

5.5.1 Morphological and structural characterization of Cyt c-ZnONPs-MWCNTs-GCE

Figure 5.26A show the TEM image of ZnONPs, which are nearly spherical and monodispersed. TEM studies were carried out to find the exact particle size of ZnONPs. The TEM image shows that the particles diameter is approximately 7 - 12 nm and matched with XRD data (AbdElhady et al., 2012, Taunk et al., 2015). The morphological structure of MWCNTs where the crystalline tubular structure of nanotubes is indicated in **Figure 5. 26B**, with the nanotubes having clear inner channels. **Figure 5. 26C** shows the TEM images of MWCNTs decorated with ZnONPs, which clearly show the ZnO nanoparticles agglomerated and distribute homogeneously on the

MWCNTs. Our study revealed that such a complex lends itself as a potential precursor for ZnONPs synthesis through thermal decomposition.

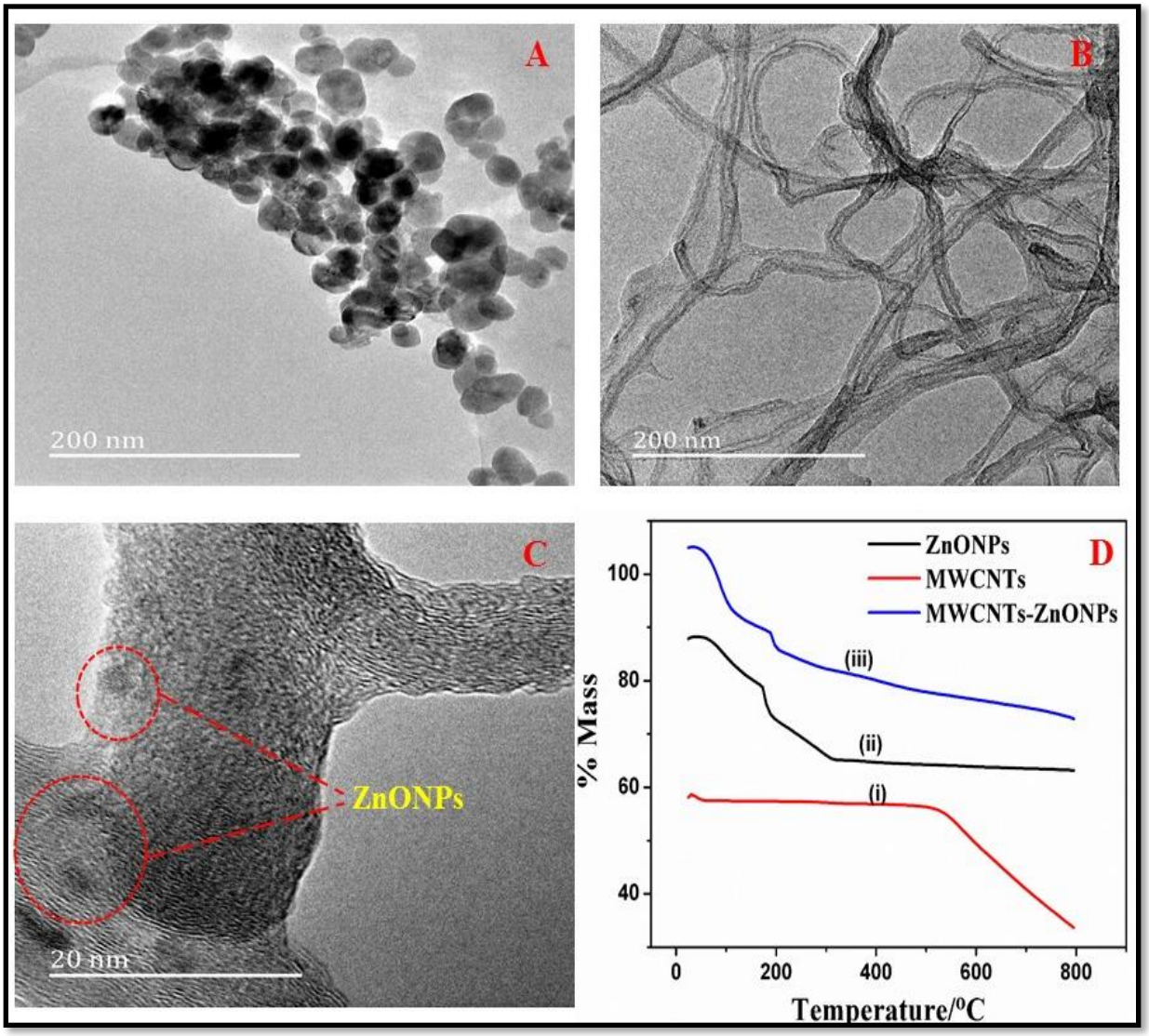

Figure 5.26: TEM images for (A) ZnONPs (B) pure MWCNTs (C) ZnONPs decorated on MWCNTs (D) TGA curves for (i) MWCNTs (ii) ZnONPs (iii) MWCNTs-ZnONPs

TGA analyses of the ZnONPs, MWCNTs and ZnONPs-MWCNTs were conducted from room temperature to 800 °C. **Figure 5. 26D** reveals the TGA curves for a typical precursor, at 200 °C the ZnONPs loses a high rate of mass due to the evaporation of water absorbed on the surface (Mohamed et al., 2015), and the maximum mass losses occurs at 375 °C also indicating a high rate of degradation of ethyl alcohol into volatile combustible products (Khalil et al., 2014). The thermograms for pure MWCNTs are shown with definite mass losses at 570 °C and are due to the carbon oxidation (black line **Figure 5. 26D**). Furthermore, the ZnONPs-MWCNTs shows minor weight losses below 100 °C due to the release of moisture and a reliable loss of weight at 200 °C. This may be attributed to desorption of moisture and solvents (Becheri et al., 2008). FT-IR studies were carried out in order to determine the purity and nature of the metal oxide nanoparticles. The metal oxide nanoparticles generally give adsorption bands in fingerprint regions below 1000 cm^{-1}, arising from inter atomic vibrations. ZnONPs mainly shows adsorption bands at 440 – 500 cm^{-1} which suggest Zn-O stretching (Becheri et al., 2008). The peaks at 2350 and 3450 cm^{-1} specify the presence of C = O and – OH residues, which may be due to the atmospheric moisture and CO_2 respectively (Becheri et al., 2008, Zak et al., 2011). The peaks which are located at 2937 and 2885 cm^{-1} are due to the symmetric and asymmetric C-H bonds respectively (Zak et al., 2011). The XRD pattern of the synthesized ZnONPs are already discussed in section 5.4.1.

5.5.2 Electrochemical characterization of the modified electrode

The elctrochemical response of the STN at bare electrode and amended electodes was examined by cyclic voltammmetry and differntial pulse voltammetry in 0.1 M PBS at pH 7.0. STN showed anodic and cathodic peaks in 0.1 M PBS at pH 7.0, and the potential window from -0.2 to 0.6 V.

Moreover, for all electrochemical assays with STN, the buffer solution was purged with nitrogen gas flow in order to remove the interference of the oxygen reduction reaction. Figure 5.27 shows the cyclic voltammogramms of 0.1 mM STN at the bare GCE (curve i), MWCNTs-GCE (curve ii), ZnONPs-MWCNTs-GCE (curve iii) and Cyt c-ZnONPs-MWCNTs-GCE (curve iv) separately. In addition all modified electrodes showed quasi-reversable redox peaks with various currents. The Cyt c-ZnONPs-MWCNTs-GCE (185 µA) showed greater electrochemical responses than that of GCE (12 µA), MWCNTs-GCE (27 µA) and ZnONPs-MWCNTs-GCE (92 µA), which might be sensibly attributed to the extraordinary electron transfer among the STN and electrode surface. Therefore, Cyt c-ZnONPs-MWCNTs-GCE was selected as the electrochemical biosensor for the studying the electrochemical behaviour of STN in the following experiments.

5.5.3 Effect of pH

The effect of pH on working electrolyte in the determination of STN (0.1mM) is significant for the performance of the electrochemical biosensor. Hence, the effect of pH in the range of 3 to 10 was examined by the cyclic voltammetry, as shown in **Figure 5.27B**. The peak current intensities increased by the raising the pH values from 3 to 10, and it reaches a maximum at pH 7.0. In addition, increase the pH value the current responses are gradually decreased. Therefore, PBS of pH 7.0 was selected as the optimal pH, and was used for the subsequent experiment. Moreover, if the pH is increased the peak potentials are move towards the negative potential values indicating the participation of the H^+ ions in the electrode reactions. The linear regression equation was found to be $E_P = 0.0963pH + 0.483$ ($R^2 = 0.9974$). The resultant slope of the plots

in the pH range 3 to 10 also demonstrates that the number of electrons and protons are equal in the electrochemical redox reaction of STN, as previously reported.

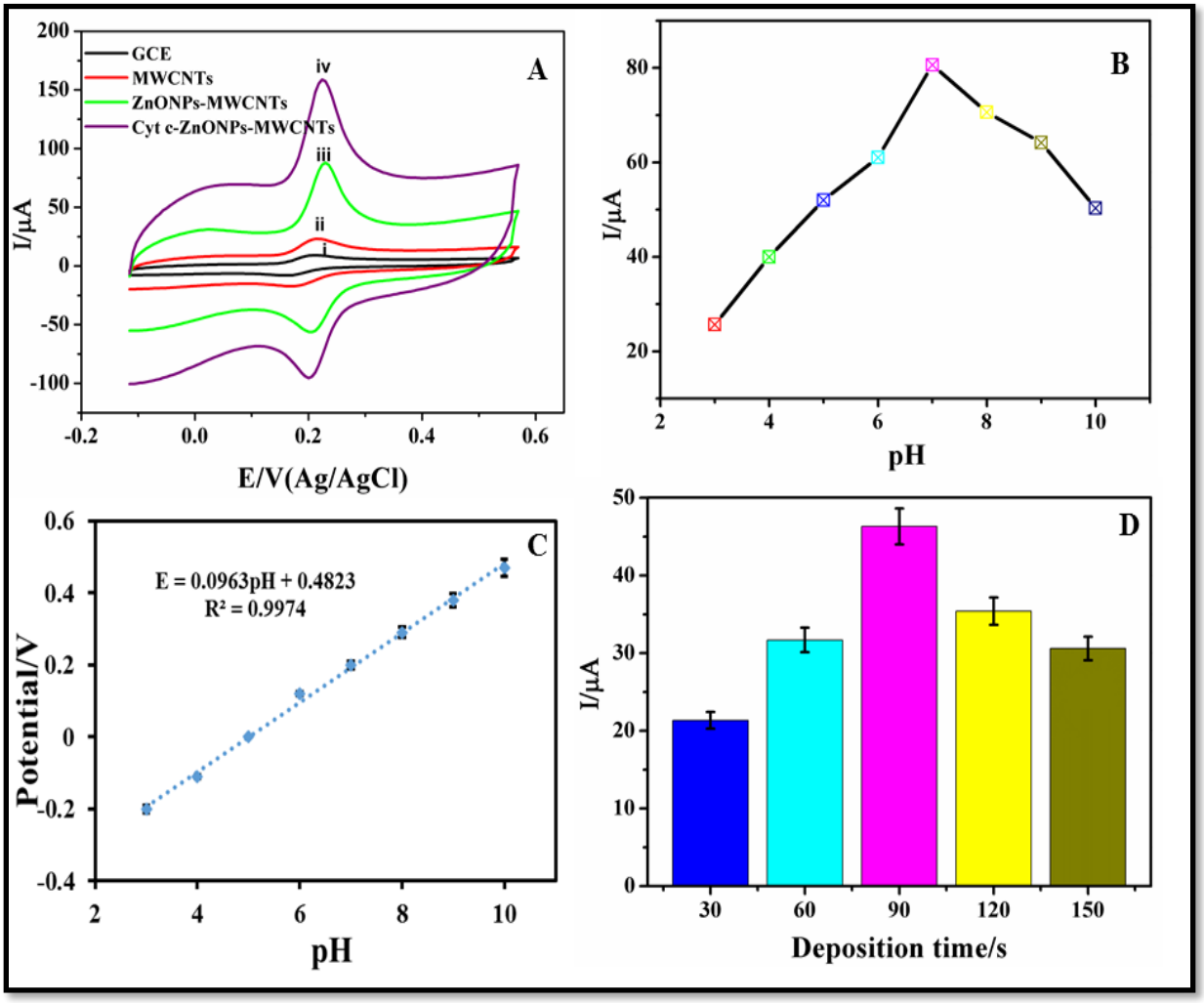

Figure 5.27: (A) Cyclic voltammograms of STN (0.1 mM) at bare GCE (i), MWCNTs-GCE (ii), ZnONPs-MWCNTs-GCE (iii) and Cyt c-ZnONPs-MWCNTs-GCE (iv) in 0.1 M PBS (pH 7.0). (B) Cyclic voltammograms of STN (0.1 mM) in different pH of solutions: (3.0, 4.0, 5.0, 6.0, 7.0, 8.0, 9.0 and 10.0). (C) The plot of peak potential (Ep) of anodic wave versus pH (pH 3-9). (D) Various deposition times (30, 60, 90, 120, and 150 s) on peak current

5.5.4 Deposition time

Due to the adsorptive nature of STN at the electrode surface, cyclic voltammetry and differential pulse voltammetry methods were selected as a sensitive technique for the detection of STN. Deposition of STN successfully increases the electrochemical response. Moreover, the effect of deposition time on the CV signal of 0.1 mM STN was examined. In addition, with increasing deposition time from 30 to 90 s, the peak currents are gradually increased as shown in **Figure 5. 27D**. However, at 90 s the peak current is at a maximum thereafter the peak currents gradually decrease, due to the saturation of the electrode surface. Therefore, 90 s was chosen as the optimized deposition time for entire study.

5.5.5 Influence of scan rates variation

The effect of the potential scan rate on electrochemical properties of the Cyt c-ZnONPs-MWCNTs-GCE was investigated in 0.1 mM PBS (pH) by using the cyclic voltammetry (see **Figure 5.28A**). Initially the redox peaks of STN increased steadily with the increase of the potential scan rates from 0.01 to 0.1 mV s^{-1}, resulting two in linear relationships amongst the peak currents and the scan rates. **Figure 5. 28B** shows the various scan rates from 0.01 to 0.1 mV s^{-1} solution of STN indicating, a linear dependence of the redox reaction up on the scan rate (υ) was observed and demonstrates an adsorption controlled procedure. **Figure 5. 28C** displays the plots of logarithm (of peak currents) and logarithm (of scan rates) and it gives straight lines with slopes of 1.283 and 1.269 for both peak currents respectively. Moreover, the values of the slope are very close to the theoretical value of the 1.12, which stands estimated for an ideal adsorption controlled electrochemical reaction, thus confirming the above results. In addition, with the scan rates increasing the anodic peak potential (E_{pa}) change to the positive direction and the cathodic

peak potential (E_{pc}) moved to negative direction. Therefore, the peak to peak separation (E_p) was somewhat increased and this behaviour demonstrates that the electrochemical process is quasi reversible. In order to determine the electrochemical limitations, difference of the peak potentials with logarithm of scan rates at high scan rate was further plotted according to the Laviron equation 5.15 (Gowda and Nandibewoor, 2014).

$$E_{pa} = E^0 - \frac{2.3\,RT}{\alpha\, nF}\, logv \tag{5.13}$$

$$E_{pc} = E^0 + \frac{2.3\,RT}{(1-\alpha)\, nF}\, logv \tag{5.14}$$

$$\log k_s = \alpha \log(1-\alpha) + (1-\alpha) - \log\left(\frac{RT}{nFv}\right) - \alpha(1-\alpha)\left(\frac{nF\Delta Ep}{2.3RT}\right) \tag{5.15}$$

where α the electron transfer coefficient, k_s is the apparent electron transfer rate constant, n is the number of electron transfer, R is the universal gas constant, T is the temperature and ΔE_p is the peak to peak separation, i.e. E_{pa} - E_{pc}. The fabrication procedure for the proposed electrochemical biosensor is illustrated in **scheme 5.7**.

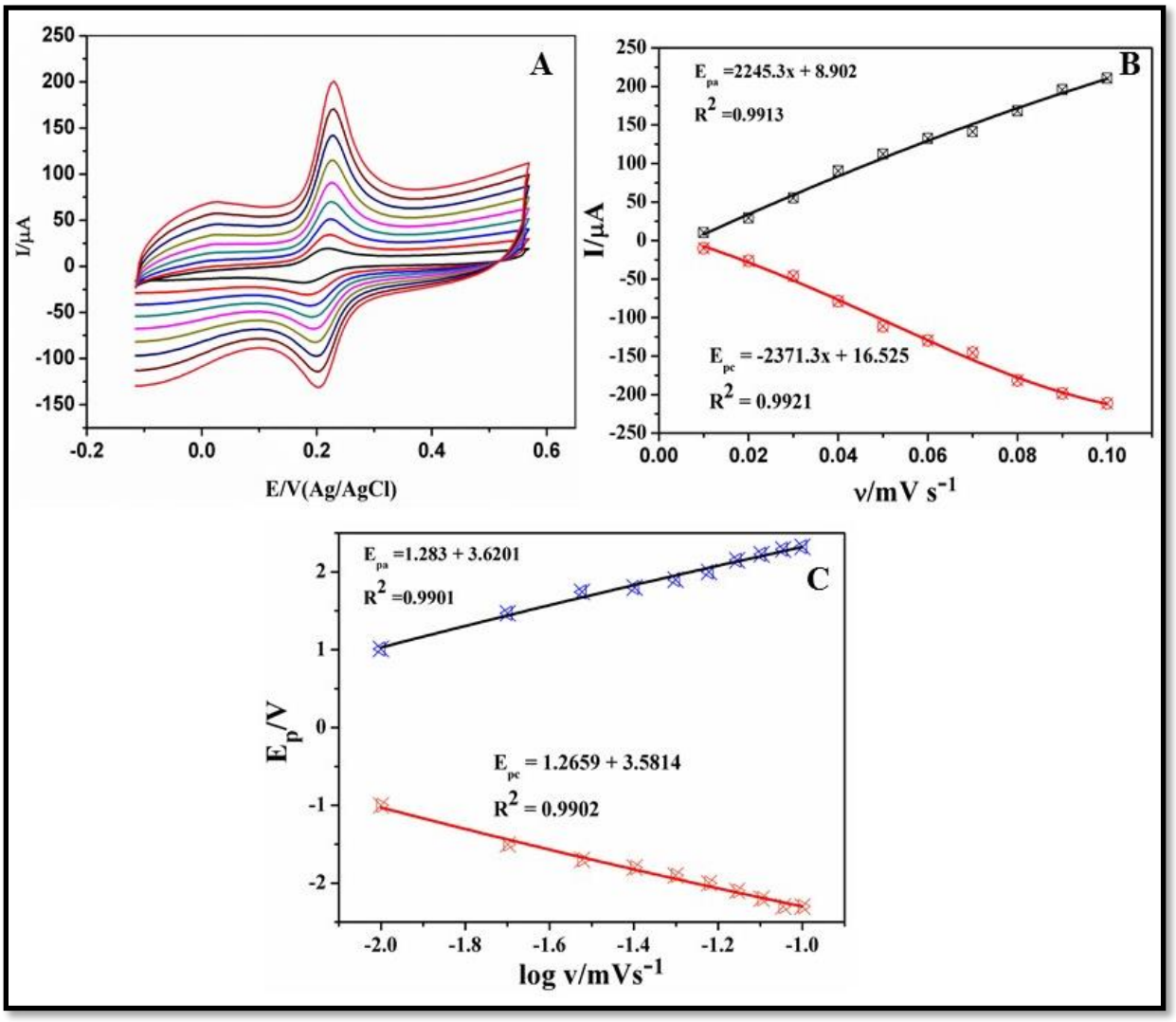

Figure 5.28: (A) CV responses of the modified electrode in PBS buffer solution (pH 7) at scan rates (inner to outer) 0.01, 0.02, 0.03, 0.04, 0.05, 0.06, 0.07, 0.08, 0.09 and 0.1mV s^{-1}. (B) The plot of anodic and cathodic peak current vs. scan rate (C) is the variation of anodic and cathodic potential vs. logarithm of scan rate.

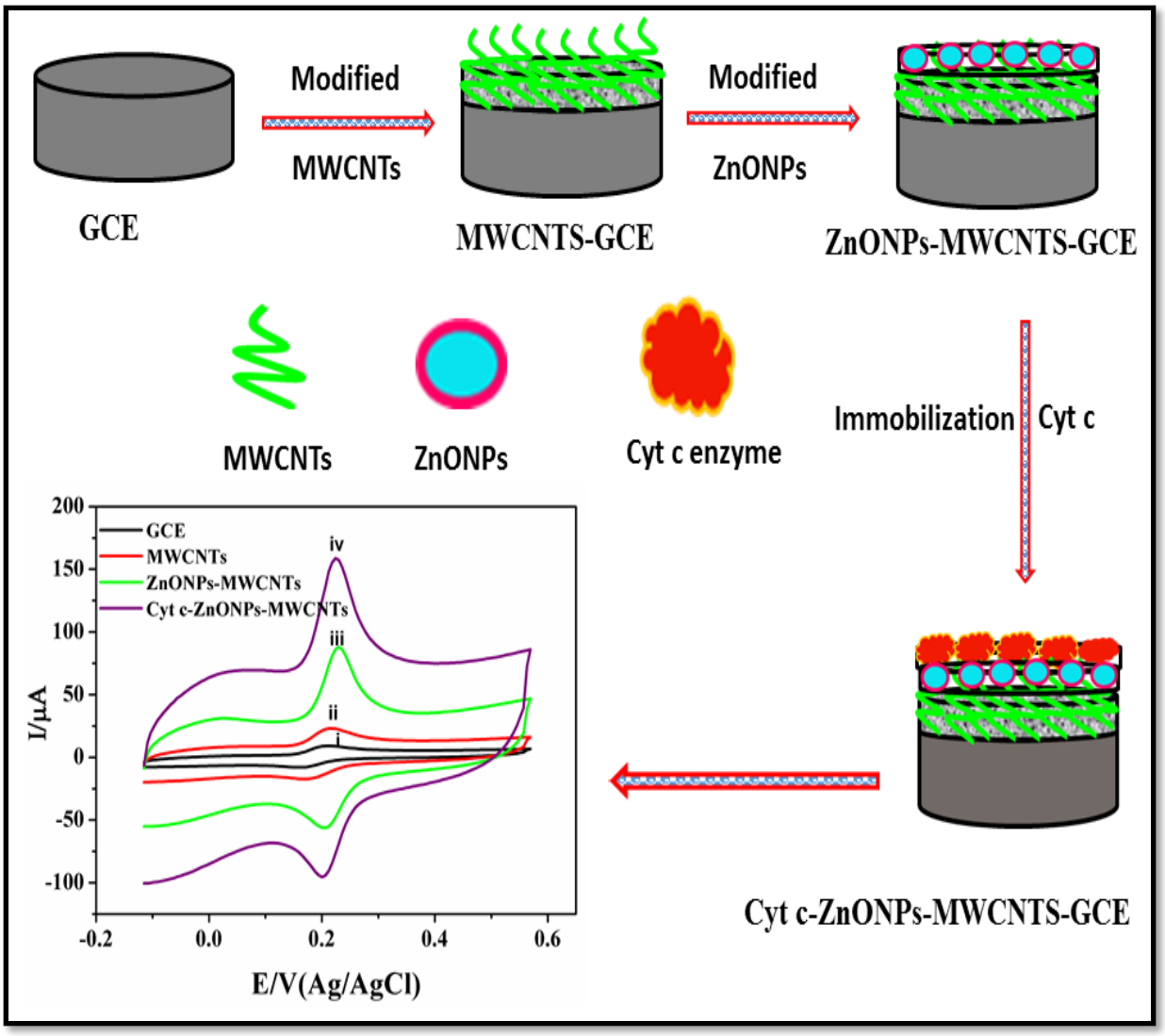

Scheme 5.7: Schematic illustration of the STN electrochemical biosensor based on Cyt c-ZnONPs-MWCNTs nanocomposite

5.5.6 Optimization of incubation time of Cyt c

In order to optimize enzyme incubation, time is one of the most significant parameter. For the determination of STN it was monitored from 5 to 20 min at ambient temperature as shown in **Figure 5.29**. In addition, it was initially found that various incubation times of STN produced a visible difference in the decrease of peak currents. The results show that the peak current response steadily increased with prolonged incubation time and achieved equilibrium at 10 min, after 10 min the peak currents gradually decreased due to the saturation of the electrode surface. Therefore, 10 min was chosen as the incubation time for the determination of STN.

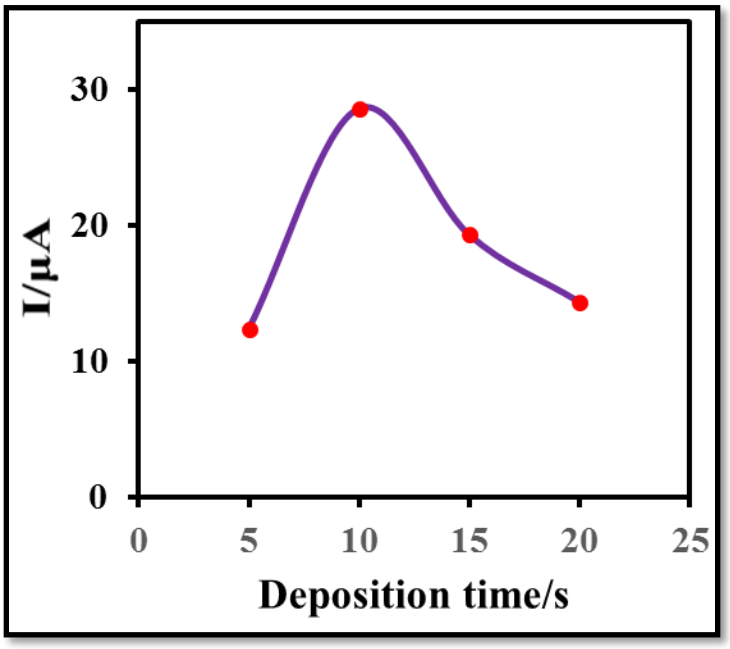

Figure 5.29: Effect of incubation time on the response of HRP-ZnONPs-RGO-GCE

5.5.7 Reproducibility and stability of the biosensor

To investigate the applicability of the proposed electrode the repeatability, stability and reproducibility of the electrochemical biosensor optimized experimental conditions were chosen. In order to examine the reproducibility of the electrode preparation process, six modified electrodes constructed on the same fabrication procedure were prepared and used for the detection of 0.1 mM STN solution by the DPV technique. Hence, from six parallel determinations, the relative standard deviation (RSD) for the determination of STN was calculated and found to be 2.86 %, which showed good sensor-to-sensor reproducibility. Furthermore, the repeatability of the proposed electrochemical biosensor was examined by detection of 0.1 mM STN and variation coefficient of 3.12 % was observed for six successive assays. The peak current response of the Cyt c-ZnONPs-MWCNTs-GCE still remained up to 96.8 % of its initial value, after 10 successive assays (RSD 2.21 %). In addition, the stability of the proposed electrochemical biosensor was investigated by its voltammetric response peak current to 0.1 mM STN over 30 days. The activity of the sensor retained about 93 % of its initial peak current response in the first 15 days. Moreover, after 15 days the electrochemical biosensor responses gradually decreased. The Cyt c-ZnONPs-MWCNTs-GCE showed 89 % of the initial performance even after 30 days, indicating that the proposed electrochemical biosensor showed good long term stability. Hence, the results illustrate that the Cyt c-ZnONPs-MWCNTs-GCE has shown good repeatability, long term stability and reproducibility.

5.5.8 Calibration curve for electrochemical detection of STN

Due to higher peak current sensitivity and superior peak separation, differential pulse voltammetry technique was used for the sensitive detection of STN at the Cyt c-ZnONPs-MWCNTs-GCE. Under the optimal experimental settings (accumulation potential 0.18 V, accumulation time 60 s, voltage step time 0.38 s, pulse amplitude 0.051 V, scan rate 0.0 12 V s^{-1}, voltage step 0.21 V, 0.1 M phosphate buffer and pH 7.0) DPV technique was used for the sensitive detection of STN. Furthermore, a sequence of DPVs were recorded at several concentrations of STN to determine its calibration curve. The response of the Cyt c-ZnONPs-MWCNTs-GCE to STN were found to increase with increasing STN concentrations. **Figure 5.30** displays DPV curves recorded on the Cyt c-ZnONPs-MWCNTs-GCE using different STN concentrations in the range of 0.2 µM to 2.2 µM. In addition, repeated measurements exposed passivation of the electrode, possibly by products of the electrode reaction or adsorption of the analyte onto the electrode surface, resulting in shifting the peaks toward more positive potentials. The linear regression equation was I_{pa} (µA) = 48.724 C + 6.6471 (R^2 = 0.9904) with 0.0028 µM of LOD and 0.0562 µM of LOQ at signal to noise ratio of 3. Therefore, this electrochemical biosensor is appreciated and effective for the detection of STN in pharmaceutical samples.

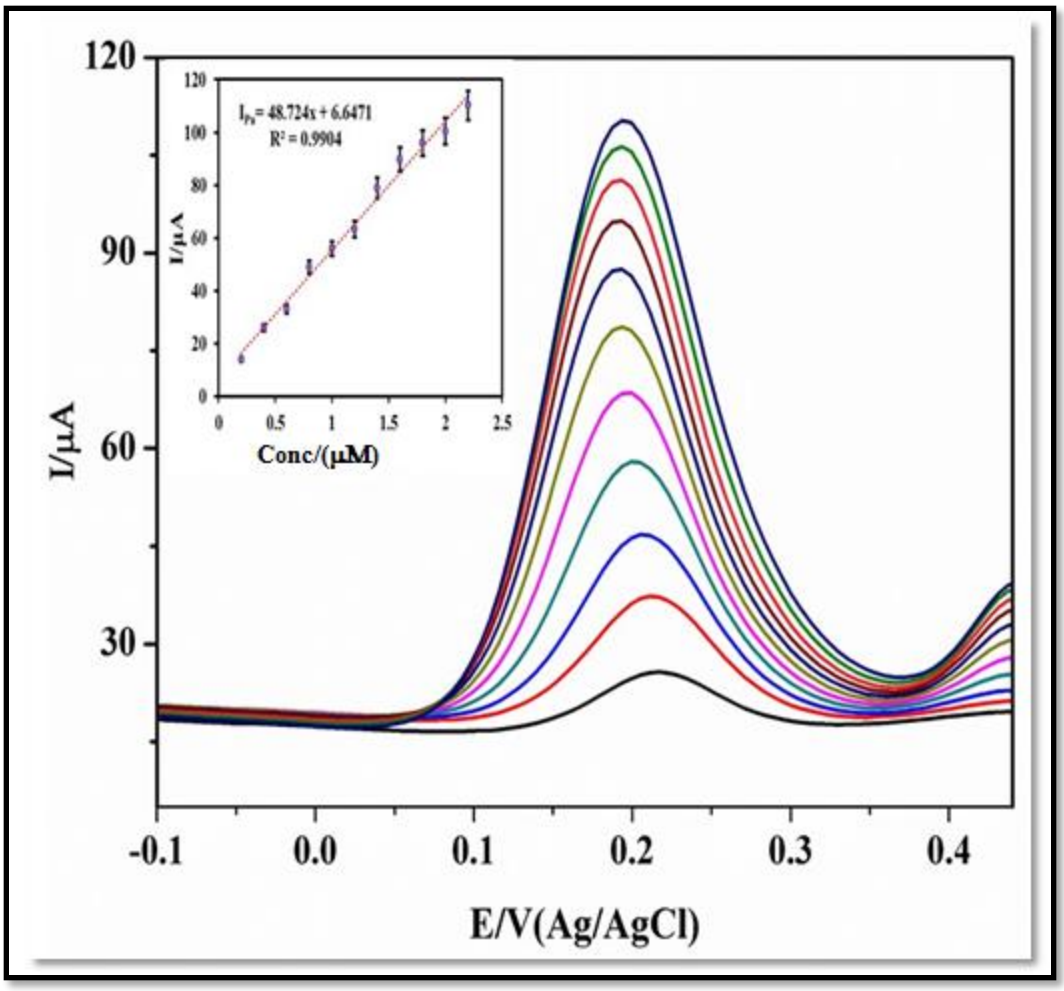

Figure 5.30: DPV curves recorded on Cyt c-ZnONPs-MWCNTs-GCE with the successive addition of STN from 0.2 to 2.2 µM. Insert the calibration plot of the concentration of STN peak current on Cyt c-ZnONPs-MWCNTs-GCE

5.5.9 Interference studies

Under optimized conditions to determine the selectivity of Cyt c-ZnONPs-MWCNTs-GCE, the interference effects of the many interfering substances i.e. organic substances and inorganic substances on the determination of STN were investigated. The developed biosensor was employed in 0.1 µM STN solutions mixed with various interference substances with different concentrations for competing reactions for 15 min. This was followed by using differential pulse voltammetry to detect the interfering ions in 10 mL of 0.1 mM PBS at pH 7. The concentrations of various interferences substances and the signal changes are shown in **Table 5. 12**. Moreover, the tolerance limit was defined as the maximum concentration of interference substances which can cause an error ± 4% in the determination of STN. These results indicated that the proposed biosensor possessed good anti-interference abilities for the determination of STN.

Table 5.12: The influences of some inorganic salts and important biological substances on the peak current of 0.1 µM streptomycin at Cyt c-ZnONPs-MWCNTs-GCE

Interferents	Concentration/µM	Signal change/%
NaCl	500	1.88
$AgNO_3$	500	1.95
$CaCl_2$	250	0.93
$NaSO_4$	500	1.86
Sucrose	500	0.25
Glucose	500	0.29
Urea	250	2.2
Ascorbic acid	250	3.89
Dopamine	250	1.20
Citric acid	250	1.61

5.5.10 Analytical application for the proposed sensor

In order to examine the applicability of the proposed electrochemical biosensor, Cyt c-ZnONPs-MWCNTs-GCE was utilised to determine the STN content in various pharmaceutical tablet samples by using the DPV techniquie. The real sample preparation was explained under section 3.3 in Chapter 3. Moreover, for real sample analysis an appropiate amount was directly dissloved in deionised water, followed by serial dilution of 10 mL phosphate buffer solution (pH 7.0). Three tablet samples were analyzed using three independently prepared electrodes. Moreover, each sample was detected five times and the detection value was the average of five results. The recovery was in the range 95 to 105 %, and the results are summarized and listed in **Table 5.13**. Satisfactory recoveries for real samples confirmed that the proposed electrochemical biosensor held great potential for reliable and sensitive application in the field of pharmaceutical analysis.

Table 5.13: Determination of STN in various pharmaceutical samples using Cyt c-ZnONPs-MWCNTs-GCE (n=5)

Tablet samples	Added/µM	Found/µM	Recovery/%	RSD/%
Tablet 1	10	9.5	95	0.75
Tablet 2	15	14.89	99	1.95
Tablet 3	20	21.01	105	1.82

CHAPTER 6

SUMMARY AND CONCLUSIONS

Pharmaceutical analysis by electrochemical techniques is quite a promising field as the study can be complete by simple techniques which are extremely selective and sensitive. Micromolar limits of detection with microelectrodes makes them a good platform suitable for drug analyses. The advances in material science further enhance the field of electrochemistry for various analysis. The development of sensitive and precise methods for the quantitative determination of anti-tuberculosis drugs is a challenging task for scientists. The main purpose of this study was to develop electrochemical biosensor methods for detection of first line anti TB drugs such as isoniazid (INZ), pyrazinamide (PZM), rifampicin (RIF), ethambutol (ETB) and streptomycin (STN). Many analytical methodologies were established and validated for their potential use in the determination of high concentration of anti TB drugs. Furthermore, nanomaterials in combination with electro analytical methods resulted in high performance biosensors being established for the sensitive detection of INZ, PZM, RIF, ETB and STN.

The prime focus of the dissertation was to modify the voltammetric sensors for anti TB drugs and their applications to real samples. The glassy carbon electrode was used as a probe for the present investigations. The efficiency of this electrode as a sensor for pharmaceutical analysis can be enhanced by modifying its surface chemically with metal oxide nanoparticles, nanotubes and enzyme etc. This will contribute to chemically modified electrodes (CME) in the field of electrochemical sensor technology. The primary objective towards the overall goal of this project involved the determination of INZ, PZM, RIF, ETB and STN by using voltammetric techniques.

A facile MWCNT-TiO_2NPs-HRP-GCE biosensor was successfully developed for the determination of INZ in different pharmaceuticals samples. The issue of high detection limits of the reported electrochemical methods were the rhodium modified glassy carbon electrode (Cheemalapati et al., 2014). The linearity ranges from 70 – 1300 µM with the detection limit of 13 µM. Our results showed that the present method is a fast, efficient method for the quantification of INZ in various pharmaceuticals. The synthesized nanoparticles and developed sensor were characterized with TGA, TEM, XRD, and FT-IR. The electrochemical sensing abilities of INZ with different electrodes, viz., bare GCE, MWCNT-GCE, MWCNT-TiO_2NPs-GCE and MWCNT-TiO_2NPs-HRP-GCE were successfully compared using cyclic voltammetry studies. The developed sensor showed fast electron transfer capability, good electronic conductivity, and large electroactive surface area. The CV results obtained reveal outstanding electrochemical sensing performance of the enzyme-induced sensor with an increase (approximately 8-fold) of anodic peak currents. In the DPV technique, the calibration plot gave a good correlation coefficient of R^2 = 0.998 with LOD and LOQ values of 0.0335 µM and 0.1118 µM, respectively. This clearly indicates the developed sensor showed a high capability for detecting the INZ in µM concentration without any interferences. In addition, the fabricated sensor exhibited good repeatability and long-term stability, with negligible current variations. Moreover, the real sample analysis gave satisfactory results with good percentages of recovery.

Furthermore, combining the unique properties of the fabricated material such as high surface area, increased electrocatalytic activity and greater adsorptive properties, a Cyt c-CuONPs-MWCNTs-GCE was developed for the determination of PZM. In the present work, the developed sensor also showed good catalytic activity towards PZM, due to the increased

electrochemical sensing mechanism for PZM. The modified electrode was successfully characterized by the TEM, FT-IR, TGA and XRD techniques. The CV results obtained showed well-defined anodic and cathodic peaks at the peak potentials -0.77 V and -0.80 V respectively, and also revealed good electrocatalytic activity of Cyt c-CuONPs-MWCNTs-GCE towards PZM. From the measured DPV results, the limit of detection (LOD) and limit of quantification (LOQ) of the developed sensor were calculated, and found to be 0.0038 μM and 0.0129 μM respectively. The fabricated biosensor exhibited enhanced peak currents. The proposed biosensor also showed excellent sensitivity, selectivity and low detection limits. In addition, the developed sensor was applied for the determination of PZM in real pharmaceutical samples, which reflect good recovery percentages. It is evident that the proposed method will possibly serve as a standard protocol for the determination of PZM in various pharmaceutical samples.

In the third part of this study, a novel and facile electrochemical method for the modification of GCE with MWCNTs, MWCNTs-Fe_3O_4NPs and Co en-q for the determination of RIF. The resulting MWCNTs, MWCNTs-Fe_3O_4NPs have been successfully characterized by using FT-IR, XRD and TEM. The electrochemical behaviour of RIF on the bare GCE and modified Co en-q-Fe_3O_4-MWCNTs-GCE were observed using cyclic voltammetry. The obtained cyclic voltammetry results indicate the outstanding electrochemical sensing performance of the biosensor, with an increase (approximately 8-fold) of anodic peak currents. The RIF shows two anodic peaks at + 0.10 V and + 0.72 V in the phosphate buffer solution at pH 7.5. This indicates the high electrochemical response ability of the developed biosensor towards the oxidation of RIF compared to GCE, MWCNTs-GCE, MWCNTs-Fe_3O_4NPs-GCE. Under the optimal experimental conditions, the anodic peak currents of RIF increased linearly within the concentration range 2-20 μM bearing the correlation coefficients of R^2 = 0.998, and R^2 = 0.997

respectively. The LOD and LOQs were calculated and found to be 0.032 µM, 0.413 µM and 1.069 µM, 1.258 µM for peak I and peak II respectively. This also reveals the high sensitivity and selectivity of the fabricated biosensor without significant interference from interferents. The biosensor exhibited good reproducibility and stability as well as successful analytical application. The proposed biosensor was certainly adequate for the determination of RIF in the commercial pharmaceutical sample.

In the fourth part of this work, the potential scan up to high potential was proposed to improve the electrocatalytical activity of modified HRP-ZnONPs-RGO-GCE towards the electrochemical redox reaction of ETB. The morphological characterization of the developed sensor was studied by FT-IR, TEM, XRD and TGA techniques. This method has been developed for the detection of ETB in various pharmaceutical samples. The HRP-ZnONPs-RGO-GCE showed an oxidation peak at -0.2 V and a reduction peak at -0.22 V in CV. Statistical analysis proved that the biosensor showed good repeatability, selectivity and sensitivity for the determination of the ETB in various pharmaceutical samples. The ZnONPs-RGO nanocomposite provides an appropriate environment for HRP enzyme attachment, and promotes the rapid catalytic action, moreover it is facilitated by the electron transfer between the active sites of enzyme and electrode surface. The HRP-ZnONPs-RGO-GCE was significantly improved by the electrochemical oxidation and reduction signals of ETB compared with the ZnONPs-RGO nanocomposite, GCE and RGO. The proposed biosensor exhibits the low limit of detection 0. 0214 µM, and limit of quantification 0.6713 µM respectively. Based on the detection limit, sensitivity, and stability of the proposed HRP-ZnONPs-RGO-GCE could be used for monitoring ETB in biological and pharmaceutical samples, as one of the reliable routine laboratory analytical methods.

In last part of this work, electrochemical behaviour of STN were examined and presented. STN was electrochemically energetic in the pH range at 3.0 – 10.0, but the peak currents of STN were higher at pH 7. Furthermore, GCE was fabricated with MWCNTs which enhanced the response of STN. However, by the addition of ZnONPs to the MWCNTs to form a nanocomposite electrode, and then immobilizing composite electrode with Cyt c, resulted in the electrochemical biosensor showed significantly higher peak currents, and the response of the STN was appreciably increased. Moreover, this also lead to an expansion of the novel electrode and proposed that the metal oxide nanocomposite electrodes when immobilized with biomolecules can fruitfully be used for analytical application of STN with simplicity, time saving and reduced costs. Hence, a novel electroanalytical technique for the determination of STN was proposed synchronously with varied linear range from 2 to 10 µM, and the detection limit and limit of quantifications was found to be 0.0028 µM and 0.5628 µM respectively (S/N=5). After the experimental limitations affecting the response sensitivity of the biosensor were optimized in detail, the resulting biosensor not only exhibited high sensitivity and selectivity for STN, but also showed much better reproducibility and repeatability.

The development of chemically modified electrode based voltammetric sensors remain an exciting and developing the area of analytical research. The main principle of this work is reducing the detection limits to true trace levels, and there are significant advances in the area of material, active mechanism design, and clearly the results of the present study are extremely promising and fruitful.

CHAPTER 7

REFERENCES

ABBASI, H. & HELLENAS, K.E. 1998. Modified determination of dihydrostreptomycin in kidney, muscle and milk by HPLC. *Analyst*, 123, 2725-2727.

ABDELHADY, M. 2012. Preparation and characterization of chitosan/zinc oxide nanoparticles for imparting antimicrobial and UV protection to cotton fabric. *International Journal of Carbohydrate Chemistry*, 2012, 1-6.

ABSALAN, G., AKHOND, M., SOLEIMANI, M. & ERSHADIFAR, H. 2016. Efficient electrocatalytic oxidation and determination of isoniazid on carbon ionic liquid electrode modified with electrodeposited palladium nanoparticles. *Journal of Electroanalytical Chemistry*, 761, 1-7.

ADAMS, E., RAFIEE, M., ROETS, E. & HOOGMARTENS, J. 2000. Liquid chromatographic analysis of streptomycin sulfate. *Journal of Pharmaceutical and Biomedical Analysis*, 24, 219-226.

ADRIANA, F., LUIZA, F. & JULIANA, P. 2011. Ethambutol analysis by Copper complexation in pharmaceutical formulations: Spectrophotometry and Crystal structures. *Journal of Brazilian Chemical Society*, 22, 867-874.

AGBOKPONTO, J.E., GONG, C., ASSANHOU, A.G., ACHEAMPONG, D.O., ALOLGA, R.N., MFONO OKE, Y.N. & DING, L. 2014. Sensitive liquid chromatography-mass

spectrometry determination of isoniazid: Elimination of matrix effects. *African Journal of Pharmacy and Pharmacology*, 8, 1228-1234.

AHIRWAL, G.K. & MITRA, C.K. 2009. Direct electrochemistry of horseradish peroxidase-gold nanoparticles conjugate. *Sensors*, 9, 881-894.

AHMAD, S., RIAZ, U., KAUSHIK, A. & ALAM, J. 2009. Soft template synthesis of super paramagnetic Fe_3O_4 nanoparticles a novel technique. *Journal of Inorganic and Organometallic Polymers and Materials*, 19, 355-360.

AJAYAN, P.M. & ZHOU, O.Z. 2001. Applications of carbon nanotubes. Carbon nanotubes. *Springer*, 391-425.

AJAYI, R.F., SIDWABA, U., FELENI, U., DOUMAN, S.F., TOVIDE, O., BOTHA, S., BAKER, P., FUKU, X.G., HAMID, S., WARYO, T.T., VILAKAZI, S., TSHIHKUDO, R. & IWUOHA, E.I. 2014. Chemically amplified cytochrome P450-2E1 drug metabolism nanobiosensor for rifampicin anti-tuberculosis drug. *Electrochimica Acta*, 128, 149-155.

ALKIRE, R.C., GOGOTSI, Y. & SIMON, P. 2008. Nanostructured materials in electrochemistry, *John Wiley & Sons*.

ALLANA, S., SHASHKINA, E., MATHEMA, B., BABLISHVILI, N., TUKVADZE, N., SHAH, N.S., KEMPKER, R.R., BLUMBERG, H.M., MOODLEY, P. & MLISANA, K. 2017. pncA Gene Mutations Associated with Pyrazinamide Resistance in Drug-Resistant Tuberculosis, South Africa and Georgia. *Emerging Infectious Diseases*, 23, 491-495.

ALLANSON, A., COTTON, M., TETTEY, J. & BOYTER, A. 2007. Determination of rifampicin in human plasma and blood spots by high performance liquid chromatography with UV detection: a potential method for therapeutic drug monitoring. *Journal of pharmaceutical and biomedical analysis*, 44, 963-969.

ALLEN, W.S., ARONOVIC, S.M., BRANCONE, L.M. & WILLIAMS, J.H. 1953. Determination of the Pyrazinamide Content of Blood and Urine. *Analytical Chemistry*, 25, 895-897.

ALMANI, K., MEMON, A., MUGHAL, U., MAHESHWARI, M. & KHUHAWER, M. 2013. Spectrophotometric Determination of Isoniazid from Pharmaceutical Preparations Using Natural Aldehyde. *Asian Journal of Chemistry*, 25, 2522-2527.

ALONSO LOMILLO, M.A., DOMINGUEZ RENEDO, O. & ARCOS MARTINEZ, M.J. 2005. Optimization of a cyclodextrin-based sensor for rifampicin monitoring. *Electrochimica Acta*, 50, 1807-1811.

ALONSO LOMILLO, M.A., KAUFFMANN, J.M. & ARCOS MARTINEZ, M.J. 2003. HRP-based biosensor for monitoring rifampicin. *Biosensors and Bioelectronics*, 18, 1165-1171.

AMAN, T., RASHID, A., KULSOOM, R. & KHOKHAR, I. 1995. Spectrophotometric determination of streptomycin. *Analytical letters*, 28, 881-892.

ANDREESCU, S. & MARTY, J.L. 2006. Twenty years research in cholinesterase biosensors: from basic research to practical applications. *Biomolecular engineering*, 23, 1-15.

ANUSHA, A. & SREEDEVI, B. 2014. Simultaneous estimation of isoniazid and rifampicin in bulk and pharmaceutical formulations by RP-HPLC method. *International Journal of Innovative Technology and Research*, 2, 1243-1247.

AOKI, K. & OSTERYOUNG, J. 1980. Theory of differential pulse polarography at expanding or stationary planar electrodes for quasi-reversible or totally irreversible reactions. *Journal of Electroanalytical Chemistry and Interfacial Electrochemistry*, 110, 19-36.

APARNA, Y., RAO, K.V. & SUBBARAO, P.S. 2012. Preparation and characterization of CuO Nanoparticles by novel sol-gel technique. *Journal of Nano-and Electronic Physics*, 4, 3005-3010.

AREVALO, F.J., OSUNA-SANCHEZ, Y., SANDOVAL-CORTES, J., DI TOCCO, A., GRANERO, A.M., ROBLEDO, S.N., ZON, M.A., VETTORAZZI, N.R., MARTÍNEZ, J.L., SEGURA, E.P., ILINA, A. & FERNANDEZ, H. 2017. Development of an electrochemical sensor for the determination of glycerol based on glassy carbon electrodes modified with a copper oxide nanoparticles/multiwalled carbon nanotubes/pectin composite. *Sensors and Actuators B: Chemical*, 244, 949-957.

ARGEKAR, A., KUNJIR, S. & PURANDARE, K. 1996. Simultaneous determination of rifampicin, isoniazid and pyrazinamide by high performance thin layer chromatography. *Journal of pharmaceutical and biomedical analysis*, 14, 1645-1650.

ARROWOOD, S., HOYT, A.M. & WOODS, M.W. 1991. Determination of streptomycin in pharmaceutical preparations by gas chromatography. *Journal of Separation Science*, 14, 808-810.

ARSALANI, N., FATTAHI, H. & NAZARPOOR, M. 2010. Synthesis and characterization of PVP-functionalized superparamagnetic Fe_3O_4 nanoparticles as an MRI contrast agent. *Express Polym Lett*, 4, 329-38.

ASADPOUR-ZEYNALI, K. & BAGHALABADI, V. 2017. Electrocatalytic Determination of Isoniazid by a Glassy Carbon Electrode Modified with Poly (Eriochrome Black T). *Analytical and Bioanalytical Chemistry Research*, 4, 31-40.

ASADPOUR-ZEYNALI, K. & MOLLARASOULI, F. 2017. Novel electrochemical biosensor based on PVP capped $CoFe_2O_4$@CdSe core-shell nanoparticles modified electrode for ultra-trace level determination of rifampicin by square wave adsorptive stripping voltammetry. *Biosensors and Bioelectronics*, 92, 509-516.

ASADPOUR-ZEYNALI, K. & SOHEILI-AZAD, P. 2010. Simultaneous polarographic determination of isoniazid and rifampicin by differential pulse polarography method and support vector regression. *Electrochimica Acta*, 55, 6570-6576.

ASADPOUR-ZEYNALI, K., SHABANGOLI, Y. & NEJATI, K. 2015. Electrochemical synthesis of Fe/Al-layered double hydroxide on a glassy carbon electrode: application for electrocatalytic reduction of isoniazid. *Journal of the Iranian Chemical Society*, 13, 29-36.

ASHAD, H., WASEEM, H. & KHALIQ, R. 2012. Simple and rapid method on high performance liquid chromatography (HPLC) for estimation of streptomycin sulphate. *Journal of World Applied Sciences*, 19, 645-649.

ASHOUR, R.M., ABDEL-MAGIED, A.F., ABDEL-KHALEK, A.A., HELALY, O.S. & ALI, M. M. 2016. Preparation and characterization of magnetic iron oxide nanoparticles functionalized by l-cysteine: Adsorption and desorption behavior for rare earth metal ions. *Journal of Environmental Chemical Engineering*, 4, 3114-3121.

ATTA, N.F., GALAL, A. & AHMED, R.A. 2011. Voltammetric behavior and determination of isoniazid using PEDOT electrode in presence of surface active agents. *International Journal of Electrochemical Science*, 6, 5097-5113.

AUTHOR, A. 1957. Congress on Modern Analytical Chemistry in Industry St. Andrews, June 24th to 28th, 1957. *Royal Society of Chemistry*.

AYYAPPAN, J. 2011. Development and validation of a stability indicating high-performance liquid chromatography (HPLC) method for the estimation of isoniazid and its related substances in fixed dose combination of isoniazid and ethambutol hydrochloride tablets. *African Journal of Pharmacy and Pharmacology*, 5, 1513-1521.

AZAD, U.P. & GANESAN, V. 2012. Efficient electrocatalytic oxidation and selective determination of isoniazid by $Fe(tmphen)_3^{2+}$-exchanged Nafion®-modified electrode. *Journal of Solid State Electrochemistry*, 16, 2907-2911.

AZAD, U.P., PRAJAPATI, N. & GANESAN, V. 2015. Selective determination of isoniazid using bentonite clay modified electrodes. *Bioelectrochemistry*, 101, 120-125.

Bathinapatla, A., Kanchi, S., Singh, P., Sabela, M.I. and Bisetty, K., 2016. An ultrasensitive performance enhanced novel cytochrome c biosensor for the detection of rebaudioside A. *Biosensors and Bioelectronics*, *77*, 116-123.

BAGELOVA, J., ANTALIK, M. & TOMORI, Z. 1997. Effect of polyglutamate on the thermal stability of ferricytochrome c. *International Union of Biochemistry and Molecular Biology*, 43, 891-900.

BAIER, A., NDOH, V.N., LACY, P. & EITZEN, G. 2014. Rac1 and Rac2 control distinct events during antigen-stimulated mast cell exocytosis. *Journal of leukocyte biology*, 95, 763-774.

BALBAO, M.S., BERTUCCI, C., BERGAMASCHI, M.M., QUEIROZ, R.H.C., MALFARA, W.R., DREOSSI, S.A.C., DE PAULA MELLO, L. & QUEIROZ, M.E.C. 2010. Rifampicin determination in plasma by stir bar-sorptive extraction and liquid chromatography. *Journal of pharmaceutical and biomedical analysis*, 51, 1078-1083.

BALGOBIND, K., KANCHI, S., SHARMA, D., BISETTY, K. & SABELA, M. I. 2016. Hybrid of ZnONPs/MWCNTs for electrochemical detection of aspartame in food and beverage samples. *Journal of Electroanalytical Chemistry*, 774, 51-57.

BARD, A.J. & FAULKNER, L.R. 2001. Fundamentals and applications. *Electrochemical Methods*, 2, 1-850.

BARON-JAIMEZ, J., JOYA, M. & BARBA-ORTEGA, J. Anodic stripping voltammetry ASV for determination of heavy metals. *Journal of Physics: Conference Series*, 2013. IOP Publishing, 012023.

BARSOUM, N., KAMEL, M.S. & DIAB, M.M. 2008. Spectrophotometric determination of isoniazid and rifampicin from pharmaceutical preparations and biological fluids. *Research Journal of Agricultural and Biological Sciences*, 4, 471-484.

BARTLETT, J.G., DOWELL, S.F., MANDELL, L.A., FILE JR, T.M., MUSHER, D.M. & FINE, M.J. 2000. Practice guidelines for the management of community-acquired pneumonia in adults. *Clinical infectious diseases*, 31, 347-382.

BAS, B., JAKUBOWSKA, M. & KOWALSKI, Z. 2006. Rapid pretreatment of a solid silver electrode for routine analytical practice. *Electroanalysis*, 18, 1710-1717.

BASI, 2017. https://www.basinc.com/manuals/EC_epsilon/Techniques/CycVolt/cv_analysis, Accessed on 26 February 2018.

BATHINAPATLA, A., KANCHI, S., SINGH, P., SABELA, M.I. & BISETTY, K. 2015. Fabrication of copper nanoparticles decorated multiwalled carbon nanotubes as a high performance electrochemical sensor for the detection of neotame. *Biosensors and Bioelectronics*, 67, 200-207.

BAXTER, G., FERGUSON, J., OCONNO, M. & ELLIOTT, C. 2001. Detection of streptomycin residues in whole milk using an optical immunobiosensor. *Journal of agricultural and food chemistry*, 49, 3204-3207.

BECHERI, A., DURR, M., LO NOSTRO, P. & BAGLIONI, P. 2008. Synthesis and characterization of zinc oxide nanoparticles: application to textiles as UV-absorbers. *Journal of Nanoparticle Research*, 10, 679-689.

BELAL, F.F., EL-DIN, M.K.S., EID, M.I. & EL-GAMAL, R.M. 2013. Micellar HPLC method using monolithic column for the simultaneous determination of linezolid and rifampicin in pharmaceuticals and biological fluids. *Analytical Methods*, 5, 6165-6176.

BELLEI PERANTONI, C., SOARES CARBOGIM, L.G., SILVA SEMAAN, F., CAMARGO MATOS, R. & LOWINSOHN, D. 2011. Flow Injection Analysis of Ethambutol in Antituberculosis Drugs Using a Graphite Paraffin Electrode as Amperometric Detector. *Electroanalysis*, 23, 2582-2585.

BENETTON, S.A., KEDOR-HACKMANN, E.R.M., SANTORO, M.I.R.M. & BORGES, V.M. 1998. Visible spectrophotometric and first-derivative UV spectrophotometric determination of rifampicin and isoniazid in pharmaceutical preparations. *Talanta*, 47, 639-643.

BENVENISTE, R., YAMADA, T. & DAVIES, J. 1970. Enzymatic adenylylation of streptomycin and spectinomycin by R-factor-resistant Escherichia coli. *Infection and immunity*, 1, 109-119.

BENVIDI, A., NIKMANESH, M., TEZERJANI, M.D., JAHANBANI, S., ABDOLLAHI, M., AKBARI, A. & REZAEIPOOR-ANARI, A. 2017. A comparative study of various electrochemical sensors for hydrazine detection based on imidazole derivative and different nano-materials of MCM-41, RGO and MWCNTs: Using net analyte signal (NAS) for simultaneous determination of hydrazine and phenol. *Journal of Electroanalytical Chemistry*, 787, 145-157.

BERGAMINI, M.F., SANTOS, D.P. & ZANONI, M.V.B. 2010. Determination of isoniazid in human urine using screen-printed carbon electrode modified with poly-L-histidine. *Bioelectrochemistry*, 77, 133-138.

BERGAMINI, M.F., SANTOS, D.P. & ZANONI, M.V.B. 2013. Electrochemical behavior and voltammetric determination of pyrazinamide using a poly-histidine modified electrode. *Journal of Electroanalytical Chemistry*, 690, 47-52.

BERNARDES-GENISSON, V., DERAEVE, C., CHOLLET, A., BERNADOU, J. & PRATVIEL, G. 2013. Isoniazid: an Update on the Multiple Mechanisms for a Singular Action. *Current Medicinal Chemistry*, 20, 4370-4385.

BERTRAND, G., COSTE, J., SEGARRA, C., SCHVED, J., COMMES, T., BEUM, P., KENNEDY, A., LI, Y., PAWLUCZKOWYCZ, A. & TAYLOR, R. 2004. Belleville, E., Dufva, M., Aamand, J., Bruun, L., Clausen, L. and Christensen, CBV, Quantitative microarray pesticide analysis (286) 219 Ben-Porat, L., see Janetzki, S. (291) 175 Berenguer, M., see Lopez-Labrador, FX (287) 91. *Journal of Immunological Methods*, 284, 197-214.

BHAJANTHRI, N., ARUMUGAM, V., CHOKKAREDDY, R. & REDHI, G.G. 2016. Ionic liquid based high performance electrochemical sensor for ascorbic acid in various foods and pharmaceuticals. *Journal of Molecular Liquids*, 222, 370-376.

BHANDARI, R. 2012. A Sensitive HPLC Method for Determination of Isoniazid in Rat Plasma, Brain, Liver and Kidney. *Journal of Chromatography & Separation Techniques*, 3, 1-5.

BINEE, Z. & CHANGQINE, H. 2002. Development and validation of liquid chromatographic method for the determination of the related substances of rifampicin. *Journal of Chinese Pharmaceutical Sciences*, 11.

BOFFITO, M., TIJA, J., REYNOLDS, H.E., HOGGARD, P.G., BONORA, S., DI PERRI, G. & BACK, D.J. 2002. Simultaneous determination of rifampicin and efavirenz in plasma. *Therapeutic drug monitoring*, 24, 670-674.

BOHM, D.A., STACHEL, C.S. & GOWIK, P. 2010. Confirmatory method for the determination of streptomycin in apples by LC–MS/MS. *Analytica Chimica Acta*, 672, 103-106.

BOHM, D.A., STACHEL, C.S. & GOWIK, P. 2012. Confirmatory method for the determination of streptomycin and dihydrostreptomycin in honey by LC–MS/MS. *Food Additives & Contaminants: Part A*, 29, 189-196.

BOXER, G.E., JELINEK, V.C. & LEGHORN, P M. 1947. The colorimetric determination of streptomycin in clinical preparations, urine, and broth. *Journal of Biological Chemistry*, 169, 153-165.

BREDA, M., MARRARI, P., PIANEZZOLA, E. & STROLIN BENEDETTI, M. 1996. Determination of ethambutol in human plasma and urine by high-performance liquid chromatography with fluorescence detection. *Journal of Chromatography A*, 729, 301-307.

BROUARD, A., BARRETEAU, H., MERDJAN, H., PAILLET, M., FREDJ, G. & MICOUD, M. 1985. Rapid determination of pyrazinamide in biological fluids by high-performance liquid chromatography. *Journal of Chromatography B: Biomedical Sciences and Applications*, 345, 453-456.

BURDA, C., CHEN, X., NARAYANAN, R. & EL-SAYED, M.A. 2005. Chemistry and properties of nanocrystals of different shapes. *Chemical reviews*, 105, 1025-1102.

CAI, J., YANG, J. & JONES, D. 1998. Mitochondrial control of apoptosis: the role of cytochrome c. *Biochimica et Biophysica Acta (BBA) - Bioenergetics*, 1366, 139-149.

CALLEJA, I., BLANCO-PRIETO, M. A. J., RUZ, N., RENEDO, M.J. & DIOS-VIEITEZ, M. A.C. 2004. High-performance liquid–chromatographic determination of rifampicin in plasma and tissues. *Journal of Chromatography A*, 1031, 289-294.

CALLERI, E., DE LORENZI, E., FURLANETTO, S., MASSOLINI, G. & CACCIALANZA, G. 2002. Validation of a RP-LC method for the simultaneous determination of isoniazid, pyrazinamide and rifampicin in a pharmaceutical formulation. *Journal of Pharmaceutical and Biomedical Analysis*, 29, 1089-1096.

CAO, X., RUI, J., WANG, Y., LI, J., MA, B., YANG, Z. & LIU, Y. 2012. Simultaneous Determination of Isoniazid and Acetylisoniazid in Human Plasma by Hydrophilic Interaction Liquid Chromatography Tandem Mass Spectrometry and Its Application to a Pharmacokinetics Related to N-Acetyltransferase2 Genetic Polymorphism. *Analytical Letters*, 45, 2125-2135.

CARA, M.C., DUMITREL, G.A., GLEVITZKY, M., MISCHIE, C. & SILAGHI-PERJU, D. 2013. Thermal degradation of streptomycin residues in honey during storage. *Food Technology and Biotechnology*, 51, 429-433.

CHATTERJEE, K., KUO, C.W., CHEN, A. & CHEN, P. 2015. Detection of residual rifampicin in urine via fluorescence quenching of gold nanoclusters on paper. *Journal of nanobiotechnology*, 13, 1-9.

CHEEMALAPATI, S., CHEN, S.M., ALI, M.A. & AL-HEMAID, F.M. 2014. Enhanced electrocatalytic oxidation of isoniazid at electrochemically modified rhodium electrode for biological and pharmaceutical analysis. *Colloids and Surfaces B: Biointerfaces*, 121, 444-450.

CHEEMALAPATI, S., DEVADAS, B. & CHEN, S.M. 2014. Highly sensitive and selective determination of pyrazinamide at poly-l-methionine/reduced graphene oxide modified electrode by differential pulse voltammetry in human blood plasma and urine samples. *Journal of colloid and interface science,* 418, 132-139.

CHEEMALAPATI, S., DEVADAS, B., CHEN, S.M., ALI, M.A. & AL-HEMAID, F. M. 2014. Electrochemical determination of selected antihypertensive and antituberculosis drugs at a tyrosine-modified electrode. *Analytical Methods*, 6, 6774-6782.

CHEEMALAPATI, S., PALANISAMY, S. & CHEN, S.M. 2013. Electrochemical determination of isoniazid at electrochemically reduced graphene oxide modified electrode. *International Journal of Electrochemical Science*, 8, 3953-3962.

CHELLINI, P.R., LAGES, E.B., FRANCO, P.H., NOGUEIRA, F.H., CESAR, I.C. & PIANETTI, G.A. 2015. Development and Validation of an HPLC Method for Simultaneous Determination of Rifampicin, Isoniazid, Pyrazinamide, and Ethambutol Hydrochloride in Pharmaceutical Formulations. *Journal of AOAC International*, 98, 1234-9.

CHEN, W.C., UNNIKRISHNAN, B. & CHEN, S.M. 2012. Electrochemical oxidation and amperometric determination of isoniazid at functionalized multiwalled carbon

nanotube modified electrode. *International Journal of Electrochemical Science*, 7, 9138-9149.

CHEN, X., SONG, B., JIANG, H., YU, K. & ZHONG, D. 2005. A liquid chromatography/tandem mass spectrometry method for the simultaneous quantification of isoniazid and ethambutol in human plasma. *Rapid Commun Mass Spectrom*, 19, 2591-6.

CHENEVIER, P., MASSIAS, L., GUEYLARD, D. & FARINOTTI, R. 1998. Determination of ethambutol in plasma by high-performance liquid chromatography after pre-column derivatization. *Journal of Chromatography B: Biomedical Sciences and Applications*, 708, 310-315.

CHENNA, G.P., SHETTY, S.K., PAI, J.B., GOPINATH, B. & AHMED, M. 2011. Development of spectrophotometric methods for the estimation of pyrazinamide in bulk and pharmaceutical formulations. *International Journal of ChemTech Research*, 3, 737-741.

CHEMICOOL DICTIONARY, 2017, https://www.chemicool.com/definition/coulometry.html, Accessed on 26 February 2018.

CHIKAMA, K., MASTUBARA, K., OYAMA, S. & TOMITA, Y. 2008. Three-dimensional confocal Raman imaging of volume holograms formed in ZrO_2 nanoparticle-photopolymer composite materials. *Journal of Applied Physics*, 103, 1-7.

CHOKKAREDDY, R., BHAJANTHRI, N.K. & REDHI, G.G. 2017. An Enzyme-Induced Novel Biosensor for the Sensitive Electrochemical Determination of Isoniazid. *Biosensors*, 7, 1-12.

CHOKKAREDDY, R., BHAJANTRI, N.K., REDHI, G.G., & DHIRENDRA, G.R. 2017. Ultra-Sensitive Electrochemical Sensor for the Determination of Pyrazinamide. *Current Analytical Chemistry*, 13, 1-8.

CHRISTIE, J.H., TURNER, J.A. & OSTERYOUNG, R. 1977. Square wave voltammetry at the dropping mercury electrode: theory. *Analytical Chemistry*, 49, 1899-1903.

CLARK, L.C. & LYONS, C. 1962. Electrode systems for continuous monitoring in cardiovascular surgery. *Annals of the New York Academy of sciences*, 102, 29-45.

CONTE, J.E., LIN, E. & ZURLINDEN, E. 2000. High-performance liquid chromatographic determination of pyrazinamide in human plasma, bronchoalveolar lavage fluid, and alveolar cells. *Journal of chromatographic science*, 38, 33-37.

CONTE, J.E., LIN, E., ZHAO, Y. & ZURLINDEN, E. 2002. A High-Pressure Liquid Chromatographic-Tandem Mass Spectrometric Method for the Determination of Ethambutol in Human Plasma, Bronchoalveolar Lavage Fluid, and Alveolar Cells. *Journal of Chromatographic Science*, 40, 113-118.

CONTE-PERALES, L., RICO, A. J., BARROSO-CHINEA, P., GOMEZ-BAUTISTA, V., RODA, E., LUQUIN, N., SIERRA, S. & LANCIEGO, J. L. 2011. Pallidothalamic-projecting neurons in Macaca fascicularis co-express GABAergic and glutamatergic

markers as seen in control, MPTP-treated and dyskinetic monkeys. *Brain Structure and Function*, 216, 371-386.

COOKSEY, R.C., MORLOCK, G.P., MCQUEEN, A., GLICKMAN, S.E. & CRAWFORD, J.T. 1996. Characterization of streptomycin resistance mechanisms among Mycobacterium tuberculosis isolates from patients in New York City. *Antimicrobial agents and chemotherapy*, 40, 1186-1188.

COUTO, R.A. & QUINAZ, M.B. 2016. Development of a Nafion/MWCNT-SPCE-Based Portable Sensor for the Voltammetric Analysis of the Anti-Tuberculosis Drug Ethambutol. *Sensors*, 16, 1015.

DA SILVA, J.A.F., DE CASTRO, N.V., DE JESUS, D. P., FARIA, A.F., DE SOUZA, M.V. & DE OLIVEIRA, M.A.L. 2010. Fast determination of ethambutol in pharmaceutical formulations using capillary electrophoresis with capacitively coupled contactless conductivity detection. *Electrophoresis*, 31, 570-574.

DANESHGAR, P., NOROUZI, P., DOUSTY, F., GANJALI, M.R. & MOOSAVI-MOVAHEDI, A.A. 2009. Dysprosium hydroxide nanowires modified electrode for determination of rifampicin drug in human urine and capsules by adsorptive square wave voltammetry. *Current Pharmaceutical Analysis*, 5, 246-255.

DE LIMA, C.A., DA SILVA, P.S. & SPINELLI, A. 2014. Chitosan-stabilized silver nanoparticles for voltammetric detection of nitrocompounds. *Sensors and Actuators B: Chemical*, 196, 39-45.

DE OLIVEIRA NEVES, A.C., SOARES, G.M., DE MORAIS, S.C., DA COSTA, F.S.L., PORTO, D.L. & DE LIMA, K.M.G. 2012. Dissolution testing of isoniazid, rifampicin, pyrazinamide and ethambutol tablets using near-infrared spectroscopy (NIRS) and multivariate calibration. *Journal of Pharmaceutical and Biomedical Analysis*, 57, 115-119.

DE OLIVEIRA, R.C., PASCHOAL, J.A.R., SISMOTTO, M., DA SILVA AIROLDI, F.P. & REYES REYES, F.G. 2009. Development and validation of an LC-APCI-MS-MS analytical method for the determination of streptomycin and dihydrostreptomycin residues in milk. *Journal of chromatographic science*, 47, 756-761.

DE VELDE, F., ALFFENAAR, J.W., WESSELS, A.M., GREIJDANUS, B. & UGES, D.R. 2009. Simultaneous determination of clarithromycin, rifampicin and their main metabolites in human plasma by liquid chromatography-tandem mass spectrometry. J *Chromatogr B Analyt Technol Biomed Life Sci*, 877, 1771-1777.

DEMIRCI, H., FRANK MURPHY, I., MURPHY, E., GREGORY, S.T., DAHLBERG, A.E. & JOGL, G. 2013. A structural basis for streptomycin-induced misreading of the genetic code. *Nature communications*, 4, 1-17.

DEMIRKAYA-MILOGLU, F., OZNULUER, T., OZDURAK, B. & MILOGLU, E. 2016. Design and Optimization of a New Voltammetric Method for Determination of Isoniazid by Using PEDOT Modified Gold Electrode in Pharmaceuticals. Iranian *Journal of Pharmaceutical Research*, 15, 65-73.

DESSAU, F., BURGER, F., YEAGER, R. & KULISH, M. 1952. A method for the determination of in vitro sensitivity of tubercle bacilli to pyrazinamide (aldinamide). *American Review of Tuberculosis and Pulmonary Diseases*, 65, 635-639.

DEVADAS, B., CHEEMALAPATI, S., CHEN, S.M., ALI, M.A. & AL-HEMAID, F.M. 2015. Highly sensing graphene oxide/poly-arginine-modified electrode for the simultaneous electrochemical determination of buspirone, isoniazid and pyrazinamide drugs. *Ionics*, 21, 547-555.

DEVANI, M.B. & SHAH, S.A. 1990. Spectrophotometric determination of ethambutol hydrochloride and its dosage forms. *Indian Journal of Pharmaceutical Sciences*, 52, 121-122.

DHAL, S. & SHARMA, R. 2009. Development and validation of RP-HPLC method for simultaneous determination of pyridoxine hydrochloride, isoniazid, pyrazinamide and rifampicin in pharmaceutical formulation. *Chemia Analityczna*, 54, 1487-1500.

DO, J. A., LEE, M.Y., CHO, Y.J., CHANG, M.I., HONG, J.H. & OH, J.H. 2015. Determination of streptomycin in kiwifruit samples using LC-ESI-MS/MS. *Koreascience*, 28, 299-307.

DODOO-ARHIN, D., LEONI, M. & SCARDI, P. 2012. Microemulsion synthesis of copper oxide nanorod-like structures. *Molecular Crystals and Liquid Crystals*, 555, 17-31.

DORMESHKIN, D., GILEP, A., SERGEEV, G. & USANOV, S. 2016. Development of CYB5-fusion monitoring system for efficient periplasmic expression of multimeric proteins in Escherichia coli. *Protein expression and purification*, 128, 60-66.

DREADEN, E.C., ALKILANY, A.M., HUANG, X., MURPHY, C.J. & EL-SAYED, M.A. 2012. The golden age: gold nanoparticles for biomedicine. *Chemical Society Reviews*, 41, 2740-2779.

DRUMMOND, M.C., LEWIS, G.T. & CUMMINGS, M.M. 1951. The effect of heat on streptomycin and para-aminosalicylic acid in tuberculósis culture medium. *Diseases of the Chest*, 19, 158-164.

DUDA, E. 1973. A new, sensitive method for the determination of streptomycin. *Analytical Biochemistry*, 51, 651-653.

DUTT, M. & CHUA, T. 1964. Spectrophotometric determination of isoniazid in excess p-aminosalicylate. *Journal of Pharmacy and Pharmacology*, 16, 696-699.

EDDER, P., COMINOLI, A. & CORVI, C. 1999. Determination of streptomycin residues in food by solid-phase extraction and liquid chromatography with post-column derivatization and fluorometric detection. *Journal of chromatography A*, 830, 345-351.

EDRINGTON, T.S., HARVEY, R.B., FARRINGTON, L.A. & NISBET, D.J. 2002. Determination of MICs of streptomycin for resistant Salmonella isolates in swine and poultry using a micro-broth dilution system. *Journal of food protection*, 65, 563-566.

EGGINS, B. R. 2008. Chemical sensors and biosensors, *John Wiley & Sons*.

EMRANI, A.S., DANESH, N.M., LAVAEE, P., RAMEZANI, M., ABNOUS, K. & TAGHDISI, S.M. 2016. Colorimetric and fluorescence quenching aptasensors for detection of

streptomycin in blood serum and milk based on double-stranded DNA and gold nanoparticles. *Food Chemistry*, 190, 115-121.

ESPINOSA-MANSILLA, A., VALENZUELA, M.A., DE LA PENA, A.M., SALINAS, F. & CANADA, F.C. 2001. Comparative study of partial least squares and a modification of hybrid linear analysis calibration in the simultaneous spectrophotometric determination of rifampicin, pyrazinamide and isoniazid. *Analytica chimica acta*, 427, 129-136.

ETHIRAJ, A.S. & KANG, D.J. 2012. Synthesis and characterization of CuO nanowires by a simple wet chemical method. *Nanoscale research letters*, 7, 70.

FEDORCHUK, V., PUCHKOVSKAYA, E., ANISIMOVA, L. & SLEPCHENKO, G.B. 2005. Use of voltammetry for determining antibiotics streptomycin and azitromycin. *Journal of Analytical Chemistry*, 60, 518-522.

FERRAZ, B.R.L., LEITE, F.R.F. & MALAGUTTI, A.R. 2016. Simultaneous determination of ethionamide and pyrazinamide using poly (l-cysteine) film-modified glassy carbon electrode. *Talanta*, 154, 197-207.

FESTENSTEIN, G.N., HEATON, F.W., LOWE, J.S & MORTON, R.A. 1955. A constituent of the unsaponifiable portion of animal tissue lipids (λmax. mμ.). *Biochemical Journal*, 59, 558-556.

FIEVET, F., LAGIER, J., BLIN, B., BEAUDOIN, B. & FIGLARZ, M. 1989. Homogeneous and heterogeneous nucleations in the polyol process for the preparation of micron and submicron size metal particles. *Solid State Ionics*, 32, 198-205.

FINKEL, J., PITTILLO, R. & MELLETT, L. 1971. Fluorometric and microbiological assays for rifampicin and the determination of serum levels in the dog. *Chemotherapy*, 16, 380-388.

FLOYD, K., BLANC, L., RAVIGLIONE, M. & LEE, J.W. 2002. Resources required for global tuberculosis control. *Science*, 295, 2040-2041.

FORBES, M., KUCK, N. & PEETS, E. 1962. Mode of action of ethambutol. *Journal of bacteriology*, 84, 1099-1103.

FRIEDRICH, M.G., GIEB, F., NAUMANN, R., KNOLL, W., ATAKA, K., HEBERLE, J., HRABAKOVA, J., MURGIDA, D.H. & HILDEBRANDT, P. 2004. Active site structure and redox processes of cytochrome c oxidase immobilised in a novel biomimetic lipid membrane on an electrode. *Chemical Communications*, 21, 2376-2377.

FRUGERI, P.M., LAGO, A.C.D., WISNIEWSKI, C. & LUCCAS, P.O. 2014. A spectrophotometric flow injection system for streptomycin determination in veterinary samples. *Spectrochimica Acta Part A: Molecular and Biomolecular Spectroscopy*, 117, 304-308.

GALUS, Z. 2015. Professor Kemula School of Electrochemistry and Electroanalytical Chemistry at the University of Warsaw in Time of a Divided World. Electrochemistry in a Divided World. *Springer*, 315-331.

GAN, T., SHI, Z., WANG, K., SUN, J., LV, Z. & LIU, Y. 2015. Rifampicin determination in human serum and urine based on a disposable carbon paste microelectrode modified

with a hollow manganese oxide mesoporous silica oxide core-shell nanohybrid. *Canadian Journal of Chemistry*, 93, 1061-1068.

GERHARDT, G.C., SALISBURY, C. & MACNEIL, J.D. 1994. Determination of streptomycin and dihydrostreptomycin in animal tissue by on-line sample enrichment liquid chromatography. *Journal of AOAC International*, 77, 334-337.

GHONEIM, M.M., EL-BARADIE, K.Y. & TAWFIK, A. 2003. Electrochemical behavior of the antituberculosis drug isoniazid and its square-wave adsorptive stripping voltammetric estimation in bulk form, tablets and biological fluids at a mercury electrode. *Journal of Pharmaceutical and Biomedical Analysis*, 33, 673-685.

GHOULIPOUR, V., SHOKRI, M. & WAQIF-HUSAIN, S. 2011. Separation and determination of streptomycin by ion exchange-high-performance thin-layer chromatography. *JPC-Journal of Planar Chromatography-Modern TLC*, 24, 520-523.

GIROUSI, S.T., GHERGHI, I. & KARAVA, M.K. 2004. DNA-modified carbon paste electrode applied to the study of interaction between rifampicin (RIF) and DNA in solution and at the electrode surface. *Journal of Pharmaceutical and Biomedical Analysis*, 36, 851-858.

GLASS, B., AGATONOVIC-KUSTRIN, S., CHEN, Y. & WISCH, M. 2007. Optimization of a stability-indicating HPLC method for the simultaneous determination of rifampicin, isoniazid, and pyrazinamide in a fixed-dose combination using artificial neural networks. *Journal of chromatographic science*, 45, 38-44.

GNANASEKARAN, L., HEMAMALINI, R. & RAVICHANDRAN, K. 2015. Synthesis and characterization of TiO_2 quantum dots for photocatalytic application. *Journal of Saudi Chemical Society*, 19, 589-594.

GOICOECHEA, H.C. & OLIVIERI, A.C. 1999. Simultaneous determination of rifampicin, isoniazid and pyrazinamide in tablet preparations by multivariate spectrophotometric calibration. *Journal of Pharmaceutical and Biomedical Analysis*, 20, 681-686.

GOLABI, S. & ZARE, H.R. 1999. Electrocatalytic oxidation of hydrazine at glassy carbon electrode modified with electrodeposited film derived from caffeic acid. *Electroanalysis*, 11, 1293-1300.

GOU, X., WANG, G., YANG, J., PARK, J. & WEXLER, D. 2008. Chemical synthesis, characterisation and gas sensing performance of copper oxide nanoribbons. *Journal of Materials Chemistry*, 18, 965-969.

GOWDA, B.G., MELWANKI, M.B., SEETHARAMAPPA, J. & SRINIVASA MURTHY, K.C. 2002. Spectrophotometric determination of isoniazid in pure and pharmaceutical formulations. *Analytical sciences*, 18, 839-841.

GOWDA, J.I. & NANDIBEWOOR, S.T. 2014. Electrochemical behavior of paclitaxel and its determination at glassy carbon electrode. *Asian Journal of Pharmaceutical Sciences*, 9, 42-49.

GOWTHAMAN, N.S.K., KESAVAN, S. & JOHN, S.A. 2016. Monitoring isoniazid level in human fluids in the presence of theophylline using gold@platinum core@shell

nanoparticles modified glassy carbon electrode. *Sensors and Actuators B: Chemical*, 230, 157-166.

GRANADOS, O. & MEZA, G. 2007. A direct HPLC method to estimate streptomycin and its putative ototoxic derivative, streptidine, in blood serum: application to streptomycin-treated humans. *Journal of pharmaceutical and biomedical analysis*, 43, 625-630.

GRANJA, R.H.M.M., NINO, A.M.M., ZUCCHETTI, R.A.M., NINO, R.E.M., PATEL, R. & SALERNO, A.G. 2009. Determination of streptomycin residues in honey by liquid chromatography–tandem mass spectrometry. *Analytica Chimica Acta*, 637, 64-67.

GUERMOUCHE, S. & GUERMOUCHE, M.H. 2004. Solid-phase extraction and HPTLC determination of isoniazid and acetylisoniazid in serum. Comparison with HPLC. *Journal of chromatographic science*, 42, 250-253.

GUMEDE, N.J. 2008. Harmonization of internal quality tasks in analytical laboratories case studies: water analysis methods using polarographic and voltammetric techniques. 1-260.

GUPTA, P., JADAUN, G., DAS, R. & GUPTA, U. 2006. Simultaneous ethambutol & isoniazid resistance in clinical isolates of Mycobacterium tuberculosis. *Indian Journal of Medical Research*, 123, 125-130.

GUPTA, V. 2003. Preparation of ethambutol–copper(II) complex and fabrication of PVC based membrane potentiometric sensor for copper. *Talanta*, 60, 149-160.

GURUMURTHY, P., GAYATHRI, T., BHAGAVATHY, S. & VENKATESAN, P. 2004. Standardization of the method for estimation of ethambutol in pharmaceutical preparations and biological fluid. *Indian Journal of Experimental Biology*, 42, 68-73.

HAHN, Y. & SHIN, S. 2001. Electrochemical behavior and differential pulse polarographic determination of rifampicin in the pharmaceutical preparations. *Archives of pharmacal research*, 24, 100-104.

HAKKIMANE, S.S. & GURU, B.R. 2017. Nano Formulation Analysis: Analytical Method Development of Isoniazid and Simultaneous Estimation of Anti-Tubercular Drugs Isoniazid and Rifampicin by Rp-Hplc. *Asian Journal of Pharmaceutical and Clinical Research*, 10, 330-335.

HAMMAM, E., BELTAGI, A.M. & GHONEIM, M.M. 2004. Voltammetric assay of rifampicin and isoniazid drugs, separately and combined in bulk, pharmaceutical formulations and human serum at a carbon paste electrode. *Microchemical Journal*, 77, 53-62.

HANKO, V. & ROHRER, J. 2015. Determination of Streptomycin and Impurities Using HPAE-PAD. *Thermo Fisher Scientific, Sunnyvale*, CA, USA, 1-12.

HARVEY, D. 2017, Coulometric Methods,

https://chem.libretexts.org/Textbook_Maps/Analytical_Chemistry_Textbook_Maps/Map%3A_Analytical_Chemistry_2.0_(Harvey)/11_Electrochemical_Methods/11.3%3A_Coulometric_Methods, Accessed on 26 February 2018.

HARVEY, D. 2002. Electrochemical Methods. *Current Separations*, 20 (2), 51-53.

HASSAN, S.S., MAHMOUD, W.H. & OTHMAN, A.H.M. 1997. A novel potassium ion membrane sensor based on rifamycin neutral ionophore. *Talanta*, 44, 1087-1094.

HEIFETS, L., HIGGINS, M. & SIMON, B. 2000. Pyrazinamide is not active against Mycobacterium tuberculosis residing in cultured human monocyte-derived macrophages [Unresolved issues]. *The International Journal of Tuberculosis and Lung Disease*, 4, 491-495.

HEYROVSKY, J. 1956. The development of polarographic analysis. *Analyst*, 81, 189-192.

HOLDINESS, M.R., ISRAILI, Z.H. & JUSTICE, J.B. 1981. Gas chromatographic mass spectrometric determination of ethambutol in human plasma. *Journal of Chromatography B: Biomedical Sciences and Applications*, 224, 415-422.

HOLZE, R. 2009. Experimental electrochemistry, *John Wiley & Sons*.

HORIE, M., SAITO, H., NATORI, T., NAGATA, J. & NAKAZAWA, H. 2004. Determination of streptomycin and dihydrostreptomycin in honey by liquid chromatography–electrospray mass spectrometry. *Journal of liquid chromatography & related technologies*, 27, 863-874.

HORIE, M., YOSHIDA, T., KIKUCHI, Y. & NAKAZAWA, H. 2001. Determination of streptomycin and dihydrostreptomycin in meat by liquid chromatography/mass spectrometry. Shokuhin eiseigaku zasshi. *Journal of the Food Hygienic Society of Japan*, 42, 374-378.

HORMAZABAL, V. & YNDESTAD, M. 1995. Determination of dihydrostreptomycin sulfate in milk by HPLC using ion-pair and postcolumn derivatization. *Journal of Liquid Chromatography & Related Technologies*, 18, 2695-2702.

HRABANKOVA, E., DOLEZAL, J. & BERAN, P. 1969. Cathodic stripping voltammetry of lead. *Journal of Electroanalytical Chemistry and Interfacial Electrochemistry*, 22, 203-206.

HSU, K. Y. & HO, Y. 1989. Determination of isoniazid methanesulphonate and its metabolites in rabbit blood by high-performance liquid chromatography. *Journal of Chromatography B: Biomedical Sciences and Applications*, 493, 305-312.

https://www.123rf.com/stock-photo/mycobacterium_tuberculosis.html?sti=lmhicvdq1a10qttrgg|, accessed on 30th November 2017.

HU, S., LU, Q. & XU, Y. 2008. CHAPTER 17 - Biosensors based on direct electron transfer of protein A2 - Zhang, Xueji. In: JU, H. & WANG, J. (eds.) Electrochemical Sensors, Biosensors and their Biomedical Applications. San Diego: *Academic Press*.

HUA, M.Y., LIN, Y.C., TSAI, R. Y., CHEN, H.C. & LIU, Y.C. 2011. A hydrogen peroxide sensor based on a horseradish peroxidase/polyaniline/carboxy-functionalized multiwalled carbon nanotube modified gold electrode. *Electrochimica Acta*, 56, 9488-9495.

HUANG, J., YIN, Y., XU, J.Z., LIU, Y., CHEN, G., ZHANG, X., YANG, W., SHENG, C., CHEN, H. & ZHANG, R. 2014. Determination of streptomycin and

dihydrostreptomycin in pollens by high performance liquid chromatography-tandem mass spectrometry. *Se pu Chinese journal of chromatography*, 32, 566-572.

HURTUBISE, R. 1974. Determination of disodium edetate dihydrate in streptomycin by atomic absorption spectrophotometry. *Journal of pharmaceutical sciences*, 63, 1131-1133.

HUTTEMANN, M., PECINA, P., RAINBOLT, M., SANDERSON, T.H., KAGAN, V.E., SAMAVATI, L., DOAN, J.W. & LEE, I. 2011. The multiple functions of cytochrome c and their regulation in life and death decisions of the mammalian cell: From respiration to apoptosis. *Mitochondrion*, 11, 369-381.

IRIMINESCU, D., CARCU-DOBRIN, M., HANCU, G., MIRCIA, E., KELEMEN, H., RUSU, A. & TILINCA, M. 2016. Simultaneous determination of Isoniazid an Drifampicin by micellar electrokinetic chromatography. *Studia Universitatis Vasile Goldis Seria Stiintele Vietii* (Life Sciences Series), 26. 353-357.

JADAUN, G., AGARWAL, C., SHARMA, H., AHMED, Z., UPADHYAY, P., FAUJDAR, J., GUPTA, A. K., DAS, R., GUPTA, P. & CHAUHAN, D. 2007. Determination of ethambutol MICs for Mycobacterium tuberculosis and Mycobacterium avium isolates by resazurin microtitre assay. *Journal of Antimicrobial Chemotherapy*, 60, 152-155.

JANSSON, M., BEISSNER, M., PHILLIPS, R.O., BADZIKLOU, K., PITEN, E., MAMAN, I., SARFO, F.S., HUBER, K.L., RHOMBERG, A. & SYMANK, D. 2014. Comparison of two assays for molecular determination of rifampin resistance in clinical samples from patients with Buruli ulcer disease. *Journal of clinical microbiology*, 52, 1246-1249.

JEBA, J. 2015. A Survey on Side Effects of Anti-Tuberculosis Drugs in Dhaka, *Bangladesh. East West University*.

JENA, B.K. & RAJ, C.R. 2010. Au nanoparticle decorated silicate network for the amperometric sensing of isoniazid. *Talanta*, 80, 1653-1656.

JIA, J., Wei, C. 2014. The prevalence of mild cognitive impairment and its etiological subtypes in elderly Chinese. *Alzheimer's & Dementia*, 10, 439-447.

JIANG, Z., WANG, H. & LOCKE, D.C. 2002. Determination of ethambutol by ion-pair reversed phase liquid chromatography with UV detection. *Analytica Chimica Acta*, 456, 189-192.

JOHNSON, D.C. & LACOURSE, W.R. 1990. Liquid chromatography with pulsed electrochemical detection at gold and platinum electrodes. *Analytical Chemistry*, 62, 589-597.

JOHNSSON, K., KING, D.S. & SCHULTZ, P.G. 1995. Studies on the mechanism of action of isoniazid and ethionamide in the chemotherapy of tuberculosis. *Journal of the American Chemical Society*, 117, 5009-5010.

KAKA, J.S. 1994. Rapid Simplified Analysis of Pyrazinamide in Rat Plasma by HPLC. *Journal of Liquid Chromatography*, 17, 3793-3801.

KALAMBATE, P.K., RAWOOL, C.R. & SRIVASTAVA, A.K. 2016. Voltammetric determination of pyrazinamide at graphene-zinc oxide nanocomposite modified carbon paste electrode employing differential pulse voltammetry. *Sensors and Actuators B: Chemical*, 237, 196-205.

KARIMI, M.A., MAZLOUM-ARDAKANI, M., MASHHADIZADEH, M.H. & BANIFATEMEH, F. 2009. Simultaneous kinetic spectrophotometric determination of hydrazine and isoniazid using H-point standard addition method and partial least squares regression in micellar media. *Croatica Chemica Acta*, 82, 729-738.

KARLSON, A. G. 1961a. The in Vitro Activity of Ethambutol (Dextro-2, 2′-[Ethylenediimino]-Di-l-Butanol) Against Tubercle Bacilli and Other Microorganisms. *American Review of Respiratory Disease*, 84, 905-906.

KARLSON, A. G. 1961b. Therapeutic Effect of Ethambutol (Dextro-2, 2′-[Ethylenediimino]-Di-l-Butanol) on Experimental Tuberculosis in Guinea Pigs. *American Review of Respiratory Disease*, 84, 902-904.

KAUFFMANN, J.M. & VIRE, J.C. 1993. Pharmaceutical and biomedical applications of electroanalysis: a critical review. *Analytica chimica acta*, 273, 329-334.

KERMAN, K., VESTERGAARD, M. D. & TAMIYA, E. 2007. Label-free electrical sensing of small-molecule inhibition on tyrosine phosphorylation. *Analytical Chemistry*, 79 (17), 6881-6885.

KHALIL, M.I., AL-QUNAIBIT, M.M., AL-ZAHEM, A.M. & LABIS, J.P. 2014. Synthesis and characterization of ZnO nanoparticles by thermal decomposition of a curcumin zinc complex. *Arabian Journal of Chemistry*, 7, 1178-1184.

KHAMAR, J.C. & PATEL, S.A. 2012. Q-Absorbance Ratio Spectrophotometric Method for the Simultaneous Estimation of Rifampicin and Piperine in their Combined Capsule Dosage, *Journal of Applied Pharmaceutical Science*, 2, 137-141

KHUHAWAR, M. & ZARDARI, L. 2006. Capillary gas chromatographic determination of isoniazid in pharmaceutical preparations and blood by precolumn derivatization with trifluoroacetylacetone. *Journal of Food and Drug analysis*, 14, 323-328.

KHUHAWAR, M.Y. & RIND, F.M.A. 2002. Liquid chromatographic determination of isoniazid, pyrazinamide and rifampicin from pharmaceutical preparations and blood. *Journal of Chromatography B*, 766, 357-363.

KHUHAWAR, M., RIND, F. & RAJPER, A. 2005. High-performance liquid chromatographic determination of isoniazid, pyrazinamide, and indomethacin in pharmaceutical preparations. *Acta chromatographica*, 15, 269-275.

KISA, O., ALBAY, A., BEDIR, O., BAYLAN, O. & DOGANCI, L. 2003. Evaluation of FASTPlaqueTB-RIF™ for determination of rifampicin resistance in Mycobacterium tuberculosis complex isolates. *The International Journal of Tuberculosis and Lung Disease*, 7, 284-288.

KISSINGER, P. & HEINEMAN, W.R. 1996. Laboratory Techniques in Electroanalytical Chemistry, revised and expanded, *CRC press*.

KOPPENOL, W. & BUTLER, J. 1984. The radiation chemistry of cytochrome c. *Israel Journal of Chemistry*, 24, 11-16.

KOWALSKI, P., OLEDZKA, I., OKONIEWSKI, P., SWITALA, M. & LAMPARCZYK, H. 1999. Determination of streptomycin in eggs yolk by capillary electrophoresis. *Chromatographia*, 50, 101-104.

KRISHNA, A. C., SARAVANAN, R., JEEVANANTHAM, S., VIGNESH, R. & KARTHIK, P. 2012. Determination of pyrazinamide in human plasma samples containing fixed dose combination molecules by using liquid chromatography tandem mass spectrometry. *Adv. Pharmacoepidemol. Drug Saf*, 4, 66-75.

KSHIRSAGAR, J.M., SHRIVASTAVA, R. & ADWANI, P.S. 2017. Preparation and characterization of copper oxide nanoparticles and determination of enhancement in critical heat flux. *Thermal Science*, 21, 233-242.

KUBO, H., KOBAYASHI, Y. & KINOSHITA, T. 1986. Fluorescence determination of streptomycin in serum by reversed-phase ion-pairing liquid chromatography. *Analytical chemistry*, 58, 2653-2655.

KUMARI, M.K., KASTHURI, J. K., BABU, B.H., SATYANARAYANA, P. & TCHALEU, B. N. 2015. A Validated Liquid Chromatographic Method for the Determination of Rifampicin and Isoniazid in Pharmaceutical Formulations. *Analytical chemistry* 7(4), 299-307.

KURNIATI, Z., RIYANTO, S. & ROHMAN, A.A. 2016. Determination of Rifampicin, Isoniazid, Pyrazinamide and Ethambutol Hydrochloride in 4FDC Tablet by FTIR Spectrophotometry in Combination with Multivariate Calibration. *Journal of Food and Pharmaceutical Sciences*, 4, 25-30.

KUROSAWA, N., KURIBAYASHI, S., OWADA, E., ITO, K., NIOKA, M., ARAKAWA, M. & FUKUDA, R. 1985. Determination of streptomycin in serum by high-performance liquid chromatography. *Journal of Chromatography B: Biomedical Sciences and Applications*, 343, 379-385.

LACHAU, S., ROCHAS, M., TUFENKJI, A., MARTIN, N., LEVILLAIN, P. & HOUIN, G. 1992. First derivative spectroscopic determination of binding characteristics of rifampicin to human albumin and serum. *Journal of pharmaceutical sciences*, 81, 287-289.

LACROIX, C., GUYONNAUD, C., CHAOU, M., DUWOOS, H. & LAFONT, O. 1988. Interaction between allopurinol and pyrazinamide. *European Respiratory Journal*, 1, 807-811.

LATA, S., BATRA, B., KUMAR, P. & PUNDIR, C. 2013. Construction of an amperometric d-amino acid biosensor based on d-amino acid oxidase/carboxylated mutliwalled carbon nanotube/copper nanoparticles/polyalinine modified gold electrode. *Analytical biochemistry*, 437, 1-9.

LEE, A. C., LIU, G., HENG, C.K., TAN, S.N., LIM, T.M. & LIN, Y. 2008. Sensitive Electrochemical Detection of Horseradish Peroxidase at Disposable Screen-Printed Carbon Electrode. *Electroanalysis*, 20, 2040-2046.

LEECH, D., WANG, J. & SMYTH, M.R. 1990. Electrocatalytic detection of streptomycin and related antibiotics at ruthenium dioxide modified graphite-epoxy composite electrodes. *Analyst*, 115, 1447-1450.

LEVIN, M.E. & HATFULL, G.F. 1993. Mycobacterium smegmatis RNA polymerase: DNA supercoiling, action of rifampicin and mechanism of rifampicin resistance. *Molecular microbiology*, 8, 277-285.

LI, B., HE, Y., LV, J. & ZHANG, Z. 2005. Simultaneous determination of rifampicin and isoniazid by continuous-flow chemiluminescence with artificial neural network calibration. *Analytical and Bioanalytical Chemistry*, 383, 817-824.

LIANG, Y.D., SONG, J.F. & XU, M. 2007. Electrochemiluminescence from successive electro- and chemo-oxidation of rifampicin and its application to the determination of rifampicin in pharmaceutical preparations and human urine. *Spectrochim Acta A Mol Biomol Spectrosc*, 67, 430-436.

LIMA, A., LUZ, G., BATISTA, N., LONGO, E., CAVALCANTE, L. & SANTOS, R. 2015. Determination of Ethambutol in Aqueous Medium Using an Inexpensive Gold Microelectrode Array as Amperometric Sensor. *Electroanalysis*, 28, 985-989.

LIMA, K. C.M.S., SANTOS, A.C.F., FERNANDES, R.N., DAMOS, F.S. & DE CASSIA SILVA LUZ, R. 2016. Development of a novel sensor for isoniazid based on 2,3-dichloro-5,6-dicyano-p-benzoquinone and graphene: Application in drug samples utilized in the treatment of tuberculosis. *Microchemical Journal*, 128, 226-234.

LINGANE, J. J. 1958. *Electroanalytical chemistry*. Interscience Publishers.

LIU, B., TANG, D., ZHANG, B., QUE, X., YANG, H. & CHEN, G. 2013. Au(III)-promoted magnetic molecularly imprinted polymer nanospheres for electrochemical determination of streptomycin residues in food. *Biosensors and Bioelectronics*, 41, 551-556.

LIU, B., ZHANG, B., CUI, Y., CHEN, H., GAO, Z. & TANG, D. 2011. Multifunctional gold–silica nanostructures for ultrasensitive electrochemical immunoassay of streptomycin residues. *ACS applied materials & interfaces*, 3, 4668-4676.

LIU, J., SUN, J., ZHANG, W., GAO, K. & HE, Z. 2008. HPLC determination of rifampicin and related compounds in pharmaceuticals using monolithic column. *Journal of Pharmaceutical and Biomedical Analysis*, 46, 405-409.

LIU, L., LI, Y., TIAN, L., GUO, T., CAO, W. & WEI, Q. 2015. A label-free voltammetric immunoassay based on 3D-structured rGO–MWCNT–Pd for detection of human immunoglobulin G. *Sensors and Actuators B: Chemical*, 211, 170-176.

LOMILLO, M.A.A., RENEDO, O.D. & MARTINEZ, M.J.A. 2005. Optimization of a cyclodextrin-based sensor for rifampicin monitoring. *Electrochimica acta*, 50, 1807-1811.

LOMILLO, M.A., KAUFFMANN, J. & MARTINEZ, M.A. 2003. HRP-based biosensor for monitoring rifampicin. *Biosensors and Bioelectronics*, 18, 1165-1171.

LONNROTH, K., MIGLIORI, G.B., ABUBAKAR, I., DAMBROSIO, L., DE VRIES, G., DIEL, R., DOUGLAS, P., FALZON, D., GAUDREAU, M.A. & GOLETTI, D. 2015. Towards tuberculosis elimination: an action framework for low-incidence countries. *European Respiratory Journal*, 45, 928-952.

LORYUENYONG, V., TOTEPVIMARN, K., EIMBURANAPRAVAT, P., BOONCHOMPOO, W. & BUASRI, A. 2013. Preparation and characterization of reduced graphene oxide

sheets via water-based exfoliation and reduction methods. *Advances in Materials Science and Engineering*, 2013, 1-5.

LOUVEAU, B., FERNANDEZ, C., ZAHR, N., SAUVAGEON-MARTRE, H., MASLANKA, P., FAURE, P., MOURAH, S. & GOLDWIRT, L. 2016. Determination of rifampicin in human plasma by high-performance liquid chromatography coupled with ultraviolet detection after automatized solid–liquid extraction. *Biomedical Chromatography*, 30, 2009-2015.

LOVE, J.C., ESTROFF, L.A., KRIEBEL, J.K., NUZZO, R.G. & WHITESIDES, G.M. 2005. Self-assembled monolayers of thiolates on metals as a form of nanotechnology. *Chemical reviews*, 105, 1103-1170.

LUBERT, K. H. & KALCHER, K. 2010. History of electroanalytical methods. *Electroanalysis*, 22, 1937-1946.

MA, Y., ZHANG, B.T., ZHAO, L.X., GUO, G. S. & LIN, J.M. 2008. Determination of Rifampicin by Peroxomonosulfate Cobalt (II) Chemiluminescence System. *Chinese Journal of Chemistry*, 26, 905-910.

MAHJOUB, A.A., KHAN, A.H., SULAIMAN, S.A.S., LAJIS, R., MAN, C.N. & ALI, I.A.H. 2016. Simultaneous determination of isoniazid and pyrazinamide in plasma by high performance liquid chromatography. *Tropical Journal of Pharmaceutical Research*, 15, 2475-2481.

MAJIDI, M.R., JOUYBAN, A. & ASADPOUR-ZEYNALI, K. 2006. Voltammetric behavior and determination of isoniazid in pharmaceuticals by using overoxidized polypyrrole

glassy carbon modified electrode. *Journal of Electroanalytical Chemistry*, 589, 32-37.

MAN, S.C., LY, D., WHITTAKER, M.R., THICKETT, S.C. & ZETTERLUND, P.B. 2014. Nano-sized graphene oxide as sole surfactant in miniemulsion polymerization for nanocomposite synthesis: Effect of pH and ionic strength. *Polymer*, 55, 3490-3497.

MANI, S., CHEEMALAPATI, S., CHEN, S.M. & DEVADAS, B. 2015. Anti-tuberculosis Drug Pyrazinamide Determination at Multiwalled Carbon Nanotubes/Graphene Oxide Hybrid Composite Fabricated Electrode. *International Journal of Electrochemical. Science*, 10, 7049-7062.

MAO, Y., LI, N., HAN, Y., LIU, N., GAO, Z. & ZHOU, Z. 2013. Synchronous Fluorescence Determination of Streptomycin in Biological Fluids with CdTe/CdSe Quantum Dots as Fluorescence Probe. *Asian Journal of Chemistry*, 25, 2552-2558.

MARIA, N., GEORGIANA, S. & CATERINA, B.A. 2015. Simple and rapid method on High Performance Liquid Chromatography for simultaneous determination of benzylpenicillin potassium, streptomycin sulphate and related substances in Ascomicin–a veterinary use ointment. *Medicamentul Veterinar*. 9, 75-82.

MARKOVIC, N., GASTEIGER, H. & ROSS, P.N. 1997. Kinetics of oxygen reduction on Pt (hkl) electrodes: implications for the crystallite size effect with supported Pt electrocatalysts. *Journal of The Electrochemical Society*, 144, 1591-1597.

MARTIN, A., TAKIFF, H., VANDAMME, P., SWINGS, J., PALOMINO, J.C. & PORTAELS, F. 2006. A new rapid and simple colorimetric method to detect pyrazinamide

resistance in Mycobacterium tuberculosis using nicotinamide. *Journal of Antimicrobial Chemotherapy*, 58, 327-331.

MEHMEDAGIC, A., VERITE, P., MENAGER, S., THARASSE, C., CHABENAT, C., ANDRE, D. & LAFONT, O. 1997. Determination of pyrazinamide and its main metabolites in rat urine by high-performance liquid chromatography. *Journal of Chromatography B: Biomedical Sciences and Applications*, 695, 365-372.

MILAN-SEGOVIA, R., PEREZ-FLORES, G., TORRES-TIRADO, J., HERMOSILLO-RAMIREZ, X., VIGNA-PÉREZ, M. & ROMANO-MORENO, S. 2007. Simultaneous HPLC determination of isoniazid and acetylisoniazid in plasma. *Acta Chromatographica*, 19, 110-116.

MITCHELL, P. 1975. The protonmotive Q cycle: a general formulation. *FEBS letters*, 59, 137-139.

MITIC, S.S., SUNARIC, S.M. & TOSIC, S.B. 2006. Determination of streptomycin in a pharmaceutical sample based on its degradation by hydrogen peroxide in the presence of copper (II). *Analytical sciences*, 22, 753-756.

MOHAMED, A.M.I., MOHAMED, F.A.F., ATIA, N.N. & BOTROS, S.M. 2015. Ethambutol-Cobalt (II) ions complexation spectral characteristics and applications for quantitative analysis. *Pakistan journal of pharmaceutical sciences*, 1, 603-609.

MOHAMED, A.M.I., MOHAMED, F.A., ATIA, N.N. & BOTROS, S.M. 2013. A novel spectrofluorimetric determination of four anti-TB drugs in their pure and pharmaceutical dosage forms by quenching effect on the fluorescence of NBS-

phenothiazine product. *Asian Journal of Biomedical and Pharmaceutical Sciences*, 3, 21-27.

MOHAMED, M.A., SHANTIER, S.W., MOHAMED, M.A., GADKARIEM, E.A. & ISMAIL, E. M. 2015. Spectrophotometric Method for the Simultaneous Determination of Isoniazid and Rifampicin in Bulk and Tablet Forms. *International Journal of Pharmaceutical Science Reviews*, 32, 154-156.

MOHAMED, M., SALLEH, W., JAAFAR, J. & ISMAIL, A. 2015. Structural characterization of N-doped anatase–rutile mixed phase TiO_2 nanorods assembled microspheres synthesized by simple sol–gel method. *Journal of Sol-Gel Science and Technology*, 74, 513-520.

MOHAMMAD DANESH, N., RAMEZANI, M., SARRESHTEHDAR EMRANI, A., ABNOUS, K. & TAGHDISI, S. M. 2016. A novel electrochemical aptasensor based on arch-shape structure of aptamer-complimentary strand conjugate and exonuclease I for sensitive detection of streptomycin. *Biosensors and Bioelectronics*, 75, 123-128.

MONTHIOUX, M. & FLAHAUT, E. 2007. Meta-and hybrid-CNTs: A clue for the future development of carbon nanotubes. *Materials Science and Engineering: C*, 27, 1096-1101.

MORALES, J., SANCHEZ, L., MARTIN, F., RAMOS-BARRADO, J.R. & SANCHEZ, M. 2004. Nanostructured CuO thin film electrodes prepared by spray pyrolysis: a simple method for enhancing the electrochemical performance of CuO in lithium cells. *Electrochimica Acta*, 49, 4589-4597.

MSAGATI, T.A. & NGILA, C.J. 2003. Voltammetric determination of a benzimidazole anthelmintic mixture at a poly (3-methylthiophene)-modified glassy carbon electrode. *South African Journal of Chemistry*, 56, 5-9.

MULYANI, E., DARMAWAN, E., PERWITASARI, D., MULYANI, U., ATTHOBARI, J., KUSUMA, D.Y., HIDAYAH, Q., AJI, O.R., WINANDA, R.S. & INAYATI, S. Validation of pyrazinamide in human plasma using Hplc-Uv for therapeutic drug monitoring. AIP Conference Proceedings, 2016. *AIP Publishing*, 020031.

MURPHY, C.J., GOLE, A.M., HUNYADI, S.E., STONE, J.W., SISCO, P.N., ALKILANY, A., KINARD, B.E. & HANKINS, P. 2008. Chemical sensing and imaging with metallic nanorods. *Chemical Communications*, 5, 544-557.

MUSSER, J.M. 1995. Antimicrobial agent resistance in mycobacteria: molecular genetic insights. *Clinical microbiology reviews*, 8, 496-514.

NAMDAR, R., EBERT, S.C. & PELOQUIN, C.A. 2005. Drugs for tuberculosis. Drug interactions in infectious diseases. *Springer*.

NEGI, S., SINGH, U., GUPTA, S., KHARE, S., RAI, A. & LAL, S. 2009. Characterization of RPO B gene for detection of rifampicin drug resistance by SSCP and sequence analysis. *Indian journal of medical microbiology*, 27, 226-229.

NESE, G. & OMLAND, T. 1959. Determination of streptomycin in various parts of the tuberculous lung. *APMIS*, 46, 343-348.

NGECE, R.F., WEST, N., NDANGILI, P.M., OLOWU, R.A., WILLIAMS, A., HENDRICKS, N., MAILU, S., BAKER, P. & IWUOHA, E. 2011. a silver nanoparticle/poly (8-

anilino-1-naphthalene sulphonic acid) bioelectrochemical biosensor system for the analytical determination of ethambutol. *International Journal of Electrochemical Science*, 6, 1820-1834.

NGO, S.C., ZIMHONY, O., CHUNG, W.J., SAYAHI, H., JACOBS, W.R. & WELCH, J.T. 2007. Inhibition of isolated Mycobacterium tuberculosis fatty acid synthase I by pyrazinamide analogs. *Antimicrobial agents and chemotherapy*, 51, 2430-2435.

NICHOLSON, R.S. & SHAIN, I. 1964. Theory of stationary electrode polarography. Single scan and cyclic methods applied to reversible, irreversible, and kinetic systems. *Analytical Chemistry*, 36, 706-723.

NXUSANI, E., NDANGILI, P., OLOWU, R., JIJANA, A., WARYO, T., JAHED, N., AJAYI, R., BAKER, P.G.L. & IWUOHA, E.I. 2012. 3-Mercaptopropionic acid capped Ga2Se3nanocrystal-CYP3A4 biosensor for the determination of 17-alpha-ethinyl estradiol in water. *Nano Hybrids, Trans Tech Pub*, 1,1-22.

OGA, E. F. & ENOCHE, F. 2010. Spectrophotometric determination of isoniazid in pure and pharmaceutical formulations using vanillin. *International Journal of Pharmaceutical Science*, 2, 55-58.

OKAYAMA, A., KITADA, Y., AOKI, Y., UMESAKO, S., ONO, H., NISHII, Y. & KUBO, H. 1988. Fluorescence Hplc determination of Streptomycin in meat using Ninhydrin as a postcolumn labeling agent. *Bunseki Kagaku*, 37, 221-224.

OLDFIELD, S., BERG, J., STILES, H. & BUCKLEY, B. 1986. Measurement of rifampicin and 25-desacetylrifampicin in biological fluids using high-performance liquid

chromatography with direct sample injection. *Journal of Chromatography B: Biomedical Sciences and Applications*, 377, 423-429.

OLITZKI, A. 1952. The determination of the most probable numbers of streptomycin-fast cells in Brucella cultures and their variability in growing and ageing cultures. *Microbiology*, 6, 166-174.

OLIVEIRA, P.R.D., OLIVEIRA, M.M., ZARBIN, A.J.G., MARCOLINO-JUNIOR, L.H. & BERGAMINI, M. F. 2012. Flow injection amperometric determination of isoniazid using a screen-printed carbon electrode modified with silver hexacyanoferrates nanoparticles. *Sensors and Actuators B: Chemical*, 171, 795-802.

ORGANIZATION, W.H. 2000. The world health report 2000: health systems: improving performance, *World Health Organization*.

ORTOLANI, L., CADELANO, E., VERONESE, G.P., DEGLI ESPOSTI BOSCHI, C., SNOECK, E., COLOMBO, L. & MORANDI, V. 2012. Folded graphene membranes: mapping curvature at the nanoscale. *Nano letters*, 12, 5207-5212.

OSWALD, S., PETERS, J., VENNER, M. & SIEGMUND, W. 2011. LC-MS/MS method for the simultaneous determination of clarithromycin, rifampicin and their main metabolites in horse plasma, epithelial lining fluid and broncho-alveolar cells. *Journal of Pharmaceutical and Biomedical Analysis*, 55, 194-201.

PANCHAGNULA, R., SOOD, A., SHARDA, N., KAUR, K. & KAUL, C. L. 1999. Determination of rifampicin and its main metabolite in plasma and urine in presence

of pyrazinamide and isoniazid by HPLC method. *Journal of Pharmaceutical and Biomedical Analysis*, 18, 1013-1020.

PARK, S.H. & BLACKSTONE, C. 2010. Further assembly required: construction and dynamics of the endoplasmic reticulum network. *EMBO reports*, 11, 515-521.

PINZAUTI, S., PIAZ, V.D. & PORTA, E.L. 1974. Chloramine-T as titrimetric reagent in potentiometric determination of isoniazid, phenelzine, and dihydralazine. *Journal of pharmaceutical sciences*, 63, 1446-1448.

PLAMBECK, J.A. 1982. Electroanalytical Chemistry: Basic Principles and Applications, New York; Toronto: *Wiley*.

PRAMER, D. & STARKEY, R.L. 1962. Determination of Streptomycin in soil and the effect of soil colloidal material on its activity. *Soil Science*, 94, 48-54.

PRASANTHI, B., RATNA, J.V. & PHANI, R.S.C. 2015. Development and validation of RP-HPLC method for simultaneous estimation of rifampicin, isoniazid and pyrazinamide in human plasma. *Journal of Analytical Chemistry*, 70, 1015-1022.

PRUSINER, S.B., SCOTT, M., FOSTER, D., PAN, K.M., GROTH, D., MIRENDA, C., TORCHIA, M., YANG, S.L., SERBAN, D. & CARLSON, G.A. 1990. Transgenetic studies implicate interactions between homologous PrP isoforms in scrapie prion replication. *Cell*, 63, 673-686.

PUGNO, N.M. 2006. On the strength of the carbon nanotube-based space elevator cable: from nanomechanics to megamechanics. *Journal of Physics: Condensed Matter*, 18, 1971-1975.

PULLAN, S.T., ALLNUTT, J.C., DEVINE, R., HATCH, K.A., JEEVES, R.E., HENDON-DUNN, C.L., MARSH, P.D. & BACON, J. 2016. The effect of growth rate on pyrazinamide activity in Mycobacterium tuberculosis-insights for early bactericidal activity. *BMC infectious diseases*, 16, 1-11.

PUMERA, M. 2009. Electrochemistry of graphene: new horizons for sensing and energy storage. *The Chemical Record*, 9, 211-223.

QUE, X., LIU, B., FU, L., ZHUANG, J., CHEN, G. & TANG, D. 2013. Molecular imprint for electrochemical detection of streptomycin residues using enzyme signal amplification. *Electroanalysis*, 25, 531-537.

RA, E.J., AN, K.H., KIM, K.K., JEONG, S.Y. & LEE, Y.H. 2005. Anisotropic electrical conductivity of MWCNT/PAN nanofiber paper. *Chemical Physics Letters*, 413, 188-193.

RAGEH, A.M.I.M., MOHAMED, F.A., ATIA, N.N. & BOTROS, S.M. 2015. Simultaneous densitometric determination of first line anti-TB drugs in binary, ternary, and quaternary mixtures. *Journal of Liquid Chromatography & Related Technologies*, 38, 1061-1067.

RAGONESE, R., MACKA, M., HUGHES, J. & PETOCZ, P. 2002. The use of the Box–Behnken experimental design in the optimisation and robustness testing of a capillary electrophoresis method for the analysis of ethambutol hydrochloride in a pharmaceutical formulation. *Journal of Pharmaceutical and Biomedical Analysis*, 27, 995-1007.

RAMAKRISHNAN, T., MURTHY, P.S. & GOPINATHAN, K. 1972. Intermediary metabolism of mycobacteria. *Bacteriological reviews*, 36, 65-108.

RAMASWAMY, S.V., AMIN, A.G., GÖKSEL, S., STAGER, C.E., DOU, S.J., EL SAHLY, H., MOGHAZEH, S.L., KREISWIRTH, B.N. & MUSSER, J.M. 2000. Molecular Genetic Analysis of Nucleotide Polymorphisms Associated with Ethambutol Resistance in Human Isolates of Mycobacterium tuberculosis. *Antimicrobial agents and chemotherapy*, 44, 326-336.

RAMESH, C., HARIPRASAD, M., RAGUNATHAN, V. & JAYAKUMAR, N. 2012. A novel route for synthesis and characterization of green Cu2O/PVA nano composites. *European Journal of Applied Engineering and Scientific Research*, 1, 201-206.

RAMEZANI, M., ABNOUS, K. & TAGHDISI, S.M. 2017. Optical and Electrochemical Aptasensors for Sensitive Detection of Streptomycin in Blood Serum and Milk. In: PRICKRIL, B. & RASOOLY, A. (eds.) *Biosensors and Biodetection*: *Methods and Protocols*, Volume 2: *Electrochemical*, *Bioelectronic*, Piezoelectric, Cellular and Molecular Biosensors. New York, NY: *Springer* New York.

RAO, N.S. & RAO, M.V.B. 2015. Structural and Optical Investigation of ZnO Nanopowders Synthesized from Zinc Chloride and Zinc Nitrate. *American Journal of Materials Science*, 5, 66-68.

RASTGAR, S. & SHAHROKHIAN, S. 2014. Nickel hydroxide nanoparticles-reduced graphene oxide nanosheets film: layer-by-layer electrochemical preparation, characterization and rifampicin sensory application. *Talanta*, 119, 156-163.

RAVIGLIONE, M.C. & PIO, A. 2002. Evolution of WHO policies for tuberculosis control, 1948–2001. *The Lancet*, 359, 775-780.

RAZA SIDDIQUI, M., MOHAMMAD WABAIDUR, S., AL OTHMAN, Z.A., ALI, S. & ALAM, S. 2014. Kinetic spectrophotometric method for the quantitative analysis of streptomycin sulfate. *Journal of the Chilean Chemical Society*, 59, 2550-2554.

RAZMI, H. & MOHAMMAD-REZAEI, R. 2013. Graphene quantum dots as a new substrate for immobilization and direct electrochemistry of glucose oxidase: application to sensitive glucose determination. *Biosensors and Bioelectronics*, 41, 498-504.

REENA, K. & SHANTHI, V. 2013. Evolution of In vitro Drug Susceptibility Testing of Pyrazinamide. *Biosciences Biotechnology Research Asia*, 10, 803-809.

RESNIKOFF, S., PASCOLINI, D., ETYAALE, D., KOCUR, I., PARARAJASEGARAM, R., POKHAREL, G.P. & MARIOTTI, S.P. 2004. Global data on visual impairment in the year 2002. *Bulletin of the world health organization*, 82, 844-851.

REVANKAR, S., DESAI, N., VAIDYA, A., BHATT, A. & ANJANEYULU, B. 1994. Determination of pyrazinamide in human by high performance liquid chromatography. *Journal of Postgraduate Medicine*, 40, 7-9.

ROHRER, V.P.H.J.S. 2007. Determination of Streptomycin, Dihydrostreptomycin and Impurities Using Anion-Exchange Chromatography with Electrochemical Detection. *Journal Chromatography*, 2, 150-156.

RONKAINEN, N.J., HALSALL, H.B. & HEINEMAN, W.R. 2010. Electrochemical biosensors. *Chemical Society Reviews*, 39, 1747-1763.

ROTE, A.R. & SHARMA, A.K. 1997. Simultaneous spectrophotometric determination of rifampicin, isoniazid and pyrazinamide by first-derivative UV spectrophotometry in combined pharmaceutical dosage forms. *Indian journal of pharmaceutical sciences*, 59, 119-123.

ROY RESEARCH GROUP, 2017. http://people.clarkson.edu/~droy/Corrosion_EIS.htm, Accessed on 26 February 2018.

RÜDEL, U., GESCHKE, O. & CAMMANN, K. 1996. Entrapment of enzymes in electropolymers for biosensors and graphite felt based flow-through enzyme reactors. *Electroanalysis*, 8, 1135-1139.

SABITHA, P., RATNA, J.V. & REDDY, K.R. 2010. A new RP-HPLC method for the determination of isoniazid in plasma. *Drug Invention Today*, 2, 331-334.

SABR, A.K., Biosensors. *American Journal of Biomedical Engineering*, 6, 170-179, 2016.

SALFINGER, M. & HEIFETS, L.B. 1988. Determination of pyrazinamide MICs for Mycobacterium tuberculosis at different pHs by the radiometric method. *Antimicrobial agents and chemotherapy*, 32, 1002-1004.

SAMPATH, K., TERISH, J., KUMAR, S., RAMESH, N. & SASIJITH, S. 2011. Method Development and Validation of Ethambutol in Human Plasma by Using LCMS/MS. *International Journal of Pharmaceutical Bio Science*, 1, 1-6.

SATYANARAYANA, M., REDDY, K.K. & GOBI, K.V. 2014. Multiwall carbon nanotube ensembled biopolymer electrode for selective determination of isoniazid in vitro. *Analytical Methods*, 6, 3772-3778.

SAYANNA, JYOTHI, M., VEERAIAH, T., VENKATA RAMANA REDDY, C.H. 2016. Spectrophotometric determination of Ethambutol in pure and pharmaceutical forms using Triphenyl methane dyes. *International Journal of Pharmaceutical Science Research*, 7, 4191-4199.

SCARDI, V. & BONAVITA, V. 1957. A New Colorimetric Method for the Determination of Isoniazid in Biologic Fluids. *Clinical chemistry*, 3, 728-731.

SCHOLZ, F. 2011. The anfractuous pathways which led to the development of electrochemical stripping techniques. *Journal of Solid State Electrochemistry*, 15, 1509-1521.

SCHULTZ, B.E. & CHAN, S.I. 2001. Structures and proton-pumping strategies of mitochondrial respiratory enzymes. *Annual review of biophysics and biomolecular structure*, 30, 23-65.

SEIFART, H.I., GENT, W.L., PARKIN, D.P., VAN JAARSVELD, P.P. & DONALD, P.R. 1995. High-performance liquid chromatographic determination of isoniazid, acetylisoniazid and hydrazine in biological fluids. *Journal of Chromatography B: Biomedical Sciences and Applications*, 674, 269-275.

SENSI, P. 1983. History of the development of rifampin. *Review of Infectious Diseases*, 5, 402-406.

SHAH, J. & WILKINS, E. 2003. Electrochemical biosensors for detection of biological warfare agents. *Electroanalysis*, 15, 157-167.

SHAH, U., PATEL, S., RAVAL, M. & DESAI, P. 2015. Chemometric assisted spectrophotometric methods for the simultaneous determination of Rifampicin and

Piperine in bulk and capsule. chemistry, *Indian Journal of Pharmaceutical Education and Research*, 49, 200-207.

SHAH, Y., KHANNA, S., JINDAL, K. & DIGHE, V. 1992. Determination of rifampicin and isoniazid in pharmaceutical formulations by HPLC. *Drug development and industrial pharmacy*, 18, 1589-1596.

SHAHROKHIAN, S. & ASADIAN, E. 2010. Simultaneous voltammetric determination of ascorbic acid, acetaminophen and isoniazid using thionine immobilized multi-walled carbon nanotube modified carbon paste electrode. *Electrochimica Acta*, 55, 666-672.

SHAHROKHIAN, S. & AMIRI, M. 2007. Multi-walled carbon nanotube paste electrode for selective voltammetric detection of isoniazid. *Microchimica Acta*, 157, 149-158.

SHALABY, T.I., FIKRT, N., MOHAMED, M. & EL KADY, M. 2014. Preparation and characterization of iron oxide nanoparticles coated with chitosan for removal of Cd(II) and Cr(VI) from aqueous solution. *Water Science and Technology*, 70, 1004-1010.

SHAO, C., WEI, Y., LI, S. & LI, C. 2008. Determination of ethambutol at glassy carbon electrode modified with multiwall carbon nanotubes. *Chemia analityczna*, 53, 511-521.

SHARMA, S., RAHMANA, N., AZMI, H. & NAJMUL, S. 2011. Spectrophotometric determination of U (VI) with rifampicin in soil samples. *Journal of the Chinese Chemical Society*, 58, 127-135.

SHERIGARA, B.S., KUTNER, W. & DSOUZA, F. 2003. Electrocatalytic properties and sensor applications of fullerenes and carbon nanotubes. *Electroanalysis*, 15, 753-772.

SHETTY, D.N., NARAYANA, B. & SAMSHUDDIN, S. 2012. Novel Reagents for the Spectrophotometric Determination of Isoniazid. *ISRN Spectroscopy*, 2012, 1-5.

SHEWIYO, D.H., KAALE, E., RISHA, P.G., DEJAEGHER, B., SMEYERS-VERBEKE, J. & VANDER HEYDEN, Y. 2012. Optimization of a reversed-phase-high-performance thin-layer chromatography method for the separation of isoniazid, ethambutol, rifampicin and pyrazinamide in fixed-dose combination antituberculosis tablets. *Journal of Chromatography A*, 1260, 232-238.

SHI, R., ITAGAKI, N. & SUGAWARA, I. 2007. Overview of anti-tuberculosis (TB) drugs and their resistance mechanisms. *Mini reviews in medicinal chemistry*, 7, 1177-1185.

SHI, W., ZHANG, X., JIANG, X., YUAN, H., LEE, J.S., BARRY RD, C.E., WANG, H., ZHANG, W. & ZHANG, Y. 2011. Pyrazinamide inhibits trans-translation in *mycobacterium tuberculosis*. *Science*, 333, 1630-1632.

SIDDHARTHA, T.S., PRASANTHI, B., SANTOSH, T. & RATNA, J.V. 2012. Development and validation of high performance liquid chromatographic method for the determination of rifampicin in human plasma. *International Journal of Pharma Pharmaceutical Sciences*, 4, 3621-3367.

SIDWABA, U., AJAYI, R.F., FELENI, U., DOUMAN, S., BAKER, P.G.L., VILAKAZI, S.L., TSHIKHUDO, R. & IWUOHA, E.I. 2014. Polyanilino-Carbon Nanotubes

derivatised cytochrome P450 2E1 Nanobiosensor for the determination of pyrazinamide Anti-tuberculosis drugs. *Nano Hybrids, Trans Tech Publ*, 59-73.

SILVA, V., ANDRADE, P., SILVA, M., VALLADARES, L.D.L.S. & AGUIAR, J.A. 2013. Synthesis and characterization of Fe_3O_4 nanoparticles coated with fucan polysaccharides. *Journal of Magnetism and Magnetic Materials*, 343, 138-143.

SIMIONI, N.B., SILVA, T.A., OLIVEIRA, G.G. & FATIBELLO-FILHO, O. 2017. A nanodiamond-based electrochemical sensor for the determination of pyrazinamide antibiotic. *Sensors and Actuators B: Chemical*, 250, 315-323.

SISTANI, P., SOFIMARYO, L., MASOUDI, Z. R., SAYAD, A., RAHIMZADEH, R. & SALEHI, B. 2014. A penicillin biosensor by using silver nanoparticles. *International Journal of Electrochemical Science*, 9, 6201-6212.

SIVARAM, V., HEMANTHKUMAR, A. & RAMACHANDRAN, G. 2015. UHPLC/MS method for the estimation of ethambutol in human plasma and its application in tuberculosis patients. *Asian Journal of Biomedical and Pharmaceutical Sciences*, 5, 1-6.

SMITH, P., VAN DYK, J. & FREDERICKS, A. 1999. Determination of rifampicin, isoniazid and pyrazinamide by high performance liquid chromatography after their simultaneous extraction from plasma. *The International Journal of Tuberculosis and Lung Disease*, 3, 325-328.

SONG, S. H., JUN, S.H., PARK, K.U., YOON, Y., LEE, J.H., KIM, J.Q. & SONG, J. 2007. Simultaneous determination of first-line anti-tuberculosis drugs and their major

metabolic ratios by liquid chromatography/tandem mass spectrometry. *Rapid Commun Mass Spectrom*, 21, 1331-1338.

SONG, P., FISHER, A. C., WADHAWAN, J. D., COOPER, J. J., WARD, H. J. & LAWRENCE, N. S. 2016. A mechanistic study of the EC′ mechanism–the split wave in cyclic voltammetry and square wave voltammetry. *RSC Advances*, 6 (74), 70237-70242.

SPIES, F. S., DA SILVA, P.E.A., RIBEIRO, M.O., ROSSETTI, M.L. & ZAHA, A. 2008. Identification of mutations related to streptomycin resistance in clinical isolates of Mycobacterium tuberculosis and possible involvement of efflux mechanism. *Antimicrobial agents and chemotherapy*, 52, 2947-2949.

STATS, S. 2014. Poverty trends in South Africa: An examination of absolute poverty between 2006 and 2011. Pretoria: Statistics South Africa.

STETS, S., TAVARES, T.M., PERALTA-ZAMORA, P.G., PESSOA, C.A. & NAGATA, N. 2013. Simultaneous Determination of Rifampicin and Isoniazid in Urine and Pharmaceutical Formulations by Multivariate Visible Spectrophotometry. *Journal of the Brazilian Chemical Society*, 24, 1198 - 1205.

STIRLING, M., REES, H., KASEDDE, S. & HANKINS, C. 2008. Introduction: Addressing the vulnerability of young women and girls to stop the HIV epidemic in southern Africa. *Aids*, 22, 1-3.

STREETER, I., WILDGOOSE, G.G., SHAO, L. & COMPTON, R.G. 2008. Cyclic voltammetry on electrode surfaces covered with porous layers: an analysis of electron transfer

kinetics at single-walled carbon nanotube modified electrodes. *Sensors and Actuators B: Chemical*, 133, 462-466.

STRUSHKEVICH, N., MACKENZIE, F., CHERKESOVA, T., GRABOVEC, I., USANOV, S. & PARK, H.W. 2011. Structural basis for pregnenolone biosynthesis by the mitochondrial monooxygenase system. *Proceedings of the National Academy of Sciences*, 108, 10139-10143.

STURKENBOOM, M., VAN DER LIJKE, H., JONGEDIJK, E., KOK, W.T., GREIJDANUS, B., UGES, D. & ALFFENAAR, J.W.C. 2015a. Quantification of isoniazid, pyrazinamide and ethambutol in serum using liquid chromatography-tandem mass spectrometry. *Journal of Applied Bionalysis*, 1, 89-98.

SUAREZ, J., RANGUELOVA, K., JARZECKI, A.A., MANZEROVA, J., KRYMOV, V., ZHAO, X., YU, S., METLITSKY, L., GERFEN, G.J. & MAGLIOZZO, R.S. 2009. An oxyferrous heme/protein-based radical intermediate is catalytically competent in the catalase reaction of Mycobacterium tuberculosis catalase-peroxidase (KatG). *Journal of Biological Chemistry*, 284, 7017-7029.

SUZUKI, M., ONO, T. & TAKITANI, S. 1991. Determination of ethambutol in plasma by high-performance liquid chromatography with fluorescence detection. *Analytical sciences*, 7, 949-950.

SVANCARA, I., PRIOR, C., HOCEVAR, S.B. & WANG, J. 2010. A decade with bismuth-based electrodes in electroanalysis. *Electroanalysis*, 22, 1405-1420.

SWAMY, N., PRASHANTH, K.N. & BASAVAIAH, K. 2014. Redox-Reaction Based Spectrophotometric Assay of Isoniazid in Pharmaceuticals. *ISRN Analytical Chemistry*, 2014, 1-11.

SWART, K. & PAPGIS, M. 1992. Automated high-performance liquid chromatographic method for the determination of rifampicin in plasma. *Journal of Chromatography A*, 593, 21-24.

SYAL, K., SRINIVASAN, A. & BANERJEE, D. 2013. Streptomycin interference in Jaffe reaction possible false positive creatinine estimation in excessive dose exposure. *Clinical biochemistry*, 46, 177-179.

SZLOSARCZYK, M., PIECH, R., BATOR, B., MASLANKA, A., OPOKA, W. & KRZEK, J. 2012. Voltammetric determination of isoniazid using cyclic renewable mercury film silver based electrode. *Pharmaceutica Analytica Acta*, 3, 1-5.

TABAK, D. 1988. Determination of ethambutol hydrochloride in air by using fluoropore® filter sampling and a derivatization-gas chromatographic procedure. *American Industrial Hygiene Association Journal*, 49, 620-623.

TAFANI, M., KARPINICH, N.O., HURSTER, K.A., PASTORINO, J.G., SCHNEIDER, T., RUSSO, M.A. & FARBER, J.L. 2002. Cytochrome c release upon Fas receptor activation depends on translocation of full-length bid and the induction of the mitochondrial permeability transition. *Journal of Biological Chemistry*, 277, 10073-10082.

TALAM, S., KARUMURI, S.R. & GUNNAM, N. 2012. Synthesis, characterization, and spectroscopic properties of ZnO nanoparticles. *ISRN Nanotechnology*, 2012, 1-12.

TATARCZAK, M., FLIEGER, J. & SZUMILO, H. 2005. High-Performance Liquid-Chromatographic Determination of Rifampicin in Complex Pharmaceutical Preparation and In Serum Mycobacterium Tuberculosis-Infected Patients. *Acta Poloniae Pharmaceutica-Drug Research*, 62, 251-256.

TAUNK, P., DAS, R., BISEN, D. & KUMAR TAMRAKAR, R. 2015. Structural characterization and photoluminescence properties of zinc oxide nano particles synthesized by chemical route method. *Journal of Radiation Research and Applied Sciences*, 8, 433-438.

THAMAPHAT, K., LIMSUWAN, P. & NGOTAWORNCHAI, B. 2008. Phase characterization of TiO_2 powder by XRD and TEM. *Kasetsart Journal of National Science*, 42, 357-361.

TILINCA, M., HANCU, G., MIRCIA, E., IRIMINESCU, D., RUSU, A., VLAD, R.A. & BARABAS, E. 2017. Simultaneous determination of isoniazid and rifampicin by uv pectrophotometry. *Farmacia*, 65, 219-224.

TIMMINS, G.S. & DERETIC, V. 2006. Mechanisms of action of isoniazid. *Molecular Microbiology*, 62, 1220-1227.

TIMMINS, G.S., MASTER, S., RUSNAK, F. & DERETIC, V. 2004. Nitric oxide generated from isoniazid activation by KatG: source of nitric oxide and activity against

Mycobacterium tuberculosis. Antimicrobial agents and chemotherapy, 48, 3006-3009.

TOBALINA, F., PARIENTE, F., HERNANDEZ, L., ABRUNA, H. & LORENZO, E. 1999. Integrated ethanol biosensors based on carbon paste electrodes modified with [Re (phen-dione) $(CO)_3Cl$] and [Fe(phen-dione)$_3$]$(PF_6)_2$. *Analytica chimica acta*, 395, 17-26.

TZENG, C.W.D., CAO, H.S.T., LEE, J.E., PISTERS, P.W., VARADHACHARY, G.R., WOLFF, R.A., ABBRUZZESE, J.L., CRANE, C.H., EVANS, D.B. & WANG, H. 2014. Treatment sequencing for resectable pancreatic cancer: influence of early metastases and surgical complications on multimodality therapy completion and survival. *Journal of gastrointestinal surgery*, 18, 16-25.

UMAPATHI, P., AYYAPPAN, J. & QUINE, D. 2010. Reverse Phase High Pressure Liquid Chromatographic Determination of Rifampin Quinone and Hydrazone in Anti-Tuberculosis Fixed-Dose Formulations Containing Sodium Ascorbate as Anti-oxidant. *Tropical Journal of Pharmaceutical Research*, 9, 587-593.

UNRUH, K., CHIEN, C. & EDELSTEIN, A. 1996. Nanomaterials: Synthesis, Properties and Applications. *Institute of Physics Publishing Bristol*: *Magnetic and electron transport properties of granular films*, 374-380.

UNIVERSITY OF CAMBRIDGE, 2017 Department of Chemical Engineering and Biotechnology, https://www.ceb.cam.ac.uk/research/groups/rg-eme/teaching-notes/hydrodynamic-voltammetry, Accessed on 26 February 2018.

VEITCH, N.C. 2004. Horseradish peroxidase: a modern view of a classic enzyme. *Phytochemistry*, 65, 249-259.

VERMA, M., SINGH, M., KAKKAR, V. & KAUR, I. 2012. Applicability of a colorimetric method for evaluating streptomycin sulphate loaded solid lipid nanoparticle. *International Journal of pharma and pharmacetical Science*, 4, 50-53.

VITORIA, M., GRANICH, R., GILKS, C. F., GUNNEBERG, C., HOSSEINI, M., WERE, W., RAVIGLIONE, M. & DE COCK, K. M. 2009. The global fight against HIV/AIDS, tuberculosis, and malaria: current status and future perspectives. *American journal of clinical pathology*, 131, 844-848.

WALASH, M., BELAL, F., METWALLY, M. & HEFNAWY, M.M. 1993. Spectrophotometric determination of rifampin in the presence of its degradation products in pharmaceutical preparations. *Analytical letters*, 26, 1905-1917.

WANG, J. & MAHMOUD, J.S. 1986. Determination of traces of streptomycin and related antibiotics by adsorptive stripping voltammetry. *Analytica Chimica Acta*, 186, 31-38.

WANG, J. 2002. Real-time electrochemical monitoring: toward green analytical chemistry. *Accounts of chemical research*, 35, 811-816.

WANG, J., ZHANG, H., SHENG, W., LIU, W., ZHENG, L., ZHANG, X. & WANG, S. 2013. Determination of streptomycin residues in animal-derived foods by a reliable and accurate enzyme-linked immunosorbent assay. *Analytical Methods*, 5, 4430-4435.

WANG, W., WANG, L., ZOU, L., LI, G. & YE, B. 2016. Electrochemical behavior of arctigenin at a novel voltammetric sensor based on Iodide/SWCNTs composite film modified

electrode and its sensitive determination. *Journal of Electroanalytical Chemistry*, 772, 17-26.

WEHRLI, W. 1983. Rifampin: mechanisms of action and resistance. *Review of Infectious Diseases*, 5, 407-411.

WEI, L., BAOXIN, L. & ZHUJUN, Z. 2002. A Chemiluminescence Method for the Determination of Rifampicin. *Chinese Journal of Analytical Chemistry*, 1, 22-26.

WEI, X.N., WANG, H.L., LI, Z.D., HUANG, Z.Q., QI, H.P. & JIANG, W.F. 2016. Fabrication of the novel core-shell MCM-41@mTiO_2 composite microspheres with large specific surface area for enhanced photocatalytic degradation of dinitro butyl phenol (DNBP). *Applied Surface Science*, 372, 108-115.

WEN, X.R. & TU, C.Q. 2014. Spectrophotometric Determination of Isoniazid in Pharmaceutical Sample by Silicomolybdenum Blue. *Advanced Materials Research, Trans Tech Publ*, 548-551.

WEN, Y., LIAO, X., DENG, C., LIU, G., YAN, Q., LI, L. & WANG, X. 2017. Imprinted voltammetric streptomycin sensor based on a glassy carbon electrode modified with electropolymerized poly(pyrrole-3-carboxy acid) and electrochemically reduced graphene oxide. *Microchimica Acta*, 184, 935-941.

WHALL, T. 1981. Determination of streptomycin sulfate and dihydrostreptomycin sulfate by high-performance liquid chromatography. *Journal of Chromatography A*, 219, 89-100.

WOLF, D.E., HOFFMAN, C.H., TRENNER, N.R., ARISON, B.H., SHUNK, C.H., LINN, B. O., MCPHERSON, J.F. & FOLKERS, K. 1958. Coenzyme QI Structure studies on the coenzyme Q group. *Journal of the American Chemical Society*, 80, 4751-4752.

WU, J.W., SHIH, H.H., WANG, S.C. & TSAI, T.H. 2004. Determination and pharmacokinetic profile of pyrazinamide in rat blood, brain and bile using microdialysis coupled with high-performance liquid chromatography and verified by tandem mass spectrometry. *Analytica Chimica Acta*, 522, 231-239.

WU, W.Y., YANG, J.Y., DU, L.M., WU, H. & LI, C.F. 2011. Determination of ethambutol by a sensitive fluorescent probe. *Spectrochimica Acta Part A: Molecular and Biomolecular Spectroscopy*, 79, 418-422.

XIAO, L., WILDGOOSE, G.G. & COMPTON, R.G. 2009. Exploring the origins of the apparent "electrocatalysis" observed at C 60 film-modified electrodes. *Sensors and Actuators B: Chemical*, 138, 524-531.

XIAOMENG, S., GUANGXIN, Y., LIHUA, Z., JINGBO, S., HONGYU, L. & XUEBING, J. 2011. Determination of isoniazid and isonicotinic acid contents in tablets by HPLC. Human Health and Biomedical Engineering (HHBE), 2011 *International Conference on, 2011. IEEE*, 324-327.

YAACOB, M. H., ZAINUDIN, N. & MUSLIM, N.Z.M. 2014. Cathodic Stripping Voltammetry (CSV) Analysis of Reactive Black 5 (RB5) Dye Using Hanging Mercury Electrode (HMDE) in Basic Medium from Sources to Solution. *Springer*, 33-36.

YAGHI, O.M., LI, H., DAVIS, C., RICHARDSON, D. & GROY, T.L. 1998. Synthetic strategies, structure patterns, and emerging properties in the chemistry of modular porous solids. *Accounts of Chemical Research*, 31, 474-484.

YAN, H., XIAO, H., XIE, Q., LIU, J., SUN, L., ZHOU, Y., ZHANG, Y., CHAO, L., CHEN, C. & YAO, S. 2015. Simultaneous electroanalysis of isoniazid and uric acid at poly (sulfosalicylic acid)/electro reduced carboxylated graphene modified glassy carbon electrode. *Sensors and Actuators B: Chemical*, 207, 167-176.

YAN, L., LI, S., YU, H., SHAN, R., DU, B. & LIU, T. 2016. Facile solvothermal synthesis of Fe_3O_4/bentonite for efficient removal of heavy metals from aqueous solution. *Powder Technology*, 301, 632-640.

YAN, M., GUO, T., SONG, H., ZHAO, Q. & SUI, Y. 2007. Determination of ethambutol hydrochloride in the combination tablets by precolumn derivatization. *Journal of chromatographic science*, 45, 269-272.

YAN, X., BO, X. & GUO, L. 2011. Electrochemical behaviors and determination of isoniazid at ordered mesoporous carbon modified electrode. *Sensors and Actuators B: Chemical*, 155, 837-842.

YANG, G., WANG, C., ZHANG, R., WANG, C., QU, Q. & HU, X. 2008. Poly (amidosulfonic acid) modified glassy carbon electrode for determination of isoniazid in pharmaceuticals. *Bioelectrochemistry*, 73, 37-42.

YAO, S., LI, W., SU, X., ZUO, X. & WEI, W. 1999. A sensitive and specific method for isoniazid determination based on selective adsorption using an isoniazid ion-selective piezoelectric sensor. *Talanta*, 50, 469-480.

YEAGER, R., MUNROE, W. & DESSAU, F.I. 1952. Pyrazinamide (aldinamide) in the treatment of pulmonary tuberculosis. *American Review of Tuberculosis and Pulmonary Diseases*, 65, 523-546.

YIN, J., GUO, W., QIN, X., PEI, M., WANG, L. & DING, F. 2016. A regular "signal attenuation" electrochemical aptasensor for highly sensitive detection of streptomycin. *New Journal of Chemistry*, 40, 9711-9718.

YOLA, M.L., GUPTA, V. K., EREN, T., SEN, A.E. & ATAR, N. 2014. A novel electro analytical nano sensor based on graphene oxide/silver nanoparticles for simultaneous determination of quercetin and morin. *Electrochimica Acta*, 120, 204-211.

YOU, T., NIU, L., GUI, J.Y., DONG, S. & WANG, E. 1999. Detection of hydrazine, methylhydrazine and isoniazid by capillary electrophoresis with a 4-pyridyl hydroquinone self-assembled micro disk platinum electrode. *Journal of pharmaceutical and biomedical analysis*, 19, 231-237.

YU, M.F., LOURIE, O., DYER, M.J., MOLONI, K., KELLY, T.F. & RUOFF, R.S. 2000. Strength and breaking mechanism of multiwalled carbon nanotubes under tensile load. *Science*, 287, 637-640.

YUN XIA, H. & YA HU, X. 2005. Determination of isoniazid using a gold electrode by differential pulse voltammetry. *Analytical letters*, 38, 1405-1414.

ZAK, A.K., MAJID, W.A., DARROUDI, M. & YOUSEFI, R. 2011. Synthesis and characterization of ZnO nanoparticles prepared in gelatin media. *Materials Letters*, 65, 70-73.

ZHANG, H. & FENG, P.X. 2010. Fabrication and characterization of few-layer graphene. *Carbon*, 48, 359-364.

ZHANG, Y., SCORPIO, A., NIKAIDO, H. & SUN, Z. 1999. Role of acid pH and deficient efflux of pyrazinoic acid in unique susceptibility of Mycobacterium tuberculosis to pyrazinamide. *Journal of Bacteriology*, 181, 2044-2049.

ZHAO, H.Z., DU, Q., LI, Z.S. & YANG, Q.Z. 2012. Mechanisms for the direct electron transfer of cytochrome c induced by multi-walled carbon nanotubes. *Sensors*, 12, 10450-10462.

ZHAO, Y., WANG, Z.B. & XU, J.X. 2003. Effect of Cytochrome c on the Generation and Elimination of O and H2O2 in Mitochondria. *Journal of Biological Chemistry*, 278, 2356-2360.

ZHENG, X., ZHIHUI, G. & ZHANG, Z. 2001. Flow-injection electrogenerated chemiluminescence determination of isoniazid using luminol. *Analytical sciences*, 17, 1095-1099.

ZHIFENG, Z., LINGYUN, C., PENG, L., MEI, S. & FEI, Z. 2010. Simultaneous determination of isoniazid, pyrazinamide, rifampicin and acetylisoniazid in human plasma by high-performance liquid chromatography. *Analytical Sciences*, 26, 1133-1138.

ZHOU, W.H., LU, C.H., GUO, X.C., CHEN, F.R., YANG, H.H. & WANG, X.R. 2010. Mussel-inspired molecularly imprinted polymer coating superparamagnetic nanoparticles for protein recognition. *Journal of Materials Chemistry*, 20, 880-883.

ZHU, X., XU, J., DUAN, X., LU, L., ZHANG, K., YU, Y., XING, H., GAO, Y., DONG, L., SUN, H. & YANG, T. 2015. Controlled synthesis of partially reduced graphene oxide: Enhance electrochemical determination of isoniazid with high sensitivity and stability. *Journal of Electroanalytical Chemistry*, 757, 183-191.

ZIMHONY, O., COX, J.S., WELCH, J.T., VILCHEZE, C. & JACOBS, W.R. 2000. Pyrazinamide inhibits the eukaryotic-like fatty acid synthetase I (FASI) of Mycobacterium tuberculosis. *Nature medicine*, 6, 1043-1047.

ZOSIWE, M.S.E. 2015. Cytochrome P450 2E1/Nickel-Poly (propylene imine) dendrimeric nanobiosensor for pyrazinamide-A first line TB Drug, 1-99.

ZUMLA, A.I., GILLESPIE, S.H., HOELSCHER, M., PHILIPS, P.P., COLE, S.T., ABUBAKAR, I., MCHUGH, T.D., SCHITO, M., MAEURER, M. & NUNN, A.J. 2014. New antituberculosis drugs, regimens, and adjunct therapies: needs, advances, and future prospects. *The Lancet Infectious Diseases*, 14, 327-340.

ZUMLA, A., GEORGE, A., SHARMA, V., HERBERT, R. H. N., OXLEY, A. & OLIVER, M. 2015. The WHO 2014 global tuberculosis report further to go. *The Lancet Global Health*, 3, 10-12.

APPENDICES

Definitions

Accuracy:

The degree to which the result of a measurement, calculation or specification conforms to the standard value.

Bias:

The change between the expectation of the test results and a known reference value.

Calibration curve:

In analytical chemistry, a calibration curve, also identified as a standard curve, is a common technique for determining the concentration of an analyte in an unknown sample by relating the unknown to a set of standard samples of known concentration.

Interference:

An interference is a substance, other than the assayed quantifiable, that can be measured by the chosen analytical method or that can prevent the assayed material from being measured.

Limit of detection:

The final content that can be measured with reasonable statistical certainty.

Limit of quantitation:

The content equal to or greater than the lowest concentration point on the calibration curve.

Precision:

The familiarity of agreement amid independent test results obtained under stipulated conditions.

Sensitivity:

The change in the response of a measuring instrument divided by the corresponding change the stimulus.

Appendix 1: Definitions

Specificity or selectivity:

The ability of a method to measure only what it is intended to measure.

Stability:

Ability of a material to persist unchanged a period of time under the expected conditions of storage and use.

Recovery:

Yield of a preconcentration or extraction for an analyte divided by the amount of analyte initially present in the original sample.

Repeatability:

Precision under repeatability situations, i.e. conditions where independent test results are found with the same technique on identical test items in the same laboratory by the same operator using the same equipment within short intervals of time.

Reproducibility:

Precision under reproducibility conditions, i.e. conditions where test results are attained with the same technique on identical test items in various laboratories with different operators using different equipment.

Relative standard deviation:

Relative standard deviation is a quantity of precision in data analysis. Relative standard deviation is measured by dividing the standard deviation of a series of values by the average of the values.

Reproducibility standard deviation:

The standard deviation of test results obtained under reproducibility conditions

Robustness:

The robustness of an analytical procedure is a measure of its capacity to remain unaffected by small, but considered variations in technique parameters and offers an indication of its reliability during normal usage.

Validation:

Confirmation by examination and provision of objective evidence that the specific requirements for a definite intended use are fulfilled.

biosensors

MDPI

Article

An Enzyme-Induced Novel Biosensor for the Sensitive Electrochemical Determination of Isoniazid

Rajasekhar Chokkareddy, Natesh Kumar Bhajanthri * and Gan G. Redhi *

Electroanalytical Laboratory, Department of Chemistry, Durban University of Technology, Durban 4000, South Africa; chokkareddys@gmail.com

* Correspondence: nateshkumar786@gmail.com (N.K.B.); redhigg@dut.ac.za (G.G.R.); Tel.: +27-31-373-3004 (N.K.B); +27-31-373-2936 (G.G.R); Fax: +27-866-740-243 (G.G.R.)

Academic Editor: Jeff D. Newman
Received: 3 March 2017; Accepted: 27 May 2017; Published: 5 June 2017

Abstract: In this present work, a glassy carbon electrode (GCE) was modified primarily with multiwalled carbon nanotubes (MWCNTs) and a composite of MWCNTs and titanium oxide nanoparticles (TiO_2NPs). The enzyme horseradish peroxidase (HRP) was immobilized to enhance the sensing ability of GCE. The proposed biosensor was used for the sensitive determination of isoniazid (INZ) in various pharmaceutical samples. The electrochemical behaviour of the developed MWCNT-TiO_2NPs-HRP-GCE biosensor was studied by using cyclic voltammetry (CV) and differential pulse voltammetric (DPV) techniques. Fourier transform infrared spectroscopy (FT-IR), X-ray diffraction (XRD), thermogravimetry (TGA) and transmission electron microscopy (TEM) techniques were used to characterize the developed sensor. Phosphate buffer solution (PBS) with pH 7 was used as supporting electrolyte in the present investigation. The cyclic voltammetric results revealed that the increment of anodic peak currents for the enzyme-induced sensor was almost 8-fold greater than that of a bare GCE. The DPV technique exhibited good limit of detection and limit of quantification values, viz., 0.0335 μM and 0.1118 μM, respectively. Moreover, the developed sensor showed long-lasting stability and repeatability without any interferents. This strongly indicates that the fabricated sensor shows outstanding electrochemical performance towards INZ, with excellent selectivity and sensitivity. The developed sensor was successfully applied to pharmaceutical samples and gave good percentages of recoveries.

Keywords: enzyme-based biosensor; isoniazid; cyclic voltammetry; differential pulse voltammetry; pharmaceutical samples

1. Introduction

Pyridine-4-carboxylic acid hydrazide (INZ) is commonly used in chemotherapy for pulmonary tuberculosis along with pyrazinamide, rifampicin and ethambutol [1]. However, regular overdoses of INZ cause hepatotoxicity and may lead to death [2]. The World Health Organization (WHO) suggested that a daily dose of INZ per adult should be 4–6 mg/kg of their body weight [3]. INZ possesses both bacteriostatic and bactericidal action to interfere with the metabolism of nucleic acids, bacterial proteins, carbohydrates, and lipids. Hence, INZ plays a vital role in the therapeutic treatment of tuberculosis disease. Therefore, there is scope to develop a simple, rapid and robust method for the sensitive determination of INZ in various pharmaceutical samples. As per previous literature reports, INZ was analysed by using high performance liquid chromatography [4], capillary electrophoresis [5], fluorimetry [6], titrimetry [7,8], chemiluminescence [9] and electrochemical methods [10]. Electrochemical methods showed superior advantages like rapid, low-cost instrumentation, less time-consuming analyses and simple sample preparation, with reduced chemical consumption [11].

In electrochemical methods, the modification electrode results in the enhanced of sensitivity of the electrode. Various types of electrode coating agents like gold and platinum core shell nanoparticles [12], thionine-immobilized multi-walled carbon nanotubes [13], mercury film silver [14], poly3,4-ethylenedioxy thiophene films [15], modified multiwalled carbon nanotubes [16], and graphene oxide poly arginine [17] have been used for the determination of INZ. However, the above mentioned methods showed a lack of fast electron-transferring ability. Hence, there is a need to search for new nanocomposites, which exhibit good sensitivity with fast electron-transferring ability for the determination of INZ. Multiwalled carbon nanotubes (MWCNTs) exhibit larger surface area and high electronic conductivity by nature, resulting in good conductivity. MWCNTs are used in various batteries, supercapacitor electronics, and sensors [18]. TiO_2NPs possess more advantageous characteristics like low cost, nontoxicity, long-term stability, and multi-functionality. Therefore, they are widely used as antiseptics, in anti-bacterial compositions, and as catalysts to promote various electrochemical reactions [19]. MWCNTs are combined with TiO_2NPs and formed as an innovative class of carbon-based functional nanomaterials with good electrical, optical and catalyst properties [20]. The enzyme horseradish peroxidase (HRP) shows greater affinity for coupling with the nanocomposite for electrochemical transduction due to the presence of amino groups in the HRP enzyme. In addition, HRP has good catalysing properties, as well as a strong oxygenation nature for oxidization of a wide variety of organic substrates [21]. Moreover, HRP immobilized with a nanocomposite results in the formation of a biosensor with high stability and good efficiency.

The present work is designed and based on the fabrication of GCE with new generation nano-structured composites like the MWCNT-TiO_2NPs-HRP composite for the sensitive determination of INZ. Furthermore, the modified sensor was applied to pharmaceutical samples to evaluate the realistic performance of the proposed sensor.

2. Experimental

2.1. Apparatus

The 797 VA Computrace (Metrohm, Herisau, Switzerland) with 1.3.1 software was used for the electrochemical investigations of INZ. A conventional three-electrode system with a glassy carbon electrode (GCE) or modified electrode was used as a working electrode, whilst a Ag/AgCl (3 M KCl) reference electrode and platinum wire were used as an auxiliary electrode. A Crison micro pH 2000 digital meter was used to prepare the supporting electrolyte. A Varian 800 Scimitar Fourier transform infrared spectroscopy (FT-IR) (SMM Instruments. Durban, South Africa) was used for the FT-IR characterization. A Transmission electron microscopy (TEM) JEM 2100 with a Lab 6 emitter (Max oxford instrument, JEOL Inc., Peabody, MA, USA) was employed for the study of surface morphology of the nanoparticles and biosensor. A Labcon 5019U ultra sonicator (Lasec, Durban, South Africa) was used for the ultrasonification of reagents. A Thermo Gravimetric Analysis (TGA) Differential Scanning Calorimetry (DSC) 1SF model 1346 (Columbus, OH, USA) with a STAR^e software version 9.20 (Mettler Toledo) instrument was used for the thermogravimetric characterization of the nanocomposite and the biosensor.

2.2. Chemicals and Reagents

All the regents used in this experiment were analytical reagent grade. Isoniazid and MWCNTs (Outer diameter (O.D).-L 6–9 nm–5 μM, catalogue number 724,769) were purchased from Sigma Aldrich (Durban, South Africa). The MWCNTs were prepared using chemical vapour deposition with cobalt, and molybdenum as a catalyst. Sodium dihydrogen orthophosphate, disodium hydrogen phosphate, sodium hydroxide, sulphuric acid, titanium tetra chloride, urea and N, N-dimethyl formamide (DMF) were purchased from Capital lab suppliers (Durban, South Africa). Alumina powder (3.0 μM) was purchased from Metrohm. The stock solution of 1 M INZ was prepared by dissolving the appropriate amount in a 50-mL volumetric flask. Upon serial dilution, working standard solution was also prepared.

All the working standard solutions were prepared with deionized water, and kept in a refrigerator at 4 °C to ensure stability. According to the previous literature [22] with slight modification, 25 mL of $TiCl_4$ was made up to a 100 mL volumetric flask with deionized water, in an ice cold bath. Likewise, 13 g of urea was dissolved in another 250-mL volumetric flask with deionized water. The urea solution was then slowly added to the contents of $TiCl_4$, and then subjected to heating at 110 °C on a hot plate, with a magnetic stirrer for about 30 min. After the completion of the reaction, a white colloidal solution was obtained. The colloidal solution was centrifuged at 1000 revolutions per minute with rotational centrifugal force for 15 min. After centrifugation of the product, the residue was washed repeatedly with deionized water, and then dried at 60 °C for 3–4 h. The newly formed TiO_2NPs were then stored in the refrigerator at 4 °C, for further use. A stock solution of INZ (1 M) was prepared by dissolving an appropriate amount in a 50-mL volumetric flask. Upon serial dilution, working standard solutions were made. Phosphate buffer solution (PBS) of 0.1 M with pH 7.0 was used as a supporting electrolyte throughout the experiment.

2.3. Fabrication of Nanocomposite Electrode

Prior to modification, the bare GCE was polished to a mirror-like surface with alumina slurry on a wet polished cloth and then further washed with deionized water. A total of 5 mg of MWCNTs was dissolved in 5 mL of DMF and thereafter kept for ultrasonification for about 30 min at 50 °C. The suspension was used for the modification of the GCE. Further, 10 mg of MWCNTs and 10 mg of TiO_2NPs were dissolved in 10 mL of N,N-dimethyl formamide (DMF) followed by ultrasonification for about 1 h, to form a stable black suspension of MWCNTs-TiO_2NPs. This was then used for the modification of the GCE. The MWCNT modified GCE and MWCNT-TiO_2NPs modified GCE was prepared by dropping 5 µL of MWCNT suspension onto the cleaned electrode, which was then dried at 50 °C for 10 min.

2.4. Preparation of the MWCNT-TiO_2NPs-HRP-GCE Enzyme Electrode

The HRP enzyme was immobilized on the MWCNT-TiO_2NPs nanocomposite fabricated on the surface of GCE. The MWCNT-TiO_2NPs-HRP-GCE sensor was fabricated by dropping 5 µL of the HRP solution onto the surface of the MWCNT-TiO_2NPs-GCE. The modified electrode was dried and then stored in the refrigerator at 4 °C [23].

2.5. Electrochemical Measurements with the MWCNT-TiO_2NPs-HRP-GCE

A total of 10 mL of the 0.1 M of PBS with pH 7.0 was added into the electrochemical cell in which the working electrode was immersed prior to the electrochemical measurements. The cell was purged with nitrogen gas for 5 min to remove the content of dissolved oxygen. To optimize the background current readings, several cyclic sweeps were carried out. The INZ sample was added into the electrochemical cell and stirred at 1000 rpm with a deposition time of 120 s, and equilibrating time of 5 s, and the sweeping was done at an optimum scan rate of 0.09 $V \cdot s^{-1}$ in differential pulse voltammetric (DPV) mode.

3. Results and Discussion

3.1. Characterization of the MWCNT-TiO_2NPs-HRP-GCE

The MWCNT-TiO_2NPs-HRP-GCE was characterized using FT-IR, X-ray diffraction (XRD), transmission electron microscopy (TEM), and thermogravimetry (TGA). FT-IR was performed to assess characteristic stretching variations for synthesized TiO_2NPs. Figure 1A reveals the presence of a sharp peak at 523 cm^{-1} indicating the presence of Ti-O stretching vibrations. A well-defined sharp peak appeared at 1403 cm^{-1}, indicating the Ti-O-Ti stretching vibrations. The peak at 1163 cm^{-1} is responsible for C-O stretching [24]. In addition, peaks at 3132 cm^{-1} were attributed to the presence of O-H stretching. Figure 1B shows the XRD data, with Miller indices (101,110, and 111) attributed to the

body-centred cubic, crystalline nature of the TiO_2NPs. The broad diffraction peaks are an indication of the nano-size of crystalline compound. The experimental XRD pattern agrees with the 2θ peak at 25.4° and confirms the TiO_2 anatase structure [25]. The strong diffractions at 25° and 48° were also attributed to TiO_2NPs in the anatase phase [26]. The above evidence confirmed the synthesized TiO_2NPs.

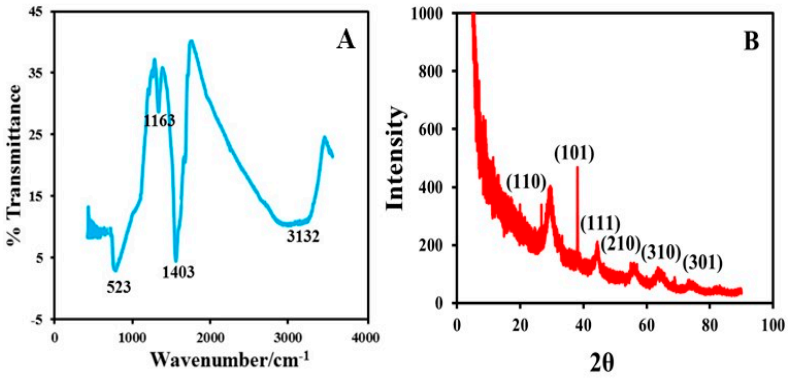

Figure 1. (**A**) Fourier transform infrared spectroscopy (FT-IR) characterization of titanium oxide nanoparticles (TiO_2NPs). (**B**) X-ray diffraction (XRD) image of TiO_2NPs.

Figure 2A is the TEM image of the TiO_2NPs, which clearly indicates the spherical shape geometry of TiO_2NPs with an average diameter of 25 nm. Figure 2B shows TEM of pure MWCNTs as having tubular network-like structure. Figure 2C clearly shows the adherence of TiO_2NPs on the surface of the MWCNTs. Figure 2D shows the thermogravimetric curves of pure MWCNTs, TiO_2NPs and MWCNTs-TiO_2NPs. The TGA curve of MWCNTs (black line in Figure 2D) exhibited definite mass loss at 570 °C, which may possibly be due to the carbon oxidation. The TGA curve of TiO_2NPs showed nearly flat characteristics with minor mass loss observed before 100 °C, and this may be due to loss of water, whereas at 400 °C this may signify loss of nitrogen content. The TGA curve of MWCNTs-TiO_2NPs also showed slight mass loss in two stages around at 100 °C and 250 °C, respectively; this may be due to the evaporation of solvent. Beyond that temperature, the composite was highly stable due to the dispersion of TiO_2NPs on the surface of MWCNTs.

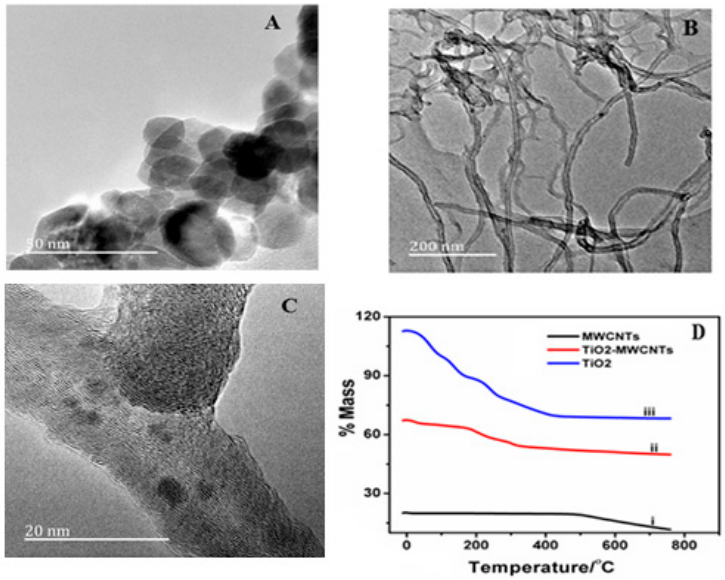

Figure 2. (**A**) Transmission electron microscopy (TEM) image of TiO_2NPs (**B**) Pure multiwalled carbon nanotubes (MWCNTs) (**C**) MWCNTs-TiO_2NPs (**D**) Thermogravimetry (TGA) curves for: (1) MWCNTs; (2) MWCNTs-TiO_2NPs; and (3) TiO_2NPs.

3.2. Method Optimization

The effect of pH played an important role in the electrochemical signal amplification of INZ. The effect of pH with peak current was studied in the range of 3.0–10.0. As the pH increases, peak currents gradually increase until pH 7, and then decrease beyond pH 7. The changes in the anodic peak currents and peak potentials responses were monitored by varying the pH (Figure 3B). According to the obtained results from Figure 3B, the anodic peak current of INZ reaches a maximum at pH 7, and decreases beyond 7. Due to this observation, a pH of 7 was selected as optimum for the entire study. In addition, the effect of deposition time was also monitored from 30 to 150 s (Figure 3C). Based on the obtained results, deposition time with 120 s was selected as optimum deposition time for the present study. Further, the most effective parameter, notably, scan rate, was examined in the range of 0.1 to 1.0 $V \cdot s^{-1}$. The obtained results showed that 0.9 $V \cdot s^{-1}$ was the optimum potential scan rate. The effect of incubation temperature was also tested with the activity of HRP immobilized on the surface of the MWCNT-TiO_2NPs-GCE. The anodic peak current response was observed with different incubated temperatures ranging from 5 to 50 °C (Figure 3D). The fabricated MWCNT-TiO_2NPs-HRP-GCE showed maximum peak currents at 30 °C. Therefore, 30 °C was selected as the optimum temperature for the successful experiment. At 5–30 °C the increase in current responses of the modified sensor was due to the increase in the activation energy of the reaction. After 30 °C, the current responses were decreased due to enzyme denaturation. The enzyme reaction rate increases as the incubation temperature increases up to an optimum temperature, and after that the enzyme activity declines rapidly. Moreover, the immobilized enzyme shows no changes in the optimum temperature when compared with free enzyme. The enzyme incubation time is also an important parameter in the method optimization, which was monitored from 5 to 25 min at room temperature, and the corresponding current responses were measured. Figure S1 showed the current responses gradually increased with sustained enzyme incubation time. The enzyme-fabricated electrode showed good peak current response at 15 min. Based on the current response and adsorption equilibrium of the enzyme, 15 min was selected as the optimum incubation time for the entire study. After 15 min the current response gradually decreased with prolonged incubation time.

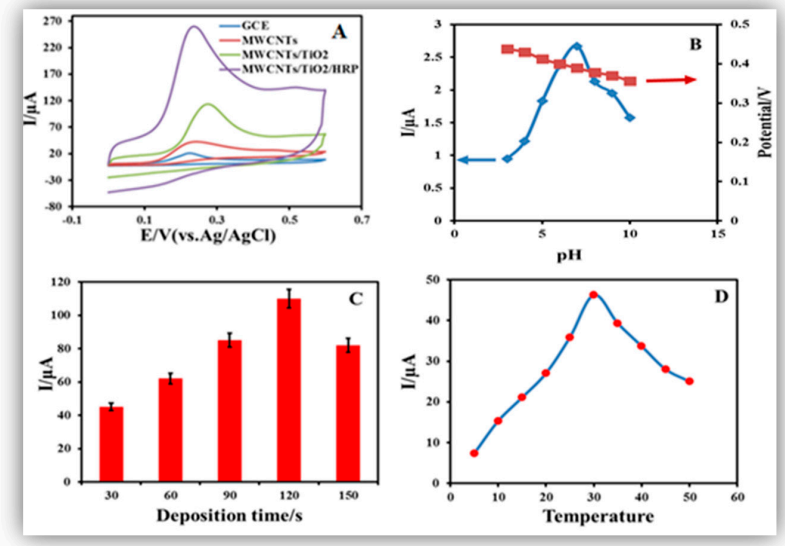

Figure 3. (**A**) Cyclic voltammograms of 0.1 mM isoniazid (INZ) with: (1) a bare glassy carbon electrode (GCE); (2) MWCNT-GCE; (3) MWCNT-TiO_2NPs-GCE; and (4) MWCNT-TiO_2NPs-horseradish peroxide (HRP)-GCE. (**B**) Peak potential and peak currents response with pH at 3.0, 4.0, 5.0, 6.0, 7.0, 8.0, 9.0 and 10.0. respectively (**C**) Peak current responses vs. different deposition times of 30, 60, 90, 120 and 150 s. (**D**) Effect of temperature on the current response of the MWCNT-TiO_2NPs-HRP-GCE.

3.3. Electrochemical Behavior of INZ on the MWCNT-TiO_2NPs-HRP-GCE

The MWCNT-TiO_2NPs-HRP-GCE was electrochemically analysed by CV and DPV techniques. The modified electrode surface area calculation was justified by using the Randles–Sevick [27] Equation (1).

$$i_{pa} = 2.69 \times 10^5 A C_0 n^{3/2} {D_R}^{1/2} v^{1/2} \quad (1)$$

where i_{pa} is the anodic peak current, A is the surface area of the electrode, C_0 is the concentration of INZ, n is the number of electrons transferred, D_R is the diffusion coefficient, and V is the scan rate. Based on Equation (1), the MWCNT-TiO_2NPs-HRP-GCE and GCE surface areas were calculated and found to be 19.32 and 3.14 mm^2, respectively. This indicated that the MWCNT-TiO_2NPs-HRP-GCE sensor was exhibiting approximately a six times larger surface area than the GCE. This implies that the fabricated sensor provides a high surface area for INZ to undergo electrochemical oxidation [28] (Scheme 1).

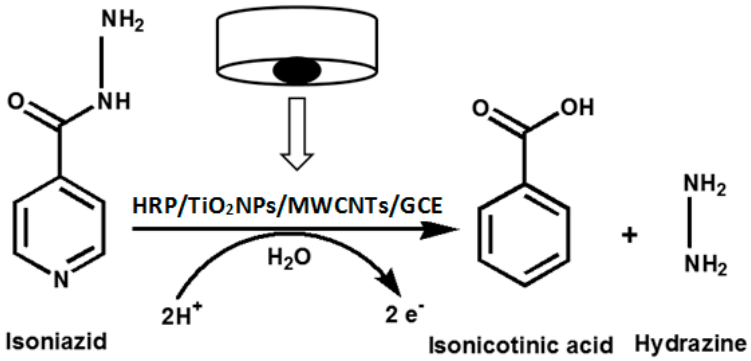

Scheme 1. Electrochemical oxidation mechanism of INZ with the MWCNT-TiO_2NPs-HRP-GCE.

The electrochemical sensing ability of the MWCNT-TiO_2NPs-HRP-GCE was compared with the bare GCE, MWCNTs and MWCNTs-TiO_2NPs (Figure 3A). The potentials scale was monitored in the range of −0.1 to +0.7 V for the appearance of anodic peak. The GCE exhibited a much lower current of 25 µA, while the MWCNT-GCE and MWCNT-TiO_2NPs-GCE showed moderate current responses of 56 µA and 110 µA, respectively (Figure S2). The final MWCNT-TiO_2NPs-HRP-GCE showed much greater peak current responses with 200 µA (Figure 4A). Figure 4B shows the linear relationship between log i_{pa} and log v, and it is suggested the diffusion of INZ at the surface of the MWCNT-TiO_2NPs-HRP-GCE can be expressed by the following Equation (2).

$$\log\ i_{pa} = 0.7841\ \log\ v + 1.5351 \quad (2)$$

Figure 4C shows that the oxidation of INZ at the MWCNTs-TiO_2NPs-HRP-GCE is similar to the diffusion-controlled process owing to the linear relationship between anodic peak current and the square root of the scan rate. The fitted regression line can be expressed as i_{pa} = 0.2642 $v^{1/2}$ + 0.2891; R^2 = 0.9822. This clearly indicates the outstanding performance of the MWCNT-TiO_2NPs-HRP-GCE compared to the other three electrodes.

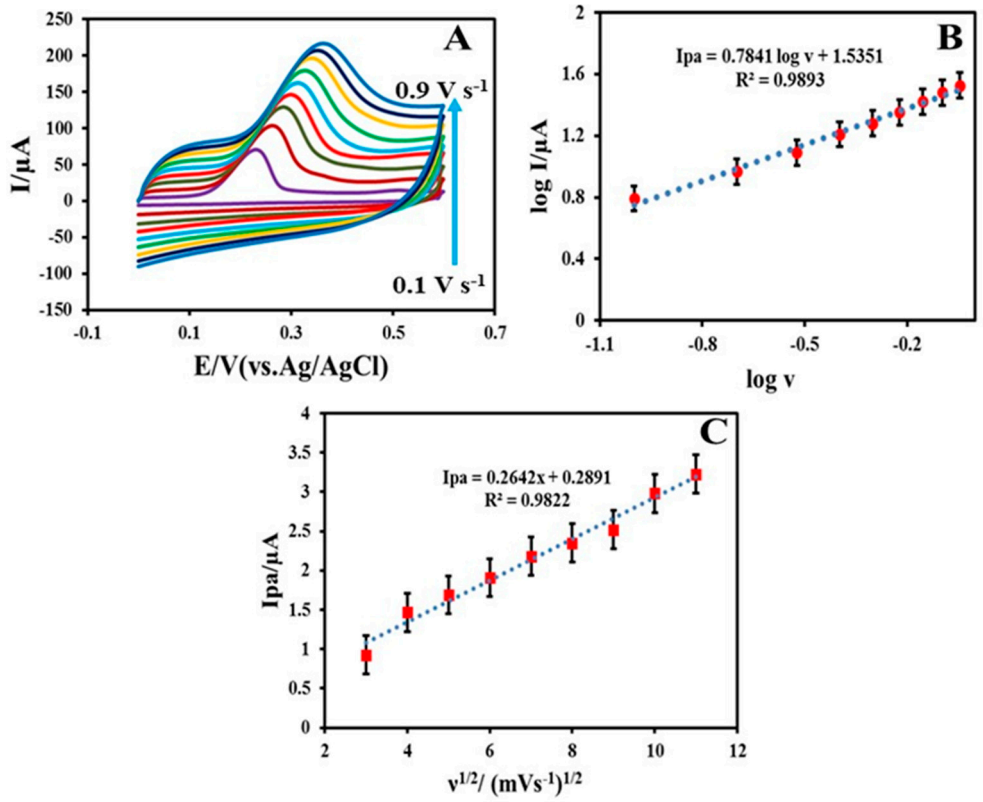

Figure 4. (**A**) Cyclic voltammograms of 0.1 mM of INZ at scan rates of 0.1, 0.2, 0.3, 0.4, 0.5, 0.6, 0.7, 0.8 and 0.9 V·s^{-1}. (**B**) Graph of (log anodic peak current) versus log (scan rate) for 0.1 mM INZ in 0.1 M phosphate buffer solution (PBS; pH 7.0) with different scan rates for the MWCNT-TiO_2NPs-HRP-GCE. (**C**) Linear plot of (anodic peak current) against the square root of the scan rate (n = 5, average standard deviation).

3.4. Quantitative Analysis of INZ

DPV was carried out with a 0.5 to 5 µM of INZ, via the standard addition method. The MWCNT-TiO_2NPs-HRP-GCE gave a well-defined anodic peak at 0.2 V (vs. Ag/AgCl) with the optimized working parameters (scan rate of 0.09 V·s^{-1}, deposition time 120 s, pulse amplitude 0.050 V, voltage step 0.00935 V, voltage step time 0.1 s and pulse time 0.040 s). It was shown that as the concentration of INZ was increased, the anodic peak currents were gradually increased (Figure 5).

A calibration graph was plotted for the concentration of INZ against anodic peak currents. The obtained regression equation (i_{pa} =12.22 c + 0.375) showed a good correlation coefficient of R^2 = 0.998 for DPV. The limit of detection (LOD) and limit of quantification (LOQ) were calculated based on signal to noise ratios by using the Equations (3) and (4). In terms of the instrument signal, we are interested in determining the smallest signal that is distinguishable from the background (baseline) noise.

$$\text{LOD} = (3 \times \text{SD}/\text{Slope}) \quad (3)$$

$$\text{LOQ} = (10 \times \text{SD}/\text{Slope}) \quad (4)$$

where SD is the standard deviation of the peak currents for three different runs and slope of the calibration curve. The limit of detection and limit of quantification for INZ is 0.0335 µM and 0.1118 µM, respectively. The comparison of current fabricated sensor method with previous methods (27–37) used in the determination of INZ is listed in Table 1. This indicates our method showed lower LOD and LOQ values for the determination of INZ compared to previous reports.

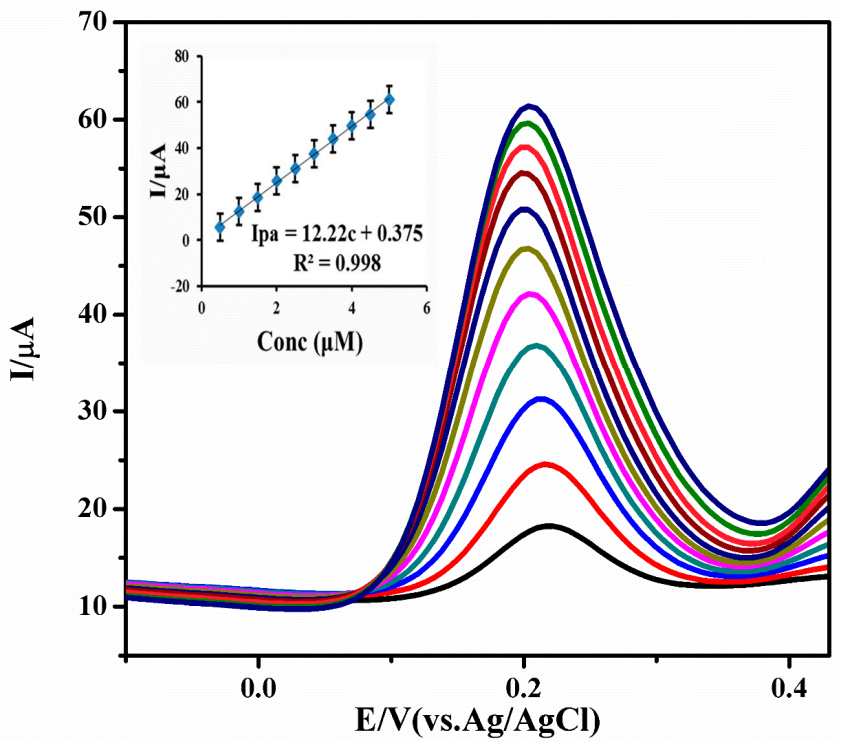

Figure 5. Differential pulse voltammetric (DPV) response of 0.5 to 5 µM INZ with the MWCNT-TiO_2NPs-HRP-GCE at pH 7.0, scan rate: 0.09 $V \cdot s^{-1}$, deposition time: 120 s, pulse amplitude: 0.050 V and pulse time: 0.040 s. (Inset calibration plot) (n = 5, average SD).

Table 1. Comparison of some characteristics of the previously reported modified electrodes with the MWCNT-TiO_2NPs-HRP-GCE.

Electrode	Technique	Detection Limits/(µM)	Linear Range/(µM)	Buffer and pH	References
Nf/Fe/GCE [a]	CV	13.00	50–20,000	Na_2SO_4 (9)	[29]
LDH/GCE [b]	DPV	4.00	4.9–770	BR (9)	[30]
4-pyridyl hydroquinone SAM/platinum electrode [c]	CV	20.0	-	PBS (7.2)	[31]
poly-L-histidine/SPE [d]	DPV	0.50	-	PBS (7)	[32]
Gold electrode [e]	DPV	0.09	-	NaOH (13.6)	[33]
PdNP/CPE [f]	CV	0.47	-	PBS (7)	[27]
Hanging mercury drop electrode [g]	SWADCS	1.18	-	BR (5.5)	[34]
GO/GCE [h]	LSV	0.17	2–70	PBS (7)	[35]
F-MWCNT/GCE [i]	CV	0.27	1–70	AB (4)	[36]
Rh/GCE [j]	CV	13.00	70–130	PBS (7)	[37]
Bentonite clay/GCE [k]	LSV	0.80	-	Na_2SO_4 (13.5)	[38]
MWCNT-TiO_2NPs-HRP-GCE	DPV	0.03	0.5–5	PBS (7)	Present work

[a] Nf/Fe/GCE—Nafion on iron-coated GCE; [b] LDH/GCE—layered double hydroxide-coated GCE; [c] 4-pyridyl hydroquinone SAM/platinum electrode-4-pyridyl hydroquinone self-assembled monolayer-coated platinum electrode; [d] poly-L-histidine/Screen printed electrode (SPE)-poly-L-histidine coated on a SPE ; [f] PdNP/CPE—palladium nanoparticle-coated CPE; [h] GO/GCE—graphene oxide-coated GCE; [i] F-MWCNT/GCE—functionalized multi-wall carbon nanotube-coated GCE; [j] Rh/GCE—rhodium nanoparticle-coated GCE; [k] bentonite clay/GCE—bentonite clay-modified GCE; SWADCS—square-wave adsorptive anodic stripping voltammetry; LSV—linear sweep voltammetry; CPE—carbon paste electrode; SPE—screen-printed electrode; CV—cyclic voltammetry; PBS—phosphate buffer solution.

3.5. Repeatability and Stability

The repeatability efficiency of the proposed sensor was examined with 0.1 mM INZ solution DPV under the optimized parameters. After each determination the used fabricated electrode underwent five to six sweeps in 0.1 M PBS (pH 7.0), to remove any adsorbents and yield a reproducible electrode surface. The peak current response of INZ was determined with five electrodes under the same conditions. From the five parallel determinations, the Relative Standard Deviation (RSD) of INZ determination was found to be 4.12%. Based on the results, the proposed sensor showed good repeatability. The long-term stability of the sensor was tested after 80 days. When not used, the sensor was stored at 4 °C. The stability studies were carried out with the MWCNT-TiO2NPs-HRP-GCE for the detection of INZ. This study was carried out in two batches. In the first batch, the stability of the modified electrode was observed from day 1 to day 40, in terms of electrochemical signalling. It was observed that for 40 days, the average electrochemical signal was found to be 91%. In the second batch, the stability study was carried out for an additional 40 days with the same materials and electrode. Interestingly, it was now observed that the electrochemical signal was found to be 87%. This implies only 4.39% of the electrochemical signal decreased. These results indicate that the fabricated electrode showed good repeatability and long-term stability.

3.6. Interference Studies

To evaluate the selectivity ability of developed sensor, interference studies were also performed for INZ with coexisting compounds like uric acid, glucose, and ascorbic acid. In this analysis, the peak current of INZ was recorded (Ip_1). The excess amount of the potential interferent species was added to the mixture and DPV was recorded (Ip_2). The tolerance limit was defined as the maximum concentration of the interfering components that caused an error less then ±5% (Ip_1/Ip_2 = 95–105%). In addition, the influence of some common ions such as Fe^{3+}, Al^{3+}, Cl^-, Na^+, and K^+ were studied and the results indicated that these ions have no significant influence on the determination of INZ (Table 2).

Table 2. The influences of some anions, cations and important biological substances on the peak current of 0.1 mM INZ with the MWCNT-TiO_2NPs-HRP-GCE.

Interferents	Concentration/(μM)	Signal Change (%)
Ascorbic acid	250	4.03
Uric acid	250	1.24
Glucose	500	0.34
Fe^{3+}	500	0.81
Al^{3+}	500	1.27
Cl^-	500	0.67
Na^+	500	2.01
K^+	500	1.35

3.7. Real Sample Analysis

Commercially-available INZ tablets (100 mg) were purchased from the local pharmacy. The samples (tablets) were used to evaluate the realistic performance of the MWCNT-TiO_2NPs-HRP-GCE. Approximately ten tablets were taken into a mortar and crushed to fine powder with pestle. A 0.1 mM INZ tablet sample solution was prepared by dissolving the appropriate amount of powder sample in a 10 mL volumetric flask and adding 10 mL of PBS. Finally, real sample analysis was carried out with 0.1 mM INZ by the DPV technique via the standard addition method. The results with respect to the analytical performances of the MWCNT-TiO_2NPs-HRP-GCE obtained were then tabulated (Table 3). The two pharmaceutical samples showed good RSD values (1.69 and 1.98) with an excellent percentage of recovery (99.2% and 98.9%). This indicates that the developed sensor exhibited good recovery capability towards INZ in various pharmaceutical samples.

Table 3. Determination of INZ in various pharmaceutical samples using the developed sensor (n = 5).

Declared Amount Tablet (mg)	Found (mg)	Recovery (%)	Relative Standard Deviation (RSD) (%)	Added (mg)	Found (mg)	Recovery (%)	RSD (%)
Sample 1 (100 mg)	99.2	99.2	1.69	20	19.3	96.5	0.32
Sample 2 (100 mg)	98.9	98.9	1.98.	10	9.5	95.0	0.79

n: average determinations.

4. Conclusions

A facile MWCNT-TiO_2NPs-HRP-GCE biosensor was successfully developed for the determination of INZ in different pharmaceuticals samples. The synthesized nanoparticles and developed sensor were characterized with TGA, TEM, XRD, and FT-IR. The electrochemical sensing abilities of INZ with different electrodes, viz., bare GCE, MWCNT-GCE, MWCNT-TiO_2NPs-GCE and MWCNT-TiO_2NPs-HRP-GCE were successfully compared using cyclic voltammetry studies. The developed sensor showed fast electron transfer capability, good electronic conductivity, and large electroactive surface area. The CV results obtained reveal the outstanding electrochemical sensing performance of the enzyme-induced sensor with an increase (approximately 8-fold) of anodic peak currents. In the DPV technique, the calibration plot gave a good correlation coefficient of R^2 = 0.998 with LOD and LOQ values of 0.0335 µM and 0.1118 µM, respectively. This clearly indicates the developed sensor showed a high capability for detecting the INZ in µM concentration without any interferences. In addition, the fabricated sensor exhibited good repeatability and long-term stability, with negligible current variations. Moreover, the real sample analysis gave satisfactory results with good percentages of recoveries. The devolved sensor may have scope for use in the pharmaceutical industries in the near future.

Supplementary Materials: The following are available online at http://www.mdpi.com/2079-6374/7/2/21, Figure S1: The effect of the enzyme incubation time on the current responses of modified electrode. Figure S2: Cyclic Voltammograms of INZ with (A) Bare GCE, (B) MWCNTs-GCE, (C) MWCNTs-TiO_2NPs-GCE at various scan rates ranges 0.1, 0.2, 0.3, 0.4, 0.5, 0.6, 0.7, 0.8 and 0.9 $V \cdot s^{-1}$

Acknowledgments: The authors gratefully acknowledge financial support for this work from the Durban University of Technology, Durban, South Africa.

Author Contributions: Rajasekhar Chokkareddy conducted the main experiments and wrote the manuscript. Natesh Kumar Bhajanthri did the material characterization. Gan G. Redhi conceived, designed and supervised the experimental work.

Conflicts of Interest: The authors declare no conflict of interest.

References

1. Rastogi, P.K.; Ganesan, V.; Azad, U.P. Electrochemical determination of nanomolar levels of isoniazid in pharmaceutical formulation using silver nanoparticles decorated copolymer. *Electrochim. Acta* **2016**, *188*, 818–824. [CrossRef]
2. Arshad, N.; Yunus, U.; Razzque, S.; Khan, M.; Saleem, S.; Mirza, B.; Rashid, N. Electrochemical and spectroscopic investigations of isoniazide and its analogs with ds.DNA at physiological pH: Evaluation of biological activities. *Eur. J. Med. Chem.* **2012**, *47*, 452–461. [CrossRef] [PubMed]
3. Becker, C.; Dressman, J.B.; Amidon, G.L.; Junginger, H.E.; Kopp, S.; Midha, K.K.; Shah, V.P.; Stavchansky, S.; Barends, D.M. International Pharmaceutical Federation, Biowaiver monographs for immediate release solid oral dosage forms: Isoniazid. *J. Pharm. Sci.* **2007**, *96*, 522–531. [CrossRef] [PubMed]
4. Fang, P.F.; Cai, H.L.; Li, H.D.; Zhu, R.H.; Tan, Q.Y.; Gao, W.; Xu, P.; Liu, Y.P.; Zhang, W.Y.; Chen, Y.C.; et al. Simultaneous determination of isoniazid, rifampicin, levofloxacin in mouse tissues and plasma by high performance liquid chromatography-tandem mass spectrometry. *J. Chromatogr. B Anal. Technol. Biomed. Life Sci.* **2010**, *878*, 2286–2291. [CrossRef] [PubMed]

5. Liu, J.; Zhou, W.; Tianyan, Y.; Fenglei, L.; Wang, E.; Dong, S. Detection of Hydrazine, Methyl hydrazine, and Isoniazid by Capillary Electrophoresis with a Palladium-Modified Micro disk Array Electrode. *Anal. Chem.* **1996**, *68*, 3350–3353. [CrossRef] [PubMed]
6. Rui Lapa, A.S.; Jose Lima, L.F.C.; Joao Santos, L.M. Fluorimetric determination of isoniazid by oxidation with cerium(IV) in a multi commutated flow system. *Anal. Chem.* **2000**, *419*, 17–23.
7. El-Brashy, A.M.; El-Ashry, S.M. Colorimetric and titrimetric assay of isoniazid. *J. Pharm. Biomed. Anal.* **1992**, *10*, 421–426. [CrossRef]
8. Verma, K.K.; Palod, S. The Titrimetric Determination of 4-Pyridine Carboxylic Acid Hydrazide (Isoniazid) in Drug Formulations with Thallium (III). *Anal. Lett.* **1985**, *18*, 11–19. [CrossRef]
9. Haghighi, B.; Bozorgzadeh, S. Flow injection chemiluminescence determination of isoniazid using luminol and silver nanoparticles. *Microchem. J.* **2010**, *95*, 192–197. [CrossRef]
10. Miloglu, F.D.; Oznuluer, T.; Ozdurak, B.; Miloglu, E. Design and optimization of a new voltammetric method for determination of Isoniazid by using PEDOT modified gold electrode in pharmaceuticals. *Iran. J. Pharm.* **2016**, *15*, 65–73.
11. Janin, Y.L. Antituberculosis drugs: Ten years of research. *Bioorg. Med. Chem.* **2007**, *15*, 2479–2513. [CrossRef] [PubMed]
12. Gowthaman, N.S.K.; Kesavan, S.; John, S.A. Monitoring isoniazid level in human fluids in the presence of theophylline using gold platinum core shell nanoparticles modified glassy carbon electrode. *Sens. Actuators B Chem.* **2016**, *230*, 157–166. [CrossRef]
13. Shahrokhian, S.; Asadian, E. Simultaneous voltammetric determination of ascorbic acid, acetaminophen and isoniazid using thionine immobilized multi-walled carbon nanotube modified carbon paste electrode. *Electrochim. Acta* **2010**, *55*, 666–672. [CrossRef]
14. Szlosarczyk, M.; Piech, R.; Bator, B.P.; Maslanka, A.; Opoka1, W.; Krzek, J. Voltammetric determination of isoniazid using cyclic renewable mercury film silver based electrode. *Pharm. Anal. Acta* **2012**, *3*, 1–5.
15. Regis, L.; Ferraz, B.; Roberto, F.; Leite, F.; Malagutti, A.R. Simultaneous determination of ethionamide and pyrazinamide using poly (l-cysteine) film-modified glassy carbon electrode. *Talanta* **2016**, *154*, 197–207.
16. Shahrokhian, S.; Amiri, M. Multi-walled carbon nanotube paste electrode for selective voltammetric detection of isoniazid. *Microchim. Acta* **2006**, *157*, 149–158. [CrossRef]
17. Guo, Z.; Wang, Z.Y.; Wang, H.H.; Huang, G.Q.; Li, M.M. Electrochemical sensor for Isoniazid based on the glassy carbon electrode modified with reduced graphene oxide-Au nanomaterials. *Mater. Sci. Eng. C Mater. Biol. Appl.* **2015**, *57*, 197–204. [CrossRef] [PubMed]
18. Madan, J.; Dwivedi, A.K.; Singh, S. Estimation of ant tubercular drugs combination in pharmaceutical formulations using multivariate calibration. *Anal. Chim. Acta* **2005**, *538*, 345–353. [CrossRef]
19. Bagheri, S.; Muhd Julkapli, N.; Bee Abd Hamid, S. Titanium dioxide as a catalyst support in heterogeneous catalysis. *Sci. World J.* **2014**, *96*, 72–74. [CrossRef] [PubMed]
20. Trocino, S.; Donato, A.; Latino, M.; Donato, N.; Leonardi, S.G.; Neri, G. Pt-TiO_2/MWCNTs Hybrid Composites for Monitoring Low Hydrogen Concentrations in Air. *Sensors* **2012**, *12*, 12361–12373. [CrossRef]
21. Ahirwal, G.K.; Mitra, C.K. Direct Electrochemistry of Horseradish Peroxidase-Gold Nanoparticles Conjugate. *Sensors* **2009**, *9*, 881–894. [CrossRef] [PubMed]
22. Strushkevicha, N.; MacKenziea, F.; Cherkesovab, T.; Grabovecb, I.; Usanovb, S.; Park, H.-W. Structural basis for pregnenolone biosynthesis by the mitochondrial monooxygenase system. *Proc. Natl. Acad. Sci. USA* **2011**, *108*, 10139–10143. [CrossRef] [PubMed]
23. Hua, M.Y.; Lin, Y.C.; Tsai, R.Y.; Chen, H.C.; Liu, Y.C. A hydrogen peroxide sensor based on a horseradish peroxidase/polyaniline/carboxy-functionalized multiwalled carbon nanotube modified gold electrode. *Electrochim. Acta* **2011**, *56*, 9488–9495. [CrossRef]
24. Azad, U.P.; Ganesan, V. Efficient electrocatalytic oxidation and selective determination of isoniazid by Fe_3^{2+} exchanged Nafion modified electrode. *J. Solid State Electrochem.* **2012**, *16*, 2907–2911. [CrossRef]
25. Zeynali, K.A.; Shabangoli, Y.; Nejati, K. Electrochemical synthesis of Fe/Al-layered double hydroxide on a glassy carbon electrode: Application for electrocatalytic reduction of isoniazid. *J. Iran. Chem. Soc.* **2015**, *13*, 29–36. [CrossRef]
26. You, T.; Niu, L.; Gui, J.Y.; Dong, S.; Wang, E. Detection of hydrazine, methyl hydrazine and isoniazid by capillary electrophoresis with a 4-pyridyl hydroquinone self-assembled micro disk platinum electrode. *J. Pharm. Biomed. Anal.* **1999**, *19*, 231–237. [CrossRef]

27. Chen, W.C.; Unnikrishnan, B.; Chen, S.M. Electrochemical oxidation and amperometric determination of Isoniazid at functionalized multiwalled carbon nanotube modified electrode. *Int. J. Electrochem. Sci.* **2012**, *7*, 9138–9149.
28. Devadas, B.; Cheemalapati, S.; Chen, S.M.; Ajmal Ali, M.; Al-Hemaid, F.M.A. Highly sensing graphene oxide/poly-arginine-modified electrode for the simultaneous electrochemical determination of buspirone, isoniazid and pyrazinamide drugs. *Ionics* **2015**, *21*, 547–555. [CrossRef]
29. Bergamini, M.F.; Santos, D.P.; Zanoni, M.V. Determination of isoniazid in human urine using screen-printed carbon electrode modified with poly-L-histidine. *Bioelectrochemistry* **2010**, *77*, 133–138. [CrossRef] [PubMed]
30. Xia, H.Y.; Hu, X.Y. Determination of Isoniazid Using a Gold Electrode by Differential Pulse Voltammetry. *Anal. Lett.* **2005**, *38*, 1405–1414.
31. Absalan, G.; Akhond, M.; Soleimani, M.; Ershadifar, H. Efficient electrocatalytic oxidation and determination of isoniazid on carbon ionic liquid electrode modified with electrodeposited palladium nanoparticles. *J. Electroanal. Chem.* **2016**, *761*, 1–7. [CrossRef]
32. Ghoneim, M.M.; El-Baradie, K.Y.; Tawfik, A. Electrochemical behaviour of the anti-tuberculosis drug isoniazid and its square-wave adsorptive stripping voltammetric estimation in bulk form, tablets and biological fluids at a mercury electrode. *J. Pharm. Biomed. Anal.* **2003**, *33*, 673–685. [CrossRef]
33. Cheemalapati, S.; Palanisamy, S.; Chen, S.M. Electrochemical determination of Isoniazid at electrochemically reduced graphene oxide modified electrode. *Int. J. Electrochem. Sci.* **2013**, *8*, 3953–3962.
34. Cheemalapati, S.; Chen, S.M.; Ali, M.A.; Al-Hemaid, F.M. Enhanced electrocatalytic oxidation of isoniazid at electrochemically modified rhodium electrode for biological and pharmaceutical analysis. *Colloids Surf. B* **2014**, *121*, 444–450. [CrossRef] [PubMed]
35. Azad, U.P.; Prajapati, N.; Ganesan, V. Selective determination of isoniazid using bentonite clay modified electrodes. *Bioelectrochemistry* **2015**, *101*, 120–125. [CrossRef] [PubMed]
36. Wei, X.N.; Wang, H.L.; Li, Z.D.; Huang, Z.Q.; Qi, H.P.; Jiang, W.F. Fabrication of the novel core-shell MCM-41@mTiO_2 composite microspheres with large specific surface area for enhanced photo catalytic degradation of di nitro butyl phenol (DNBP). *Appl. Surf. Sci.* **2016**, *372*, 108–115. [CrossRef]
37. Gnanasekaran, L.; Hemamalini, R.; Ravichandran, K. Synthesis and characterization of TiO_2 quantum dots for photo catalytic application. *J. Saudi Chem. Soc.* **2015**, *19*, 589–594. [CrossRef]
38. Thamaphat, K.; Limsuwan, P.; Ngotawornchai, B. Phase Characterization of TiO2 Powder by XRD and TEM. *Kasetsart J. (Nat. Sci.)* **2008**, *42*, 357–361.

Send Orders for Reprints to reprints@benthamscience.ae

Current Analytical Chemistry, **2017,** *13,* **000-000**

RESEARCH ARTICLE

Ultra-Sensitive Electrochemical Sensor for the Determination of Pyrazinamide

R Chokkareddy[1], N K Bhajanthri[1,*], Gan G Redhi[1,*] and Dhirendra G Redhi[2]

[1]*Department of Chemistry, Durban University of Technology, Durban- 4000, South Africa;* [2]*Pharmacy, Mediclinic Victoria, Tongaat-4400, South Africa*

Abstract: ***Background:*** A simple and novel electrochemical sensor was developed for the determination of pyrazinamide (PZM) in various pharmaceutical samples. The sensor was developed by modifying the glassy carbon electrode (GCE) in 3 different stages; GCE modified with multi walled carbon nano tubes MWCNTs (GCE/MWCNTs), further it was coated with copper oxide nanoparticles (CuONPs). Finally Cytochrome c (Cyt c) was immobilized on the surface of the pre-coated electrode. Cyclic voltammry and differential pulse voltammetric techniques were employed for the electrochemical investigations. The CV results obtained showed well-defined anodic and cathodic peaks at the peak potentials -0.77 V and -0.80 V respectively, and also revealed good electrocatalytic activity of Cyt c/CuONPs/MWCNTs/GCE towards PZM. From the measured DPV results, the limit of detection and limit of quantification of the developed sensor were calculated, and found to be 0.0038 μM and 0.0129 μM respectively. Furthermore, the proposed sensor was successfully applied to the analysis of PZM in the various commercial pharmaceutical samples.

Pyrazinamide (PZM) is an antimycobacterial and a chief component of multidrug therapy for tuberculosis (TB). It is crucial for the prevention or treatment of TB infections. PZM has become an important component of short-term (6 months) multiple-drug therapy for tuberculosis. Owing to the high medical significance of PZM, it is necessary to develop a simple and rapid methodology for the analysis of PZM in various pharmaceutical is crucial. Ectrochemical methods with modified sensors have been exhibiting greater advantages in the current progressive scientific world. In the present manuscript a novel high sensitive electrochemical sensor was developed for the determination of PZM in various pharmaceutical samples. The developed sensor shows realistic behaviour towards pharmaceutical samples which is successfully monitored and tabulated in the present work.

Methodology: Voltammetric measurements were carried out with 797 VA Computrace system with version 1.3.1 software from Metrohm (Switzerland). PZM stock and standard solutions were made with 0.1 M phosphate buffer solution (PBS). The CuONPs were synthesized according to the previous report with slight modification. Electrode modification was performed in three different stages with MWCNTs, CuONPs and Cyt c to develop the finalized sensor. 10 ml of the PBS (pH 7) was introduced into the electrochemical cell. Thereafter a bare and modified GCE was dipped into the electrochemical cell followed by purging nitrogen gas for about 10 min and then the CV/DPV experiment was performed. An aliquot of the PZM solution was then introduced into the electrochemical cell, at 1000 rpm of rotating disc speed and the optimized pre-concentration potential was fixed for the voltammetric measurements. The cyclic and differential pulses voltammograms were monitored at the scan rate of 0.1 V s^{-1} with the potentials increasing towards the positive direction. In addition the real pharmaceutical samples were also analysed via standard addition method.

Results: Infrared spectroscopy and X-ray diffraction study characterization reveals the confirmation of formed CuONPs. Transmission electron microscopic studies confirmed the surface characterization of finalized sensor. Additionally, thermogravimetric analyses support the confirmation of the formed nanocomposite coated on the surface of GCE. Randles-Sevick equation reveals the high surface area of the modified sensor. This indicates the development of a suitable platform for electrochemical redox mechanism of PZM on the surface of the final sensor. The utmost electrochemical parameters like pH, scan rate, and deposition time were optimized. The developed sensor showed enhanced electrochemical sensing peak currents in cyclic voltammetry. The differential pulse voltammetry showed the linear range 3-30 μM with good LOD and LOQ of 0.0038 μM and 0.0129 μM respectively. The developed sensor showed good percentages of recovery viz., 99.5% and 98.2% respectively.

Conclusion: In the present work the developed sensor showed good catalytic activity towards PZM, due to the increased electrochemical sensing mechanism for PZM. The modified electrode was successfully characterized by the TEM, FT-IR, TGA and XRD techniques. The fabricated sensor showed enhanced peak currents and low detection limits with PZM. The proposed sensor showed excellent sensitivity, selectivity and low detection limits. In addition the developed sensor was applied for the determination of PZM in real pharmaceutical samples, and reflects good recovery percentages. It is evident that the proposed method will serve as a standard protocol for the determination of PZM in various pharmaceutical samples, and would be of great help to pharmaceutical industries in the future.

ARTICLE HISTORY

Received: February 21, 2017
Revised: April 21 2017
Accepted: May 11, 2017

DOI:
10.2174/1573411013666170530105000

Keywords: An electrochemical sensor, pyrazinamide, cyclic voltammetry, different pulse voltammetry, pharmaceutical samples.

*Address correspondence to this author at the Department of Chemistry, Faculty of Applied Sciences, Durban University of Technology, P.O. Box: 1334, Durban, South Arica, 4000; Tel: +27 - 0313732936; E-mails: redhigg@dut.ac.za; nateshkumar786@gmail.com

1. INTRODUCTION

Tuberculosis (TB) is a deadly disease generally caused by the bacterium *"Mycobacterium tuberculosis"* [1]. TB af-

1573-4110/17 $58.00+.00

fects almost one third of the world's population, and after 2006 the death rate was slightly decreased [2]. Pyrazine-2-carboxamide is commercially known as pyrazinamide (PZM) and it is the most significant drug amongst all the first line anti tuberculosis drugs. A combination of isoniazid, rifampicin and ethambutol was prescribed to TB patients along with PZM in order to cure the disease [3, 4]. Its use has shortened the time of the treatment, however the regular intake of PZM drug causes more side effects such as liver injury, anorexia, nausea, vomiting, fever, sideroblastic anemia and severe hepatic damages [5-7]. To minimize side effects and control the PZM dosages in biological fluids, several analytical methodologies have been developed. They are capillary electrophoresis [8], UV–visible methods [9], square-wave polarography methods [10], chromatographic methods [11, 12], spectrophotometry [13], fluorimetry [14] and electrochemical methods [15]. Electrochemical methods have great advantages like high sensitivity, less expensive instrumentation costs and simple methodologies, compared to other methods. Electrochemical method investigations via bare glassy carbon electrode (GCE) show less sensitivity and selectivity in the field of pharmaceutical formulations.

In the past two decades chemically modified electrodes have been widely used in sensor development, since they show larger surface area with easy electron transferable nature [16]. The electrode is generally modified with basic electrode coating materials like graphene oxide (GO) and multi walled carbon nano tubes (MWCNTs). These coating materials exhibit excellent electrical and thermal conductivity [17]. MWCNTs possess very high tensile strength, high flexibility and elasticity [18]. These properties make MWCNT a suitable modifier for the coating of different working electrodes [19]. Hence MWCNTs was used as a basic electrode coating material in this present investigation. Furthermore, metal oxides nano particles such as CuO, ZnO, TiO_2, MnO_2, and Fe_3O_4NPs are also widely used as one of the coating materials in electrochemical sensors, due to its low cost, high abundance, greater electrical conductivity, and easy synthetic procedures [20]. Among all other nano materials, CuONPs exhibit good electrochemical response, are non-toxic, have a large surface area and show excellent degree of biocompatibility [21]. Due to the numerous advantages of CuONPs, it was incorporated as one of the fabricating materials [22-24] in the present developed sensor. Cytochrome c is a low mass, highly stabled heme as a prosthetic moiety containing conjugated protein. The major role of cytochrome c is to transfer electrons from complex III (QH2-cytochrome c reductase) to complex IV (cytochrome c oxidase) in the respiratory chain and occurs in the mitochondria of vertebrates [25, 27]. It generally carries an electron and is responsible for a redox mechanism in cell biology as well [26]. Therefore, cytochrome c was also used as one of the electrode coating materials in the present investigation in order to increase the electrochemical sensing ability of the developed sensor.

2. EXPERIMENTAL

2.1. Apparatus

Voltammetric measurements were carried out with 797 VA Computrace system with version 1.3.1 software from Metrohm (Switzerland). A three-electrode system comprised of a platinum wire which served as a counter electrode, Ag/AgCl (3.0 M KCl) acted as a reference electrode and the Cytochrome c/CuONPs/MWCNTs/GCE was used as a working electrode. The thermo gravimetric analysis of the CuONPs/MWCNTs hybrid was performed with TGA (TGA/DCS1SF/1346 model by METTLER TOLEDO) and the transition electron microscopic characterization was done with TEM model (JEM 2100 equipped with a Lab6 emitter, Max Oxford instrument). Fourier transformation infrared (FTIR) characterization was performed by a Varian 800 FTIR scimitar series (by SMM instruments). An ultrasonic bath (Labcon model 5019 U) was used to prepare modifier suspensions. A (CRISON digital micro pH 2000) pH meter was used for the preparation of the buffer solutions. Deionized water was provided by the Aqua Max TM Basic 360 system.

2.2. Chemicals

Pyrazinamide, di sodium hydrogen orthophosphate, sodium di hydrogen phosphate, sodium hydroxide, copper (II) chloride pentahydrate and MWCNTs (O.D.-L 6-9 nm-5 μM) were purchased from Sigma Aldrich. Ethanol (99.9%), sulphuric Acid, and N, N-dimethyl formamide (DMF) were purchased from Capital Lab Supplies (Durban, South Africa).

2.3. Preparation of Working Standard Solutions

An analytical reagent grade pyrazinamide (PZM) was used in the present investigation. The stock and standard solutions were made by dissolving an appropriate quantity of PZM with the desired volume. A 0.1 M phosphate buffer solution (PBS) was prepared from the mixture of di sodium hydrogen orthophosphate and sodium di hydrogen phosphate, and the desired pH was adjusted with 0.02 M H_2SO_4 or 0.1 M NaOH.

The CuONPs were synthesized according to the previous report with slight modification [28], 1.59 g of $CuSO_4$ was dissolved in 150 mL of deionized water to prepare 0.2 M $CuSO_4$. This initially appeared as a green coloured solution, and to this 1 mL of acetic acid was added. In another vessel 8 g of NaOH was dissolved in 25 mL of deionized water to get 8 M NaOH. In a drop, wise manner, NaOH was added to the contents of $CuSO_4$ with continuous stirring, and was subjected to heating at 90 ^oC. This gave a black coloured precipitate immediately. The precipitate was then centrifuged, repeatedly washed 4 to 5 times with deionized water and oven dried at 60 ^oC for 3 hours. This powder was further used for the characterization of CuONPs.

2.4. Fabrication of Cyt c/CuONPs/MWCNTs/GCE

The bare GCE surface was initially treated with alumina slurry on a wet polishing pad and washed with deionized water, followed by ultra-sonication with an equal amount of ethanol and deionized water for about 15 min. 0.25 g of MWCNTs were then dispersed into 5 mL of DMF, the resulting mixture was sonicated for 30 min at 50 ^oC, to give a black suspension. The resulting mixture was used for the coating of MWCNTS on the GCE. Equal quantities (0.30 g) of pure MWCNTs and CuONPs were dispersed into a 10 mL

of DMF, the resulting mixture was sonicated for 60 min at 50 °C resulting in black suspension. Thereafter, the GCE was immobilized in two different stages. In first stage 5 µL of CuONPs/MWCNTs paste was coated on the surface of the bare GCE and dried at 50 °C for 15 min, whilst in the second stage the modified GCE was cooled at room temperature and then dipped in to the 1 mg mL^{-1} Cyt c solution for 7-10 h at 4 °C. It was then dried at room temperature for another 10 min. Cyt c was successfully adsorbed on the surface of MWCNTs/CuONPs coating.

2.5. Voltammetric Measurements with Cyt c/CuONPs/MWCNTs/GCE

10 mL of the PBS (pH 7) was introduced into the electrochemical cell. Thereafter a bare and modified GCE was dipped into the electrochemical cell followed by purging nitrogen gas for about 10 min and then the CV/DPV experiment was performed. An aliquot of the PZM solution was then introduced into the electrochemical cell, at 1000 rpm revolution of rotating disc speed and the optimized preconcentration potential was fixed for the voltammetric measurements. The cyclic and differential pulses voltammograms were monitored at the scan rate of 0.1 V s^{-1} with the potentials increasing towards the positive direction.

2.6. Pharmaceutical Samples

The proposed electrochemical sensor was used to examine its performance towards the determination of PZM in real pharmaceutical formulated samples. PZM tablets (400 mg and 500 mg) were purchased from the local pharmacy. Randomly 15 tablets of PZM were selected, accurately weighed and finely grounded with mortar and pestle. An appropriate quantity of PZM was then weighed and carefully transferred into a 50 mL volumetric flask, along with 40 mL of 0.1 M PBS (pH 7.0) followed by 30 min ultra-sonication. In this analysis, quantitative determination of pharmaceutical samples was carried out by the standard addition method via the DPV technique.

3. RESULTS AND DISCUSSION

3.1. Characterization of Cyt c/CuONPs/MWCNTs/GCE

The Cyt c/CuONPs/MWCNTs/GCE hybrid electrode was characterized by TEM, TGA, XRD and FTIR. FT-IR spectra were recorded for the CuONPs in the range of 400-4000 cm^{-1} (Fig. **1A**). The two characteristic bands observed at 509 cm^{-1} and 604 cm^{-1} can be assigned to the CuONPs [29]. For the range from 605-660 cm^{-1} no other IR active mode was observed in CuONPs [30]. Moreover, the peak at 871 cm^{-1} was responsible for =C-H bending, 1122 cm^{-1} for C-O stretching, 1629 cm^{-1} for C = C stretching, 2195 cm^{-1} for –C ≡ C – stretching, and 3396 cm^{-1} for O-H stretching vibrations respectively [31]. The XRD pattern for the CuONPs is shown in (Fig. **1B**). The XRD peaks confirmed that the formation of CuONPs from each precursor was in monoclinic phase, no other impurity peaks was observed in the XRD pattern. According to previous literature the XRD pattern exhibits two main diffractions at 2θ = 36.6 (110) and 2θ = 38.8 (111) and these were ascribed to the formation of the CuONPs in face centered cubic (FCC) and monoclinic crystal lattice [32, 33].

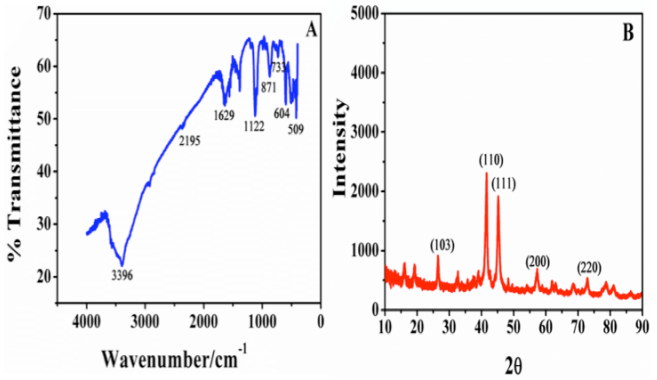

Fig. (1). (A) FT-IR characterization of CuO NPs **(B)** XRD image of CuO NPs.

Figure **2A-D** shows the transmission electron microscopic images of pure MWCNTs, CuONPs and CuONPs-MWCNTs.

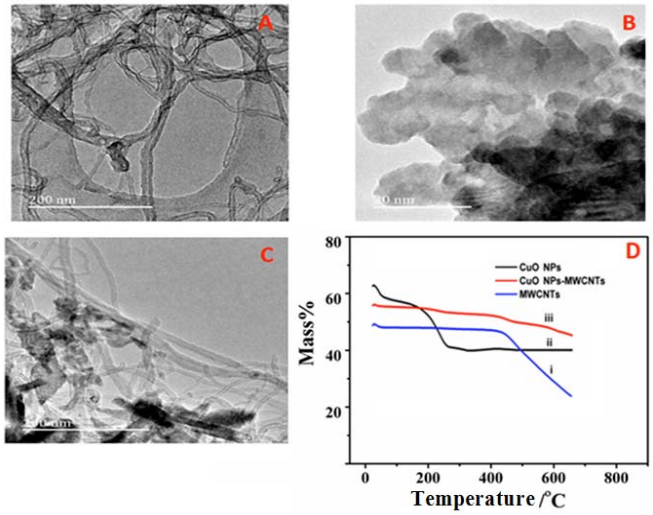

Fig. (2). (**A**) TEM image Pure MWCNTs (**B**) CuONPs (**C**) CuONPs-MWCNTs (**D**) TGA curves for (i) MWCNTs, (ii) CuONPs and (iii) CuONPs/MWCNTs.

Figure **2A** shows the morphological structure of pure MWCNTs with tube like structure. Figure **2B** shows the CuONPs which are almost spherical shape and have average diameters varying between 3-7 nm. Figure **2C** indicates the TEM image of MWCNTs decorated with CuONPs. The CuONPs and MWCNTs nano composites stability and thermal behavior was investigated by the thermo gravimetric analysis (TGA). Figure **2D** show the TGA curves for MWCNTs (i), CuONPs (ii) and CuONPs/MWCNTs (iii). MWCNTs showed one major decrement in the mass around 570 °C. The TGA curve of CuONPs shows loss of mass in two steps. In the first step it loses minor mass at 100 °C due to evaporation of water, whereas in the second step mass losses occur at above 400 °C and can be attributed to the removal of organic moieties. Finally the CuONPs decorated on the MWCNTs show different TGA curves, and it loses minor mass at below 600 °C, due to the evaporation of some organic moieties [34].

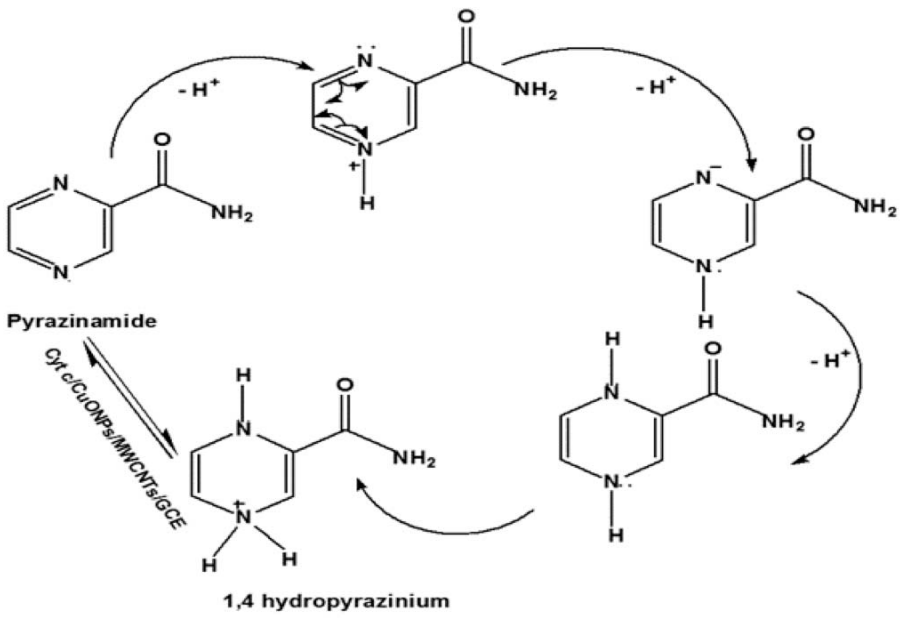

Fig. (3). Proposed electrochemical reaction of PZM at Cyt c/CuONPs/MWCNTs/GCE.

3.2. Electrochemical Behavior of PZM at Cyt c/CuONPs/MWCNTs/GCE

The electrochemical behavior of PZM was evaluated with 0.1 M PBS (pH 7.0) at different electrodes. PZM generally undergoes an electrochemical reduction reaction at the electrode surface and converts pyrazinamide to pyrazinoic acid [35]. In this reaction, two electrons and three protons are involved in the hydroxylation process. They are responsible for the generation of reduction peaks at the electrode surface, (Fig. **3**).

The Cyt c/CuONPs/MWCNTs/GCE demonstrated the good current response against PZM. The increasing anodic and cathodic currents for the different modified electrodes were calculated by using the Randles-Sevick equation [36].

$$i_{pa} = 2.69 \times 10^5 A\, C_0\, n^{3/2}\, D_R^{1/2}\, v^{1/2}$$

In the Randles-Sevick equation i_{pa} is the anodic peak current, C_0 is the concentration of PZM, A is the surface area of electrode, n is the number of electrons transferred, D_R is the diffusion coefficient and ν is the scan rate. The bare GCE anodic peak currents were used to calculate D_R. Further the surface area of the Cyt c/CuONPs/MWCNTs/GCE was calculated by using the diffusion coefficient value. The surface area of Cyt c/CuONPs/MWCNTs/GCE was calculated and found to be 15.23 mm^2, and for the bare GCE it was 3.14 mm^2. The obtained results reveal that the Cyt c/CuONPs/MWCNTs nanocomposite provides larger surface area on the GCE, and allows more PZM molecules to take part in the reduction mechanism. Cyt c is strongly adsorbed on the MWCNTs/CuONPs/GCE surface and it forms monolayer. The Cyt c had two active sites, these active sites are capable of electron transfer. Among the two active sites of Cyt c, one binds with MWCNTs/CuONPs/GCE and the second active site binds with the PZM [37].

Figure **4A** clearly shows the obtained CV curves for bare GCE, MWCNTs/GCE, MWCNTs/CuONPs/GCE and Cyt c/CuONPs/MWCNTs/GCE at an optimum scan rate of 50 mV s^{-1}. The CV measurements were done in the potential range of -1.4 to 0.1 V for all the electrodes. At the bare GCE, the anodic and cathodic peaks were obtained at the potentials of -0.75 V and -0.78 V with minor 25 μA currents responses. Under identical conditions, MWCNTs/GCE and CuONPs/MWCNTs show corresponding anodic and cathodic peaks at the potentials of -0.78 V, -0.81 V and -0.77 V, -0.80 V with modest currents of 145 μA and 780 μA respectively. Cyt c/CuONPs/MWCNTs/GCE show corresponding peaks at -0.77 V and -0.80 V with extraordinary higher current responses (1600 μA). At ambient temperature Cyt c is stable and the denaturation temperature for Cyt c is 68.4 °C [38]. Comparing all the fabricated electrodes and bare GCE, the Cyt c/CuONPs/MWCNTs/GCE showed the highest electrochemical responses towards PZM (Fig. **4D**).

3.3. Method Optimization

pH is the most significant factor that plays a key role in the determination of the analyte of interest chiefly in electrochemical investigations. In order to optimize the pH for the present study, various buffer solutions with pH ranges 3-10 were examined. Figure **4B** clearly shows the effect of pH on the peak currents and potentials of PZM. The anodic peak currents gradually increase with the increase in the pH 3-10. Moreover, the maximum peak current response was observed at pH 7, after that the peak currents are decreased because the electrode surface has become saturated. Hence the pH 7.0 was taken as optimum for duration of the experimental work.

The deposition time was studied for 30-180 sec. The peak currents increase with increase in the deposition time from 30 s to 120 s. A longer deposition time was favoured for the adsorption of a higher number of PZM molecules on the electrode surface. After 120 s the peak currents were decreased, because the electrode surface was now saturated. Hence a deposition time of 120 s was used for further analy-

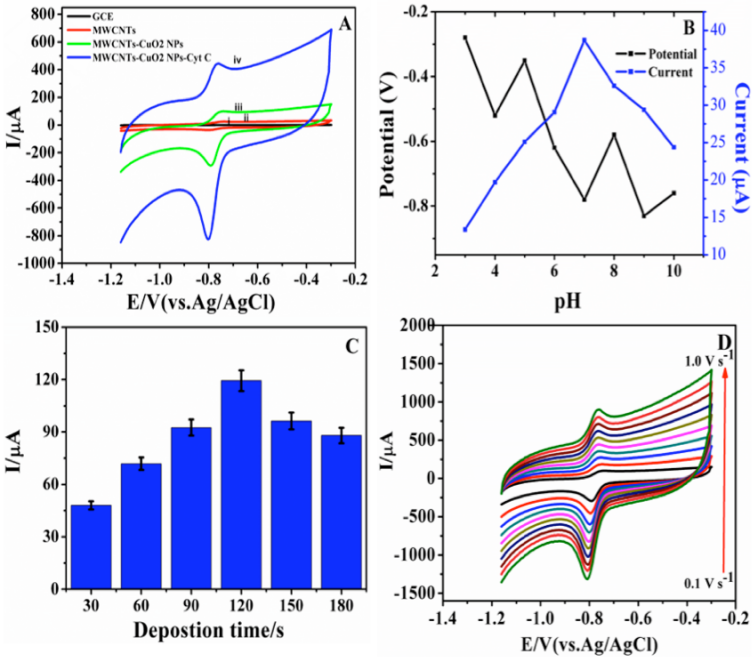

Fig. (4). (A) Cyclic Voltammograms of 0.1 mM PZM at bare **(i)** GCE, **(ii)** MWCNTs/GCE **(iii)** CuO NPs/MWCNTs/GCE, and **(iv)** Cyt c/CuO NPs/MWCNTs/GCE. **(B)** Peak potential and current response with respect to change in pH (3-10) with 0.1 mM PZM**. (C)** Various deposition times (30, 60, 90, 120,150 and 180 s) on peak current. **(D)** Cyclic Voltammograms of PZM at various scan rates from inner to outer (10,20,30,40,50,60,70,80,90 and 100 V s^{-1}).

sis (Fig. **4C**). The effect of scan rate was studied in order to investigate the nature of the surface coated electrode. The CV experiment was performed with PZM at a concentration of 0.1 mM and the redox electrochemical responses were investigated between 10 to 150 mV s^{-1}. The anodic peak currents and cathodic peak currents increase linearly with the square root of the scan rates, and the diffusion controlled oxidation and reduction process occur at Cyt c/CuONPs/ MWCNTs/GCE. The dependence of the anodic peak currents and cathodic peak currents ratios on the scan rate is different from unity, and this ratio was increased as the scan rate was increased. Based on these results, a scan rate of 50 mV s^{-1} was chosen as optimum, and used in this work.

3.6. Quantitative Analysis of PZM

The DPV method was employed with Cyt c/CuONPs/MWCNTs/GCE for the quantification of PZM. The working parameters viz., pulse time 0.045 s, potential range -1.1 to -0.6 V, pulse amplitude 0.055 V, were used for this study. The Cyt c/CuONPs/MWCNTs/GCE fabricated electrode shows one reduction peak at -0.80 V with higher currents at pH 7.0. The peak currents for PZM increase linearly with an increase in the concentration of PZM (3 to 30 μM) as shown in Fig. (**5**). The calibration curve obtained by plotting peak current verses concentration of PZM as shown as an insert in Fig. (**5**). The linear equation and correlation coefficient was found to be i_{pa} =2.249 c + 2.930 (R^2 = 0.994). Furthermore, the limit of detection and limit of quantification were calculated according to the ratio of 3 σ/b and 10 σ/b respectively, where b is the slope of the calibration curve and sigma is the standard deviation values from the five voltammetric runs for the blank electrode. The LOD and LOQ were found to be 0.0038 μM and 0.0129 μM respectively. Furthermore, the LOD and LOQ values were compared with the previous reports (Table **1**), and reveal the high performance of the developed sensor towards PZM.

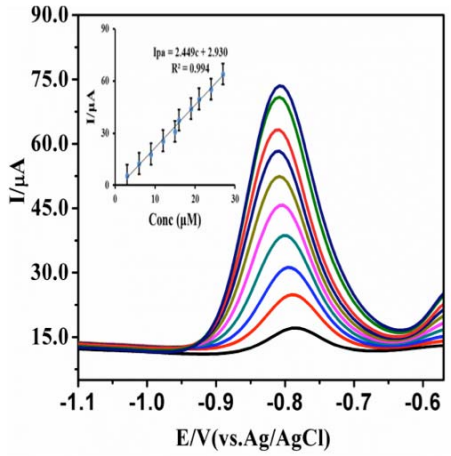

Fig. (5). DPV response of 3 to 30 μM of PZM at Cyt c/CuO NPs/MWCNTs/GCE at pH 7.0; scan rate 0.015 V s^{-1}; deposition time 120 s; pulse amplitude 0.055 V; and pulse time: 0.045 s. (Inset calibration plot)

3.7. Applications to Real Pharmaceutical Samples

The real sample analysis is a most significant application to determine electrochemical behavior of the fabricated electrode towards the analyte. The commercial pharmaceutical samples were used to determine the electrochemical performance of the Cyt c/CuONPs/MWCNTs/GCE sensor. The obtained DPV results clearly show the electrochemical enrichment of the PZM reduction peak. The developed sensor showed good percentages of recovery viz., 99.5 % and 98.2

Table 1. Comparison of electrochemical performance of the developed sensor with previous reports.

Electrode	Method	LOD	Buffer & pH	Ref
SPCE/EPH	DPV& SWV	68 μM	PBS (1.0)	[40]
GO/PAG/GCE	CV & DPV	3.28 μM	PBS (7.0)	[41]
PMET/ERGO/GCE	CV & DPV	0.16 μM	PBS, (7.0)	[42]
Poly(Gly)/GCE	CV & DPV	0.035 μM	PBS (7.5)	[43]
GNS/ZnO/CPE	CV & DPV	0.0431 μM	BRS (7.0)	[44]
Poly (L-Cys)/GCE	CV& SWV	0.113 μM	BRS (1.0)	[45]
PARS/ GCE	CV & DPV	1.2 μM	HAc-NaA c (4.5)	[46]
Cyt c/CuO NPs / MWCNTs /GCE	CV & DPV	0.0038 μM	PBS (7.0)	This work

SPCE/EPH: screen printed electrode modified with poly-histidine prepared by histidine monomer electro polymerization; GO/PAG/GCE: graphene oxide and poly arginine poly-L-methionine modified GCE; GCE: glassy carbon electrode; CPE: carbon paste electrode; PMET/ERGO/GCE: poly L methionine and reduced graphene oxide modified GCE; Poly (Gly)/GCE: poly L methionine modified GCE; GNS/ZnO/CPE: graphene zinc oxide modified CPE; Poly (L-Cys)/GCE: Poly L-cysteine (Poly(L-Cys)) modified glassy carbon electrode; PARS/ GCE: A poly-alizarin red S modified glassy carbon electrode: Cyt c/CuO NPs/MWCNTs/GCE: cytochrome c enzyme, copper dioxide, multi wall carbon nanotubes modified GCE.

Table 2. Determination of PZM in different pharmaceutical samples using proposed sensor (n = 6).

Tablet Sample (mg)	Found (mg)	Recovery (%)	Added (mg)	Found (mg)	Recovery (%)
Sample1 (400 mg)	398.2	99.5	50	49.1	98.2
Sample 2 (500 mg)	491.3	98.2	50	48.4	96.8

*n= average determinations

% respectively, for the two different pharmaceutical samples. The recovery percentages are very close to the official monograph of PZM. (Not less than 90 % and not more than 110 % of PZM are contained in real labeled samples) [39]. The results are summarized in the Table **2**.

In order to evaluate the selectivity of the proposed sensor, interference studies were performed with the real pharmaceutical samples (Antib-4 and Rimstar 4-Fdc). These tablets have some common interferents like isoniazid, rifampicin and ethambutol in its composition. The maximum concentration of the interfering substance caused an error of less than ±5% towards the determination of PZM. This indicates the extremely high selectivity of the developed sensor towards the determination of PZM in real pharmaceuticals.

3.8. Stability and reproducibility of Cyt c/CuONPs/ MWCNTs/GCE

The stability and reproducibility of the Cyt c/CuONPs/ MWCNTs/GCE were studied by using CV and DPV measurements with 0.1 mM PZM. The developed sensor was investigated by keeping the electrode in PBS (pH 7.0) for 15 days and then the CV was recorded and compared to the previous CV results. Based on the obtained results, the peak current decreased by 1.35 % for Cyt c/CuONPs/MWCNTs/ GCE after 15 days. This indicates the stability of the proposed sensor. The reproducibility of Cyt c/CuONPs/ MWCNTs/GCE was measured by performing the analysis at different time intervals (10-50 days). The fabricated sensor was stored in the refrigerator at 4 ^{o}C, and after ten days the initial response of Cyt c/CuONPs/MWCNTs/GCE was 94 %, and after 50 days it decreases to 89.32 %. According to the results obtained the fabricated electrode exhibits high stability and reproducibility.

CONCLUSION

Combining unique properties of the fabricated materials such as high surface area, increased electrocatalytic activity and greater adsorptive properties, a Cyt c/CuONPs/ MWCNTs/GCE was developed for the determination of PZM. In the present work, the developed sensor showed a good catalytic activity towards PZM, due to the increased electrochemical sensing mechanism for PZM. The modified electrode was successfully characterized by the TEM, FT-IR, TGA and XRD techniques. The fabricated sensor showed enhanced peak currents and low detection limits with PZM. The proposed sensor showed excellent sensitivity, selectivity and low detection limits. In addition, the developed sensor was applied for the determination of PZM in real pharmaceutical samples, which reflect good recovery percentages. It is evident that the proposed method will serve as a standard protocol for the determination of PZM in various pharmaceutical samples and would be of great help to pharmaceutical industries in the future.

ETHICS APPROVAL AND CONSENT TO PARTICIPATE

Not applicable.

HUMAN AND ANIMAL RIGHTS

No Animals/Humans were used for studies that are base of this research.

CONSENT FOR PUBLICATION

Not applicable.

CONFLICT OF INTEREST

The authors confirm that this article content has no conflict of interest.

ACKNOWLEDGEMENTS

This project was financially supported by the Durban University of Technology, Durban, South Africa.

REFERENCES

[1] Van den Boogaard, J.; Kibiki, G.S.; Kisanga, E.R.; Boeree, M.J.; Aarnoutse, R.E. New drugs against tuberculosis: problems, progress, and evaluation of agents in clinical development. *J Antimicrob Chemother*, **2009**, 53, 849-862.

[2] Sivakumar, M.; Cheemalapati, S.; Chen, S.M.; Devadas, B. Anti tuberculosis Drug Pyrazinamide Determination at Multiwalled Carbon Nanotubes/ Graphene Oxide Hybrid Composite Fabricated Electrode. *Int. J. Electrochem. Sci*, **2015**, 10, 7049 - 7062.

[3] Khuhawar, M.Y.; Rind, F.M.A. Liquid chromatographic determination of isoniazid, pyrazinamide and rifampicin from pharmaceutical preparations and blood. *J Chromatogr B*, **2002**, 766, 357–363.

[4] Nagaraja, P.; Srinivasa Murthy, K.C.; Yathirajan, H.S. Spectrophotometric determination of isoniazid with sodium1,2-naphthoquinone-4-sulphonate and cetyltrimethyl ammonium bromide. *Talanta*, **1996**, 43, 1075-1080.

[5] Pyrazinamide, *Tuberculosis*, **2008**, 88, 141-144.

[6] Janin, Y.L. Antituberculosis drugs: ten years of research. *Bioorg. Med. Chem. Lett*, **2007**, 15 2479-513.

[7] Tafazoli, S.; Mashregi, M.; O'Brien, P.J. Role of hydrazine in isoniazid-induced hepatotoxicity in a hepatocyte inflammation model. *Toxicol. Appl. Pharmacol*, **2008**, 22994-101.

[8] Faria, A.F.; De Souza, M.V.; Bruns, R.E.; De Oliveira, M.A. Simultaneous determination of first-line anti-tuberculosis drugs by capillary zone electrophoresis using direct UV detection. *Talanta*, **2010**, 82, 333-339.

[9] Madan, J.; Dwivedi, A.K.; Singh, S. Estimation of antitubercular drugs combination in pharmaceutical formulations using multivariate calibration. *Anal Chim Acta*, **2005**, 53, 8345-353.

[10] Maher, H.M.; Youssef, R.M. Simultaneous determination of ternary drug mixtures using square wave polarography subjected to non-parametric and chemometric peak convolution. *Chemometr. Intell. Lab*, **2008**, 94, 95-103.

[11] John Conte, E.; Emil Lin, J.; Zurlinden, E. High-Performance Liquid Chromatographic Determination of Pyrazinamide in Human Plasma, Broncho alveolar Lavage Fluid, and Alveolar Cells. *J Chromatogr*, **2000**, 38, 33-37.

[12] Bhanushali, C.J.; Zidan, A.S.; Rahman, Z.; Habib, M.J. Ion-pair chromatography for simultaneous analysis of ethionamide and pyrazinamide from their porous micro particles. *AAPS Pharm Sci Tech*, **2013**, 14, 1313-1320.

[13] Goicoechea, H.C.; Olivieri, A.C. Simultaneous determination of rifampicin, isoniazid and pyrazinamide in tablet preparations by multivariate spectrophotometric calibration. *J pharm Biomed Anal*, **1999**, 20, 681-686.

[14] Isoannou, P.C. A simple and rapid fluorimetric method for the micro determination of isonicotinic acid hydrazide. *Talanta*, **1987**, 34, 857–860.

[15] Kalambate, P.K.; Rawool, C.R.; Srivastava, A.K. Voltammetric determination of pyrazinamide at graphene-zinc oxide nanocomposite modified carbon paste electrode employing differential pulse voltammetry. *Sens. Actuators, B*, **2016**, 23, 7196-205.

[16] Mobin, S.M.; Sanghavi, B.J.; Srivastava, A.K.; Mathur, P.; Lahiri, G.K. Biomimetic sensor for certain phenols employing a copper (II) complex. *Anal. Chem*, **2010**, 82, 5983–5992.

[17] Dreyer, D.R.; Park, S.; Bielawski, C. W.; Ruoff, R.S. The chemistry of graphene oxide. *Chem. Soc. Rev*, **2010**, 39, 228-240.

[18] Cui, S.; Canet, R.; Derre, A.; Couzi, M.; Delhaes, P. Characterization of multiwall carbon nanotubes and influence of surfactant in the nanocomposite processing. *Carbon*, **2003**, 41, 797-809.

[19] Wu, X.; Chai, Y.; Yuan, R.; Zhong, X.; Zhang, J. Synthesis of multiwall carbon nanotubes-graphene oxide-thionine-Au nanocomposites for electrochemiluminescence detection of cholesterol. *Electrochim. Acta*, **2014**, 129, 441-449.

[20] Liu, B.; Ouyang, X.; Ding, Y.; Luo, L.; Xu, D.; Ning, Y. Electrochemical preparation of nickel and copper oxides-decorated graphene composite for simultaneous determination of dopamine, acetaminophen and tryptophan. *Talanta*, **2016**, 146, 114-121.

[21] Wang, G.; Gu, A.; Wang, W.; Wei, Y.; Wu, J.; Wang, G.; Zhang, X.; Fang, B. Copper oxide nanoarray based on the substrate of Cu applied for the chemical sensor of hydrazine detection. *Electrochem. Commun*, **2009**, 11, 631-634.

[22] Soomro, R.A.; Nafady, A.; Sirajuddin, N.; Memon, T.H.; Sherazi, N.H. Kalwar. L-cysteine protected copper nanoparticles as colorimetric sensor for mercuric ions. *Talanta*, **2014**, 130, 415-22.

[23] Pedrosa, V.A.; Epur, R.; Benton, J.; Overfelt, R.A.; Simonian, A.L. Copper nanoparticles and carbon nanotubes-based electrochemical sensing system for fast identification of tricresyl-phosphate in aqueous samples and air. *Sens. Actuators, B*, **2009**, 140, 92-97.

[24] Luo, J.; Jiang, S.; Zhang, H.; Jiang, J.; Liu, X. A novel non-enzymatic glucose sensor based on Cu nanoparticle modified graphene sheets electrode. *Anal. Chim. Acta*, **2012**, 709, 47-53.

[25] Dormeshkin, D.; Gilep, A.; Sergeev, G.; Usanov, S. Development of CYB5-fusion monitoring system for efficient periplasmic expression of multimeric proteins in Escherichia coli. *Protein Expr. Purif*, **2016**, 128, 60-66.

[26] Tafani, M.; Karpinich, N.O.; Hurster, K.A.; Pastorino, J.G.; Schneider, T.; Russo, M.A.; Farber, J.L. Cytochrome c release upon Fas receptor activation depends on translocation of full-length bid and the induction of the mitochondrial permeability transition. *J Biol Chem*, **2002**, 277, 10073-10082.

[27] Zhao, Y.; Wang, Z.B.; Xu, J.X. Effect of cytochrome c on the generation and elimination of O_2 and H_2O_2 in mitochondria. *J Biol Chem*, **2003**, 278, 2356-60.

[28] Aparna1, Y.; Venkateswara Rao, K.; Srinivasa Subbarao, P. Preparation and Characterization of CuO Nanoparticles by Novel Sol-Gel Technique. J.Nano Electron. phys, **2012**, 4, 1-4.

[29] Kshirsagar, J.M.; Shrivastava, R.; Adwani, P.S. Preparation and characterization of copper oxide nanoparticles and determination of enhancement in critical heat flux. *Therm Sci*, **2015**, 26-26.

[30] Ramesh, C.; Hariprasad, M.; Ragunathan, V.; Jayakumar, N. A novel route for synthesis and characterization of green Cu2O/PVA nano composites. *J. Appl. Eng. Sci. Res*, **2012**, 1, 201-206.

[31] Dodoo-Arhin, D.; Leoni, M.; Scardi, P. Micro emulsion synthesis of copper oxide nano rod-like structures. *Mol. Cryst. Liq. Cryst. Sci, Technol. Set. A*, **2012**, 555, 17-31.

[32] Ethiraj, A.S.; Kang, D.J. Synthesis and characterization of CuO nanowires by a simple wet chemical method. *Nanoscale Res Lett*, **2012**, 7, 70.

[33] Morales, J.; Sánchez, L.; Martín, F.; Ramos-Barrado, J.R.; Sánchez, M. Nanostructured CuO thin film electrodes prepared by spray pyrolysis: a simple method for enhancing the electrochemical performance of CuO in lithium cells. *Electrochim. Acta*, **2004**, 49, 4589-4597.

[34] Xinglong, G.; Wang, G.; Yang, J.; Park, J.; Wexler, D. Chemical synthesis, characterisation and gas sensing performance of copper oxide nanoribbons. *J Mater. Chem*, **2008**, 18, 965-969.

[35] Nxusani, E.; Ndangili, P.M.; Olowu, R.A.; Jijana, A.N.; Waryo, T.; Jahed, N.; Ajayi, R.F.; Baker, P.; Iwuoha, E.I. 3-Mercaptopropionic Acid Capped Ga_2Se_3nanocrystal-CYP3A4 Biosensor for the Determination of 17-Alpha-Ethinyl Estradiol in Water. *Nano Hybrids*, **2012**, 1, 1-22.

[36] Bhajanthri, N.K.; Arumugam, V.K.; Chokkareddy, R.; Redhi G.G. Ionic liquid based high performance electrochemical sensor for ascorbic acid in various foods and pharmaceuticals. *J. Mol. Liq*, **2016**, 222, 370–376.

[37] Friedrich, M.G.; Giebeta, F.; Naumann, R.; Knoll, W.; Ataka, K.; Heberle, J.; Hrabakova, J.; Murgida, D.H.; Hildebrandt, P. Active

site structure and redox processes of cytochrome c oxidase immobilized in a novel biomimetic lipid membrane on an electrode. *Chem Commun (Camb)*, **2004**, 2376-2377.

[38] Bhgelovfi, J.; Antalik, M.; Tomori, Z. Effect of polyglutamate on the thermal stability of ferricyytochrome c. *Biochem. Mol. Biol. Int.* **1997**, 43, 891-900.

[39] World health organization. Rifampicin, isoniazid and pyrazinamide dispersible tablets. http://www.who.int/medicines/publications/pharmacopoeia/QAS07/222rev1/Rif-Iso-Pyraz-dispers. final.pdf (October **2007**).

[40] Bergamini, M.F.; Santos, D.P.; Zanoni, M.V.B. Electrochemical behavior and voltammetric determination of pyrazinamide using a poly-histidine modified electrode. *J Electroanal Chem* **2013**, 690, 47-52.

[41] Devadas, B.; Cheemalapati, S.; Chen, S.M.; Ali, M.A.; Al-Hemaid, F.M.A. Highly sensing graphene oxide/poly-arginine-modified electrode for the simultaneous electrochemical determination of buspirone, isoniazid and pyrazinamide drugs. *Ionics*, **2014**, 21, 547-555.

[42] Cheemalapati, S.; Devadas, B.; Chen, S.M. Highly sensitive and selective determination of pyrazinamide at poly-L-methionine/reduced graphene oxide modified electrode by differential pulse voltammetry in human blood plasma and urine samples. *J Colloid Interface Sci*, **2014**, 418, 132-139.

[43] Ferraz, B.R.L.; Leite, F.R.F.; Malagutti, A.R. Highly sensitive electrocatalytic determination of pyrazinamide using a modified poly(glycine) glassy carbon electrode by square-wave voltammetry. *J Solid State Electrochem*, **2015**, 20, 2509-2516.

[44] Kalambate, P.K.; Rawool, C.R.; Srivastava, A.K. Voltammetric determination of pyrazinamide at graphene-zinc oxide nanocomposite modified carbon paste electrode employing differential pulse voltammetry. *Sens. Actuators, B,* **2016**, 237, 196-205.

[45] Ferraz, B.R.L.; Leite, F.R.F.; Malagutti, A.R. Simultaneous determination of ethionamide and pyrazinamide using poly (l-cysteine) film-modified glassy carbon electrode. *Talanta*, **2016**, 154, 197-207.

[46] W.li. Zhang, X.li. Niu, Q.q. Jiang, P.p. Zhang Electrochemical behaviors of pyrazinamide at poly (alizarin red S) modified electrode, *Huaxue Shiji*, **2015**, 37, 506–510.

Int. J. Electrochem. Sci., 12 **(2017)** 9190 – 9203, doi: 10.20964/2017.10.13

International Journal of ELECTROCHEMICAL SCIENCE
www.electrochemsci.org

A Novel Electrode Architecture for Monitoring Rifampicin in Various Pharmaceuticals

Rajasekhar Chokkareddy, Natesh Kumar Bhajanthri[*], *Gan G Redhi*[*]

Electroanalytical Laboratories, Department of Chemistry, Durban University of Technology, P.O Box 1334, Durban 4000, South Africa.
[*]E-mail: redhigg@dut.ac.za, nateshkumar786@gmail.com

Received: 24 March 2017 / *Accepted:* 25 July 2017 / *Published:* 12 September 2017

The present work involves the fabrication of glassy carbon electrode (GCE) with iron oxide nanoparticles (Fe_3O_4NPs) and multiwalled carbon nanotubes (MWCNTs) composite. Further it was immobilized with Coenzyme q (Co en-q/ Fe_3O_4NPs/MWCNTs/GCE) to enhance the electrochemical performance of the modified electrode for the determination of rifampicin (RIF). The designed sensor was successfully characterized by Fourier transform infrared spectroscopy (FT-IR), transmission electron microscopy (TEM), thermo gravimetry (TGA) and x-ray diffraction (XRD) studies. The electrochemical oxidation of RIF has been studied by cyclic voltammetry (CV) and differential pulse voltammetric techniques (DPV). The enzyme immobilized sensor surface area was calculated and found to be 10.03 mm^2. This larger surface area was responsible for the oxidation of more number of RIF molecules on the surface of sensor. The RIF shows two anodic peaks at + 0.10 V and + 0.72 V in phosphate buffer solution (PBS) pH 7.5. The cyclic voltammetric measurements reveals that the developed sensor exhibited an enhanced electrochemical platform with an approximately eight-fold increment in the anodic peak currents. Under the optimized conditions, a good linear relationship was observed between peak currents and RIF concentration. The studied linearity range (2 – 20 µM) showed a limit of detection (LOD) of 0.032 µM, 0.413 µM and limit of quantification (LOQ) of 1.069 µM, 1.258 µM for anodic peaks I and peaks II respectively. The proposed sensor showed longstanding stability and high reproducibility. The method was successfully applied for the determination of RIF in pharmaceutical tablets without any sample pre-treatment.

Keywords: Biosensor, Rifampicin, voltammetry, Co en-q, pharmaceutical samples

1. INTRODUCTION

Infectious diseases are fatal enemies of the global population. Tuberculosis (TB) is an infection disease caused by *Mycobacterium tuberculosis*. However, TB is found in every country of the world, and in 2012, the largest number of new cases was reported in Asia and African countries, accounting for 80% of new cases globally. In order to prevent TB, rifampicin (3-[(4-methyl-1-piperazinyl) imino]

methyl rifamycin) has been prescribed as a single combination with first line anti TB drugs (isoniazid, pyrazinamide and ethambutol) at fixed dosages [1, 2]. The over dosage of RIF produces many side effects such as headaches, kidney damages, nausea, vomiting and liver diseases [3]. A literature survey reveals that several analytical methods, such as high-performance liquid chromatography [4-6], UV-Visible spectro photometric method [7], capillary electrophoresis [8], fluorimetry [9] and electroanalytical methods have been employed for the determination of RIF. However, most of the methods are expensive, complicated, require sample pretreatment, and expert knowledge of electrochemical methods. In electrochemical methods, cyclic voltammetry, differential pulse voltammetric techniques were majorly used in RIF analysis. The electrochemical method involving modified electrodes are receiving more attentions from researchers for the analysis of pharmaceutical samples. According to the literature survey, DNA-modified carbon paste electrodes [10], cyclodextrin based sensors [11], cytochrome P450-2E1 metabolised nano biosensors [12], HRP-based biosensors [13] have been reported for RIF analysis. However, the above mentioned electrode fabrication and the methodologies involves complexity and need highly sophisticated laboratory equipment and condition.

Currently, MWCNTs are widely used as an electrode coating material, due to the favourable specialized properties. It possess large specific surface area, good adsorption properties, electrochemical bond expansion, catalytic activities as well as good chemical and thermal stability [14]. They can be modified and functionalized there by making it suitable for anchoring the nanoparticles on the external surface and improving the sensitivity of the electrochemical response [15]. Metal oxide nanoparticles have numerous advantages such as high electron conductivity, biodegradability, low cost and simple preparation methods. Owing to these advantages of metal oxide nano particles, they are extensively used as anchoring electrochemical substances in modified sensors. In recent years, many metal oxide nanoparticles (CuO_2, TiO_2, Fe_3O_4, ZnO, and Ag_2O) have been used in biosensors for the fabrication of electrodes. Among these Fe_3O_4 nanoparticles has unique properties such as smaller particle size with larger surface area, provide enhanced selectivity and sensitivity for this method, and facilitate the electron transfer process at the electrode and without interference [16, 17]. Fe_3O_4 generally conjugates with enzymes it considers as biologically and electro catalytically active [18]. The Co en-q is a fat-soluble vitamin and functions as an antioxidant. Its performs as an electron transporter in the electron transport chain [19]. This facilitates the fast transfer of electrons from RIF to the electrode surface and leads to the enrichment of electroactivity of the fabricated sensor. Additionally, it generates the electrophilic site which increase the sensitivity and limits of detection of the fabricated electrode. In the present work GCE was coated with MWCNTs, it was further capped with Fe_3O_4NPs and finally immobilized with Co en-q for the determination of RIF. The aim of this work is to explore the potentialities of the biosensor and develop a novel, rapid and accurate voltammetric method for the determination of RIF in various pharmaceutical formulations. A voltammetric sensor was optimized by testing with many methods of electrode coating, and the best results were the use of Co en-q/ Fe_3O_4NPs/MWCNTs/GCE.

2. EXPERIMENTAL

2.1. Materials

Multiwalled carbon nanotubes (O.D. × 6-9 nm, 95% Carbon) and pure analytical grade of Rifampicin and Coenzyme-Q (≥95%) were purchased from Sigma Aldrich. N, N-dimethylformamide, sodium hydroxide, disodium hydrogen phosphate, sodium dihydrogen orthophosphate, sulfuric acid, ethanol, potassium bromide, iron (II) sulphate, nickel nitrate, acetic acid, folic acid, uric acid and iron (II) chloride tetrahydrate, were purchased from Capital Lab Suppliers (Durban, South Africa).

2.2. Instrumentation

Voltammetric measurements were performed with a 797VA Computrace from Metrohm (Herisau, Switzerland) equipped with the computrace 1.31 software. A glassy carbon electrode (3.0 mm diameter) or modified Co en-q/ Fe_3O_4NPs/MWCNTs/GCE as a working electrode, Ag/AgCl (saturated with KCl) reference electrode and platinum wire counter electrode were used for the electrochemical study. A digital pH meter (CRISON model 2000) was used for preparing the buffer solutions. The FT-IR spectra were recorded on Varian 800 FTIR Scimitar series spectrometer. Transmission electron microscope (TEM) images were obtained on a JEM 2100 LaB6 field emission transmission electron microscope. The TGA was performed with TGA/DSC1SF/1346 model, supplied with STAR^e software version 9.20 (Mettler Toledo). The entire experiment was carried out at room temperature. The working stock, standard and supporting electrolytic solutions were kept in the refrigerator at 4 ^oC.

2.3. Reagents

According to previous literature [20] with slight modification, 1.21 g (0.03 M) of $FeCl_2.4H_2O$ was dissolved in a 250 ml volumetric flask with deionized water. The 4 g (1 M) NaOH was dissolved in another 100 ml volumetric flask with deionized water. Further, 150 ml of $FeCl_2.4H_2O$ was taken into the 500 ml beaker and then slowly added 50 ml of 1M NaOH and subjected to heating at 100 ^oC on a hot plate for about 30 min with continuous stirring. After the completion of the reaction the reaction mixture turns into black colour precipitate from the original wine red colour. The precipitate was then washed several times with deionized water and filtered with Whatman-1 filter paper and then dried at 50 ^oC for 2 h. The newly formed Fe_3O_4NPs was kept in refrigerator for further use.

2.4. Preparation of Co en-q/ Fe_3O_4NPs/MWCNTs/GCE

Prior to use, the GCE was polished with an alumina slurry to obtain a mirror like surface, there after washed with deionized water and sonicated with ethanol and deionized water (50:50) to remove the alumina particles on electrode surface. It was finally rinsed with deionized water and dried in an oven. 0.10 mg of MWCNTs was dissolved in 4 ml of N, N-dimethyl formamide (DMF) and then kept

for ultra-sonication for 30 min, finally resulting in a black suspension, which was used for the modification of GCE.

Afterwards, 0.20 mg Fe_3O_4 and 0.20 mg of MWCNTs was dispersed into 5 ml of N, N-dimethyl formamide (DMF) by ultra-sonication for 1 h to give a black suspension. The resulting dispersion (5 µL Fe_3O_4/MWCNTs) was dropped on the surface of GCE and kept for drying in an oven at 50 ^oC for about 10 min. The electrode was then cooled to room temperature and thereafter 2 µL of Co en-q enzyme was added, and coated electrode left undisturbed at 4 ^oC for about 15 min for the complete enzyme immobilization process to occur, finally resulting in the Co en-q/ Fe_3O_4NPs/MWCNTs/GCE.

2.5. Preparation of tablet samples

Tablet samples containing RIF were purchased from the local pharmacy (Ebsar-2 Ds, R-Cin 600). The fabricated sensor was tested to determine the RIF in commercialized tablets via following procedure. Approximately 5-10 tablets were weighed and ground as a finely powdered sample. A 50 mg tablet sample was transferred into a 100 ml volumetric flask and dissolved in PBS. The resulting mixture was sonicated for 40 min. The analyses were performed via the standard addition method in DPV technique.

3. RESULTS AND DISCUSSION

3.1. Co en-q/ Fe_3O_4NPs/MWCNTs/GCE characterization

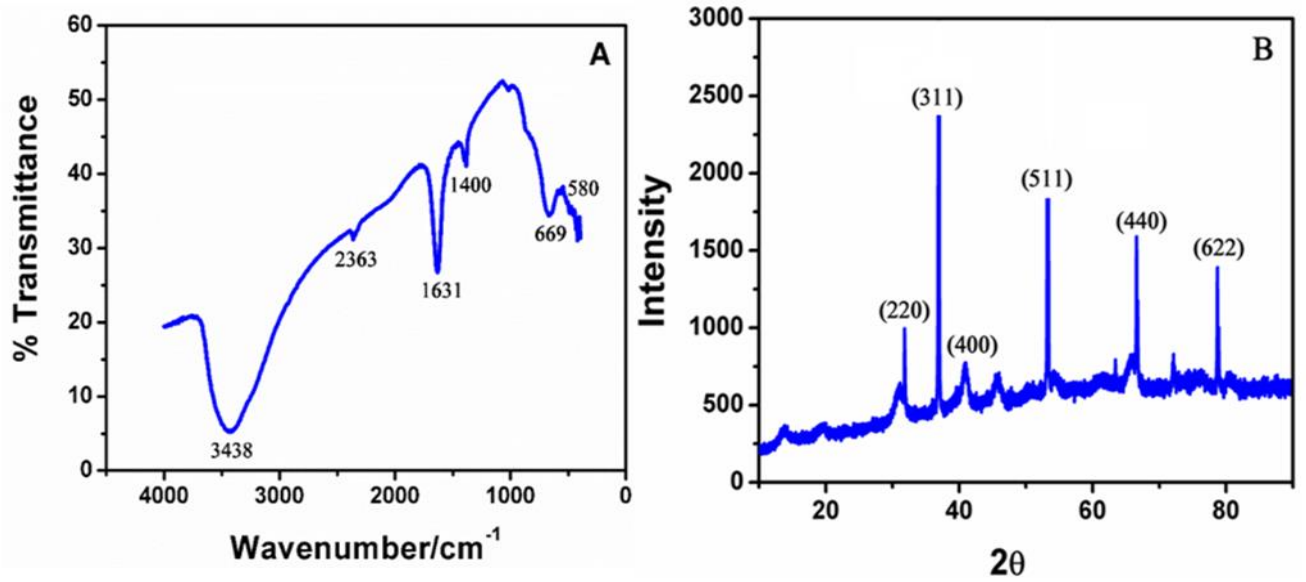

Figure 1. (A) FT-IR characterization of Fe_3O_4NPs. **(B)** XRD Image of Fe_3O_4NPs.

The FTIR spectra of the Fe_3O_4NPs are showed in fig. 1A. From the FTIR spectrum the band appeared at 580 cm^{-1} the peak associated with Fe-O presenting the tetrahedral side which can be attributed to Fe_3O_4 [21].The Fe_3O_4NPS can be seen by strong absorption band at around 669 cm^{-1} which corresponds to the Fe-O absorption. The band at 1400 cm^{-1} indicates –C-H bending vibrations.

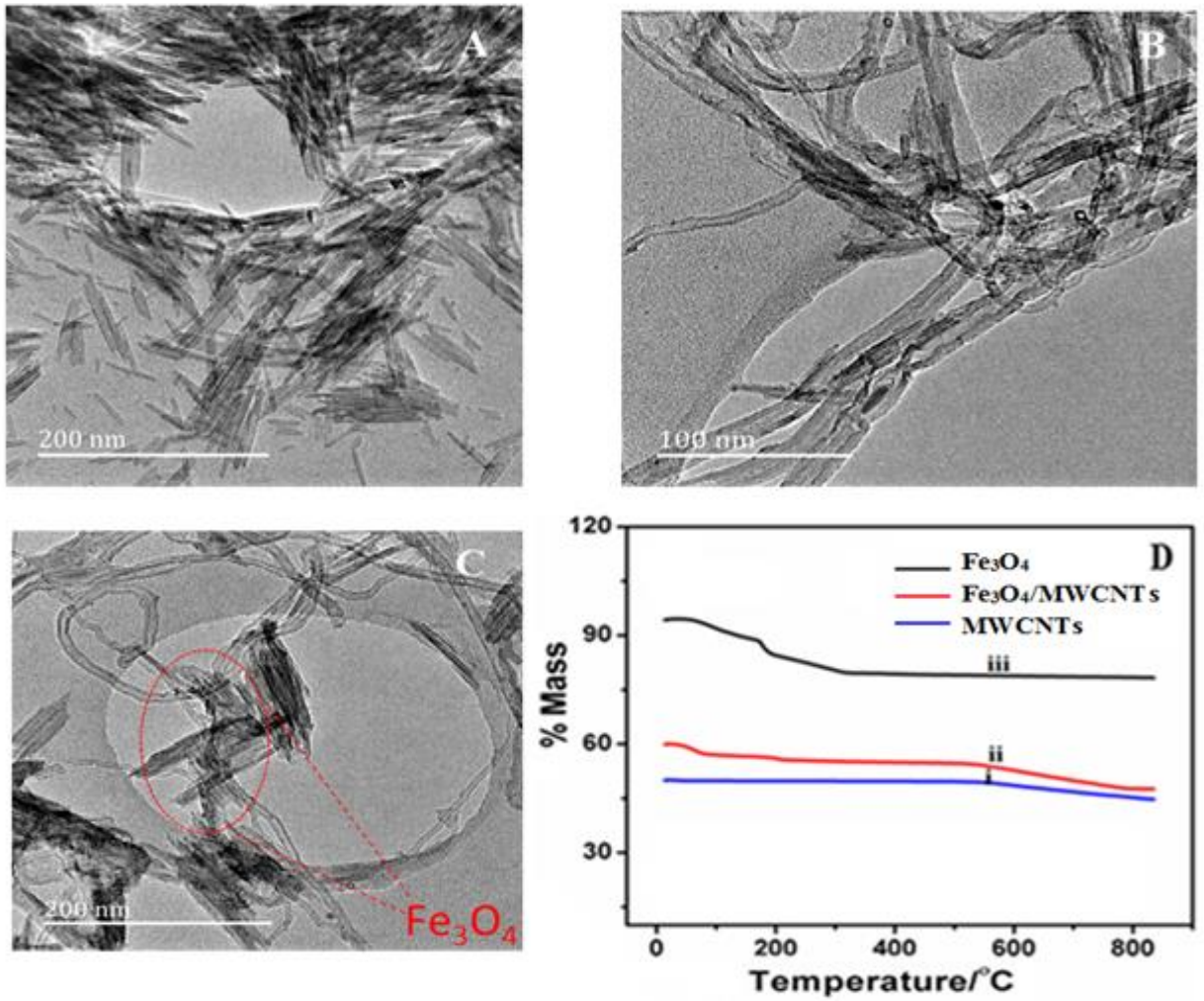

Figure 2. (A) TEM image Fe_3O_4NPs **(B)** Pure MWCNTs **(C)** MWCNTs- Fe_3O_4NPs **(D)** TGA curves for **(i)** MWCNTs **(ii)** Fe_3O_4NPs /MWCNTs and **(iii)** Fe_3O_4NPs

The intense band at 1631 cm^{-1} is attributed to stretching of OH mode of H_2O [22]. On the other hand the peak at 2363 cm^{-1} showed strong stretching of O=C=O. The peak at 3438 cm^{-1} is attributed to the stretching vibrations of OH arising from hydroxyl groups from the water on Fe_3O_4NPs [23]. Fig. 1B shown the x-ray diffraction pattern of the Fe_3O_4NPs. The Fe_3O_4NPs showed six specific peaks at 30.03^o, 35.52 ^{o}, 43.02 ^{o}, 53.6 ^{o}, 68.25 ^{o} and 76.32 ^{o}, corresponding to (220), (311), (400), (511), (440) and (622) respectively. The above strong diffraction intensities of the Fe_3O_4NPs reveals a the cubic spinal structure [24]. Fe_3O_4NPs shows a very high intensive peak at 35.52 ^{o} (311) indicating that the nanoparticles are ultrafine in nature, single cubic phase and small crystallite size. Based on the Debye-Scherer formula [25], the size of the Fe_3O_4NPs was also calculated and found to be approximately 15 nm in diameter.

$$d_{hkl} = \frac{0.9\lambda}{\beta \cos\theta} \quad (1)$$

Where β is the full width at half maximum value of XRD diffraction lines, λ is the wave length and θ is the half diffraction angle of 2θ.

Fig. 2A indicates TEM image of the synthesized Fe_3O_4NPS. These nanoparticles are in rod like geometry and they are aggregated like a bunch.

The fig. 2B clearly shown the tubular network like structure of MWCNTs. The fig. 2C shown reveals the adherence of Fe_3O_4NPS on the surface of the MWCNTs. Furthermore, the thermo gravimetric analysis of the MWCNTs, Fe_3O_4NPs/MWCNTs and Fe_3O_4NPs are shown in fig 2D. The thermograms for pure MWCNTs are shown with definite mass losses at 570 °C due to the carbon oxidation (black line fig. 2D). The Fe_3O_4NPs/MWCNTs shows that the mass losses at below 300 °C due to the loss of residual water in the sample [26]. On the other hand, the Fe_3O_4NPs losses minor mass at below 300 °C due to the evaporation of water. At 600 to 800 °C there is no significant mass loss, and this implies that there is only iron oxide at this range of temperature [27].

3.2. Electrochemical behavior of fabricated electrodes

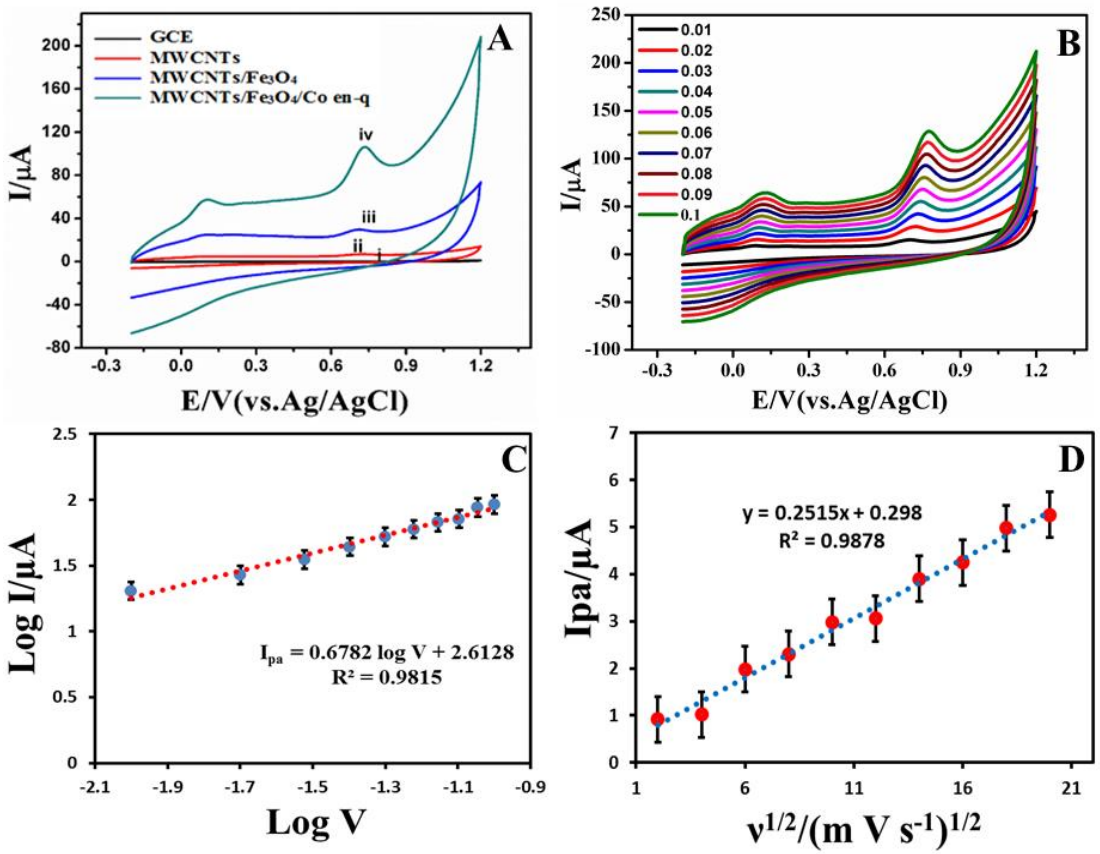

Figure 3. (A) Cyclic voltammograms of 0.1 mM RIF in 0.1M PBS (pH 7.5) **(i)** GCE, **(ii)** MWCNTs, **(iii)** MWCNTs/Fe_3O_4NPs/GCE, **(iv)** Co en-q/MWCNTs/Fe_3O_4NPs/GCE. **(B)** Cyclic voltammograms of 0.1mM RIF at scan rates 0.01, 0.02, 0.03, 0.04, 0.05, 0.06, 0.07, 0.08 0.09, and 0.1V s^{-1}. **(C)** Linear relationship of log (I_{pa}) and log (ν) **(D)** The relationship between anodic peak currents (I_{pa}) vs square root of scan rate.

Fig. 3A shows the electrochemical behaviors of RIF on bare GCE (black line), MWCNTs/GCE (red line), Fe_3O_4/MWCNTs/GCE (blue line) and Co en-q/ Fe_3O_4/MWCNTs/GCE (green line), investigated by the cyclic voltammetry.

The cyclic voltammograms of RIF gave two anodic peaks at + 0.1 V and + 0.7 V potentials. The bare GCE showed very low anodic peak currents 28 µA, whereas the MWCNTs/GCE and Fe_3O_4/MWCNTs/GCE showed 75 µA and 150 µA currents respectively (S Fig. 1). The Co en-q/ Fe_3O_4/MWCNTs/GCE showed the higher peak currents (220µA) than the remaining modified electrodes (fig. 3B). It can be concluded that the Co en-q has actively participated in the high electron transfer between the RIF molecule and fabricated electrode. Moreover, a graph drawn between log V and log I_{pa} shows a linear relationship and can be expressed as I_{pa} = 0.6782 log V+ 2.6128 (R^2 = 0.9815 fig. 3C). Simultaneously a graph was drawn between the anodic peak currents and square root of the scan rate ($\nu^{1/2}$), and the resulting linear equation can be express as $I_{pa} = 0.2515\ \nu^{1/2} + 0.298$ (R^2 = 0.9878) (fig. 3D). The results confirmed that the diffusion controlled mechanism is usual for the overall electrochemical reaction of RIF at the fabricated electrode surface [28-30]. According to these results an improved electrocatalytic effect of RIF at the fabricated electrodes is due to the increased surface to volume ratio and electronic conductivity. The fabricated electrode surface area was calculated by Randles-Sevick equation [31].

$$I_{pa} = 2.69\times10^5\ A\ C_0\ n^{3/2} D_R\ \nu^{1/2} \qquad (2)$$

Where I_{pa} denotes the anodic peak current, A the electrode area (A is surface area electrode, r_e is the radius of the rotating disc electrode, ($A=\pi r_e^2$)), C_o is the concentration of RIF, n is the number of electrons involved in the reaction, D_R is the analyte diffusion coefficient (cm^2/s), ν is scan rate ($V\ s^{-1}$). From the above equation the fabricated electrode and GCE surface area was estimated to be10.03 and 3.14 mm^2 respectively. The increased surface area and the presence of adsorptive sites in Co en-q resulting in the significant increase the anodic currents. Due to the high density of active sites and ketonic functional group in Co en-q, accelerating the electron transfer between fabricated electrode and RIF. Based on the obtained results indicates the Co en-q/ Fe_3O_4/MWCNTs/GCE sensor surface area was approximately three times greater than the GCE surface. Which is responsible for the high electrochemical oxidation of RIF (Scheme 1).

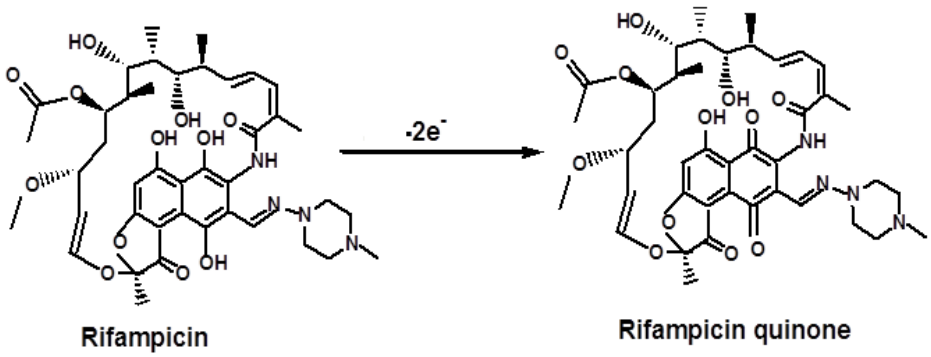

Scheme 1. Schematic illustration of the electro oxidation reaction of RIF leading to rifampicin quinone formation.

3.3. Effect of Co en-q concentration on the sensor response

The CV study was performed in order to determine the optimum concentration of Co en-q within the range of 1.2 to 14 µg mL^{-1}. The anodic peak currents were gradually increasing with the increase in concentrations Co en-q, from 1.2 to 6 µg mL^{-1} (Fig. 4). Beyond the concentration 6 µg mL^{-1} the current response decreased gradually. This is due to the steric hindrance of more accumulation of enzyme on the surface of the electrode, leading to inhibition of the electronic communication between RIF and the fabricated electrode. The concentration of Co en-q was (6 µg mL^{-1}) selected as optimum for the present study.

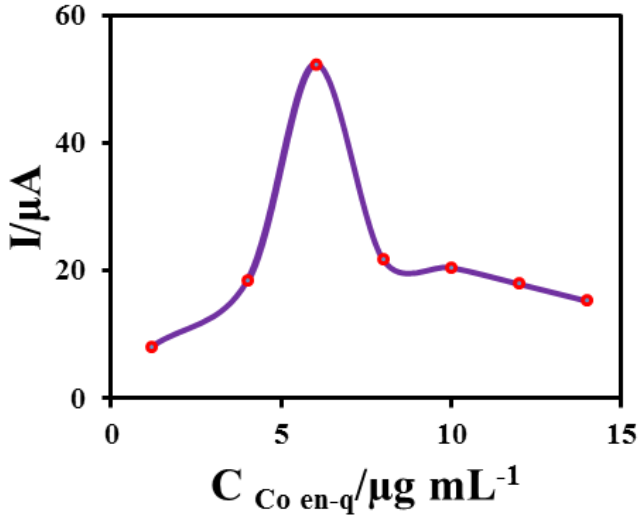

Figure 4. Effect of the Co en-q concentration on the response of the Co en-q/ Fe_3O_4/MWCNTs/GCE in 0.1 mM of RIF with PBS (pH 7.5) at ambient temperature.

3.4. Influence of pH, scan rates and deposition time

The electrochemical oxidation of RIF basically depends upon the range of the supporting electrolyte pH, because it affects of the responses of peak currents and peak potentials. Fig. 5A shows the electrochemical sensing abilities of modified electrode in the pH ranges from 2.5 to 9.5. The RIF gave well-defined anodic peak with high current response at pH 7.5, beyond pH 7.5 the peak current responses gradually decreased. According to these results pH 7.5 was choosen as optimum pH. Additionally, the relationship between peak potentials and pH values were plotted and shown in fig 5B.

The linear regression equation obtained in fig. 5B, E_p (V) = - 0.0688 pH + 0.8579 with correlation coefficient with R^2 = 0.9877 was approximately equal to the previously reported regression equation E_p (V) = -0.0591 pH + 0.3296 with R^2 = 0.9897[32, 33]. Based on the above results it is evident that two electrons were involved in electrode oxidation process. Fig. 3B shows the effect of scan rates ranges from 0.01 to 0.1 mVs^{-1} on the current response of RIF at the fabricated electrode. It can be seen that by increasing the scan rates, the anodic peak currents increase linearly with maximum peak current 0.1 m V s^{-1}. Thus 0.1 m V s^{-1} was used as an optimum scan rate for this study. It was

possible to calculate current efficiency of RIF at electrode deposition process based on the polarization curves (Fig.5C). The effect of deposition time was also monitored from 30 to 150 s at scan rate of 0.1 mV s^{-1} at pH 7.5 resulted in a deposition potential of -0.187 V. The current responses were maximum at 90 s, thus it is preferred as optimum deposition time for the entire study (Fig. 5C).

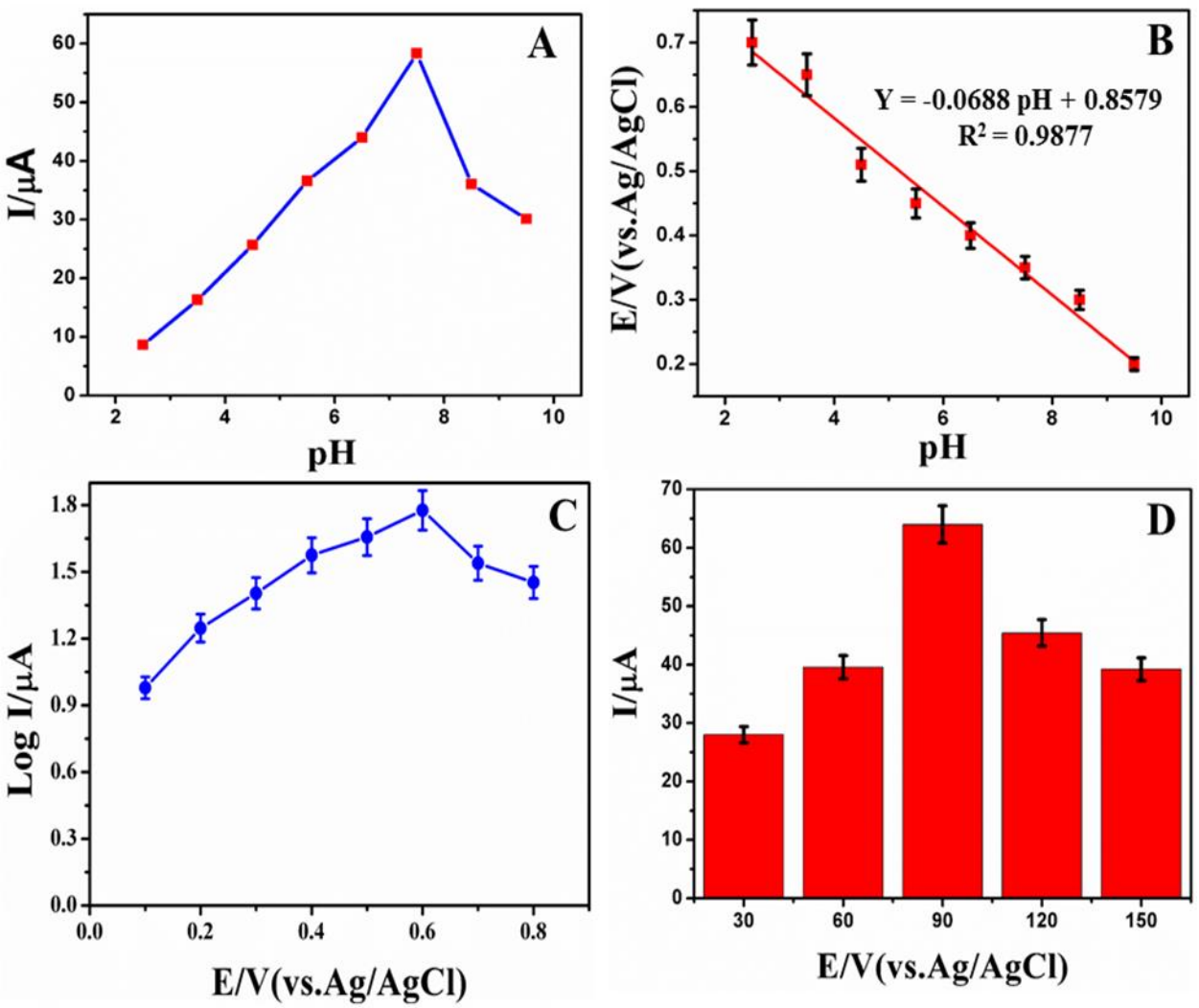

Figure 5. (A) Peak potential and peak currents response with pH ranges 2.5, 3.5, 4.5, 5.5, 6.5, 7.5, 8.5, and 9.5. **(B)** Peak potentials and pH **(C)** Polarization curve of Co en-q/ Fe_3O_4/MWCNTs/GCE. **(D)** Peak current responses vs different deposition time ranges 30, 60, 90, 120 and 150 s.

3.5. Determination of sensitivity of the developed sensor

DPV was used to evaluate the sensitivity of the fabricated sensor towards RIF. The working method parameters (scan rate 0.1 V s^{-1}, deposition time 90 s, pulse amplitude 0.050 mV and pulse time 0.040 s) were employed for the differential pulse voltammetric determination. The peak current responses on the concentration of RIF were obtained in the linear range 2 to 20 μM. The calibration

curves were linear over the concentration ranges from 2 to 20 μM for DPV. The calibration curve was then plotted for the concentration of RIF versus peak currents (Fig. 6).

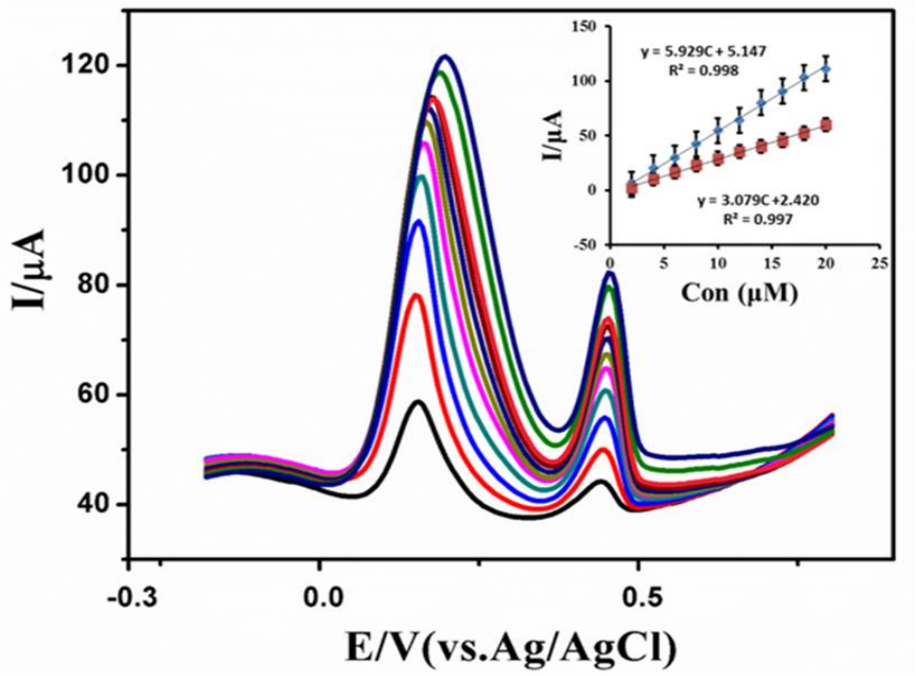

Figure 6. DPV recorded at Co en-q/Fe_3O_4NPs/MWCNTs/GCE at different concentrations of RIF (2–20 μM), inset: plot show for linear dependence of I_{pa} versus RIF. (Conditions for DPV pH: 7.5, accumulation time: 90 s, accumulation potential: 0.1Vs^{-1}, pulse amplitude: 0.050 V, pulse time 0.040 s).

Table 1. Comparison of some characteristics of the previously reported modified electrodes with Co en-q/ Fe_3O_4NPs/MWCNTs/GCE.

Electrode	Technique	LOD/ (μM)	Linear Range/ (μM)	Buffer/ pH	Ref
β-CD/PPY/Pt[1]	CA	1.69	10-50	PBS;7.06	[11]
AgNPs/PANSA/EGCYP2E1[2]	CV;DPV	0.05	2 - 14	PBS;7.4	[12]
CPE[3]	SWAdASV	0.05	0.1-6	PBS;7	[34]
$Ni(OH)_2$–RGO–GCE[4]	LSV	2.34	0.004–10	PBS;7	[13]
Co en-q/ Fe_3O_4NPs/MWCNTs/GCE[5]	CV; DPV	0.032	2-20	PBS;7	This work

β-CD/PPY/Pt- ß-cyclodextrin-polypyrrole coated on platinum electrode; Au/PVP-AgNPs/PANSA/EG-CYP2E1- Polyvinyl pyrrolidone/silver nanoparticles/poly (8-anilino-1-naphthalene sulphonicacid); CPE-Carbon paste electrode; $Ni(OH)_2$–RGO–GCE- Nickel hydroxide nanoparticles-reduced graphene oxide nanosheets coated on glassy carbon electrode; Coenzyme q/ Fe_3O_4NPs/MWCNTs/GCE- Coenzyme q- Fe_3O4 nanoparticles-multiwall carbon nanotubes coated on GCE; CA-chronoamperometry; CV-Cyclic voltammetry; DPV- Differential pulse polarography; SWAdASV-Square-wave adsorptive anodic stripping voltammetry; LSV-Linear sweep voltammetry; PBS-Phosphate buffer solution.

The linear regression equation can be expressed as I_{pa} = 5.929 C_{RIF} (μM) + 5.147 with correlation coefficient [(R^2 = 0.998) and I_{pa} = 3.079 C_{RIF} (μM) + 2.420 with correlation coefficient (R^2 = 0.997)] was determined by DPV. The limit of detection (LOD) and limit of quantization (LOQ) was calculated based on signal to noise ratios, by using the following equations.

$$LOD = \frac{3S_B}{b} \quad (3)$$

$$LOQ = \frac{10S_B}{b} \quad (4)$$

Where S_B is the standard deviation of the blank solution for three different runs, and b is the slope of the calibration curve. The limit of detection and limit of quantification was found to be 0.032 μM, 0.413 μM and 1.069 μM, 1.258 μM for anodic peak I and peak II respectively. The results obtained indicated that the Co en-q/ Fe_3O_4NPs/MWCNTs/GCE was an excellent biosensor for the sensitive determination of RIF. Compared to previous reports sensors comparison table (Table 1).

3.6. Interference study

Table 2. Effects of interferents on the anodic peak current responses for 0.1mM RIF at Co en-q/ Fe_3O_4NPs/MWCNTs/GCE based electrochemical sensor.

Interference species	Interferents/molar ratio of RIF	Responses ratio (%)
SO_4^{-2}	200	< 1.05
	400	< 2.09
Br^-	200	< 0.9
	400	< 1.06
NO_3^-	200	< 1.35
	400	< 2.49
Ni^{2+}	200	< 0.85
	400	< 1.79
Fe^{3+}	200	< 1.02
	400	< 2.89
K^+	200	< 0.95
	400	< 2.01
Glutamic acid	200	< 1.05
	400	< 2.09
Uric acid	200	< 1.25
	400	< 2.49
Folic acid	200	< 1.09
	400	< 3.01

The interference effect of the Co en-q/ Fe_3O_4NPs/MWCNTs/GCE with 0.1 mM RIF was evaluated in the presence of some organic, inorganic, and some other foreign interfering molecules through DPV method. The inorganic interference ions like $SO4^{-2}$, Br^-, NO_3^-, Ni^{2+}, $Fe^{3+}$and K^+ do not interfere with electrochemical response of RIF. The real samples were also investigated with the possible interference of these pharmaceutical samples with RIF peaks (The real pharmaceutical sample preparations and brands are mentioned in section 2.5). In addition, the organic interference like

glutamic acid, uric acid and folic acid do not interfere with the current response (≤6%) when present in 0.1 mM concentration of RIF. Based on the current results, the fabricated electrode was successfully used for the quantification of RIF in PBS (pH 7.5) and the results of this study are summarized in Table 2.

3.7. Analytical performances of the modified sensor

The repeatability of the fabricated sensor performance was calculated by using the anodic currents generated by the various analyte concentrations taken 10 times in a day. In the following day responses of 10 different preparations of electrodes in 0.1 M RIF solution were again tested. It was found that the repeatability decreased less than 5% to original current responses. In order to investigate the stability of Co en-q/ Fe_3O_4NPs/MWCNTs/GCE was measured by the CV peak currents in PBS with 0.1 M RIF was tested after 50 days. The current responses of the final biosensor remained at 80.25% of the initial response after 40 days as indicated in S Fig. 2A.

4. CONCLUSION

The present study demonstrated a simple and facile method for the modification of GCE with MWCNTs/Fe_3O_4NPs and Co en-q for the determination of RIF. The resulting MWCNTs, MWCNTs/Fe_3O_4NPs have been successfully characterized by using FT-IR, XRD and TEM. The electrochemical behaviour of RIF on the bare GCE and modified Co en-q/ Fe_3O_4/MWCNTs/GCE were observed using cyclic voltammetry. The obtained cyclic voltammetry results indicate the outstanding electrochemical sensing performance of the biosensor, with an increase (approximately eight-folds) of anodic peak currents. This indicates the high electrochemical response ability of developed biosensor towards the oxidation of RIF compared to the previous electrodes. Under the optimal experimental conditions, the anodic peak currents of RIF increased linearly within the concentration range 2-20 µM bearing the correlation coefficients of R^2 = 0.998, and R^2 = 0.997 respectively. The LOD and LOQs were calculated and found to be 0.032 µM, 0.413 µM and 1.069 µM, 1.258 µM for peak I and peak II respectively. This also reveals the high sensitivity and selectivity of the fabricated biosensor without interferents. The biosensor exhibited good reproducibility and stability as well as the successful analytical applications. The proposed biosensor was certainly adequate for the determination of RIF in the commercial pharmaceutical sample.

SUPPLEMENTARY INFORMATION

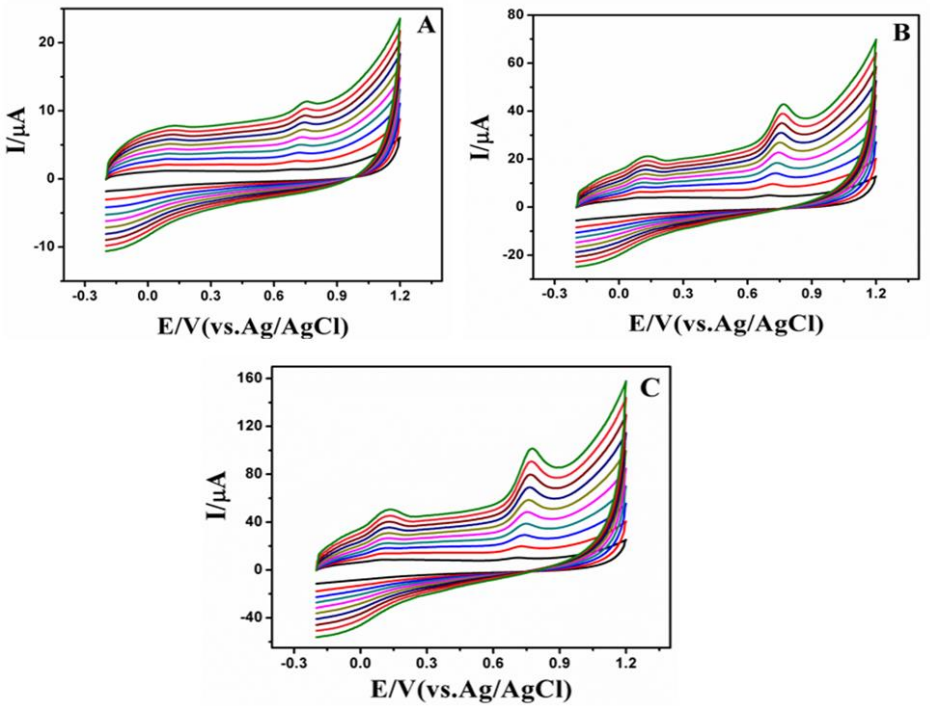

S Figure 1. Cyclic Voltammograms of RIF with **(A)** Bare GCE, **(B)** MWCNTs/GCE, (C) Fe_3O_4NPs/MWCNTs/GCE at various scan rates ranges 0.01, 0.02, 0.03, 0.04, 0.05, 0.06, 0.07, 0.08, 0.09 and 0.1V s-1.

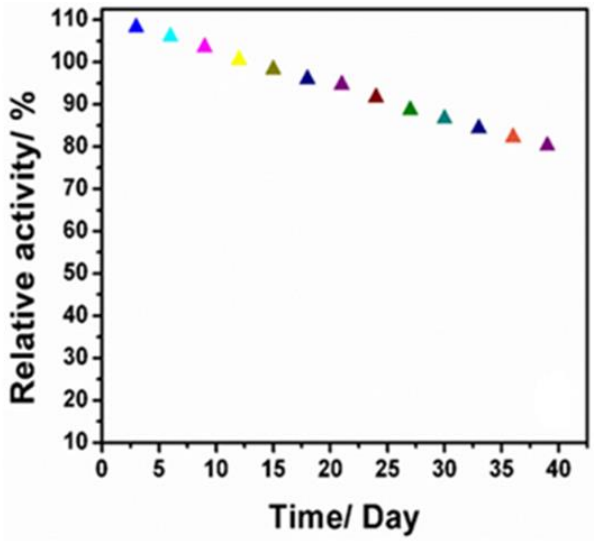

S Figure 2. (A) Stability for Co en-q/Fe_3O_4NPs/MWCNTs/GCE

References

1. W. Chen, B. Unnikrishnan, S.M. Chen, *Int. J. Electrochem. Sci.*, 7 (2012) 9138.
2. S. Cheemalapati, S. Palanisamy, S.M. Chen, *Int. J. Electrochem. Sci.*, 8 (2013) 3953.
3. M.S.M. Quintino, L. Angnes, *J. Pharm. Biomed. Anal.* 42 (2006) 400.

4. N.F. Atta, A. Galal, F.M. Abu-Attia, S.M. Azab, *Electrochim. Acta* 56 (2011) 2510.
5. A.K. Hemanth Kumar, I. Chandra, R. Geetha, K.S. Chelvi, V. Lalitha, G. Prema, *Indian J Pharmacol*, 36 (2004) 231.
6. J.B. Lecaillon, N. Febvre, J.P. Metayer, C. Souppart, *J. Chromatogr. B:Anal. Technol. Biomed. Life Sci.* 145 (1978) 319.
7. K. Asadpour-Zeynali, P. Soheili-Azad, *Electrochim. Acta* 55 (2010) 6570.
8. M. A. Karimi, A. H. Mehrjardi, M. M. Ardakani, R. B. Ardakani, M. H. Mashhadizadeh, S. Sargazi, *Int. J. Electrochem. Sci.*, 5 (2010) 1634.
9. J. van den Boogaard, G.S. Kibiki, E.R. Kisanga, M.J. Boeree, R.E. Aarnoutse, *Antimicrob. Agents Chemother.* 53 (2009) 849.
10. S.T. Girousi, I. Gherghi, M.K. Karava, *J. Pharm. Biomed. Anal.* 36 (2004) 851.
11. M.A. Alonso Lomillo, O. Domínguez Renedo, M.J. Arcos Martínez, *Electrochim. Acta* 50 (2005) 1807.
12. R.F. Ajayi, U. Sidwaba, U. Feleni, S.F. Douman, O. Tovide, S. Botha, *Electrochim. Acta* 128 (2014) 149.
13. M.A. Alonso Lomillo, J.M. Kauffmann, M.J. Arcos Martinez, *Biosens. Bioelectron.* 18 (2003) 1165.
14. R.A. Couto, M.B. Quinaz, *Sensors*, 16 (2016) 1015.
15. M. Ma, Z. Miao, DI. Zhang, X. Du, Y. Zhang, C. Zhang, J. Lin, Q. Chen, *Biosens. Bioelectron.* 64 (2015) 477.
16. K.S. Loh, Y.H. Lee, A. Musa, A.A. Salmah, I. Zamri, *Sensors* 8 (2008) 5775.
17. X. Cao, N. Wang, *Analyst*, 136 (2011) 4241.
18. R.A. Couto, M.B. Quinaz, *Sensors*, 16 (2016) 1015.
19. L. Ernster, G. Dallner, *Biochim. Biophys. Acta, Mol. Basis Dis.* 1271 (1995) 195.
20. S.A. Kahani, Z. Yagini, *Bioinorg. Chem. Appl.* 2014 (2014) 384984.
21. S. Ahmad, U. Riaz, A. Kaushik, J. Alam, *J. Inorg. Organomet. Polym.* 19 (2009) 355.
22. S. Asgari, Z. Fakharib, S. Berijanic, *JNS*, 4 (2014) 55.
23. L. Yan, S. Li, H. Yu, R. Shan, B. Du, T. Liu, *Powder Technology* 301 (2016) 632.
24. V.A.J. Silva, P.L. Andrade, M.P.C. Silva, A. Bustamante D, L. De Los Santos Valladares, J. Albino Aguiar, *J. Magn. Magn. Mater.* 343 (2013) 138.
25. S.A. Kulkarni, P. S. Sawadh, K. K. Kokate, International Conference on Benchmarks in Engineering Science and Technology ICBEST, *Proceedings published by Int. J. Computer Applications (IJCA)*, (2012) 17.
26. N. Arsalani, *eXPRESS Polymer Letters*, 4 (2010) 329.
27. W.H. Zhou, C.H. Lu, X.C. Guo, F.R. Chen, H. H. Yang, X.R. Wang, *Supplementary Material (ESI) for J. Mater. Chem.*2010.
28. R.S. Nicholson, I. Shain, *Anal. Chem.* 36 (1964) 706.
29. I. Streeter, G.G. Wildgoose, L. Shao, R.G. Compton, *Sens. Actuators B* 133 (2008) 462.
30. L. Xiao, L. Wi, G.G. Wildgoose, R.G. Compton, *Sens. Actuators B* 138 (2009) 524.
31. N.K. Bhajanthri, V.K. Arumugam, R. Chokkareddy, G.G. Redhi, *J. Mol. Liq.* 222 (2016) 370.
32. S. Rastgara, S. Shahrokhiana, *Talanta* 119 (2014) 156.
33. K. Asadpour-Zeynali, F. Mollarasouli, *Biosens. Bioelectron.* 92 (2017) 509.
34. M. Pumera, *Chem Rec*, 9 (2009) 211.